Rheological performance of seals in South Africa based on binder ageing considerations

by

Carlie Tredoux

Thesis presented in fulfilment of the requirements for the degree of Master of Engineering in Civil Engineering in the Faculty of Engineering at Stellenbosch University

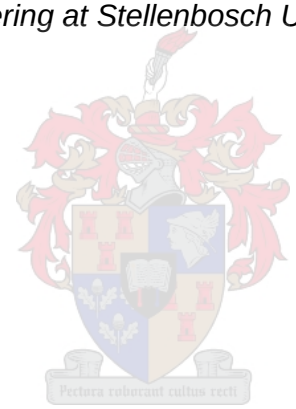

Supervisor: Prof Kim Jonathon Jenkins
Co-supervisor: Dr Chantal Eloise Rudman

March 2020

Declaration

By submitting this thesis electronically, I declare that the entirety of the work contained therein is my own, original work, that I am the sole author thereof (save to the extent explicitly otherwise stated), that reproduction and publication thereof by Stellenbosch University will not infringe any third party rights and that I have not previously in its entirety or in part submitted it for obtaining any qualification.

Carlie Tredoux : …… Date : ……

Abstract

Ageing is a fundamental phenomenon that affects the durability and performance of bituminous binders in a pavement. Ageing increases the risk of premature pavement failures whilst reducing the material durability and flexibility thus shortening pavement life.

For this reason the South African pavement industry is currently moving away from Penetration and Viscosity Grade (empirical) Specifications and towards Performance Grade (fundamental) Specifications, as the current specifications do not account for ageing in a comprehensive, fundamental manner. To facilitate the transitional process, a proposed technical specification for SA Performance Grade (PG) Specification for Bitumen (SATS 3208) was published by the South African Bureau of Standards (SABS) in 2018. Currently, this Performance Grade Specification is based on asphalt as per SHRP Superpave, hence the need for consideration of seal binders.

In order to make a meaningful contribution towards the formulation of a comprehensive PG specification for SA bituminous binders with respect to seals this study's aim is to investigate the performance of seals in South Africa. In particular, changes in the fundamental rheological properties of seal binders during ageing are of interest. These measurements provide performance-based properties that are essential as binder selection criteria.

This study was undertaken by performing laboratory testing on seal binders. It includes Dynamic Shear Rheometer (DSR) testing in accordance with SATS 3208 at intermediate temperatures and on seven different levels of ageing (unaged, RTFO, PAV2, RTFO+PAV2, PAV4, RTFO+PAV4 and recovered age). The seal binder's behavioural data was analysed with the Modified Kaelble shift factor model, CAM and GLS empirical models to determine / investigate rheological parameters that describes the durability and performance of seals in relation to ageing.

Results from the investigation show the Glover-Rowe (G-R) parameter to be the best rheological parameter to identify seal performance with age, as the Rheological Index (R) showed no correlation to seal ageing. Further investigation is required on SA seals, regarding the VET parameters influence on aggregate loss (failure mechanisms) before performance limits can be proposed for performance specifications.

Ageing influences the rheological properties of modified seal binders, as long-term artificial ageing of polymer modified seal binder provides an increased viscous component, thus showing that the polymer degrades at high temperatures as the binder ages.

Visual assessment on seal roads is recommended after 6-8 years of in-service to determine deterioration (failure mechanisms) of the pavement, based the G-R data findings of this study and others.

Opsomming

Veroudering is 'n fundamentele verskynsel wat die duursaamheid en werkverrigting van bitumen-bindmiddel in 'n plaveisel beïnvloed. Veroudering verhoog die risiko van voortydige falings tydens die plaveisel, terwyl die materiaal duursaamheid en buigsaamheid verminder word, waardeur plaveisel se lewe verkort word.

Om hierdie rede beweeg die Suid-Afrikaanse plaveiselbedryf tans weg van die Penetrasie en Viskositeit Graad (empiriese) spesifikasies en na die Werksverrigtingspesifikasies (fundamentele), aangesien die huidige spesifikasies nie op 'n omvattende, fundamentele manier veroudering in ag neem nie. Om die oorgangsproses te vergemaklik, is 'n voorgestelde tegniese spesifikasie vir SA Werksverrigtingspesifikasies vir Bitumen (SATS 3208) in 2018 deur die Suid Afrikaans Bureau van Standaarde (SABS) gepubliseer. Tans is hierdie Werksverrigtingspesifikasies gebaseer op asfalt volgens SHRP Superpave, daarom moet seëlbinders oorweeg word.

Om 'n betekenisvolle bydrae te lewer tot die formulering van 'n omvattende Werksverrigtingspesifikasie vir SA bitumen-bindmiddels ten opsigte van seëls, is hierdie studie se doel om die werkverrigting van seëls in Suid-Afrika te ondersoek.

Veral die veranderinge in die fundamentele reologiese eienskappe van seëlbinders tydens veroudering is van belang. Hierdie metings bied werkverrigting-gebaseerde eienskappe wat noodsaaklik is vir bindingseleksie-kriteria.

Hierdie studie is onderneem deur laboratoriumtoetse op seëlbinders uit te voer. Dit sluit *Dynamic Shear Rheometer* (DSR) -toetse in volgens die SATS 3208 by intermediêre temperature en op sewe verskillende verouderingsvlakke (onverouderd, RTFO, PAV2, RTFO + PAV2, PAV4, RTFO + PAV4 en herwonne ouderdom). Die gedragsgegewens van die seëlbinder is met die Aangepaste Kaelble verskuiffaktor model, CAM en GLS empiriese modelle geanaliseer om reologiese parameters te bepaal / ondersoek wat die duursaamheid en werkverrigting van seëls in verhouding tot veroudering beskryf.

Ondersoekresultate het getoon dat die Glover-Rowe (G-R) parameter die beste reologiese parameter was om seëlprestasie met ouderdom te identifiseer, aangesien die Reologiese Indeks (R) geen korrelasie met seëlveroudering getoon het nie. Verdere ondersoek is nodig op SA seëls met betrekking tot die visko-elastiese oorgangsparameters invloed op klipverlies (falingmeganismes) voordat werkverrigting limiete vir Werksverrigtingspesifikasies voorgestel kan word.

Veroudering beïnvloed die reologiese eienskappe van gemodifiseerde seëlbinders, aangesien langtermyn kunsmatige veroudering van polimeermodifiseerde seëlbindmiddels 'n verhoogde viskose komponent lewer, dit toon aan dat die polimeer by hoë temperature afbreek soos die bindmiddel verouder.

Na 6-8 jaar van diens word visuele assessering op seëlpaaie aanbeveel om die agteruitgang (falingmeganismes) van die plaveisel te bepaal, wat gebaseer is op die bevindings van die G-R data van hierdie studie en andere.

Acknowledgements

The author would like to express sincere appreciation to the following people and organisations for their motivation, support, assistance and guidance making this thesis possible:

- **Prof Kim Jonathan Jenkins** (University of Stellenbosch), my study leader for sharing his specialist knowledge on and passion for improving pavement engineering; and his patience and willingness to always help and guide me regardless of all other pressing responsibilities.
- **Dr Chantal Eloise Rudman** (University of Stellenbosch), my co-supervisor for her guidance, encouragement, support and continuous motivation in challenging times.
- **Miss Elaine Simone Goosen** (University of Stellenbosch), busy with her Doctoral, for allowing me to perform much of my research work alongside her and sharing her specialist knowledge on rheology with me.
- **Mr Gerrie van Zyl (MyCube)** for sharing his valuable industry experience on seal performance and the sourcing of samples (in-services and original) used in this thesis.
- **The National Research Foundation (NRF)** for their financial support to do my masters, making this thesis possible and giving me the opportunity to broaden my knowledge.
- **MUCH ASPHALT and their Central Laboratory Staff (Mr Colin Brooks, Mr Alec Rippenaar, Mr Morné Labuschagne, Mrs Firyaal Moos, Mr Craig Cupido)** for making their laboratory and equipment available to student of the University of Stellenbosch and assisting with tests as and when needed.
- **Mr Gavin Williams and Mr Riaan Briedenhann** for their help in the Pavement Laboratory of the University of Stellenbosch.
- **The Civil Department (Pavement Engineering)** of the University of Stellenbosch for their contribution to making my dream of becoming a successful engineer, a reality.
- **My Family and friends** for all their continuous love, support, prayers, motivation an encouragement to give my best at all times and to finish strong.
- **Most importantly the almighty LORD** for blessing me with the physical and mental ability to complete what I set out to do, to never give up, to always give my utmost best and to keep going when all seems impossible.

Table of Contents

Page

Declaration ..... **i**

Abstract ..... **ii**

Opsomming ..... **iii**

Acknowledgements ..... **iv**

Table of Contents ..... **v**

List of Figures ..... **viii**

List of Tables ..... **xi**

List of Abbreviations ..... **xii**

List of Symbols ..... **xiv**

Chapter 1: Introduction **1**

1.1 Background 1
1.2 Problem Statement 2
1.3 Aim and Objectives 3
1.4 Research Scope and Limitations 4
1.5 Thesis Overview and Layout 4

Chapter 2: Literature Study **6**

2.1 Introduction 6
2.2 Bitumen 6
2.2.1 Origin 6
2.2.2 Constitution and Structure 7
2.2.3 Application 8
2.2.4 Different products 10
2.3 Behaviour of Bitumen 12
2.4 Seals 14
2.4.1 Introduction of Seals 14
2.4.2 Function of Seals 14
2.4.3 Type of seals and construction 14
2.4.4 Components of seals influencing performance 17
2.4.5 Failure mechanisms 18
2.4.6 Measurement methods for seal selection 21
2.5 Specifications for bitumen 22
2.5.1 Performance grade specification 24
2.6 Performance Grade Testing and Rheology 28
2.6.1 Solubilisation and Recovery 28
2.6.2 Artificial Ageing / Hardening 33
2.6.3 Rheology Properties 36
2.7 Viscoelastic behaviour modelling / LVE rheological modelling 42
2.7.1 Linear Viscoelastic (LVE) limits 43

2.7.2 Time-temperature superposition principle (TTSP) 43
2.7.3 Rheological Models for Shifting 44
2.7.4 Empirical models 48
2.8 Durability and Ageing Parameters 56
2.8.1 Glover and Glover-Rowe parameter 57
2.8.2 Critical temperature difference 59
2.8.3 Viscoelastic transition (VET) stiffness and temperature 61
2.8.4 Rheological Index 62
2.8.5 Ageing Ratios 64
2.9 Summary 65

Chapter 3: Research Materials and Methods 66
3.1 Introduction 66
3.2 Experimental Design 66
3.3 Material Obtained and Selected 68
3.4 Test Methods and Material Preparation 70
3.4.1 Storage and handling temperatures of bitumen 70
3.4.2 Solubility and Recovery 70
3.4.3 Artificial Ageing Procedure 75
3.4.4 DSR Moulds 77
3.4.5 DSR test 78
3.5 Viscoelastic Modelling and Data Analysis 80
3.5.1 Master curves and Black Space diagrams 80
3.5.2 Durability and Ageing Parameters 84
3.6 Summary 86

Chapter 4: Test Results and Findings 87
4.1 Introduction 87
4.2 Solubilisation and Recovery 87
4.3 DSR Rheometry Testing 88
4.4 Modelling 90
4.4.1 Shift Factor 91
4.4.2 Master Curves and Black Space Diagrams before modelling 92
4.4.3 Empirical models 97
4.5 Suitable model 110
4.6 Durability and Ageing Parameters 111
4.6.1 Glover-Rowe (G-R) Parameter 111
4.6.2 Viscoelastic transition (VET) stiffness and temperature 116
4.6.3 Rheological Index 122
4.6.4 Ageing Ratio 124
4.7 Summary of Findings 127

Chapter 5: Conclusions and Recommendations 129
5.1 Conclusions 129
5.1.1 Recovery and artificial ageing of seal binders 129
5.1.2 DSR testing at intermediate temperatures 129
5.1.3 Modelling and identify suitable rheological indicators 130
5.2 Recommendations 130

Reference List 132

Appendix A: Modelling 140

Appendix B: Combined Master Curves & Black Space Diagrams before modelling 188

Appendix C: Measured vs modelled correlation 192

List of Figures

Page

Figure 1-1: Types of pavements based on materials 1
Figure 1-2: Overview of this research study 5
Figure 2-1: Fossil fuel formation 6
Figure 2-2: Crude oil distillation products 7
Figure 2-3: Schematic illustration of a "SOL" type bitumen 8
Figure 2-4: Schematic illustration of a "GEL" type bitumen 8
Figure 2-5: Applications of bitumen surfacing 9
Figure 2-6: Binders available in SA 12
Figure 2-7: Distribution of bituminous binders 12
Figure 2-8: Domain behaviours of bitumen depending on strain versus temperature (T) and number of cycles (N) 13
Figure 2-9: Four regions of viscoelastic behaviour 13
Figure 2-10: Surfacing types in SANRAL and Western Cape 15
Figure 2-11: Structure of a single seal 15
Figure 2-12: Structure of a double seal 16
Figure 2-13: Handling application of slurry for Cape seal 16
Figure 2-14: Structure of a cape seal 16
Figure 2-15: Slurry application in Cape seals 17
Figure 2-16: Divided failure mechanisms of seals 19
Figure 2-17: Two categories of failure mechanisms in seals 19
Figure 2-18: Criteria for binder selection 23
Figure 2-19: Simplified solubilisation and recovery procedure 28
Figure 2-20: Abson distillation method illustration 31
Figure 2-21: Rotary evaporator for polymer modified binders using a Bunsen burner 31
Figure 2-22: Typical illustration of a rotary evaporator 32
Figure 2-23: Unmodified and modified RTFO procedure 34
Figure 2-24: PAV and Vacuum Degassing Oven Apparatus 35
Figure 2-25: Ageing of bituminous binders 35
Figure 2-26: Short- and long-term ageing in terms of the viscosity 36
Figure 2-27: DSR Parallel Plate and Stain distribution 37
Figure 2-28: DSR stress-strain response 37
Figure 2-29: G* and δ related to viscoelastic behaviour 38
Figure 2-30: Example of the LVE region of a binder 39
Figure 2-31: One creep recovery cycle during MSCR test 40
Figure 2-32: Schematic and analysis of BBR 41

Figure 2-33: Step- by- step LVE rheology modelling 43
Figure 2-34: Shift factor applied to G* isotherms to form a master curve 44
Figure 2-35: Example of Kaelble compared to Arrhenius and WLF for a SBS modified binder 46
Figure 2-36: Example of PG64-22 modified binder, comparing shift factor equations with the RMSE at T_{ref} = 25°C 47
Figure 2-37: Four primary master curve parameters to characterise LVE properties 48
Figure 2-38: Christensen- Anderson (CA) model 50
Figure 2-39: CA model of unaged S-E1 binder 50
Figure 2-40: Modelling of the CAM model 52
Figure 2-41: Definition of the Standard Sigmoidal model 53
Figure 2-42: The SS model's |G*| graph with different ɣ values 54
Figure 2-43: The GLS model's log G* graph with varies λ values 55
Figure 2-44: Ductility versus Glover parameter correlation for aged unmodified binders 57
Figure 2-45: Ductility versus Glover parameter correlation for modified binders 58
Figure 2-46: Ageing of binders in the ductility-based failure planes 59
Figure 2-47: Relationship between the G-R and ΔT_c parameter 60
Figure 2-48: Extending the S and m values to the G-R concept 61
Figure 2-49: VET concept with age 62
Figure 2-50: Using R-value as damage parameter for ageing in Black Space 63
Figure 2-51: Black Space plot of Western Canadian PG64-28 binder with age 64
Figure 2-52: Effect of ageing on ω_c and R-value 65
Figure 3-1: Experimental Design flow chart 67
Figure 3-2: Retrieved and original seal samples 69
Figure 3-3: Field sample retrieving process 70
Figure 3-4: Extraction procedure 71
Figure 3-5: Centrifugation procedure 72
Figure 3-6: Rotary evaporator with vacuum pump 73
Figure 3-7: Recovered bituminous binder sample preparation 74
Figure 3-8: RTFO modified binder ageing 76
Figure 3-9: Long-term ageing apparatus 76
Figure 3-10: PAV and Degassing procedure 77
Figure 3-11: Moulding procedure 77
Figure 3-12: Testing that can be done 78
Figure 3-13: DSR equipment 79
Figure 3-14: 70/100 strain sweeps 79
Figure 3-15: G* pairwise shift and Modified Kaelble model 81
Figure 3-16: GLS model optimised for fit 83
Figure 3-17: Schematic illustration of computing VET parameters 85

Figure 3-18: Correlation between $G^*_{TINT, 10rad/s}$ and $G\text{-}R_{15°C, 0.005rad/s}$ 86
Figure 4-1: DSR strain sweeps of binders with higher and lower upper LVE limits 89
Figure 4-2: MR23_70/100_Recovery_3years DSR isotherm data 90
Figure 4-3: Typical Modified Kaelble shift equation plot 91
Figure 4-4: Combined master curves for N8/11_S-E1 93
Figure 4-5: Combined master curves R61/8_SC-E2 94
Figure 4-6: Modification of unaged binder's Black Space diagrams 95
Figure 4-7: Combined Black Space diagrams for artificially aged 70/100 binder, T_{ref} = 15°C 96
Figure 4-8: Combined Black Space diagrams N2/16_S-E1, T_{ref} = 25°C 97
Figure 4-9: Determination of the crossover frequency, ω_c 99
Figure 4-10: RMSE (%) with age for the CAM and GLS models 100
Figure 4-11: CAM model parameters of artificially aged binders 101
Figure 4-12: CAM model parameters of recovered binders 101
Figure 4-13: CAM G* data correlation, G* > 10^5 Pa 102
Figure 4-14: CAM δ data correlation, G* > 10^5 Pa 102
Figure 4-15: CAM model G* and master curves 103
Figure 4-16: CAM model Black Space diagrams 103
Figure 4-17: GLS model parameters of artificially aged binders 107
Figure 4-18: GLS model parameters of recovered binders 107
Figure 4-19: GLS G* data correlation, G* > 10^4 Pa 108
Figure 4-20: GLS δ data correlation, G* > 10^4 Pa 108
Figure 4-21: GLS model G* and master curves 109
Figure 4-22: GLS model Black Space diagram 109
Figure 4-23: G-R parameter for all recovered binders 113
Figure 4-24: Artificially aged binder's G-R values in Black Space 114
Figure 4-25: Recovered binder's G-R values with age, seal type and province 115
Figure 4-26: Goosen's recovered binder's G-R values with age, seal type and province 115
Figure 4-27: Recovered binders' G-R correlation with field performance 116
Figure 4-28: VET parameters correlation with artificial ageing 118
Figure 4-29: Development of VET for artificially aged binders 119
Figure 4-30: Development of VET for recovered binders 119
Figure 4-31: G^*_{VET} and T_{VET} correlation for recovered binders 120
Figure 4-32: Goosen's recovered binder's VET parameters correlation 121
Figure 4-33: G^*_{VET} and T_{VET} correlation for artificially aged binders 121
Figure 4-34: Recovered binders' VET parameters correlation with field performance 122
Figure 4-35: Cracking related to R-value for all binders 124
Figure 4-36: Ageing ratios (G-R) for all artificially aged binders 126
Figure 4-37: Ageing ratios (G-R) for S-E1 and SC-E2 recovered binders 126

List of Tables

Page

Table 2-1: Different compositions of modifiers 10
Table 2-2: Combinations of double seals 16
Table 2-3: Cape seal selection 17
Table 2-4: Components influencing performance of seals 18
Table 2-5: Tentative construction and PG of emulsion framework 22
Table 2-6: Concepts in the SATS 3208 Performance Grade (PG) Specifications for Bitumen in South Africa 25
Table 2-7: Traffic 25
Table 2-8: Proposed SATS 3208 Performance Grade (PG) Specifications for Bitumen in South Africa 27
Table 2-9: Solvents for extraction of bituminous binders with distillation conditions 29
Table 2-10: Testing extraction-recovery apparatus survey 33
Table 2-11: Various R-values 63
Table 3-1: Retrieved and Original seal binders selected for investigation 69
Table 3-2: Retrieved road sections centrifuge fines 72
Table 3-3: Specifications of two solvents 73
Table 3-4: RTFO ageing procedure 75
Table 3-5: DSR testing conditions 80
Table 3-6: Initial values for the model parameters 82
Table 4-1: Outline of the interpretation and discussion of the results 87
Table 4-2: Mass change of binder and % binder recovered from retrieved samples 88
Table 4-3: DSR parallel plate upper LVE strain for frequency sweeps 88
Table 4-4: DSR frequency sweep output for one temperature 89
Table 4-5: Synthesis of Abatech RHEA Modified Kaelble shift parameters at T_{ref} = 25°C 91
Table 4-6: Summary of CAM model parameters at T_{ref} = 25°C 97
Table 4-7: Summary of GLS model at T_{ref} = 25°C 104
Table 4-8: Suitable model on binder to binder basis 110
Table 4-9: G-R parameter and associated G* and δ for all the binders 112
Table 4-10: VET stiffness and temperature parameters for all the binders at 15°C and 0.005 rad/s 116
Table 4-11: Rheological Index and crossover frequency values 122
Table 4-12: Ageing ratios in terms of G-R parameters 124

List of Abbreviations

AAPA	Australian Asphalt Pavement Association
AAPT	Association of Asphalt Paving Technologists
AASHTO	American Association of State and Highway Transportation Officials
ASTM	American Society for Testing and Materials
BBR	Bending Beam Rheometer
CA	Christensen-Anderson
CAM	Christensen-Anderson-Marasteanu
CEN	European Committee for Standardisation
CMA	Cold Mix Asphalt
CSIR	Council of Scientific and Industrial Research
DSR	Dynamic Shear Rheometer
DTT	Direct Tension Tester
ELV	Equivalent Light Vehicles
EVA	Ethylene Vinyl Acetate
GLS	Generalised Logistic Sigmoidal
G-R	Glower-Rowe parameter
HMA	Hot Mix Asphalt
HiPAT	High Pressure Ageing test
LVE	Linear Viscoelastic
MEPDG	Mechanistic-Empirical Pavement Design Guide
MSCR	Multi Stress Creep Recovery
PAV	Pressure Ageing Vessel
PG	Performance Grade
PMB	Polymer Modified Binder
PP	Parallel Plate
RTFO	Rolling Thin Film Oven
RV	Rotational Viscometer

SA	South Africa
SABITA	Southern African Bitumen Association
SABS	South African Standard Organisation
SAPEM	South African Pavement Engineering Manual
SANRAL	South African National Roads Agency Limited
SANS	South African National Standards
SATS	South African Technical Specification
SBR	Styrene-Butadiene-Rubber
SBS	Styrene-Butadiene-Styrene
SHRP	Strategic Highway Research Program
SI	International System of Units
SS	Standard Sigmoidal
TG	Technical Guideline
TRH	Technical Recommendation for Highways
US	United States
VDO	Vacuum Degassing Oven
VET	Viscoelastic Transition
WLF	Williams, Landel and Ferry

List of Symbols

C_1	Arrhenius / WLF/ Kaelble constant	[-]
C_2	Arrhenius / WLF/ Kaelble constant	[-]
f	Loading frequency	[Hz]
f_r	Reduced frequency	[Hz]
G	Shear relaxation modulus	[Pa]
G"	Loss modulus	[Pa]
G*	Complex shear modulus	[Pa]
G’	Storage modulus	[Pa]
G_e	Equilibrium complex shear modulus	[Pa]
G_g	Glassy modulus	[Pa]
G-R	Glower-Rowe parameter	[kPa]
G_{VET}	Viscoelastic transition stiffness	[Pa]
J*	Complex shear compliance modulus	[Pa]
J_{nr}	Non-recoverable Creep Compliance	[kPa^{-1}]
m(t)	Slope of BBR logarithm stiffness at time, t	[Pa/s]
R	Rheological Index	[-]
RMSE	Root Mean Square Error	[%]
S(t)	BBR flexural creep modulus at time, t	[Pa]
t	Loading time	[s]
T	Testing temperature	[°C]
T_c	Critical temperature	[°C]
T_d	Defining temperature	[°C]
T_g	Glass transition temperature	[°C]
T_{int}	Intermediate temperature	[°C]
T_{max}	Maximum temperature	[°C]
T_{min}	Minimum temperature	[°C]
T_{ref}	Reference temperature	[°C]
T_{VET}	Reference temperature	[°C]
α_T	Horizontal shift factor	[-]

β_T	Vertical shift factor	[-]
δ	Phase angle	[°]
η^*	Complex shear viscosity	[Pa.s]
η_0	Steady state viscosity	[Pa.s]
η_o	Viscosity of the original bitumen	[Pa.s]
η_r	Viscosity of the recovered bitumen	[Pa.s]
ω	Angular frequency	[rad/s]
ω_c	Crossover frequency	[rad/s]
ω_r	Reduced frequency	[rad/s]
v, w	CAM fitting parameters	[-]
γ	Shear strain	[-]
γ_p	Peak shear strain	[-]
γ_r	Recovered shear strain	[-]
γ_u	Non-recoverable shear strain	[-]
τ	Shear stress	[Pa]

Chapter 1: Introduction

1.1 Background

Surfacing is the upper layer and most visible component of a pavement structure. It easily shows signs of condition deterioration, which usually leads to road user criticism.

Surfacing is also one of the key indicators for required pavement maintenance or renewal in order to counter deterioration observations. It is therefore important to have standardised specifications available for the South African (SA) pavement industry that would assist in improving the **function** of pavement surfacing, the **performance** thereof in a particular climate when subjected to certain loading conditions and to eliminate / minimise the probability of surface **failure mechanisms**, of which ageing is just one component.

Pavement types are classified by the types of material used for surfacing as shown in Figure 1-1. Flexible surfacing (asphalt and seals) is commonly used in SA, where seals are more frequently applied than asphalt not only because it is the most cost-effective method, but also because the construction is less complicated.

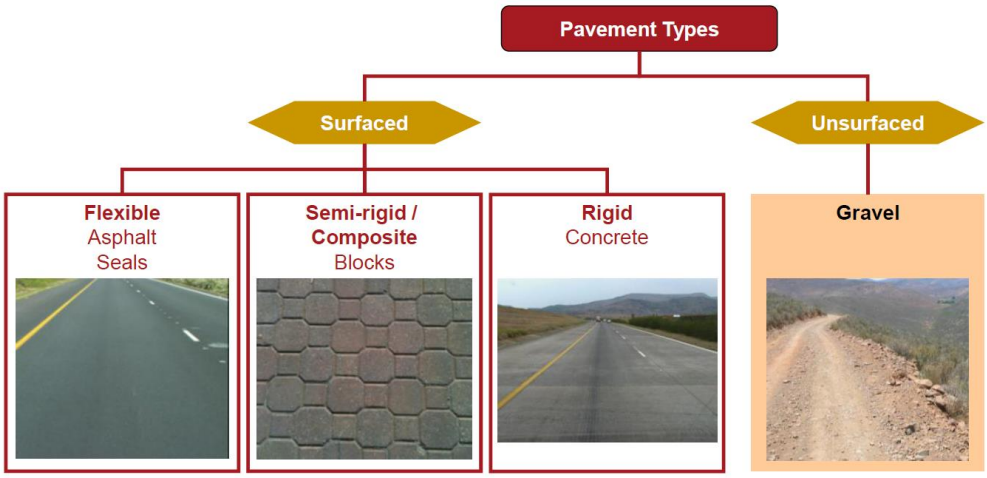

Figure 1-1: Types of pavements based on materials (South African Pavement Engineering Manual (SAPEM), 2013)

The most essential component used in road surfacing is bituminous binder products. Bitumen's flow behaviour is complex under different environments (temperatures) and traffic levels, as it can be viscous, elastic or viscoelastic. The binder's viscosity (flow) and grade (hardness) are associated with the failure mechanisms in surfacing, such as cracks and aggregate loss.

The SA pavement industry has seen momentous change in the last few years, especially the decline in using the South African National Standard Penetration Grade Specification (SANS 4001-BT1) for bitumen by engineers. The Penetration Grade Specification for unmodified bitumen in-service depends on viscosity and penetration measurements at standard temperatures and does not account for ageing completely. Accordingly, due to growing traffic demands and the necessity to minimise crack failure mechanism, with the support of the Council of Scientific and Industrial Research (CSIR) a Performance Grade (PG) Specification (fundamental properties) is currently in the process of being developed for the SA pavement industry. This will be applicable to all binders (including modification) and all bituminous road applications (asphalt and **seals**). (Australian Asphalt Pavement Association (AAPA), 2011)

The Rheology (*the study of flow*) of bitumen is the fundamental measurement for bitumen flow and deformation characteristics. Consequently the performance grade specifications parameters are derived from the rheology of binder performance indicators. (Hunter, Self & Read, 2015)

1.2 Problem Statement

Globally Penetration Grade Specifications have been used for many decades since the 20th century in order to classify the specification of unmodified bitumen. Unfortunately the SA industry growth has surpassed current Penetration Grade Specifications deliverables and requires review in order to meet current and future SA industry demands.

The Penetration Grade Specifications worked rather well for conventional (unmodified) bitumen until the arrival of modified bitumen. The modified binders introduced more complexities to bituminous materials in terms of different behavioural trends under different loading and environmental conditions. To adequately describe modified bitumen performance trends, it requires more sophisticated test methods. (Hunter *et al.*, 2015)

In 1993 the United States (US) Strategic Highway Research Program (SHRP) published the first version of the American Association of State and Highway Transportation Officials (AASHTO) performance grade binder specification primarily for asphalt binders. (Hunter *et al.*, 2015) The latest version of the US's PG specification was published in 2017, known as the 'AASHTO M320-17 Standard Specification for performance-grade asphalt binder'. The PG specification captures the fundamental properties of the material and in relation to the actual stress-strain relationship encountered in the pavement service structure, which the Penetration Grade Specifications do not contain. (Hunter *et al.*, 2015)

Bituminous specifications for Southern Africa were first published in 1951. They were revised in 1966 and again in 2014, the SANS 4001-BT1, to eliminate certain shortcomings and to bring them into line with current practice, as higher traffic volumes and loading gave rise to an increase in premature road pavement failure in SA.

Unfortunately, the binder quality assessment in the SANS 400-BT1 (empirical testing) is too limited and fails to measure the binder's ability to perform adequately when subjected to prevailing SA climate and traffic conditions. Empirical tests can therefore not effectively characterise the rheological properties of polymer modified binders, which are needed to evaluate response and damage. More advanced, fundamental rheological tests are increasingly being used throughout the world to establish specifications based on fundamental engineering properties, capable of more accurately predicting the performance of bitumen, including asphalt and seals.

Currently there are no performance classifications for binders for seals or thin surfacing for the SA pavement industry. Neither are there any set selection guidelines for SA binders.

At present the USA PG asphalt binder specification and standard test procedures for asphalt are used as basis and starting point for the SA PG Binder Specification, as the USA are still in the process of developing a PG specification for seals.

A proposed SA technical specification (SATS 3208) for a SA PG Specification for Bitumen was published by the South African Bureau of Standards (SABS) in 2018.

The SATS 3208 is only out on a two year trial release, covering a performance grading system which includes measures describing stress / strain relationships under field loading; pavement conditions including temperature, traffic speed, traffic volume and pavement structure; and compliance limits derived from fundamental analysis, experience and field performance. This specification still needs to be used in conjunction with the SANS 4004-BT1, where the empirical testing needs to be replaced within this trial period.

To address the prevailing empirical testing challenges, it is of critical importance that substantial research is conducted in relation to pavement performance. Hence this research study will contribute in this regard by investigating the rheological performance of seals in South Africa based on binder ageing considerations.

1.3 Aim and Objectives

The aim of this study on performance grade specifications is to investigate the rheological performance of seals in South Africa based on binder ageing considerations in order to:

- gain a better understanding of the durability aspects that are connected to the ageing performance of seal binders in South Africa;
- make a meaningful contribution to the formulation of a comprehensive PG specification for SA bituminous binders with respect to seals only; and to
- determine the key rheological considerations impacting on the transition from a Penetration-Viscosity Specification to a Performance Grade Specification.

In order to achieve the aforementioned aim the following four main objectives need to be met:

Objective 1: To characterise seal ageing in terms of PG specification, as the ageing process is an important component of the relaxation of bitumen in order to evaluate the failure mechanisms (fatigue and cracking) / deterioration of seal binders over time.

Objective 2: To evaluate the performance development by testing the original simulated (artificial) aged and in-service (recovered) seal binders according to the proposed SATS 3208 PG specification.

Objective 3: To identify the principles applicable and gain an understanding of analysing test data and rheological parameters in order to determine binder properties in response to the ageing process of seals. This is done by assessing the rate of ageing of the seal binders by means of rheological parameters. This includes both artificially aged conditioning levels, Rolling Thin Film Oven (RTFO) ageing followed by Pressure Ageing Vessel (PAV) ageing (plant and in-field ageing) as prescribed by industry and ageing without RTFO (only PAV) as seal binders do not go through plant ageing.

Objective 4: To identify suitable rheological indicators i.e. G-R, VET and Rheological Index parameters (not included in the SATS 3208) that can be used to describe seal behaviour / performance, by analysing the test data and rheological indicators of recovered-, original-, RTFO- and PAV-binders.

1.4 Research Scope and Limitations

This research study does not serve as a specification document, but rather contributes to finalise the formulation of the proposed SATS 3208 Performance Grade (PG) Specifications for Bitumen in South Africa in relation to seals.

Due to time constraints and the sample preparation process involved (recovery, RTFO, PAV) this research study had to be limited to:

- investigating only the structures for Cape seal and multiple seals;
- investigating only the 70/100, S-E1 and SC-E2 binder types, obtained from multiple sources, with only some original binders available from the same recovered road surface seal samples;
- recovering only a restricted amount of binder from the existing road surface samples;
- only testing at intermediate temperatures using the Dynamic Shear Rheometer (DSR); and
- not allowing any time for repetition tests in order to validate the accuracy of results.

This research study therefore **excludes**:

- Additional seal structures, such as single seal, double seal, slurry seal, sand seal or any other similar type of seals.
- Additional seal binder types, namely S-E2, SC-E1, bitumen rubber for seals (S-R1 and S-R2)
- Bending Beam Rheometer (BBR) testing, assessing the tendency of bitumen to become brittle and which measures the binders' stiffness and relaxation abilities at low temperatures.
- Multi Stress Creep Recovery (MSCR) testing with the DSR machine, evaluating the binder's susceptibility to deform permanent at high temperatures.

1.5 Thesis Overview and Layout

The thesis overview and layout is schematically illustrated in Figure 1-2, with chapters dedicated to each core element of the study, describing the research steps followed to achieve the aim and objectives of this research study, as set out in Section 1.3:

CHAPTER 2: Literature Study reflects on and discusses past and current research conducted in relation to PG specifications, providing the background of bitumen – including the origin, flow behaviour and bituminous products used in road applications. The focus being on the main failure mechanisms of seal binder in SA and the recommended test procedures and linear viscoelastic models used to analyse the rheological properties of seals in order to effectively interpret the parameters for SA PG specifications.

CHAPTER 3: Research Methodology provides an outline of the experimental design and methodology that was undertaken, including the details of the test material, material preparation, equipment used, and the testing procedures applied.

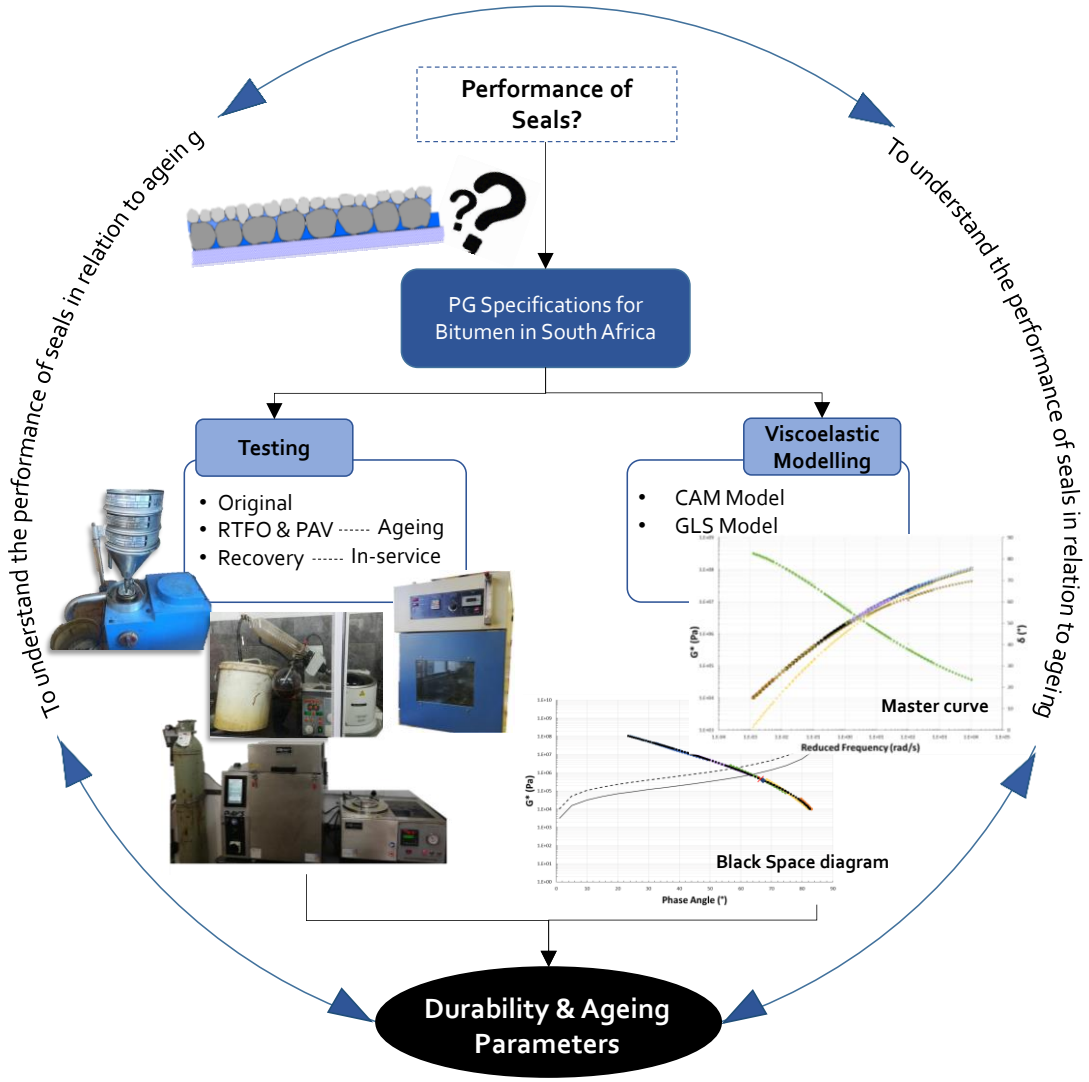

Figure 1-2: Overview of this research study

CHAPTER 4: Test Results and Findings presents, analyses and discusses the results obtained from tests conducted, including the calculation of essential parameters to define the rheological properties of the specific binder type, providing behavioural trends for the typical seal binders in SA.

CHAPTER 5: Conclusions and Recommendations summarises the conclusions drawn from findings in relation to the performance of seal binders in SA and makes recommendations to contribute to the formulation of a comprehensive SA PG specification for bituminous binders with respect to seals only.

Chapter 2: Literature Study

2.1 Introduction

In line with the topic of this thesis, “Rheological performance of seals in South Africa based on binder ageing considerations” this literature study only focusses on research already conducted in relation to performance grade (PG) specifications, with the specific focus on bitumen within seals. The study takes into account factors influencing bitumen and the performance of seals simultaneously.

2.2 Bitumen

2.2.1 Origin

Bitumen is recognised as the oldest engineering material of value to engineers, because of its exceptional properties when used as an adhesive, sealant and waterproofing agent. Bitumen is also widely used in road construction, to the extent of 90% of refined bitumen from petroleum according to South African Bitumen Association (SABITA). (Morgan, Mulder & Bitumen, 1995)

The majority of bitumen is obtained from crude oil, produced from petroleum distillation residue which is commonly manufactured during the refining process of crude oil. Crude oil accumulates naturally on ocean- and lake floors. Crude oil is a fossil fuel which is converted from remains of marine organisms and plants in an organic matter, created with the application of heat from within the earth’s crust and pressure applied by the upper layers, Figure 2-1. (Van de Ven, Rowe & Jenkins, 2017) (Morgan *et al.*, 1995)

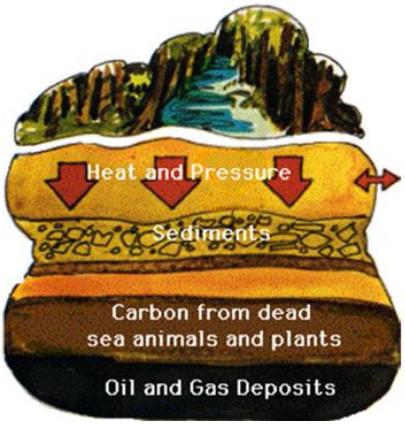

Figure 2-1: Fossil fuel formation (Van de Ven *et al.*, 2017)

Crude oil consists of a complex mixture of hydrocarbons. In order to obtain bitumen, the hydrocarbons have to be separated during the refining process (atmospheric & vacuum distillation), by heating the crude oil until it boils to ensure separation between lighter fractions (liquid petroleum gas, petrol, and diesel) and heavier fractions. The residue at the bottom (heaviest faction) of the barrel is called straight-run bitumen (unmodified bitumen), only 2.5% of the total barrel, which is used to manufacture several grades of bitumen, as illustrated by Figure 2-2. It must also be noted that crude oil cannot be used without changing it. (Southern African Bitumen Association (SABITA), 2014)

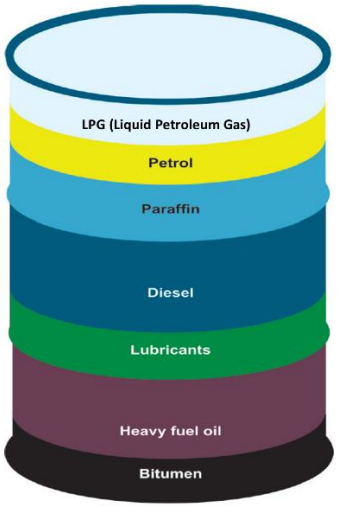

Figure 2-2: Crude oil distillation products (Southern African Bitumen Association (SABITA), 2014)

2.2.2 Constitution and Structure

A good understanding of the constitution (chemical composition) and structure (physical arrangement) of bitumen is essential to understand the characteristics of bitumen rheology (Section 2.5). It is also important to note that composition and structure of bitumen is not stereo type, as it differs according to the crude oil source from which the bitumen originates.

The chemical composition of bitumen is also a complex mixture of chemical agents, containing a large number of hydrocarbons; minor amount of oxygen, nitrogen and sulphur atoms; and traces of metals (calcium, iron, magnesium, nickel and vanadium). Although the constitution of bitumen is generally similar, it is important to note that with variation depending upon the origin of crude oil/bitumen, most bitumen compositions fall within the following range: (RAHA Bitumen Co, 2016)

- Carbon 82-88%
- Hydrogen 8-11%
- Sulphur 0-6%
- Oxygen 0-1.5%
- Nitrogen 0-1%

Bitumen can be divided in two chemical groups, i.e. asphaltenes and maltenes (includes aromatics, resins and saturates). Asphaltenes consist of high molecular weight, high polar solids and are n-heptane insoluble, where maltenes have lower molecular weight and are n-heptane soluble. (Morgan *et al.*, 1995)

The structure of bitumen particles is modelled as a colloid system, with maltenes as the continuous phase and asphaltenes as the dispersed phase. The colloid system consists of high molecular weight asphaltenes micelles (asphaltenes clusters together with an absorbed layer of high molecular weight aromatic resins) dissolved or dispersed in a lower molecular weight maltenes. (RAHA Bitumen Co, 2016)

There are two boundary types of bitumen ('SOL'- and GEL'- type) presented in Figure 2-3 and 2-4. The 'SOL'-type is when asphaltenes micelles has a good movement within the bitumen

by having a sufficient quantity of aromatics and resins, whereas in the 'GEL'-type micelles bind together and form irregular disconnected asphaltenes structure due to insufficient quantity of aromatics and resins. The 'GEL'-type behaviour of bitumen decreases when heated to high temperatures. (Morgan *et al.*, 1995)

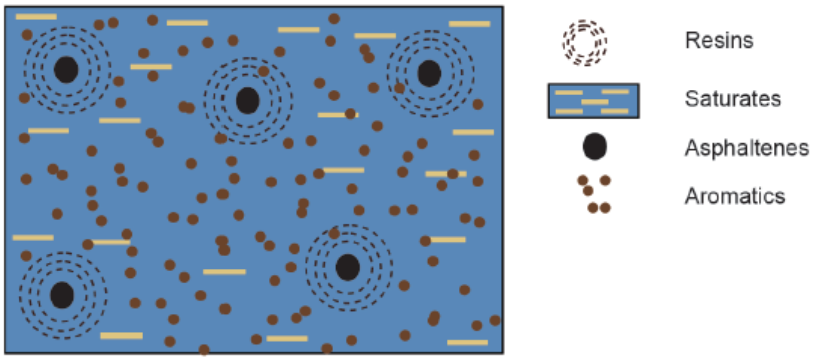

Figure 2-3: Schematic illustration of a "SOL" type bitumen (Southern African Bitumen Association (SABITA), 2014)

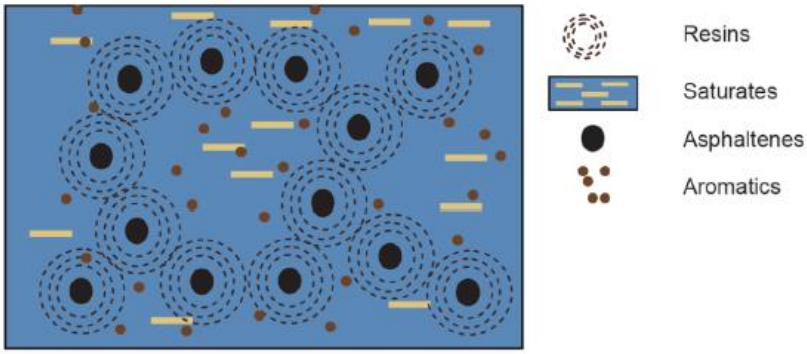

Figure 2-4: Schematic illustration of a "GEL" type bitumen (Southern African Bitumen Association (SABITA), 2014)

Morgan *et al*. (1995) has demonstrated that by keeping the asphaltenes content constant:

- An increase in aromatics reduces the shear susceptibility;
- An increase in resins hardens the bitumen, decrease shear susceptibility but rises the viscosity;
- But by sustaining a constant ratio of resins to aromatic and increasing saturates, the bitumen softens.

It is noted that the composition and structure of bitumen influences the flow behaviour and rheology properties of the bitumen. A 'SOL'-type structure leads to a Newtonian flow behaviour, whereas the 'GEL'-type structure dominates a non-Newtonian flow behaviour. (Yusoff, Shaw & Airey, 2011)

2.2.3 Application

It is unsurprising that bitumen has numerous applications as it is a low-cost thermoplastic material, with excellent properties. It is therefore widely used in industrial applications of which 90% is used in road and pavement applications (surfacing layer) and 10% used in other applications such as roofing, paints, sound roofing, pipe coating etc. (Southern African Bitumen Association (SABITA), 2014)

According to the South African National Roads Authority (SANRAL) the purpose of road surfacing is to protect the underlying pavement structure and provide a safe driving surface for road users, by providing a uniform, skid-resistant impermeable coat. (South African National Roads Agency Limited (SANRAL), 2007)

Figure 2-5 contains the three types of applications for bituminous surfacing. It is important to note that when seal costs are compared with asphalt overlayer costs in SA, that seals are much more cost effective.

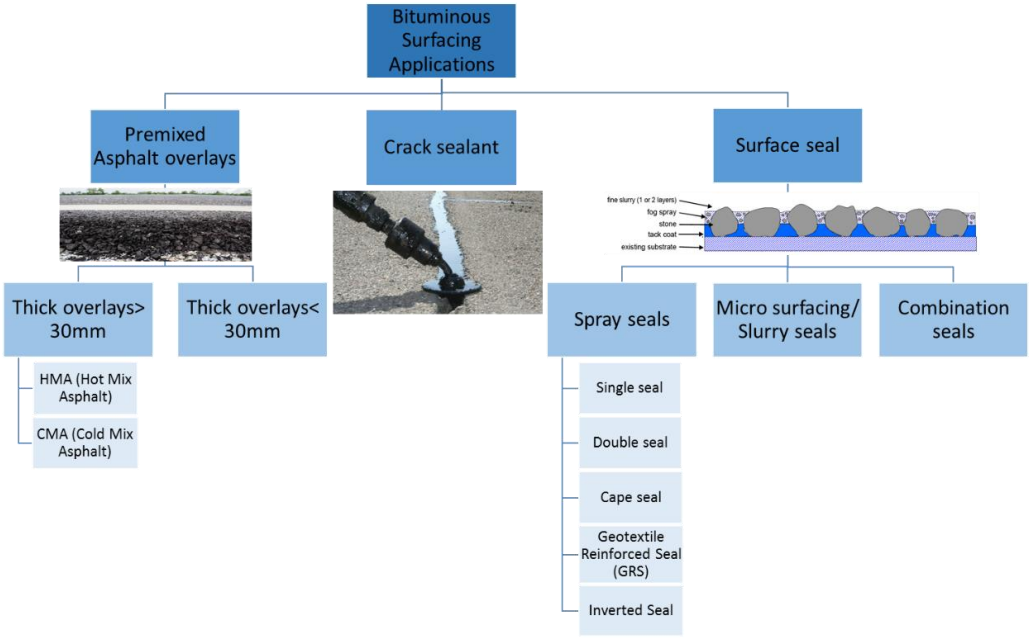

Figure 2-5: Applications of bitumen surfacing (adapted from Van Zyl (2018) and SANRAL (2007))

Seals are 15-20% more economical than asphalt and last on an average 7-10 years with relatively little maintenance. However, seals are not as strong as asphalt and should not be used in designs where heavy traffic roads are present. (Blackrock Paving & Seal coating INC., 2019)

Although asphalt and seals use the same materials, it is constructed differently. Asphalt is defined as a mixture of bitumen and aggregate, in contrast the seal method of paving is not premixed. For seals, bituminous binder is sprayed onto a clean and prepared roadbed, immediately followed with a single sized aggregate layer that is compressed on top. (Blackrock Paving & Seal coating INC., 2019)

The single, double, multiple and Cape seals are typically used in SA, where bituminous binder is applied as a: (South African National Roads Agency Limited (SANRAL), 2007)

- Prime is applied onto a granular base layer to improve adhesion between surfacing and base;
- Tack coat is the first bituminous binder sprayed on the base, providing a waterproof layer and a bonding layer for surface aggregate;
- Penetration coat is applied after the first layer of aggregate is spread and rolled onto a single seal, a second bituminous binder is applied, which makes it a double seal;
- Fog spray is the bitumen emulsion sprayed over the top layer of aggregate of a seal or as a maintenance treatment to existing bitumen surfacing; and

- Slurry layer is the layer added to a final single seal to fill the void, which is a mixture of water, fine stone, bitumen emulsion and hydrated lime or cement.

2.2.4 Different products

2.2.4.1 Modified and unmodified

Bitumen products can be divided into two groups of bituminous binders namely conventional (unmodified) and modified binders. Both these groups are used as bituminous binders for the construction of surfacing seals. Conventional binder comprises of cutback bitumen, bitumen emulsion and penetration grade bitumen, whereas modified binders include hot and cold applications. (Distin, 2008)

Often conventional binders do not meet the requirements / performance when surface treatments are under severe conditions, such as high traffic volumes and which modified binders normally do handle. For this reason modifiers are added to unmodified bitumen to improve its performance properties in relation to: (Louw, 2016)

- binder-aggregate adhesion;
- consistency;
- elasticity;
- flexibility, resilience and toughness;
- stiffness and cohesion at high road temperatures;
- resistance during in-service ageing;
- reduction of temperature susceptibility; and
- to reduce sensitivity to durability and bleeding, even at freezing temperatures.

Conventional binders are not as costly as modified binders. The arrival of modified binders has however ensured less maintenance, which led to extended pavement life which led to lower life-cycle costs and overall more cost-effective surface seal application alternatives. (South African National Roads Agency Limited (SANRAL), 2007)

To improve performance properties of improved bitumen, modifier binders such as polymer, rubber crumbs, and synthetic wax or natural occurred hydrocarbons are added. Table 2-1 provides different compositions of modified bitumen used in surface seals. (SABITA, 2019a)

Table 2-1: Different compositions of modifiers (Southern African Bitumen Association (SABITA), 2014)

Modifier type		Selections
Polymer	Elastomer	Styrene-Butadiene-Rubber (SBR) latex
		Styrene-Butadiene-Styrene (SBS)
		Rubber crumb
	Plastomer	Ethylene Vinyl Acetate (EVA)
Hydrocarbon substance	Aliphatic synthetic wax	Fisher-Tropsch (FT) wax
	Natural hydrocarbons	Gilsonite
		Durasphalt

Polymer modifier with binder, so-called polymer modified binder (PMB), can be categorised as either a plastomer (improving the bitumen's viscosity) or an elastomer (increasing the elastic and strength properties). The most commonly used modifiers used in seals in SA are elastomers, being: (Distin, 2008)

Styrene-Butadiene-Rubber (SBR) latex is widely / extensively used as cold applied bitumen emulsions (bond coat, crack sealant, micro surfacing and seals), where hot modified bitumen with SBR is used to a lesser extent (seals and in asphalt). This modified SBR binder exhibits elastic properties which make it ideal for resealing lightly cracked surfaces and tack coat in winter construction for double and Cape seals, providing: (Southern African Bitumen Association (SABITA), 2014) (Technical Guideline (TG) 1, 2019)

- improved flexibility, elasticity and adhesion; and less chip loss.

Styrene-Butadiene-Styrene (SBS) is available in crumb, pellet or powder to form modified hot bitumen, which is usually preferred above SBR due to its high elastic recovery properties and high softening points. As a result of the SBS's relative lower viscosities it allows to be applied at lower temperatures, providing:

- improved flexibility at low temperatures which inhibits cracking; elasticity at high temperatures;
- resistance to rutting and crack reflection; and
- reduced temperature susceptibility.

Rubber crumb is obtained from recycled rubber such as tyres and applied in cold crumb format due to temperature sensitivity. (Technical Guideline (TG) 1, 2019) Bitumen rubber is obtained from mixing and reaction of ± 20% rubber crumb blended with bitumen for one hour at 170 – 210 °C, which needs to be applied within six hours due to its restricted shelf life. (Southern African Bitumen Association (SABITA), 2014) Rubber crumbs are mainly used for resealing surfaces/ roads that carry more than 30 000 Equivalent Light Vehicles (ELV) or has highly active cracks, serving as a membrane inter-layer that absorbs stress and providing: (Distin, 2008)

- improved adhesion, cohesion, durability, elasticity and flexibility;
- resistance to bleeding, flushing and deformation; and
- reduced temperature susceptibility.

Binders are not only required to maintain durability and flexibility under traffic and environmental conditions, but also used to retain surfacing aggregate.

2.2.4.2 Availability in South Africa (SA)

Figure 2-6 represents the bituminous binders used / available in SA, where the distribution percentage for surface seals as last estimated in 2008 (Figure 2-7).

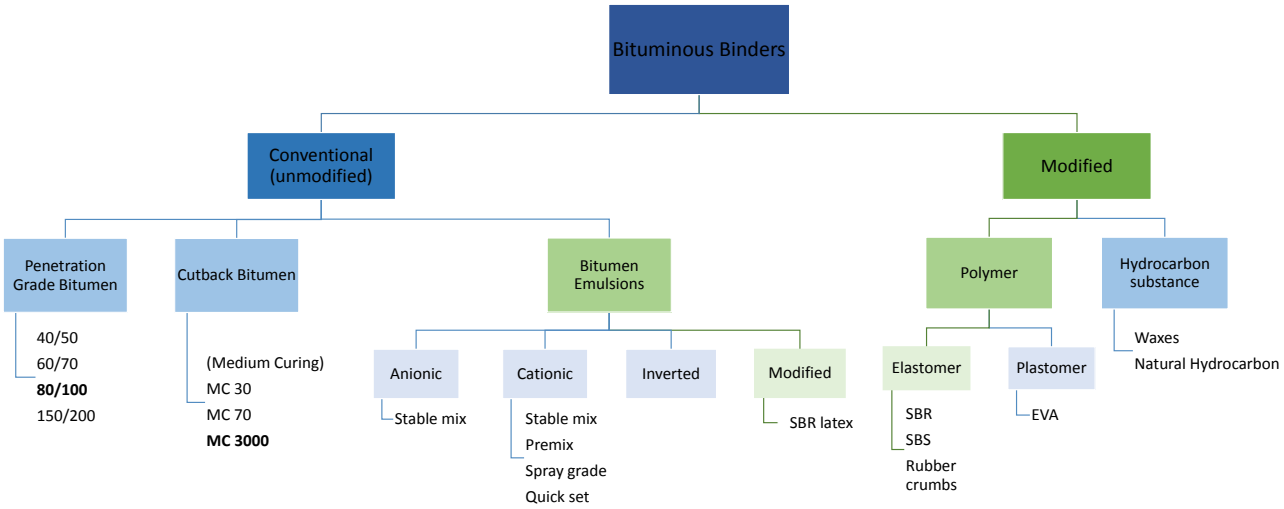

Figure 2-6: Binders available in SA (adapted from SABITA, 2019a)

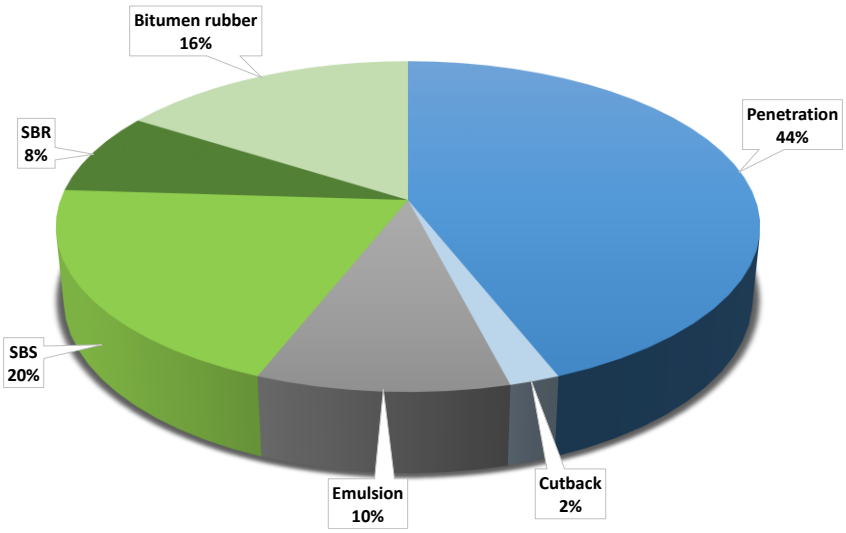

Figure 2-7: Distribution of bituminous binders (adapted from Distin, 2008)

The notable increase in traffic-loads and volumes experienced in SA has a direct impact on the need to use modified binders and alternative seals in order to expand the functional limits of road surfacing.

2.3 Behaviour of Bitumen

In Greek the word “Rheology” stands for study (*logis*) of flow (*rheo*), which defines the flow and deformation of bitumen. This term was developed in 1929 by the USA Professor Bingham, showing that bituminous binders both exhibits solid (elastic) and liquid (viscous) response to loading, leading to viscoelastic behaviour. (Hunter *et al.*, 2015)

There are two factors that influence the behaviour of bitumen performance, namely temperature and the loading duration or frequency conditions. When bitumen is subjected to low temperatures and short / quick loading time, the bitumen behaves like a stiff and elastic solid, which will completely return to its original state when the load is removed (recoverable). To the opposite at high temperatures and prolonged / slower loading times there are more flow or plastic viscous liquid behaviour, where the stress-strain response will undergo plastic deformation, i.e. deform permanently (irreversible).

Bitumen in most cases has viscoelastic behaviour. Figure 2-8 illustrates how number of cycles (loading) and how temperature affects the behaviour of bitumen. (Hunter *et al.*, 2015)

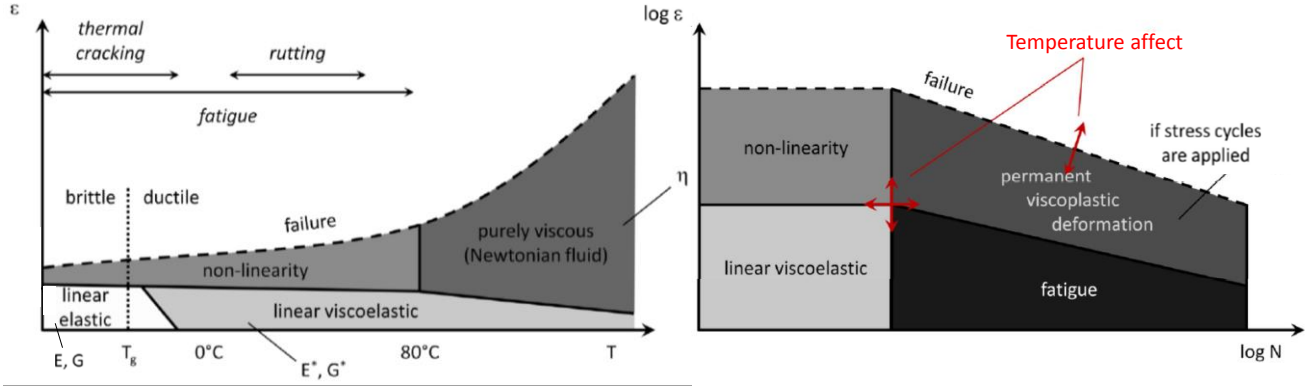

Figure 2-8: Domain behaviours of bitumen depending on strain versus temperature (T) and number of cycles (N) (Van de Ven, Jenkins & Bredenhann, 2004)

In Figure 2-8 the temperature T_g represents the glass transition temperature. According to Shaw & MacKnight (2005) there are four regions of viscoelastic behaviour. Figure 2-9 shows the four distinct regions of bitumen's viscoelastic behaviour:

- Glassy region is at low temperatures where the shear relaxation modulus (G) is above 10^9Pa and where the properties are entirely controlled by the physical-chemical character of bitumen;
- Transition region is entered by increasing the temperature from low to intermediate temperatures (ranging from 5 to 20°C), where there is a significant decrease in stiffness;
- Rubbery / Plateau region is where the storage modulus (G') is essentially independent of the temperature or frequency;
- Flow region is where the properties are mainly determined by the viscous liquid response; and
- a purely viscous behaviour will occur when temperatures increase beyond the flow region.

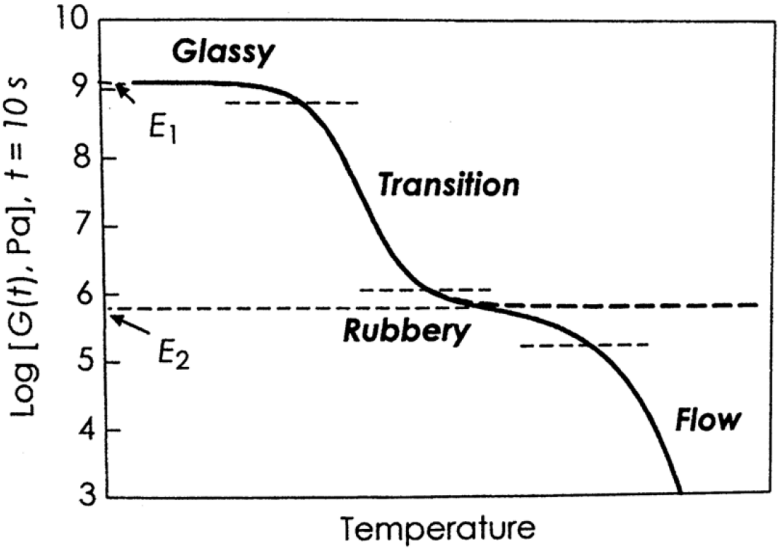

Figure 2-9: Four regions of viscoelastic behaviour (Shaw & MacKnight, 2005)

2.4 Seals

2.4.1 Introduction of Seals

As discussed in Chapter 1, there are currently no performance classification specifications for binders used in seals or for thin surfacing in SA.

More than 80% of the surfaced road network of 150 000km in South Africa has a seal as a wearing course and functional surfacing rather than a Hot Mix Asphalt (HMA), either as the opening surfacing or as a reseal for maintenance. (Distin, 2008) In addition it is noted that 90% of SA's road surface seal network is sprayed seals (Australian Asphalt Pavement Association (AAPA), 2011).

Seals in SA are expected to have an effective life span of approximately 10 years before maintenance is implemented. (Van Zyl & Jenkins, 2015) The main purpose of seals is to protect the base from moisture ingress and traffic wear, by providing adequate skid resistance for road safety purposes. (Van Zyl, 2018a)

2.4.2 Function of Seals

The Technical Recommendation for Highways (TRH 3, 2007) summarises the three main functions of a seal / surfacing as follows, which serves as the basic benefits of seals, providing: (SAPEM, 2014a)

- an impermeable layer to cover and protect the underlying pavement structure from moisture ingress;
- a durable, safe, dust-free, all-weather, riding surface for traffic with sufficient skid resistance for an acceptable level of service for road users; and
- protection to the underlying layers from the destructive and abrasive forces of traffic and the environment.

From the study that was conducted by Labi & Sinha (2003), models were developed that describes the effectiveness of seals, where these seals effectiveness models offers a basis to relate the benefits of treatments like seals by characteristics such as the environment, material, treatment type, procedure or work sources. In this study it was concluded that seals reduce the deterioration rate of the pavement and increase the pavement condition significantly.

2.4.3 Type of seals and construction

There are different kinds of seal structures commonly used in SA depending on the conditions that apply, varying from climate (environment), traffic, road gradients and / or the road authority's ability to conduct maintenance. (SABITA, 2019b)

In Figure 2-10 it is noted that seal selection varies between national and provincial roads, where the majority of seals on South African National Roads Agency Limited (SANRAL) roads are double seals, while the Western Cape Province predominantly uses single seals (over a 6 year average). This is expected as the majority of freight movements (heavy traffic volumes)

are being carried by national roads. (Van Zyl, 2018a) (Australian Asphalt Pavement Association (AAPA), 2011)

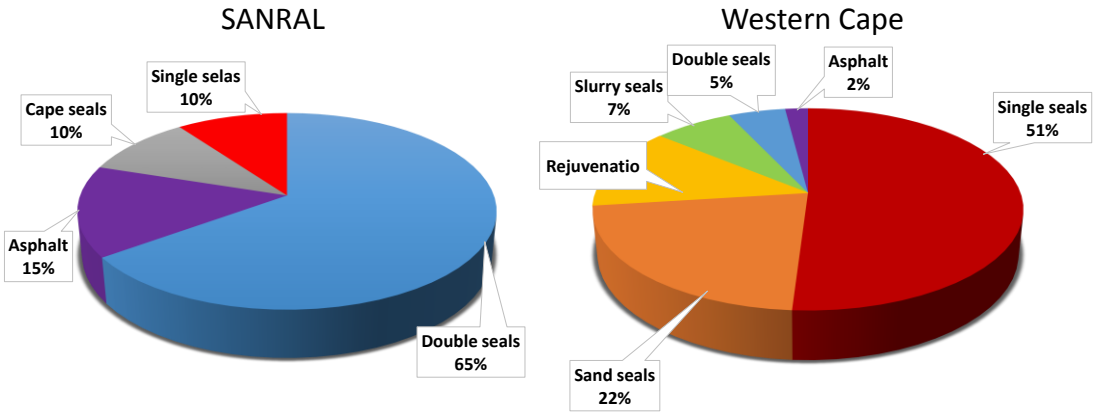

Figure 2-10: Surfacing types in SANRAL and Western Cape (adapted from Van Zyl, 2018)

Seal construction in the simplest form comprises of bituminous sprayed binder onto a clean road surface at a specific rate, covered immediately with aggregate and then mechanically rolled by a roller.

Rolling of the aggregate plays an important role as it initiates particle orientation, making it a dense matrix, filling the voids with aggregates, ensuring decent adhesion between the aggregate and the binder layer. The orientation process is continuous and is only completed after traffic is applied to the pavement surface to ultimately densify to a relatively impermeable surfacing. (SABITA, 2019b)

Although the construction techniques for different seal types are basically the same, the experience and knowledge of construction teams must be taken into consideration when selecting the seal type to be used in surfacing the roads. (South African National Roads Agency Limited (SANRAL), 2007)

Single seal (S1) is commonly used for resealing and it is constructed by a spayed bituminous binder layer and the application of a single sized aggregate, Figure 2-11.

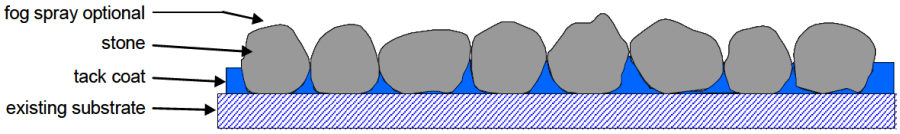

Figure 2-11: Structure of a single seal (South African National Roads Agency Limited (SANRAL), 2007)

Double seal (S2) in SA is achieved by a tight flat first layer of aggregate on top of the tack coat, containing the larger stone size, which is then rolled by a 10 to 12 tonne steel roller. Traffic is not allowable (on the first layer) until the second layer of smaller size aggregate is applied on the penetration coat, because of the potential of flushing the seal (TRH 3). This seal design increases the volume of voids caused by preventing the reorientation of larger aggregate by the smaller aggregate. Following the application of the final smaller layer of aggregate a dilute emulsion fog spray is applied to minimise ravelling (stone loss) (Figure 2-12). (Australian Asphalt Pavement Association (AAPA), 2011)

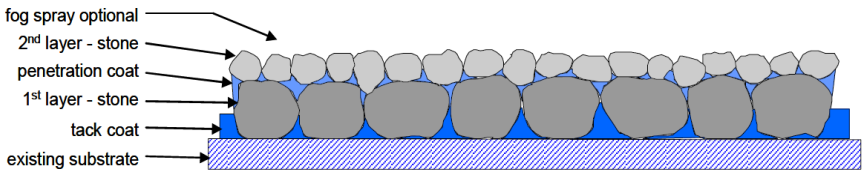

Figure 2-12: Structure of a double seal (South African National Roads Agency Limited (SANRAL), 2007)

Table 2-2 shows combination of double seals in South Africa.

Table 2-2: Combinations of double seals (South African National Roads Agency Limited (SANRAL), 2007)

Double seal (S2)	First layer aggregate	Second layer aggregate
S2 (9)	9.5 mm	sand
S2 (13)	13.2 mm	sand
S2 (13/6)	13.2 mm	6.7 mm
S2 (19/6)	19 mm	one or two 6.7 mm
S2 (19/9)	19 mm	9.5 mm

Cape seal (S4) contains 13 mm or 19 mm stone that are single seal concealed with slurry, amounting to approximately 10% of the surfacing program. Slurry is usually applied by hand (Figure 2-13) for two reasons:

- Firstly because of low employment level the Government policy prefers labour intensive methods, and
- Secondly to expose the tops of the aggregate (improving skid-resistance) by forcing the slurry between the sealing aggregates (voids).

Figure 2-13: Handling application of slurry for Cape seal (SABITA, 2011a)

The slurry can be applied to only fill the voids between aggregate or to act as a wearing surface by covering the sealing aggregate fully, Figure 2-14 and Figure 2-15.

Mechanically applying slurry is not preferred, as it involves the slurry being exposed to heavy traffic loads causing potential bleeding of the slurry. (South African National Roads Agency Limited (SANRAL), 2007) (SABITA, 2011a) (Australian Asphalt Pavement Association (AAPA), 2011)

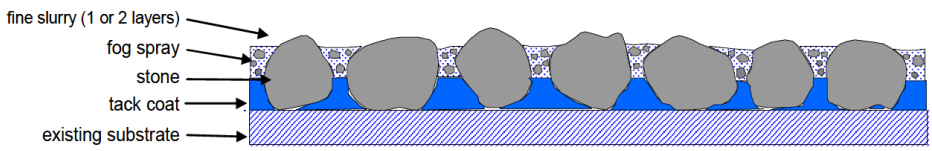

Figure 2-14: Structure of a cape seal (South African National Roads Agency Limited (SANRAL), 2007)

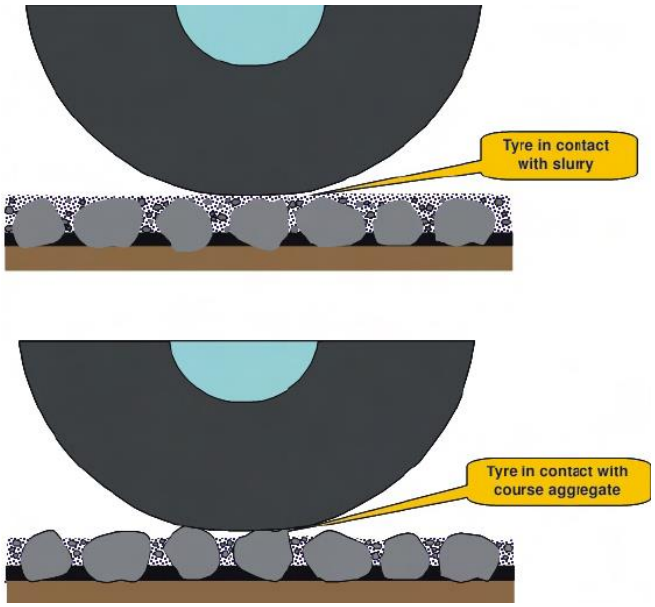

Figure 2-15: Slurry application in Cape seals (SABITA, 2011a)

Cape seal is typically used for low maintenance of new surfacing works. Cape seal is ideal and has been successfully applied to reseal areas where heavy traffic turning movements occur. (SABITA, 2011a) See Table 2-3 for selection of aggregate size for Cape seal which is depended on the traffic and required texture for appropriate skid resistance. (Australian Asphalt Pavement Association (AAPA), 2011)

Table 2-3: Cape seal selection (South African National Roads Agency Limited (SANRAL), 2007)

Cape seal (S4)		Traffic
S4 (13)	13.2 mm aggregate and one layer of slurry	< 10 000 ELV / lane / day
S4 (19)	19 mm aggregate with two layers of slurry	> 10 000 ELV / lane / day

Bitumen emulsions in many countries are referred to as the key binder type to be used as the first layer of binder onto the base for surfacing seals, known as the tack coat (Bahia, Jenkins & Hanz, 2008). The big advantage of bitumen emulsions is that it is suitable for cold weather condition sealing (SABITA, 2019b).

2.4.4 Components of seals influencing performance

The performance of seals is influenced by several factors and groupings thereof. The various factors influencing the performance of seals (as established by TRH 3) are summarised into four categories – Construction, Maintenance, Traffic and Environment as shown in Table 2-4.

It is important to note that all four of these categories are inter-related to some extent.

The material (binder or aggregate) is related to the traffic as material must provide resistance to abrasion moving wheel loads as well as skid resistance.

The environment (climate), like cold weather, could lead to initial cracking as the rainy weather conditions might result in intrusion of water in the underlying layers. Both high and low temperatures are troublesome when it comes to pavements as it can cause bleeding, ravelling and fatigue. Low temperatures cause more ravelling / fatigue, whereas high temperatures reduce ravelling, encourages breaking but reduces the impact of bleeding. (Bahia *et al.*, 2008)

In studying the comprehensive list of factors listed in the TRH 3 manual, it can be concluded that the main factors influencing the performance of seals are traffic, climate (environmental factors) and underlying layers.

Table 2-4: Components influencing performance of seals (adapted from SANRAL, 2007)

Construction	Maintenance	Traffic	Environment
Pavement Structure and Conditions ↓ Existing substrate Determines seal type, quantity of binder, size of stone and required pre-treatment Materials ↓ Aggregate / Binder Resistance to abrasion, moving wheel loads and **skid resistance** Construction and Supervision ↓ Preparation, Pre-treatment and Repairs before construction Preparation of road surface, timeous pre-treatment and repair of defects before seal work commences ➔ **VITAL to initial and long term performance of seal**	1. Selection of appropriate surfacing **E.g.:** • Spray diluted emulsion to increase and rejuvenate existing binder before **loss off aggregate** occurs • Patch small areas where de-bonding occurred 2. Apply fine slurry to isolate areas (where **ravelling** arisen/ is present)	Traffic 1. Volume 2. Loading 3. Tyre pressure 4. Vehicle type and characteristics 5. Speed 6. Traffic distribution Road geometry 1. Gradient 2. Sharp curves 3. Intersections 4. Road width	**Physical and social environment** 1. Climatic conditions 2. Drainage systems 3. Mechanical damage 4. Dust/ wind-blown sands 5. Fuel spillage/ organic matter 6. Developing areas

2.4.5 Failure mechanisms

Pavement failure is a two-phased process, namely surface and structural failures.

Failures normally start to manifest on the surface of the road, which includes surface cracks, aggregate loss (ravelling), binder condition and bleeding / flushing. If surface failures are not resealed or maintained, these failures will magnify in terms of degree, resulting in functional and structural failure of the pavement structure.

Figure 2-16 provides a schematic illustration of the failure mechanisms of seals, which can be divided into the two categories of adhesion or cohesion, as discussed below.

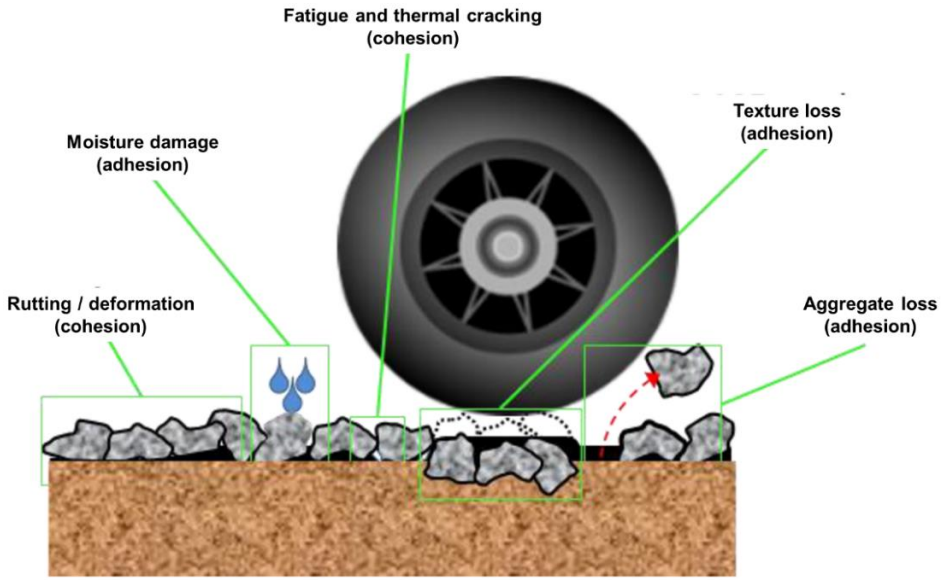

Figure 2-16: Divided failure mechanisms of seals (Adopted from Abrahams, 2015)

The performance expectation for seals can be assessed through the investigation of two primary mechanisms of distress leading to failure of seals in-service ("end of its effective service life"). Identified by Van Zyl, Jenkins and Mukandila (2015) these two categories of failures are (Figure 2-17):

- Adhesion failure, being the failure between aggregate and bitumen or bitumen and base, which leads to aggregate loss (ravelling, stripping or spalling); and

- Cohesion failure, being the fatigue cracking (intermediate temperatures) due to the ageing of binder and loss of elasticity and rutting (deformation) at high temperatures.

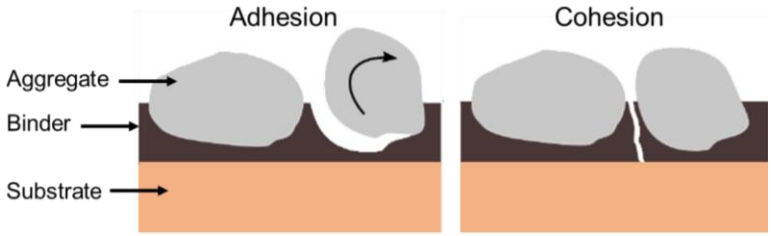

Figure 2-17: Two categories of failure mechanisms in seals (Gerber, 2016)

2.4.5.1 Adhesion

Adhesion failure is the disintegration between the aggregate and bitumen or bitumen and base. This is the form of stripping, ravelling or spalling, which can result from things such as chemical reactivity, low application rate of binder, aggregate degradation, delay in aggregate placing, cold temperatures, poor compaction, traffic abrasion, loss of bonding or binder ageing. (South African National Roads Agency Limited (SANRAL), 2007)

Adhesive strength is the ability of the binder to retain aggregate and adhesion to the pavement. (Milne, 2004)

When a seal loses its aggregate, bleeding and / or flushing will occur. Bleeding and flushing are the primary cause of texture loss, which decreases skid resistance tremendously between the seal road surface and vehicle tyre, making the road unsafe. Moisture damage is also a

failure mechanism that causes loss of adhesive strength in seals, where stripping or ravelling occurs, thus constituting aggregate loss. (Abrahams, 2015)

Stripping and ravelling adhesive failure mechanisms involves the crumbling and loss of surface aggregate. Stripping is wet ravelling and occurs when water is trapped in the surface treatments voids, which leads to separation of the adhesive bond. Ravelling is directly related to adhesive bond's fatigue damage and leads to loss of macro texture and poor skid resistance, when the base is not protected from abrasive action of traffic. In the case of thin surface treatments such as seals, this could eventually lead to the exposure of the underlying layer, where potholing will occur. (Committee for State Road Authorities, 1992) (SANRAL, 2009)

According to various sources the ravelling phenomenon occurs as a result of any of or combination of the following conditions: (SANRAL, 2009) (Van Zyl & Jenkins, 2015)

- abrasion of traffic;
- ageing of binder;
- aggregate embedment into the underlying layer;
- aggregate orientation;
- aggregate wear;
- binder rise;
- certain types of aggregate used;
- dirty aggregate;
- under rolling;
- opening the seal surface too soon to traffic before bitumen has set ;
- surfacing constructed in cold weather (cold weather related to thermal cracking);
- under spray in seal (low binder application); and / or
- moisture damage (stripping).

The stripping failure of seals is normally addressed early in maintenance by applying fog spray of diluted cationic rapid set emulsion to stop loss of surface aggregate. Whereas slurry surfacing is used to address ravelling of the surface, which is cutback binder or rejuvenation spray that extend seal pavements by 3 to 4 years. (SANRAL, 2009) (Australian Asphalt Pavement Association (AAPA), 2011)

2.4.5.2 Cohesion

Cohesion is in relation to the fracture and distortion failure of the surface. Fracture could be in the form of cracking or spalling resulting from such things as excessive loading, fatigue, thermal changes, moisture damage, slippage or contraction. Distortion comes in the form of deformation (rutting, corrugation and shoving), resulting from such things as excessive loading, creep, densification, consolidation, swelling or frost action. (South African National Roads Agency Limited (SANRAL), 2007)

Cohesive properties are the ability of the binder to perform in a viscoelastic manner without losing its integrity. (Milne, 2004)

In as far as surface cracking is concerned, there are various types of surface cracking that exist, and which can be categorised as an active or a passive crack. Active cracks are commonly initiated from the levels below the surfacing, whilst passive cracks apply to the surfacing itself. (SANRAL, 2009)

Passive cracks are normally caused by:

- Surface cracks – old and brittle surface or overstressing of surfacing layer (not limited to wheel tracks) (SAPEM, 2014b)
- Single cracks – long, transverse and random
- Crocodile cracking (in wheel path)

Surface cracks, more specifically surface fatigue cracks, are typically caused by the shrinkage of the bituminous binder as a result of decreased binder volume. This is due to the ageing of the binder and the loss of elasticity (loses its lighter oils and aromatics). Surface cracks occur commonly in dense surfacing such as Cape seals, sand seals and slurry seals. (Committee for State Road Authorities, 1992)

Surface cracks are also largely due to traffic loading, age of a specific layer, weather conditions and material types used in road layers. The main concern of surface cracks (fatigue and thermal cracking) that develop in surface treatments is that it welcomes the intrusion of water to the underlying pavement layers which usually compromises the structural integrity of the pavement system. This especially occurs in the wet season when surface cracks are left unattended, most likely leading to potholes and deterioration of the pavement condition to complete failure. (SANRAL, 2009)

2.4.6 Measurement methods for seal selection

The properties of binders need to be outlined in terms of what could or should be tested in measurement method format. This will enable the analysis of the critical characteristics of bitumen and allow determination of whether or not a particular binder will be “fit for purpose” as a seal tack and capable of resisting the relevant failure mechanism.

Thus far binder selection criteria have mostly advanced in respect of empirical methods (observations and experience), but very little in relation to practical performance guidelines for seals as pavement surfacing. According to Bahia *et al.* (2008) the lack of practical performance guidelines for seals as pavement surfacing has an undesirable impact on seals service life, as it limits the development of longer lasting bitumen seal products to extend seal service lifespans.

As discussed in Section 2.4.5 it must be noted that failure mechanisms are categorised as “in-service related failures” in Bahia *et al.* (2008). Bahia *et al.* (2008) also indicated that where “construction related failures” has been determined; the emulsion properties contribute to the successful construction of a surface seal. In such cases it is important to note that it influences the in-service performance thereof, as seal failure/s occur during construction or service.

Bahia *et al.* (2008) recognises binder properties that could be tested to analyse the critical characteristics of the bitumen in order to establish whether a particular binder will be "fit for purpose" as a seal, i.e. can resist the failure mechanism.

The tentative framework, Table 2-5, developed by Bahia *et al.* (2008) for construction and PG emulsions defines the properties that needs to explored in order to determine whether or not a seal binder will or has the potential to resist prevailing failure mechanisms, including providing suggested critical measurement methods to test these properties. This tentative framework is based on minimising the risk of premature main seal failure mechanisms and the factors affecting seal performance.

Table 2-5: Tentative construction and PG of emulsion framework (Bahia *et al.*, 2008)

Stage	Binder Property	Measurement method
Construction Performance (Tests on Emulsified Bitumen)	Storage stability	Cylinder Storage for 24 hrs
	Spray ability / Drain-out (Run-off)	Viscosity [Pa.s]
	Breaking Rate	Silica Powder [g]
	Wetting of Aggregates	Adhesion Strength [Pa]
		Pneumatic Adhesion Tension Testing Instrument (PATTI): Adhesion test (ASTM D4541)
In-Service Performance (Test on Residual Bitumen)	Fattiness Resistance (Early Aggregate Loss) @ max design pavement surface temperature	Creep stiffness [kPa] (Un-aged) - Estimated from penetration and softening point
		Creep stiffness [kPa] (RTFO-aged) - Estimated from penetration and softening point
		Early adhesion [kPa] (RTFO-aged) - Estimated from PATTI adhesion test
	Long-Term Ravelling Resistance @ avg. design pavement surface temperature	Creep stiffness [kPa] (PAV-aged)- Estimated from penetration and softening point
		Wet adhesion [kPa] (PAV-aged)- Estimated from PATTI adhesion test
		Cohesion [kPa] (PAV-aged) --Estimated from PATTI cohesion test
	Fatigue Cracking Resistance @ min design pavement surface temperature	Creep stiffness [kPa] (PAV-aged) - Estimated from penetration and softening point
		Creep rate (PAV-aged) & Elongation at break [mm/mm] (PAV-aged)
	Thermal Cracking Resistance @ low PG Grade of base bitumen +10°C	Creep stiffness [kPa] (PAV-aged)
		Creep rate (PAV-aged)
		Failure strain [%] (PAV-aged)

Note that Table 2-5's measurement method mostly includes penetration and softening point which is used in the empirical Penetration Grade Spesification, of which the industry wants to move away from.

2.5 Specifications for bitumen

Figure 2-18 shows in detail the binder selection criteria.

The penetration, softening point and viscosity (soft bitumen) dedicate to the determination of the grade of the binder. (Hunter *et al.*, 2015)

Binder grade is classified in terms of the binder's stiffness (hardness) and workability. In an ideal world one would like to design with uniform stiffness and flow behaviour over a range of temperatures that will overcome deformation and brittleness (fatigue) of the binder. Multi-grade bitumen is a step towards this ideal binder, as it is less prone to temperature, making the binder perform at low and high temperatures. Multi-grade bitumen contains hard and soft grades, where hard grades are selected for heavy traffic and warm environments; whereas soft grades are selected for low traffic levels and cooler environments. (Hunter *et al.*, 2015)

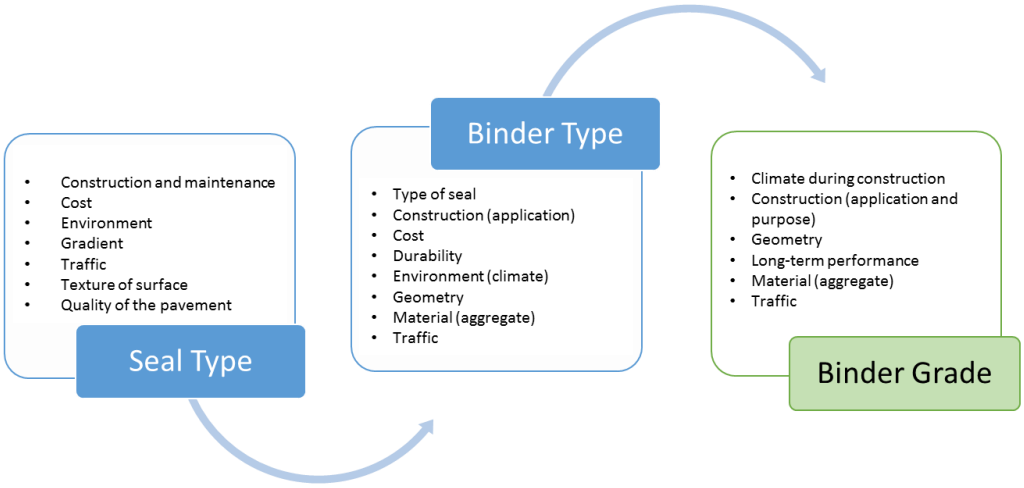

Figure 2-18: Criteria for binder selection (adapted from SANRAL, 2007)

The quality of bitumen binders required for surfacing is determined by a range of diverse standards and grading systems depending on the region, country and typical weather conditions applicable. The most recognised standards are published by AASHTO, American Society for Testing and Materials (ASTM), European Committee for Standardisation (CEN) and the South African Bureau of Standard (SABS).

South Africa has the following published specifications in terms of bitumen binder quality requirements, which are mainly based on penetration (mm), viscosity (Pa.s), softening and flash point (°C):

- South African National Standards (SANS):
  - SANS 4001-BT1: penetration grade bitumen (straight-run bitumen- unmodified bitumen) (South African National Standards (SANS) 4001, 2016)
  - SANS 4001-BT2: cutback bitumen (SANS 4001, 2012)
  - SANS 4001-BT3: anionic bitumen road emulsion (SANS 4001, 2014a)
  - SANS 4001-BT4: cationic bitumen road emulsion (SANS 4001, 2014b)
  - SANS 4001-BT5: inverted bitumen road emulsion (SANS 4001, 2014c)
- Technical Guideline (TG1) for polymer modified binder (Technical Guideline (TG) 1, 2019)

Currently the SANS 4001-BT1 Penetration Grade Bitumen and the SABITA TG1 Modified Bitumen specifications for binders are the two standards mostly used in asphalt by SA engineers. (SABITA, 2018)

2.5.1 Performance grade specification

Penetration Grade Specifications, also known as 'pen grade', are empirical and do not measure viscosity and the actual stress-strain in the pavement, which is within fundamental engineering parameters.

Rheology is a fundamental measurement that is becoming commonly used in engineering specifications such as the PG Specification for Bitumen, making the performance-related physical properties essential for the binder selecting criteria. (Hunter *et al.*, 2015) (SABITA, 2011b)

To address the SA Industry's need for implementing a performance grading system, considerable progress has been made since 2015 in the transition process of moving away from the Penetration Grade Specification to the PG Specification for Bitumen in South Africa. Thus far this has led to the SABS publication in 2018 of the SATS 3208 technical specification (SATS 3208: Performance Grade (PG) Specifications for Bitumen in SA). It is however important to note that the SATS 3208 is on a two year trail basis, as it still contains empirical methods and procedures (SANS 4001-BT1) that still needs to be replaced with a performance characteristic binder selection specification. (Technical Guideline (TG) 1, 2019) (South African Technical Specification (SATS) 3208, 2018)

As mentioned in Section 1.4, the USA Superpave PG specification is currently used as key basis and point of departure to develop a comprehensive revised SATS 3208.

Below are some benefits of the USA Superpave PG specification, addressing the limitations in other grading systems: (SABITA, 2017)

- measures the physical properties that relates to in-service performance;
- provide the test temperature criteria dependent on the environmental condition (climate) and binder grade;
- covers the performance over a range of temperatures experience by the pavement;
- different ageing characteristics of binders are tested;
- regional requirements of binder grades are more precise;
- contains tests and specifications for modified and unmodified asphalt binders;
- designed to minimise three pavement distresses: thermal cracking (low temperature cracking or single event cracking), fatigue cracking (repeated load failure) and rutting (permanent deformation);
- rheological properties give a better understanding of bitumen behaviour in field conditions; and
- uses the international system of units (SI).

The SATS 3208 were developed using Dynamic Shear Rheometer (DSR) and Bending Beam Rheometer (BBR) to measure the rheological properties and characterisation. The specifications are aimed at minimising distresses. These distresses levels include low temperature thermal cracking, fatigue cracking at intermediate temperatures and rutting (permanent deformation) at high temperatures.

Table 2-6 shows the current and new concepts that the SATS 3208 introduces. For more details on the concepts see relevant ATSM specifications.

Table 2-6: Concepts in the SATS 3208 Performance Grade (PG) Specifications for Bitumen in South Africa

<table>
<tr><th colspan="3">CURRENT CONCEPT</th><th>Description</th><th>Test Method</th></tr>
<tr><td colspan="3">Viscosity (Pa.s)</td><td>Viscosity of the binder is measured by using the rotational viscometer, which at a certain application temperature and speed measures the torque needed to rotate an object in the binder, thus giving an indication of the binder's pumpability. (Hunter et al., 2015) (SABITA, 2016)</td><td>ASTM D4402</td></tr>
<tr><td colspan="3">Flash Point (°C)</td><td>Temperature at which binder will ignite / explode when exposed to a flame.</td><td>ASTM D92</td></tr>
<tr><td colspan="3">Storage stability</td><td>Assessed on unaged (original) binder by the difference of complex shear modulus at the top and bottom of the binder in the container at T_{max}. (SABITA, 2017)</td><td>ASTM D7175</td></tr>
<tr><th colspan="3">NEW CONCEPT</th><th>Description</th><th>Test Method</th></tr>
<tr><td rowspan="3">Grading Criteria according to operating categories</td><td colspan="2">Traffic (loading)</td><td>Traffic is classified in terms of speed and volume / severity of loading condition. For example, slow moving (speed) traffic will lead to severe pavement conditions. The following Table 2-7 summarises the traffic categories of the SATS 3208. Where S, H, V, E respectively stands for Standard, Heavy, Very Heavy and Extreme traffic. (SABITA, 2018)
Table 2-7: Traffic
<table>
<tr><th rowspan="2">Design Traffic (million E80)</th><th colspan="3">Traffic Speed (km/h)</th></tr>
<tr><th><20</th><th>20-80</th><th>>80</th></tr>
<tr><td><0.3</td><td>S</td><td>S</td><td>S</td></tr>
<tr><td>0.3-3</td><td>H</td><td>S</td><td>S</td></tr>
<tr><td>>3-10</td><td>V</td><td>H</td><td>S</td></tr>
<tr><td>>10-0</td><td>E</td><td>V</td><td>H</td></tr>
<tr><td>>30</td><td>E</td><td>E</td><td>V</td></tr>
</table></td><td></td></tr>
<tr><td rowspan="2">Climate</td><td>Maximum temperature, T_{max} (°C)</td><td rowspan="2">The CSIR estimated minimum and maximum road temperatures for SA.
The minimum grading temperatures were adopted to align with the US PG specifications, as it rarely gets colder than -10°C in SA. T_{min} values are the lower temperatures at which a binder can function, determined from a single lowest temperature. The maximum temperatures for SA were adopted from the highest seven day average (58 °C, 64°C and 70°), associated with the low temperatures -22°C, -16°C and -10°C. (SABITA, 2018)
Note that low temperature is 10°C above minimum grading temperature.
T_{min} and T_{max} expected road temperatures, including the type of traffic (loading) used for binder grade definitions.</td><td rowspan="2"></td></tr>
<tr><td>Minimum grading temperature, T_{min} (°C)</td></tr>
</table>

NEW CONCEPT			Description	Test Method
Grading Criteria according to operating categories	Climate	Intermediate temperature, T_{int} (°C)	The intermediate temperature is the average between the T_{min} and T_{max} plus 4°C and represents the operational temperature where traffic loading would lead to durability (fatigue) cracking failure. (SABITA, 2018)	
DSR	Complex Shear Modulus, G* (Pa)		DSR is used to obtain binder properties at intermediate and high temperatures to represent in-service performance. Binder behaviour is assessed by measuring the G*, δ (elastic behaviour) and J_{nr} under oscillatory loading. J_{nr} is used to measure the rutting compliance.	ASTM D7175
	Phase angle, δ (°)			
	Non-recoverable Creep Compliance, J_{nr}			ASTM D7405
BBR	Stiffness at after 60 seconds loading, S(60)		BBR measures the stiffness and creep rate of a binder at the lower range of service temperature. This BBR test is carried out on aged binders under monotonic loading.	ASTM D6648
	Slope of stiffness at after 60 seconds loading, m(60)			
G* / sin δ			This parameter is measured in kPa at 10 rad/s and T_{max}. G* / sinδ has been replaced by the non-recoverable creep compliance parameter, J_{nr}, where G* / sinδ is only used for unaged binder as a quality control measure and not as a rutting parameter.	ASTM D7175
Glover-Rowe Parameter, G-R (kPa)			G-R measures the ductility of a binder at 15°C to interpret binder cracking and ageing. G-R equals G* ($\cos\delta^2$ / sinδ). (Much Asphalt, 2013)	
Critical temperature, T_c (°C)			It is the temperature of low temperature (BBR) stiffness and / or relaxation from BBR test.	ASTM D7643
Ageing ratios	RTFO		Ageing ratios are determined at intermediate temperatures to give an indication on the durability of the binder, as it gives the rate to which it ages. The complex shear modulus, G*, of the original binder and after artificial ageing (RTFO and PAV) is used to calculate this parameter. This parameter shows how sensitive a binder is to ageing.	ASTM D7175
	PAV			

The aim of the SATS 3208 is to ensure acceptable performance of flexible pavements in three distinct temperature or seasonal regimes, each associated with a different distress. Table 2-8 is the proposed SATS 3208 as it stands at present until a revision is issued.

Table 2-8: Proposed SATS 3208 Performance Grade (PG) Specifications for Bitumen in South Africa (SABITA, 2017)

Test Property	Performance Grade												Test method
	58S-22	58H-22	58V-22	58E-22	64S-16	64H-16	64V-16	64E-16	70S-10	70H-10	70V-10	70E-10	
Maximum pavement design temperature, T_{max} (°C)	58				64				70				
Minimum grading temperature, T_{min} (°C)	-22				-16				-10				
	Original binder												
G* and δ at T_{int}	Compulsory report only – see detailed description in (a)												ASTM D7175
G*/sinδ at 10 rad/s at T = T_{max} (kPa)	Compulsory report only												ASTM D7175
Viscosity at 165°C at ≥ 30 sec^{-1} (Pa.s)	≤ 0.9												ASTM D4402
Storage stability at 180°C (% diff in G* at T_{max})	≤ 15												ASTM D7175 & TG1 MB6
Flash Point (°C)	≥ 230												ASTM D92b
	After RTFO ageing												
G* and δ at T_{int}	Compulsory report only during implementation phase												ASTM D7175
Mass change (% by mass fracrtiom)	≤ 1.0												ASTM D2872 / TG1 MB3
J_{NR} at T_{max} (kPa)	≤ 4.5	≤ 2.0	≤ 1.0	≤ 0.5	≤ 4.5	≤ 2.0	≤ 1.0	≤ 0.5	≤ 4.5	≤ 2.0	≤ 1.0	≤ 0.5	ASTM D7405
Ageing ratio, $G^*_{RTFOT}/G^*_{Original}$	≤ 3.0												ASTM D7175
	After RTFO and PAV ageing												
G* and δ at T_{int}	Compulsory report only during implementation phase												ASTM D7175
Creep stiffness, S (60s) at T_{min} + 10°C , MPa	≤ 300 at -12°C				≤ 300 at -16°C				≤ 300 at 0°C				ASTM D6648
m (60s) at T_{min} + 10°C, minimum	≥ 0.3 at -12°C				≥ 0.3 at -16°C				≥ 0.3 at 0°C				ASTM D6648
$\Delta T_c = T_{s,300} - T_{m,0.3}$ (°C)	≥ -5												ASTM D7643
Ageing Ratio, $G^*_{PAV}/G^*_{Original}$	≤ 6.0												ASTM D7175

(a) Report only the isotherm at the intermediate temperature (TIT) for each of the unaged, and RTFO and PAV aged binders. This requirement is especially important during the implementation phase.

2.6 Performance Grade Testing and Rheology

This section discusses the methods and procedures required to prepare seal binders for final testing techniques (rheometry) in order to establish the rheological properties of binders. It deals with the extraction and recovery of seal samples in pavements; the artificial ageing thereof and the two main PG specification testing apparatuses (DSR and BBR) in order to determine rheological properties as shown in Table 2-8.

2.6.1 Solubilisation and Recovery

To determine the rheological properties of bitumen binders in-service, it is necessary to isolate the binder from the seal / asphalt mixture.

The validity of the evaluation of binder-aggregate mixes depends on the solubilisation and recovery procedures to resolve the mix effectively and to recover these chemical compositions without significantly changing its properties. This is generally done by a two-step process (Figure 2-19): solubilisation (extraction and centrifugal) and then recovery / distillation.

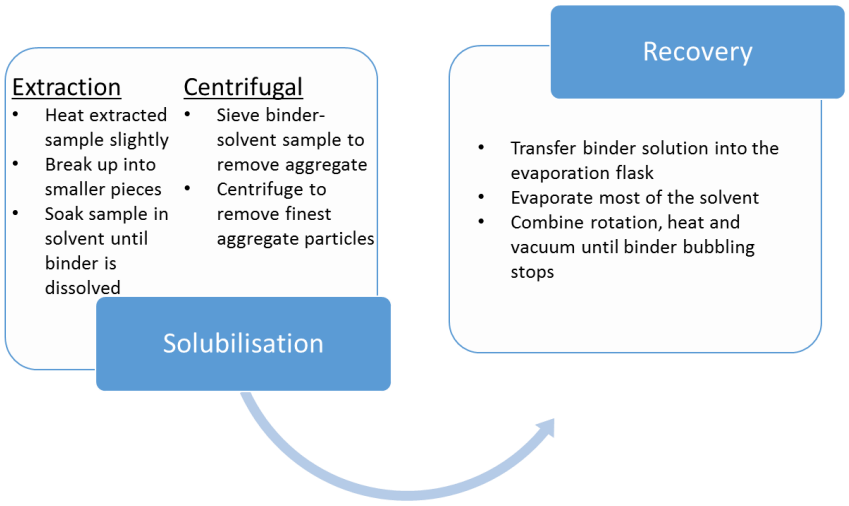

Figure 2-19: Simplified solubilisation and recovery procedure

The following components / procedures are very important in the extraction and recovery process and discussed in respect off:

- the solvent used and the period that the sample is immersed in the solvent;
- removing all the aggregate, including fines, from the binder-solvent sample; and
- the distillation / recovery process (Abson method, Rotary vacuum distillation and Bunsen burner method).

Solvents:

All the solvents currently used by construction teams are potentially unsafe and hazardous, from an environmental and health & safety perspective. Limiting exposure to hazardous solvents is therefore of utmost importance regardless of the type solvent used in the process. The majority of exposure occurs during the extraction procedure and not during the distillation phase.

Table 2-9 summarises the different solvents used depending on the method used for extraction and recovery of bituminous binder.

Table 2-9: Solvents for extraction of bituminous binders with distillation conditions (adapted from EN-12697-3, 2013)

Solvent				First Phase		Second Phase		Extra Temp.
Type	Chemical Formula	Name	Boiling Point (°C)	Temp. T_1 (°C)	Pressure P_1 (kPa)	Temp. T_2 (°C)	Pressure P_2 (kPa)	Temp. T_3 (°C)
Chlorinated hydrocarbons	CH_2Cl_2	Dichloromethane (Methylene chloride)	40,0	85	85	150	2,0	175
Chlorinated hydrocarbons	CH_3Cl_3	1,1,1-Trichloroethane	74,1	80	30	160	2,0	185
Aromatic hydrocarbon	C_6H_6	Benzene	80,1	80	30	160	2,0	185
Chlorinated hydrocarbons	C_2HCl_3	Trichloroethylene (TCE)	87,0	90	40	160	2,0	185
Aromatic hydrocarbon	C_8H_{10}	Xylene	140	120	30	180	2,0	205
Aromatic hydrocarbon	C_7H_8	Toluene	110,6	110	40	160	2,0	185
Chlorinated hydrocarbons	C_2Cl_4	Tetrachloroethylene	121	110	40	160	2,0	180

Before an extracted in-service pavement seal / asphalt sample is immersed in a solvent; if necessary, the seal / asphalt sample can be preheated at a maximum of 110°C to loosen the sample to ease the process. It helps to create a larger contact area for the binder to dissolve in the solvent. (SANS 3001, 2011)

Bituminous binders that are exposed to solvents have shown to have an inherent hardening effect, especially where two chemical processes occur, i.e. the oxidation process and molecular weight increase. Binder hardening exhibits stiffer binder properties from 5% up to 300%. (Mturi, Rippenaar, Hamraj, Naicker & Husselman, 2015)

There are six factors that affect the hardening extent of binders, namely: (Mturi *et al.*, 2015)

1. Solvent type: According to Mturi *et al.* (2015) research published in 1960,1969 and 1991 found that chlorinated solvents have greater hardening effect than aromatic hydrocarbon solvents. However in 1997 similar research conducted by Van Assen & Rust and W. Vonk (Nielsen, 2012) confirmed that chlorinated hydrocarbons do not harden binders during the extraction and recovery process, thus contradicting Mturi *et al.* (2015) research.

2. Time the binder is exposed to the solvent: The hardening of the binder increases when in long contact with the solvent. This occurs during the extraction process when the binder is immersed in the solvent until the binder is dissolved. Different specifications assign diverse maximum exposure time / specified recovery times. The exposure time ranges as follows:

    - Method A (ASTM D2172 cold extraction followed by centrifuge) employing a shorter time than method B (ASTM D2172 - hot reflux extraction process);
    - 20-60 minutes for the SANS 3001 method (part AS20: determination of the soluble binder content and particle size analysis of an asphalt mix);

- 8 hours for the Abson method (ASTM D 1856);
- 24 hours for the EN-12697-3 method; and
- no time specified for the Rotary Evaporator Method (ASTM D5404).

It is also important to note that the test duration depends not only on the methods used, but also on the type of mixture, amount of binder used and the amount of re-centrifugal needed for successful extraction of binder. (Mikhailenko & Baaj, 2017)

3. Temperature at which the solvent is exposed to the binder: It is important to note that increased temperature contact between solvent and binder, increases the hardening effect. In order to minimise hardening of extracted binder, hot-extraction procedures should be avoided if the properties of the recovered binder are to be measured. Thus, extractions should rather be performed cold. Note in Table 2-9 that the distillation condition's temperatures are solvent dependent. (Van Assen & Rust, 1997)

4. Light contact between binder and solvent: The absence of light during the extraction-recovery process will decrease the hardening effect.

5. Contact oxygen pressure: The hardening effect reduces with low presence of partial oxygen pressure.

6. Types of binder-aggregates: Similar extraction-recovery methods, depending on the binder-aggregate type, can exhibit different hardening effects.

Removal of Aggregate and Fines:

The extraction methods used internationally is the ASTM D2172 Method A and Method B.

As the cold extraction minimises the hardening effect, Method A (cold extraction process) of the ASTM D2172 is recommended, followed by centrifuge.

Part of the solubilisation processes is the centrifugal process on the extracted binder-aggregate-solvent sample. When conducting this process, it is of utmost importance that the centrifuge machine is in a fume tight sliding door cupboard with an extraction fan to ensure safe and sufficient removal of fumes during the process. The centrifuge is a machine that rotates a metal cup by way of a fixed axis, causing outward centrifugal forces to remove the fines from the sample.

The binder-solvent solution needs to be poured through a 0.063mm sieve that is positioned over the centrifuge funnel, followed by washing the binder of the aggregate until the solvent runs colourless out of the centrifuge. If the mass of the fine minerals in the centrifuge cup exceed 50g, re-centrifuging is needed, as per applicable SANS Code. (SANS 3001, 2011)

When the solubilisation process is technically performed inconsistently, incomplete removal of binder from aggregate is likely regardless of the solvent used. Similarly it is also likely that a high density solvent will retain fines, which will lead to incomplete separation of fine aggregate from the binder. An ash content analysis can be conducted to determine the fines in the contaminated recovered binder, which would results in stiffer properties. (Mturi *et al.*, 2015)

Due to the increase of modified binders used in surfacing, it is complex to establish a viable strong residue recovery procedure. (Bahia *et al.*, 2008)

Distillation / Recovery Process:

Two popular recovery / distillation methods have been identified by the CSIR (Mturi *et al.*, 2015) that are used internationally, i.e. the Abson (Figure 2-20) and Rotary Evaporator methods (Figures 2-21 and 2-22) . There is also a third recovery method identified by SABITA (2019b) TG1 and which uses a Bunsen burner (Figure 2-21). The equipment is generally used for removal of solvent under reduced pressure.

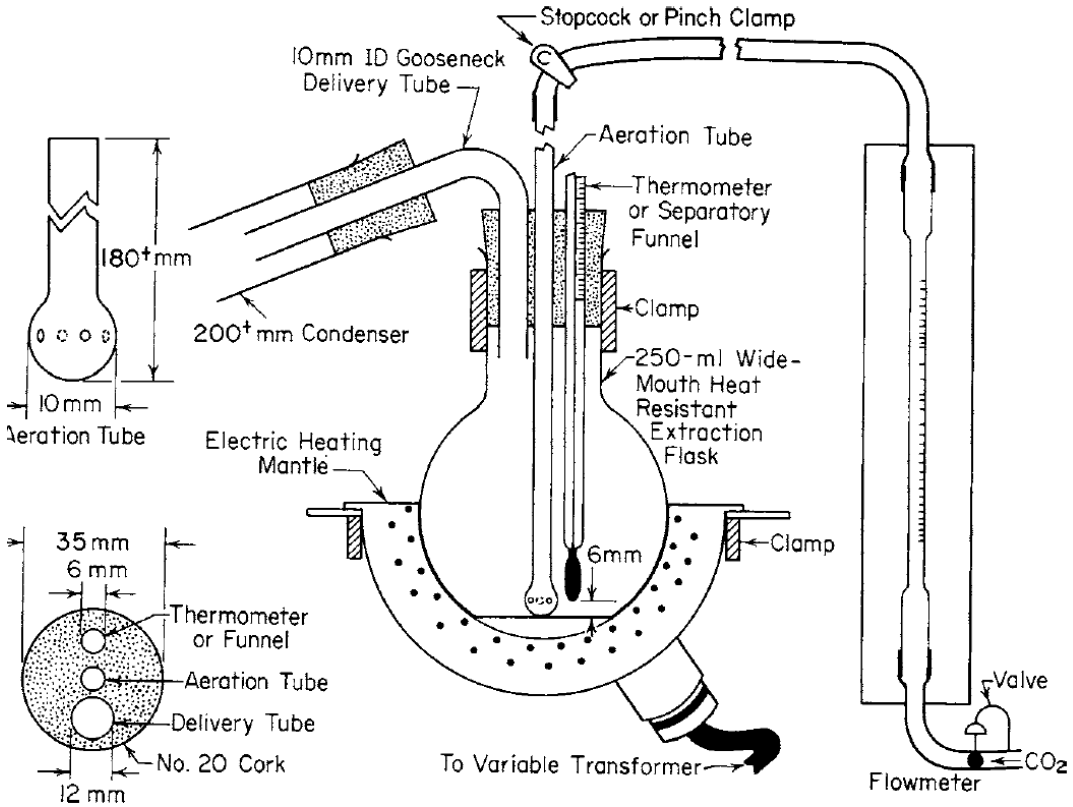

Figure 2-20: Abson distillation method illustration (American Society for Testing and Materials (ASTM) D1856, 2009)

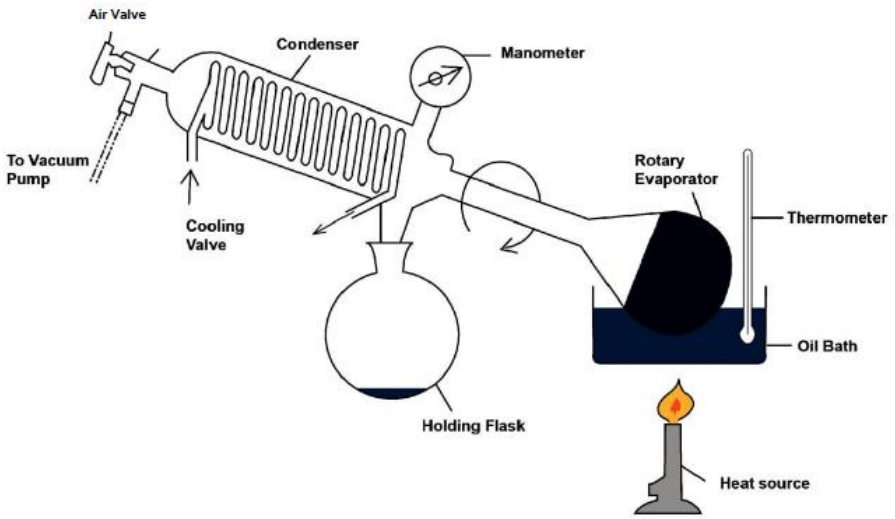

Figure 2-21: Rotary evaporator for polymer modified binders using a Bunsen burner (Technical Guideline (TG) 1, 2019)

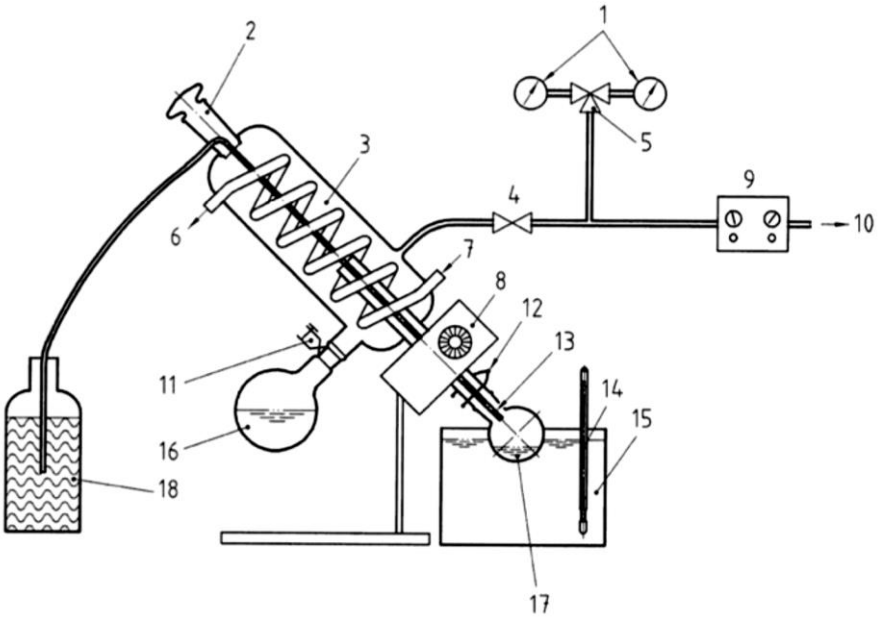

Key

1	vacuum gauge	8	rotary drive motor	14	thermometer
2	induction stopcock	9	vacuum regulator	15	oil bath
3	condenser	10	to vacuum pump	16	receiving flask
4	auxiliary air inlet	11	screw clip	17	rotating evaporating flask
5	change-over valve	12	spring clip	18	bitumen solution
6	water outlet	13	delivery tube (end approximately 1/3 of way into flask)		
7	water inlet				

Figure 2-22: Typical illustration of a rotary evaporator (European Standards (EN) -12697-3, 2013)

One of the main problems of the mentioned recovery / distillation methods is that all of them have the potential to remove the solvent insufficiently. The residual solvent in the recovered binder decreases the stiffness, resulting in softer binder properties. Thus, typically a solvent with a high boiling point will have more residual solvent in the recovered binder. The gas chromatography can be used to monitor the presence of the remaining solvent. (Mturi *et al*., 2015)

Researchers have shown that the use of the Abson Method (ASTM D1856) provides results that show a large amount of residual solvent in recovered binder compared to other methods, where the ASTM D5404 Rotary Evaporator Method has shown to have insufficient repeatability and consistency. (Mturi *et al*., 2015)

The EN-12697-3 Rotary Evaporator Method however attempts to resolve some of the Abson Method challenges by employing specific recovery temperatures for specific phases and various solvent types, as can be seen in Table 2-9. (Mturi *et al.*, 2015)

It is however very important to assess the accuracy and precision of the mentioned recovery and solubilisation methods in order to determine the most suitable and effective method/s to be applied for optimal binder extraction without significantly changing its properties. (Van Assen & Rust, 1997)

Mikhailenko & Baaj (2017) conducted a survey on the extraction-recovery procedure in relation to the apparatus used, performance, safety and the data collected by research laboratories in Canada, USA and Europe. Table 2-10 summarises the apparatus used for the mentioned extraction-recovery procedure.

Table 2-10: Testing extraction-recovery apparatus survey (adapted from Mikhailenko & Baaj, 2017)

Solvent	%	Concerns		Safety	
		Ageing	Residue solvent	Volatiles	Corrosive Chemicals
Trichloroethylene (TCE)	67%	46%	33%	88%	29%
N-Propyl Bromide	31%	27%	45%	64%	36%
Toluene	22%	63%	13%	75%	0%
Extraction Method	**%**	**Top Recovery method used with Extraction**		**Top Solvent used during Extraction**	
Centrifuge	84%	59% Rotary		72% TCE	
Automatic Extractor	16%	100% Rotary		83% TCE	
Recovery Method	**%**	**Centrifuge used before Recovery**	**Top solvent used during Recovery**	**Concerns**	
				Ageing	Residue solvent
Rotary Evaporator	63%	86%	45% TCE	36%	18%
Abson Method	51%	94%	94% TCE	44%	33%

From Mikhailenko & Baaj (2017) it is concluded that laboratories primarily use the extraction-recovery procedure to analyse Reclaimed Asphalt Pavement (RAP) and secondly to determine the binder content. 51% of the respondents found the extraction-recovery procedure to determine the binder content very consistent and the other 49% respondents found it consistent. It was also found that 54% of respondents were concerned that the binder is being modified during this process, with binder ageing being the primary concern.

2.6.2 Artificial Ageing / Hardening

Ageing is a fundamental phenomenon that affects the performance of a pavement. It was found that oxidation is the most influential aspect of binder ageing, making the binder stiffer and brittle over time, indicating that as a pavement ages the oxidation slows molecular relaxation in bituminous binder.

This oxidative (reaction with oxygen from air) process is complicated and is replicated by artificial ageing. (Hagos, 2008) There are two artificial ageing methods that simulates plant (short-term) and in-service (long-term) ageing: Rolling Thin Film Oven (RTFO) and Pressure Ageing Vessel (PAV).

For asphalt mixes there are two different ageing mechanisms, namely short-term ageing (mixing, storage and compaction) using the RTFO and long-term ageing which is simulated by using the PAV. It is however important to note that short term ageing does not occur in the case of seals, as seal binders are not subjected to plant mixing after production. (Engelbrecht, 2019)

Research conducted by O'Connell showed that seals also have two ageing / hardening processes, being: (Engelbrecht, 2019)

- Short-term ageing results from heating, transport, circulation and spraying of the binder. This ageing is normally ignored due to its short insignificant age duration, especially when there are delays and / or extended heating times.
- Long-term ageing, involves two processes that lead to the hardening of the binder:

- One is oxidative ageing which PAV simulates but does not relate in the same way as the ageing prediction for asphalt mixes.
- A very important practical hardening mechanism is the long-term co-mingling of material in two adjacent layers. These layers are dependent on the pavement structure. It is also important to remember that bitumen is not a solid, not even at 20°C when there is very slow movement of the molecules. When a thin seal is put on top of another aged seal or aged asphalt mix, the aged material from the underlying layer will move into the fresh seal binder. Thus, when these two adjacent layers are tested in the long term, the stiffness will increase as a result of this incorporation of older / harder material.

The RTFO was well-accepted in 1970 by the America and European specifications, which represents short-term binder ageing during plant mixing, storage, transportation and application. After PAV's introduction in the USA, it has also become popular in Europe to simulate long-term ageing of binders during its service life in pavement. Typically, samples are first RTFO-aged before being PAV aged. These tests are correspondingly used to predict binder rutting and fatigue performance. (Hunter *et al.*, 2015)

The RTFO method differs for unmodified and modified binders, as modified binders are exposed to more severe conditions during construction than unmodified binder. The ASTM D2872 (2004), ASSHTO T240 (2013) and EN-12607-1 describes the standard method for unmodified binder and the SA's TG 1 (2019) gives the modified binder version.

The main difference between the RTFO unmodified and modified is the type of container used (glass or metal), the amount of binder in each container and the time of the test at 163°C, as shown in Figure 2-23.

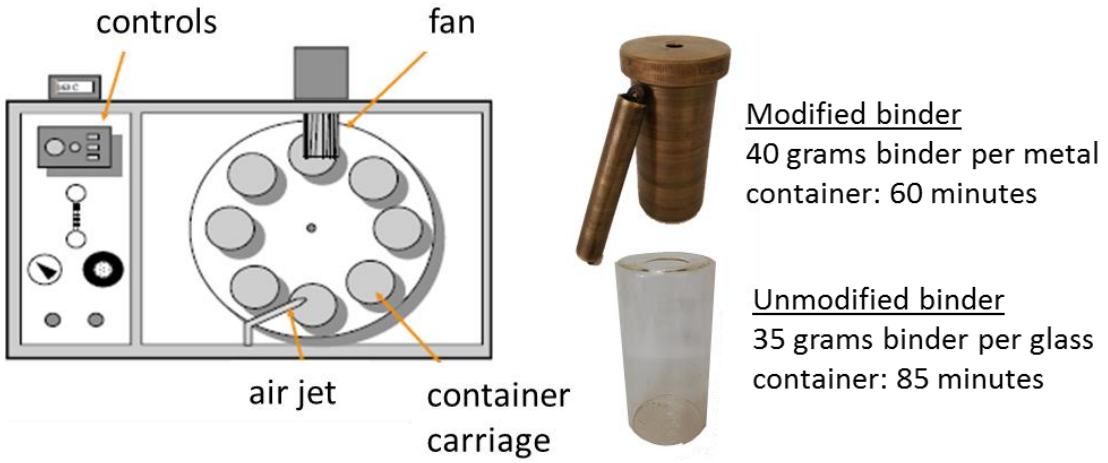

Figure 2-23: Unmodified and modified RTFO procedure (adapted from Rowe, Jenkins & Ven, 2017)

The PAV method is described in the American standard ASTM D6521 (2008) and uses raised temperatures (90-100°C) and pressure (2.07MPa) for in-service ageing of binder. PAV duration is 20 hours standard, which is identified as PAV1 and can be extended to 40 hours (PAV2), 60 hours (PAV3) and 80 hours (PAV4). It is important to note that PAV is only conducted after the binder sample is subjected to RTFO-ageing.

Vacuum degassing of samples after PAV is part of the ASTM D6521 (2008). Degassing of PAV samples are essential in order to remove bubbles, as residual bubbles will negatively affect DSR

and BBR test results. Figure 2-24 gives a schematic illustration of the PAV and vacuum degassing oven apparatus.

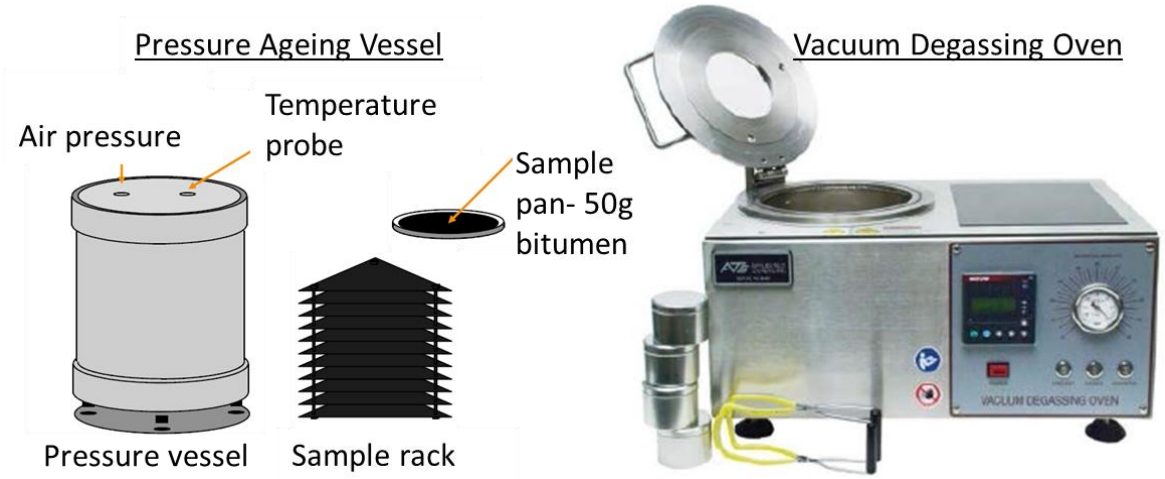

Figure 2-24: PAV and Vacuum Degassing Oven Apparatus (adapted from Rowe *et al.*, 2017)

Figure 2-25 illustrates that every binder has its own unique ageing / hardening rate. Vijaykumar (2012) believes that laboratory 20 hours PAV ageing simulates approximately one year of in-field ageing, where King, Anderson, Hanson and Blankenship (2011) researched and stipulated that PAV (20h) ageing is equal to five to ten years of field ageing. This indicates that the years the laboratory PAV-ageing simulates is still unknown in terms of binder in-service ageing.

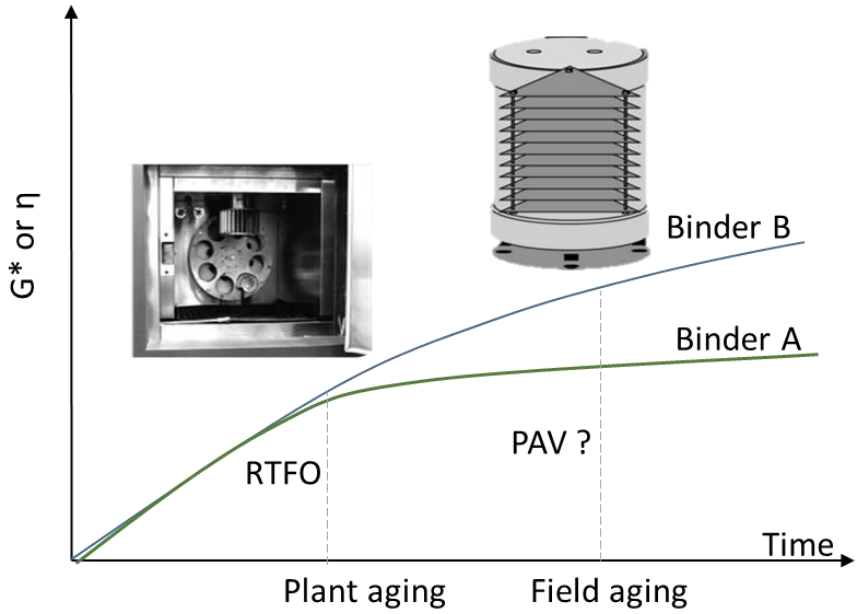

Figure 2-25: Ageing of bituminous binders (adapted from Rowe, Jenkins & Ven, 2017)

Hunter *et al*. (2015) established an ageing of bitumen graph in terms of an ageing index on the y-axis. The ageing index is a ratio of the viscosity of the aged bitumen (η_a) and the viscosity of the original bitumen (η_o). Figure 2-26 shows the Hunter *et al.* (2015) bitumen ageing graph, where significant ageing occurs during mixing.

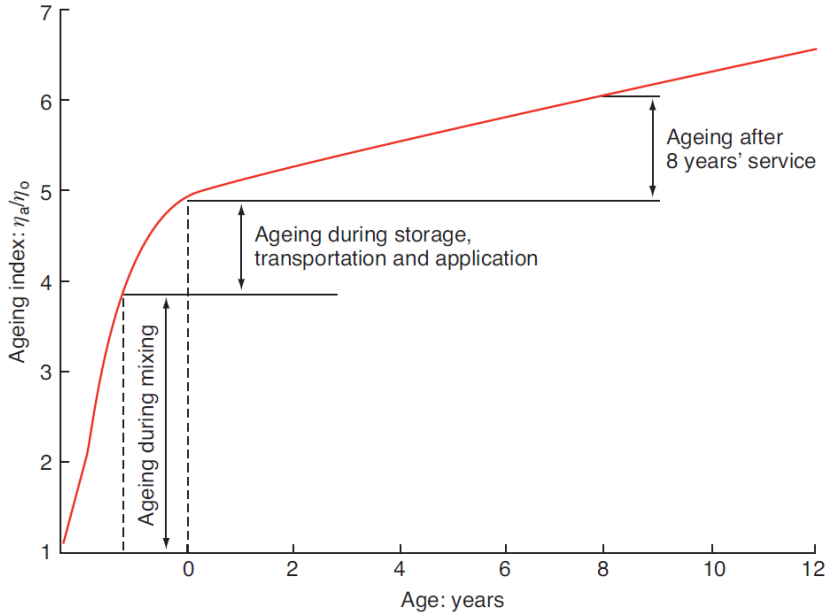

Figure 2-26: Short- and long-term ageing in terms of the viscosity (Hunter *et al.*, 2015)

2.6.3 Rheology Properties

To address the SA industry's need to have and implement a SA specific Performance Grading System, it is important to have a good understanding of the reliability, capabilities and shortcomings of current specifications.

The rheometer is the instrument that tests the viscosity and viscoelasticity of solids, semi-solids and liquids. Two rheometer testing apparatuses must be used in accordance with SATS 3208 Performance Grade (PG) Specifications for Bitumen in South Africa (Table 2-8), which is also used globally in PG specifications, namely DSR (dynamic test) and BBR (monotonic test). The DSR is used at intermediate and high temperatures to determine the relaxation and creep behaviour, where BBR is tested at low temperatures in order to determine thermal cracking and stress relaxation.

2.6.3.1 Dynamic Shear Rheometer (DSR)

DSR's most common setup is by way of the parallel plate (PP) apparatus, where the bitumen sample is placed between a plate that is fixed (temperature controller) and a plate that oscillates. The oscillation of the top plate creates a shear within the bitumen sample, whilst measuring the strain / stress response at a selected frequency.

DSR has two forms of testing, namely strain-controlled and stress-controlled. Mturi, O'Connell & Zoorob, (2011) concluded that the strain-controlled test is most commonly used, which applies a dynamic, sinusoidal strain to a binder sample to obtain resulting stress (torque) as a function of frequency.

Figure 2-27 provides a schematic illustration of the DSR parallel plate strain distribution, where r, h, θ, Ω is the plate radius, distance between the plates (gap), angular motor deflection (radians) and motor angular velocity (rad/s) respectively. (Thermal Analysis Instruments, 2019)

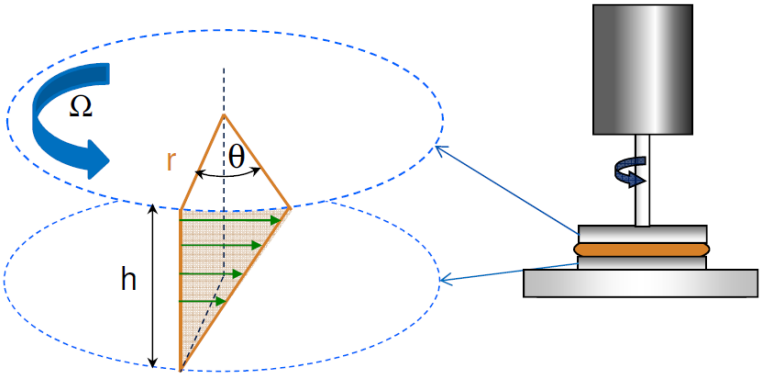

Figure 2-27: DSR Parallel Plate and Stain distribution (Thermal Analysis Instruments, 2019)

From the DSR the complex shear modulus (G*), phase angle (δ) and non-recoverable creep compliance (J_{nr}) can be calculated. From the input of target strain (%), the shear stress-strain response is plotted, as indicated in Figure 2-28, where after the G*, δ, storage modulus (G') and loss modulus (G'') can be obtained.

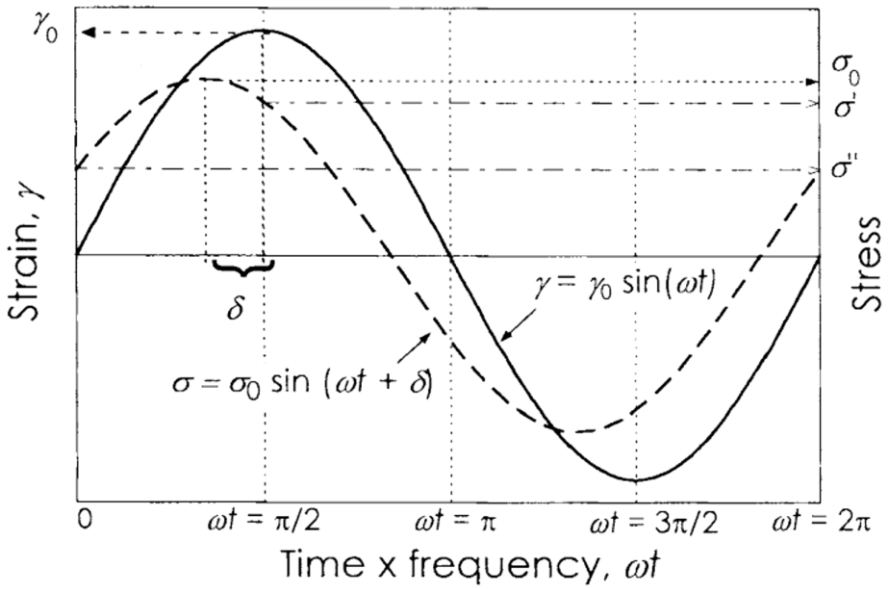

Figure 2-28: DSR stress-strain response (Shaw & MacKnight, 2005)

Complex shear modulus measures bitumen's resistance to deform when under a shear load and is calculated with Equation 2-1 (Mturi *et al.*, 2011):

$$G^*(\omega) = \frac{|\tau(\omega)|}{|\gamma(\omega)|} \qquad (2\text{-}1)$$

Where,

$G^*(\omega)$	= *complex shear modulus [Pa]*
$\tau(\omega)$	= *shear stress response [Pa]*
$\gamma(\omega)$	= *shear strain response [m/m]*
ω	= *angular frequency [rad/s]*

The phase angle (°) illustrates the bitumen's recoverable and non-recoverable deformation (SABITA, 2017). The phase angle can easily be obtained from the stress-strain maximum response difference

(Figure 2-28), with the G' and G'' components of G* that can be calculated with Equation 2-2 and 2-3 (Mturi *et al.*, 2011):

$$G'(\omega) = G^*(\omega)\cos\delta \quad (2\text{-}2)$$

$$G''(\omega) = G^*(\omega)\sin\delta \quad (2\text{-}3)$$

Where,

G' (ω) = *storage modulus / in-phase component [Pa]*

G'' (ω) = *loss modulus / out-phase component [Pa]*

By combining the complex shear modulus and phase angle the viscoelastic behaviour of bitumen can be described. If the phase angle equals zero degrees, then the bitumen is purely elastic. Bitumen will have a pure viscous behaviour if the phase angle is equal to 90 degrees, as shown in Figure 2-29. (SABITA, 2017)

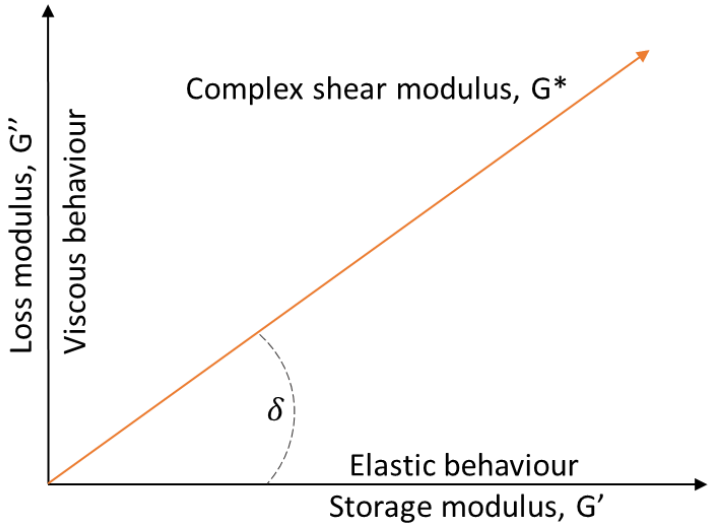

Figure 2-29: G* and δ related to viscoelastic behaviour (adapted from SABITA, 2017)

Complex shear modulus (G*) can also be used to determine other viscoelastic parameters, namely complex shear viscosity (η*) and complex shear compliance modulus (J*) (Mturi *et al.*, 2011):

$$\eta^* = \frac{G^*}{\omega} \quad (2\text{-}4)$$

$$J^* = \frac{1}{G^*} \quad (2\text{-}5)$$

Where,

*η** = *Complex shear viscosity [Pa.s]*

*J** = *complex shear compliance modulus [Pa]*

During DSR testing there are three typical tests that can be performed, namely the strain sweep, frequency sweep and Multi Stress Creep Recovery (MSCR). (Mturi *et al.*, 2011) (Vijaykumar, 2012)

Strain Sweep

Strain sweeps are tested at a constant temperature (range between -22°C and 70°C) and frequency (10rad/s) whilst an increasing strain is applied to the bitumen sample to analyse and determine the

linear viscoelastic (LVE) range of the bituminous binder. The LVE of a specific binder is the strain at which the binder can recover to its original state. When the initial complex shear modulus decreases with 5%, the upper limit of the LVE range is defined, as shown in Figure 2-30. (SABITA, 2017)

It must be noted that it is of critical importance that further testing (frequency sweep and MSCR) is conducted within the LVE range of the binder, in order to ensure safe strain levels and accurate results. Mturi et al. (2011) identified that there is a clear relationship between the LVE region and G* and with an increase in frequency, decrease in G* and decease in temperature, the LVE limit will reduce.

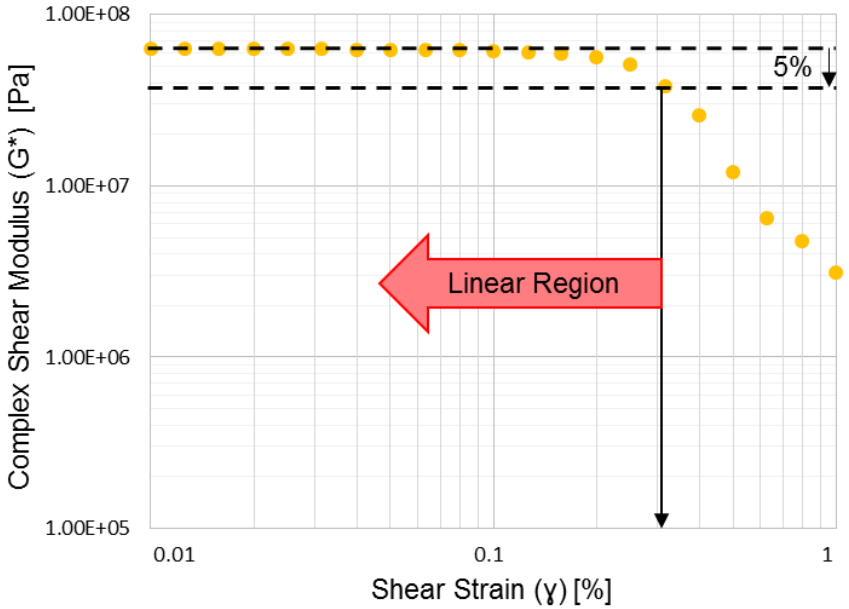

Figure 2-30: Example of the LVE region of a binder

Frequency Sweep

Before conducting frequency sweep, the strain sweep test is performed to determine the maximum strain within the LVE range, which is used for the frequency sweep test. The frequency sweep test is conducted at a constant strain (mentioned above) and temperature while a variety of loading frequencies is applied to the bitumen sample. This process is repeated at different temperatures to finally obtain stiffness isotherms, which will be used to analyse the specific binder's performance behaviour over a wide temperature spectrum. (Mturi *et al.*, 2011)

Multi Stress Creep Recovery (MSCR)

The MSCR test is performed in a DSR to simulate repeated traffic loading on a pavement. This test uses the concept of creep recovery testing to evaluate the binder's susceptibility to deform permanent. The test consists of a creep portion where the binder is loaded for one second at a constant stress, then released, allowing to recovery for nine seconds unloaded (Figure 2-31). The creep (one second loading) and recovery (nine second unloading) of binder is repeated 30 times, thus resulting in 30 cycles. (SABITA, 2017) (Vijaykumar, 2012)

The process involving the following three steps:

- conditioning the binder sample for the first 10 cycles at 0.1kPa stress level;
- followed by 10 cycles also at 0.1kPa stress level; and

- finally (last) 10 cycles at stress level 3.2kPa.

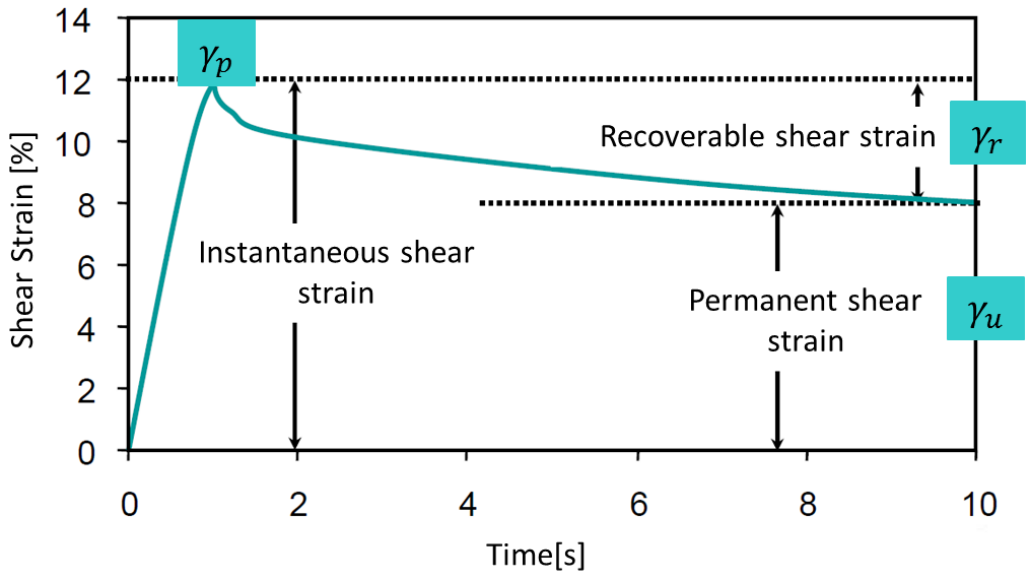

Figure 2-31: One creep recovery cycle during MSCR test (adapted from SABITA, 2017)

Two parameters are derived from the MSCR test, namely the non-recoverable creep compliance (J_{nr}) and the percentage recovery. (ASTM D7405, 2010)

The J_{nr} measures the residual strain left in the binder sample after repeated creep recovery relative to the stress applied. The J_{nr} gives an indication of the traffic grade and rutting, influenced by the temperature at which the test is done. Thus, a lower J_{nr} reduces rutting and increases the traffic grade. The percentage recovery is intended to provide a means for determining the presence of elastic response and stress dependence of polymer modified and unmodified binders. Non-recoverable creep compliance (J_{nr}) and % recovery are calculated using Figure 2-31 and, Equation 2-5 and 2-6. (SABITA, 2017) (ASTM D7405, 2010)

$$J_{nr} = \frac{non-recoverable\ shear\ strain}{applied\ shear\ stress} = \frac{\gamma_u}{\tau} \quad (2\text{-}5)$$

$$\%\ Recovery = \frac{\gamma_r}{\gamma_p} \times 100 \quad (2\text{-}6)$$

Where,

J_{nr} = *non-recoverable creep compliance [kPa^{-1}]*

τ = *applied shear stress [kPa]*

γ_u = *unrecovered shear strain [mm/mm]*

γ_r = *recovered shear strain ($\gamma_p - \gamma_u$) [mm/mm]*

γ_p = *peak shear strain [mm/mm]*

2.6.3.2 Bending Beam Rheometer (BBR)

BBR is used for low temperature rheological properties to assess the tendency of bitumen becoming brittle and measures the binders' stiffness and relaxation abilities at low temperatures. BBR is a simple test (Figure 2-32) that: (ASTM D6648, 2008) (Hunter *et al.*, 2015)

- applies a monotonic, constant creep load (980mN) to a beam of bitumen that is simply supported;
- that is submerged in cold fluid bath, at a corresponding bituminous binder's lowest in-service temperature (-36°C to 0°C) to behave like an elastic solid; and
- is tested for a period of 240 seconds, where at every 0.5 second interval the resultant deflection is measured.

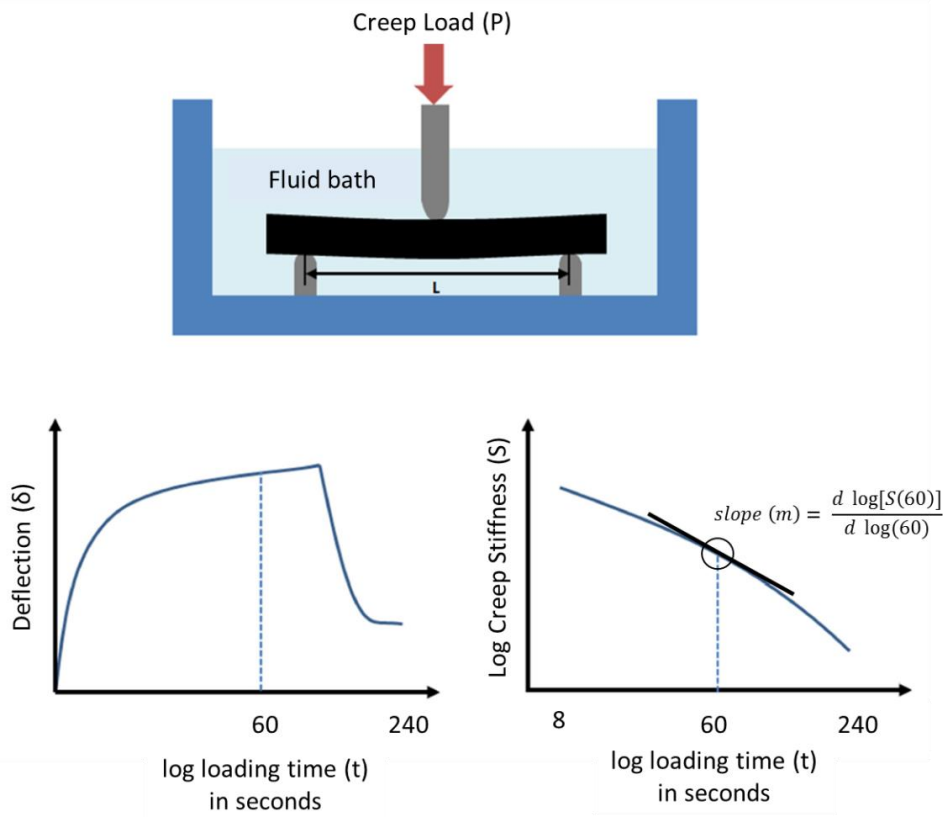

Figure 2-32: Schematic and analysis of BBR (adapted from SABITA, 2017)

The BBR test provides two output parameters which are also included in the current SATS 3208 PG Specification, namely the flexural creep stiffness (S) and the creep rate (m) after 60 seconds. The creep stiffness (S) can be described as the binder's resistance to creep loading, using the linear elastic beam theory and viscoelastic principles to calculate creep stiffness. The creep rate (stress-relaxation factor) describes the changes in binder stiffness over time during loading. (SABITA, 2017) Equations 2-7 and 2-8 are used in the ASTM D6648 (2008) to calculate abovementioned low temperature rheological properties.

$$S(t) = \frac{PL^3}{4bh^3\delta(t)} \tag{2-7}$$

$$m(t) = \left|\frac{d\log[S(t)]}{d\log(t)}\right| \tag{2-8}$$

Where,

S(t) = *flexural creep stiffness at time, t [MPa]*

P = *constant creep load [mN]*

L = *span length between the beam support [mm]*

b = *width of test bitumen beam [mm]*

h = *depth of test bitumen beam [mm]*

δ(t) = *deflection of beam at time, t [mm]*

t = *loading time [s]*

m(t) = *slope of the log[S(t)] [MPa/s]*

log[S(t)] = *logarithm of the stiffness [MPa]*

log(t) = *logarithm of loading time [s]*

Vijaykumar's (2012) research has shown strong correlation between the BBR parameters (S and m-value) at low temperatures and the DSR parameters (G*, phase angle and ω) at specified frequency and temperature. Equation 2-9 and 2-10 shows Vijaykumar (2012), S(60) and m(60) equations incorporating DSR parameters, where time is equal to 1/ω.

$$S(t) = \frac{3G^*(\omega)}{[1+0.2\sin(2\delta)]} \quad (2\text{-}9)$$

$$m = \frac{d(\log G^*)}{d(\log \omega)} \quad (2\text{-}10)$$

Where,

S(t) = *creep stiffness at time, t [Pa]*

m = *slope of G* versus ω plot at a given frequency*

G(ω)* = *Complex shear modulus at frequency, ω [Pa]*

δ = *phase angle at frequency, ω [Pa]*

2.7 Viscoelastic behaviour modelling / LVE rheological modelling

As bituminous binders are viscoelastic (behaviour) in nature, its performance properties will change with rate (or time) of loading, temperature and age.

Rheology is the engineering tool that describes bituminous binder's behaviour and performance, enabling identification of trends by producing graphs and diagrams of tested data, such as master curves and Black Space diagrams. This mathematical modelling is simplified by introducing tests within the bituminous binder's linear viscoelastic (LVE) region and enabling data to use the time-temperature superposition principle (TTSP).

In the 1950's LVE rheological properties were assessed by using nomographs from Van der Poel's non-linear multivariable model. The Nomograph Method has been replaced by empirical / mathematical equations and mechanical element modelling, as the nomograph method uses the penetration test and PG specifications are moving away from this test. (Yusoff, 2012)

These mathematical equations and mechanical element modelling are used to plot master curves and Black Space diagrams individually. It is also used to analyse the binder's response to unloading and the behaviour related to age and temperature.

Figure 2-33 provides shortened steps to model the linear viscoelastic rheology properties of bituminous binders.

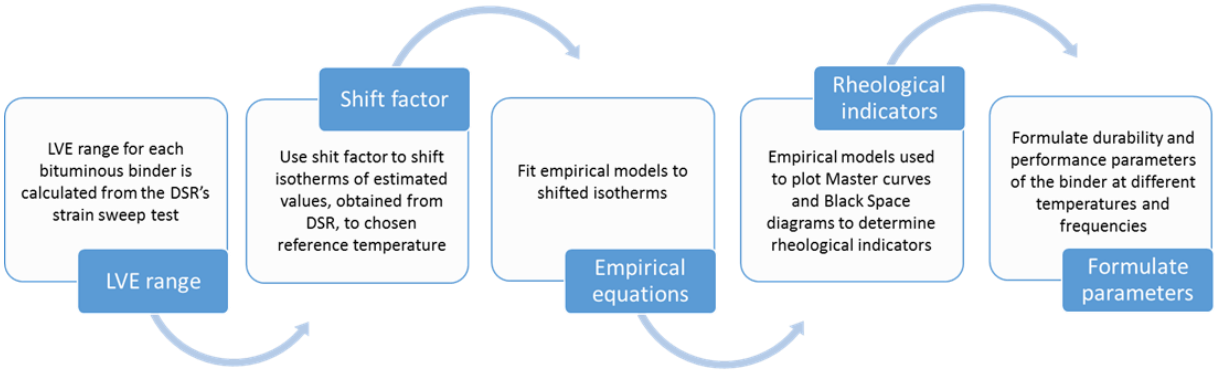

Figure 2-33: Step- by- step LVE rheology modelling

2.7.1 Linear Viscoelastic (LVE) limits

As discussed in Section 2.6.3.1, a bituminous binder will have linear viscoelastic behaviour when it is exposed to a stress or strain profile over time, where the strain that is applied is small.

Figure 2-30 in Section 2.6.3.1 provides a schematic illustration on how the LVE region of a binder is calculated.

Airey, Rahimzadeh & Collop (2002) studied the LVE range of conventional and modified binders. They found that high modified binders have a smaller LVE range than conventional binders. This could be due to the increase in stiffness of the modification, as it has been noted that a decrease of LVE limit correspond with the increase of stiffness. Their study in England showed that both conventional and modified binders at low temperatures have a strain dependent LVE range of between 2% to 6%.

It is extremely difficult to characterise non-linear viscoelastic response in practice and in a laboratory, as rheological modelling of bituminous binders is limited to the LVE range where the magnitude of stress has no influence on the stress-strain inter-relation. By limiting and simplifying the modelling to the LVE range, enables the use of TTSP. (Yusoff, 2012)

2.7.2 Time-temperature superposition principle (TTSP)

The TTSP can be used to relate the relationship between time (frequency) and temperature in the material's LVE region. This is important as the isotherms (stiffness over a range of frequencies at multiple temperatures) of a bituminous binder can be shifted to a reference temperature (Tref) to form a single continuous smooth graph, which represents the master curve that describes the material's behaviour.

The TTSP represents an influential and suitable tool for evaluating rheological data through the use of a horizontal shift factor function. Figure 2-34 illustrates how the isotherms of a complex shear modulus (G*) at several temperatures are shifted to a chosen reference temperature, constructing a smooth master curve. Note that the master curve is the G* plotted against a reduced frequency scale, ω_r (rad/s) or f_r (Hz), and is calculated by means of Equation 2-11: (Yusoff, Chailleux & Airey, 2011)

$$f_r = \alpha_T \times f \quad (2\text{-}11)$$

Where,

f_r = reduced frequency [Hz]

α_T = shift factor [-]

f = loading frequency [Hz]

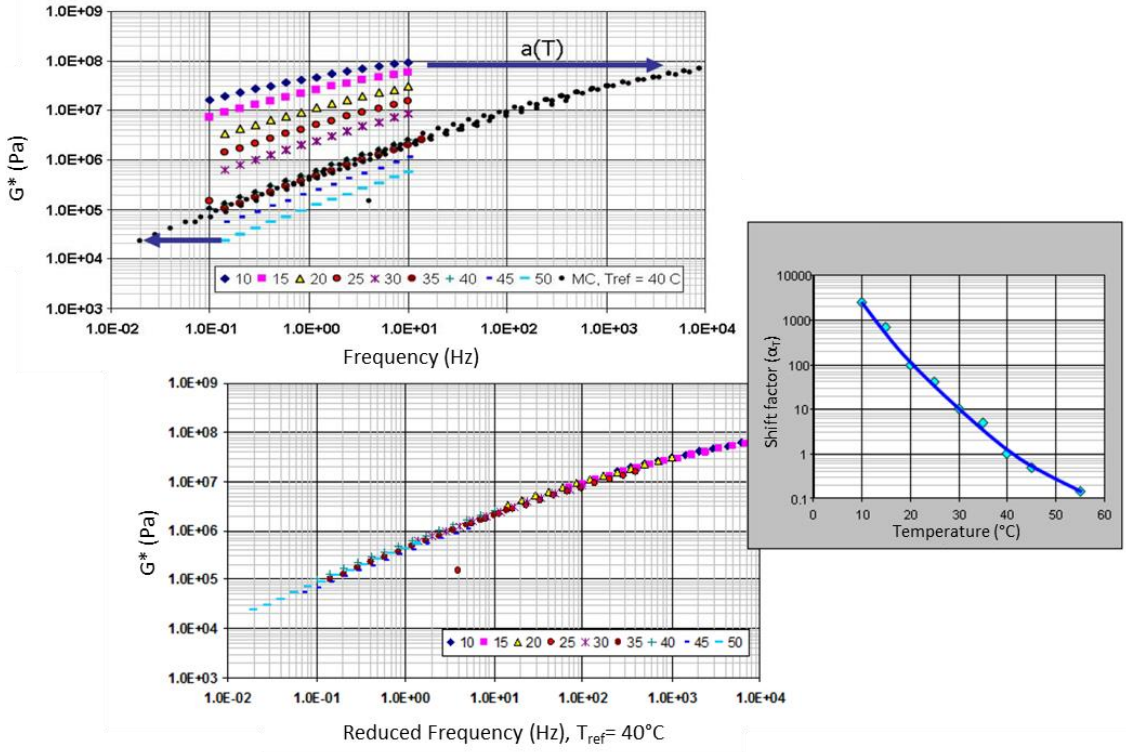

Figure 2-34: Shift factor applied to G* isotherms to form a master curve (Rowe & Sharrock, 2011)

There are two types of shifting methods that can be considered, the Constrained Empirical Shifting Method or the Non-functional Numerical Free Shifting Method. The non-functional numerical method (free / manually shifting) provides the best fit to the experimental data as it has the highest degree of freedom and is preferred when the material's temperature or frequency susceptibility is unknown. The Constrained Empirical Shifting Method has a low degree of freedom which leads to a poor fit to experimental data, but still allows simplification of inaccurate isotherm shapes (Forough, Nejad & Khodaii, 2014). In the USA the Constrained Empirical Shifting Method is the standard approach to model data to form a smooth master curve (Rowe & Sharrock, 2011).

2.7.3 Rheological Models for Shifting

Several shifting techniques have been proposed for the generation of master curves (mostly G*, S or δ versus frequency or loading time at different temperatures) using the TTSP. The following four constrained shifting equations are mostly used by researchers:

- Arrhenius

- William, Landel and Ferry (WLF) based on free volume concepts, provides good results above T_g (glass transition temperature)
- Kaelble
- Modified Kaelble

It is important to note that these equations are all empirical and might present different results under similar testing conditions for the same bituminous binder mixes (Forough *et al.*, 2014). These techniques only involve horizontal shift (α_T) and no vertical shift (β_T), as most researchers found that vertical shifting does not provide accurate temperature adjustment(s). Vertical shift allows temperatures to induce density changes. It is important to note that the horizontal shift factor is equal to one at the chosen reference temperature ($\log \alpha_T = 0$). (Yusoff *et al.*, 2011)

As mentioned, the TTSP involves a horizontal movement of isotherms, where the horizontal shift factor (α_T) indicates the temperature dependency of bitumen as expressed in Equation 2-12. It must be noted that temperature dependency does not correspond with temperature susceptibility, which is bases on the bitumen's hardness over change of temperature. (Hunter *et al.*, 2015)

$$\alpha_T = \alpha_T (T, T_{ref}) \tag{2-12}$$

Where,

T = *testing temperature [°C]*

T_{ref} = *chosen reference temperature [°C]*

The ***Arrhenius*** equation is based on the rate theory and is accurate when it is <u>below</u> the glass transition temperature (T_g) and <u>within</u> the Newtonian region (Anderson, Rowe & Christensen, 2008) (Alhaddad, 2015). The Arrhenius equation is adopted in the AASHTO, where the equation only has one constant. Rowe & Sharrock (2011) includes Arrhenius Equation 2-13 with an added constant that makes this equation define a linear relation between the shared temperature and shift factor.

$$\log \alpha_T = C_1 + C_2 \left(\frac{1}{T} - \frac{1}{T_{ref}}\right) \tag{2-13}$$

Where,

C_1, C_2 = *constants*

The ***William, Landel and Ferry (WLF)*** equation has shown to provide good material behaviour <u>above</u> the T_g (higher temperatures) and is based on a Ferry's (1971) free volume theory. (Anderson *et al.*, 2008) The WLF equation is represented by Equation 2-14, which uses temperature differences to make it more suitable for practical manipulation. (Hunter *et al.*, 2015)

$$\log \alpha_T = \frac{-C_1(T - T_{ref})}{C_2 + (T - T_{ref})} \tag{2-14}$$

In 1994, for aged and unaged bituminous binders the Arrhenius equation was found to be more accurate in shifting low temperatures (below transition point) than that for the WLF equation. As both equations are theoretical, the parameters of both provide molecular structure with an understanding of the bitumen. (Yusoff, 2012)

The transition point from where the Arrhenius best fit below the T_g to the WLF best fit above the T_g is defined as the defining temperature (T_d). Basically the T_d is regarded similar to the T_g. (Rowe & Sharrock, 2011)

The ***Kaelble*** shift equation is a modification of the hyperbolic WLF equation that introduces an inflection point at T_d, which changes the shape to sigmoidal. This modification, Equation 2-15, is due to the WLF shift factor increasing to rapidly below the inflection point at lower temperatures. (Rowe & Sharrock, 2011)

$$\log \alpha_T = \frac{-C_1(T-T_d)}{C_2+|T-T_d|} \qquad (2\text{-}15)$$

Where,

T_d = *defining temperature [°C]*

From Figure 2-35 it is evident that the Kaelble equation above inflection point temperature is identical to WLF. However below the inflection point temperature the Kaelble log (α_T) strives towards the horizontal asymptote instead of rapidly increasing to the vertical asymptote like the WLF. (Rowe & Sharrock, 2011)

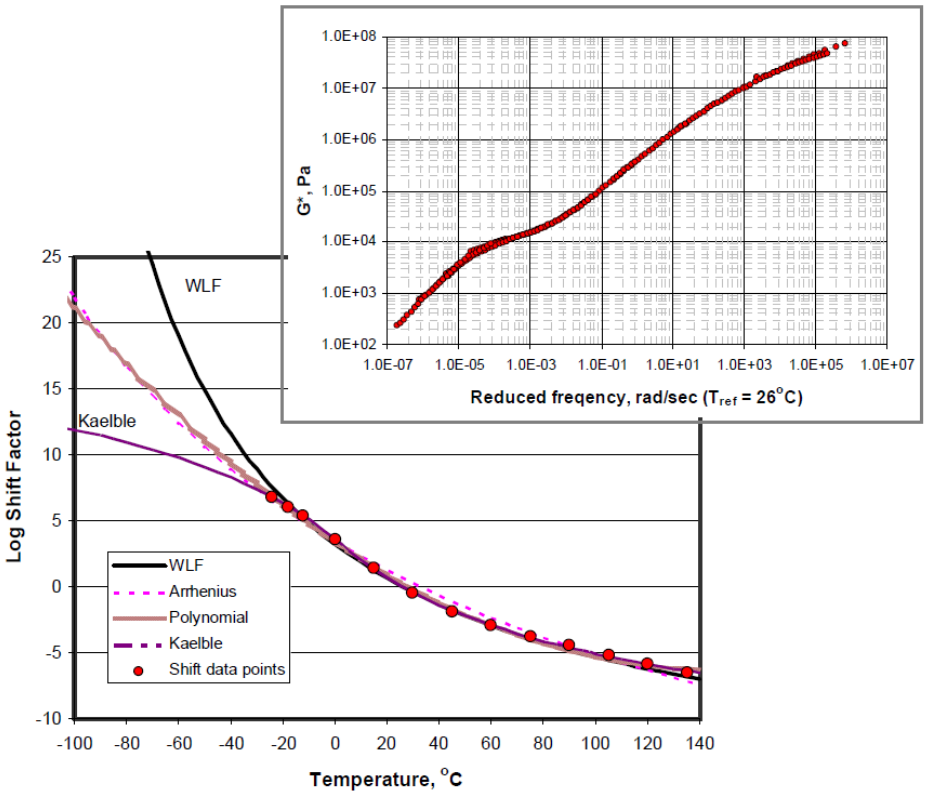

Figure 2-35: Example of Kaelble compared to Arrhenius and WLF for a SBS modified binder(Rowe & Sharrock, 2011)

The Kaelble equation however has one problem over and above that it is difficult to apply; being that the composition of the Kaelble equation points towards the reference temperature (T_{ref}) and the defining temperature (T_d) being similar. This problem is overcome by the modification of the Kaelble equation, called the ***Modified Kaelble*** that separates the T_{ref} and T_d, as shown in Equation 2-16. (Rowe & Sharrock, 2011)

$$\log \alpha_T = -C_1 \left(\frac{T - T_d}{C_2 + |T - T_d|} - \frac{T_{ref} - T_d}{C_2 + |T_{ref} - T_d|} \right) \quad (2\text{-}16)$$

Rowe & Sharrock (2011) research showed that this modification reduces the Root Mean Square Error (RMSE) from 0.8872% for Arrhenius to 0.2367% for Modified Kaelble.

Forough *et al.* (2014) found that there are three components that could affect shift factors in their "comparative study of temperature shifting techniques", being mix characteristics, ageing time and reference temperature (T_{ref}). They concluded that the aggregate gradation and binder content of a mixture does not influence the ranking order of the constrained shifting equations, with Arrhenius as the best fit, followed by WLF and Modified Kaelble. Forough *et al*. (2014) studied three ageing periods (1 year, 7.5 years and 18 years) where it was evident that ageing period applied affects the ranking order, with Arrhenius providing the best correlation for all three ageing periods. Investigation of the reference temperatures of -7, +4, +14 and +21°C revealed that Arrhenius best correlates between measured and predicted shift factors. The ranking order after Arrhenius differs, making the reference temperature an influential factor.

Yusoff *et al.* (2011) calculated goodness-of-fit statistics which included the standard error ratio, coefficient of determination (R^2), discrepancy ratio, average geometric deviation and mean normalised error for all of the abovementioned constrained shifting equations. In this study it was concluded that WLF in most cases produces the best correlation to the manual shift approach, followed by Modified Kaelble and Arrhenius. Yusoff *et al.* (2011) made the same finding as Forough *et al.* (2014), that aged binders decreases the accuracy of constrained shifting equations, and more so for polymer modified binders.

Rowe & Sharrock (2011) evaluated and ranked the constrained shifting equations by means of the RMSE looking at modified binders. As shown in Figure 2-36 Modified Kaelble is the best fit as the relative error is less than one third compared to WLF.

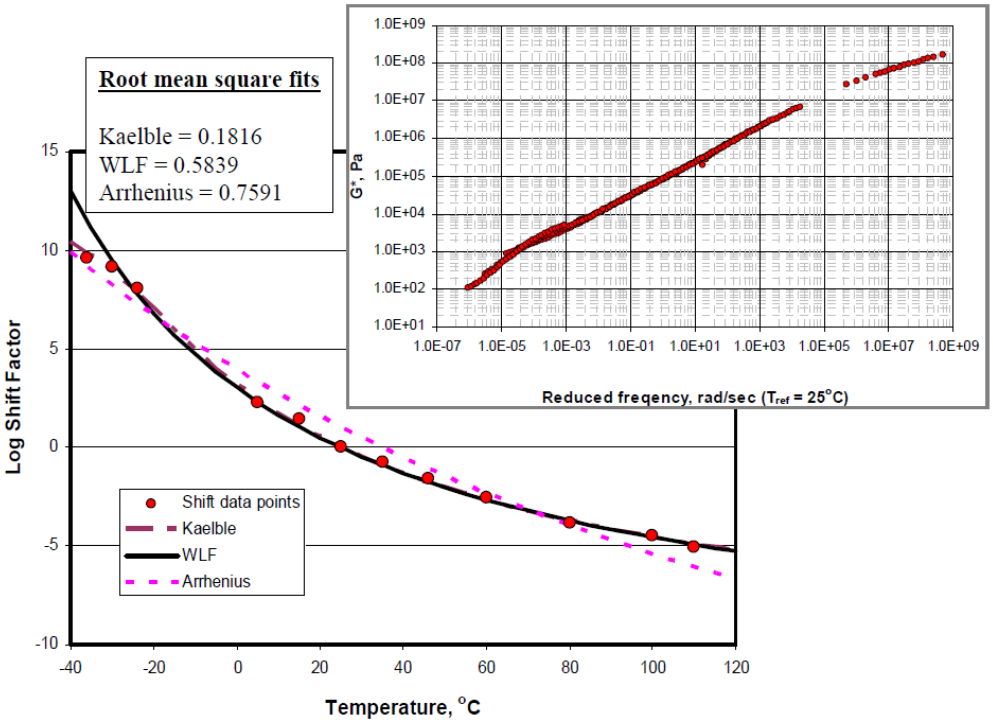

Figure 2-36: Example of PG64-22 modified binder, comparing shift factor equations with the RMSE at T_{ref} = 25°C (Rowe & Sharrock, 2011)

2.7.4 Empirical models

Binder requires a model that captures changes in binder rheology caused by long-term ageing. This needed to link binder and mixture properties related to binder “quality” and to model its needs for its application (asphalt or / and seals), in order to be compatible with molecular/ structure changes at molecular level.

Binder rheology is characterised by the use of empirical models, as it provides: (Anderson *et al.*, 2008)

- a mathematical equation that can be manipulated;
- a link between the mixture and the binder;
- quantitative parameters that characterise and identifies change in rheology; and
- a rational basis for a specification criterion.

Very well-known and common empirical models that are used to interpret viscoelastic data are:

- the Christensen - Anderson (CA) and Christensen - Anderson - Marasteanu (CAM) models;
- the Standard Sigmoidal (SS) model; and
- the Generalised Logistic Sigmoidal (GLS) model.

According to Christensen & Anderson (1992) there are four primary parameters needed to fully characterise bitumen’s LVE properties from a master curve (Figure 2-37), being the glassy modulus (G_g), the crossover frequency (ω_c), the Rheological Index (R) and finally the steady-state viscosity (η_0). When assessing empirical models, it is important to look at how ageing and modification of binders influence the master curve parameters, avoiding those empirical models that reduce the accuracy of the parameters.

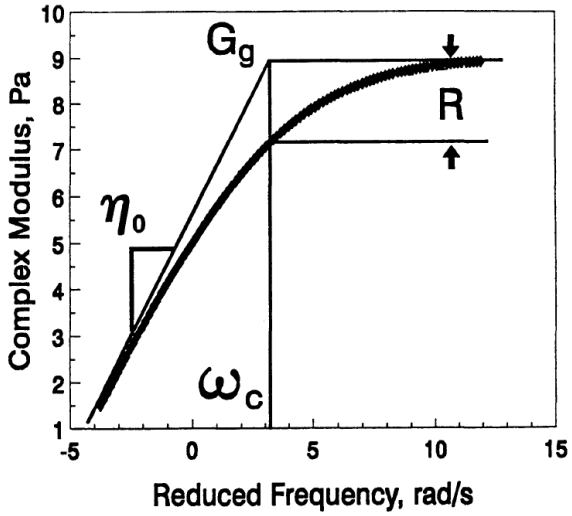

Figure 2-37: Four primary master curve parameters to characterise LVE properties (Christensen & Anderson, 1992)

The four primary master curve parameters as shown in Figure 2-37 are:

- Glassy modulus (G_g) is defined as the upper limit value of complex shear modulus (G*) at low temperatures and high frequencies. G_g values where noted to ranges from 0.6 – 1.5GPa, but 1GPa can be assumed for analysis purposes. (Christensen & Anderson, 1992)

- Crossover frequency (ω_c) is the frequency at which the storage modulus (G') and loss modulus (G'') are equal; and where the phase angle (δ) is equal to 45°, thus tan δ = 1. This parameter is binder specific and is generally considered as a hardness parameter, which indicates the binder's consistency at a chosen temperature. (Christensen & Anderson, 1992)

- Rheological Index (R) is also referred to as the R-value. This parameter gives a good indication of the change in the material's behaviour with age. Where field performance shows that cracking is related to the R-value. There are two ways of obtaining the R-value, using Equation 2-17 or calculating the difference between the upper limit of G* (glass modulus) and the G* at the crossover frequency, as illustrated in Figure 2-37. (Rowe, 2014a)

$$R = \frac{(\log 2)\log\left(\frac{G^*(\omega)}{G_g}\right)}{\log\left(1-\frac{\delta(\omega)}{90}\right)} \tag{2-17}$$

  This parameter is proportional to both the asphaltene content (Yusoff, Jakarni, Nguyen, Hainin & Airey, 2013) and relaxation spectrum, where a larger R-value exhibits a wide relaxation spectrum. (Christensen & Anderson, 1992)

- Steady-state viscosity (η_0) is the limit of complex shear viscosity (η^*) as the phase angle approaches the viscous behaviour (at 90°). (Christensen & Anderson, 1992)

Christensen & Anderson (1992) developed the ***Christensen - Anderson (CA)*** model from eight Strategic Highway Research Program (SHRP) asphalt binders. (Yusoff *et al.*, 2013) The CA model is a semi-empirical model that is based on the skewed logistic function, modelling a diagonal (viscous) and horizontal (glassy) asymptote illustrated in Figure 2-38:

$$|G^*(\omega)| = G_g\left[1+\left(\frac{\omega_c}{\omega}\right)^{\frac{\log 2}{R}}\right]^{\frac{-R}{\log 2}} \tag{2-18}$$

$$\delta(\omega) = \frac{90}{1+\left(\frac{\omega}{\omega_c}\right)^{\frac{\log 2}{R}}} \tag{2-19}$$

$$R = \frac{(\log 2)\log\left(\frac{|G^*(\omega_c)|}{G_g}\right)}{\log\left(1-\frac{\delta(\omega_c)}{90}\right)} \cong \log\left(\frac{|G^*(\omega)|}{G_g}\right) \tag{2-20}$$

Where,

$G^*(\omega)$	= *measured complex shear modulus at frequency, ω [Pa]*
$\delta(\omega)$	= *measured phase angle at frequency, ω [°]*
G_g	= *glassy modulus [Pa]*
ω_c	= *crossover frequency [rad/s]*
ω	= *frequency of interest [rad/s]*
R	= *Rheological Index [-]*

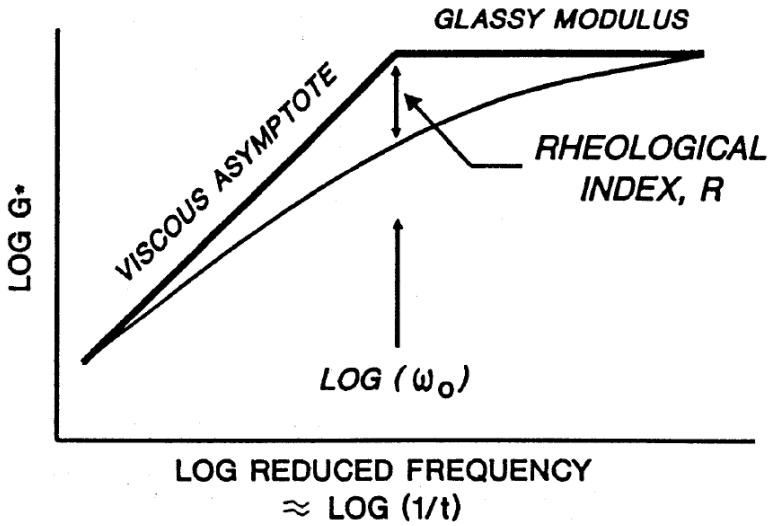

Figure 2-38: Christensen- Anderson (CA) model (Christensen & Anderson, 1992)

This CA model generates good results in the glassy region (binders with more solid type of behaviour) at low temperatures, but often generates inconsistent results when viscous flow behaviour at long loading times and / or at high temperatures is approached. (Christensen & Anderson, 1992) This is shown in Figure 2-39.

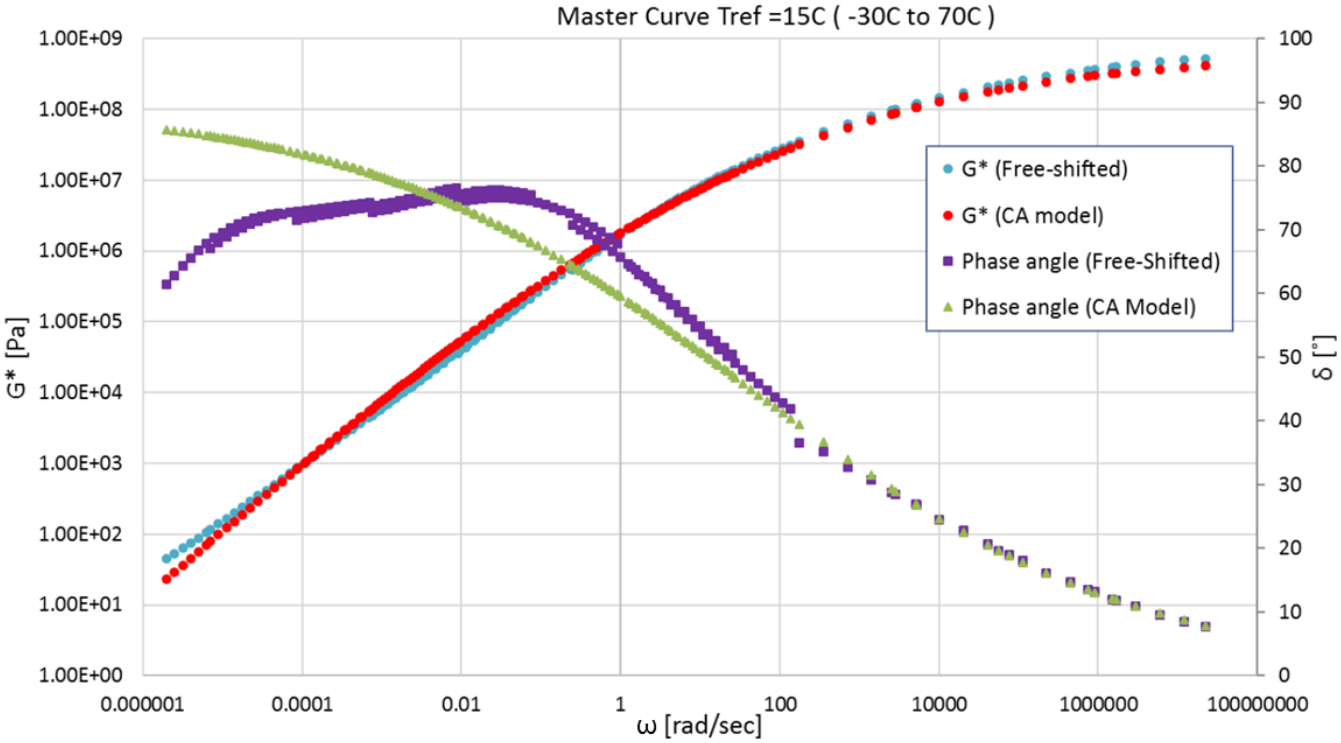

Figure 2-39: CA model of unaged S-E1 binder (Engelbrecht, 2018)

The CA model assumes a G_g value of 10^9 Pa for in shear and $3 \cdot 10^9$ Pa for flexure or extension, where the crossover frequency and R-value is fitted. The R- value describes the relaxation spectra and gives the best result near the crossover frequency, where the phase angle equals 45°, but it is still rather accurate when the phase angle is between 10 and 70°. However, when the viscous flow behaviour of a binder is reached, permanent deformation becomes a concern, but can be controlled by the loading time and steady state viscosity where the R-value can be assumed to be 0.81. (Christensen & Anderson, 1992)

Yusoff, Shaw & Airey (2011) found that the CAM model showed lack of fit for modified binders, as it lacks to describe the LVE rheological properties of modified binders.

Yusoff *et al.* (2013) observed that for the CA model, the R-value reduces while the ω_c increases for modified and aged binders. They further concluded that the CA model is unable to describe the Ethylene Vinyl Acetate (EVA) polymer behaviour accurately.

The **Christensen - Anderson - Marasteanu (CAM)** model was developed in 1999 by Anderson and Marasteanu by modifying the CA model (Yusoff, 2012). The CAM model attempts to improve the correlation in the higher and lower zones of the frequency range, by modelling both modified and unmodified binders at low and high temperatures. The additional parameter w describes how slow or fast the G*- or δ- data converges to asymptotes (diagonal and horizontal) as frequency goes to infinity or zero; and is related to the slope of the diagonal (viscous) asymptote. (Anderson & Marasteanu, 2010) (Mensching, Rowe, Daniel & Bennert, 2015)

$$|G^*(\omega)| = G_g \left[1 + \left(\frac{\omega_c}{\omega}\right)^v\right]^{-\frac{w}{v}} \quad (2\text{-}21)$$

$$\delta(\omega) = \frac{90w}{1+\left(\frac{\omega}{\omega_c}\right)^v} \quad (2\text{-}22)$$

Where,

v = *fitting / shape parameter [-]*

w = *fitting / shape parameter that controlling the arc length between asymptotes [-]*

It should also be noted that the v fitting parameter is equivalent to the CA model's log2/R. (Yusoff, 2012) For this reason, in numerous research literature, the G_g is assumed to be 10^9 Pa, with ω_c, v, w being fitted (Yusoff *et al.*, 2013).

Yusoff *et al.* (2013) observed that the CAM model for unmodified binders increases the R-value and decreases the ω_c with age and that it is in contrast with the CA model where a higher R-value will result in a smaller relaxation spectrum for the CAM model. As for the two fitting parameters, v decreases with age, while the w reduces with modification. These researchers concluded that although the CAM model is able to improve the CA model by adequately describing the unaged and aged conventional binder's properties, it still lacks to fit at extreme temperatures (Figure 2-40). (Yusoff, Shaw, *et al.*, 2011)

The CAM model works well in limited range 10^5 to 10^9 Pa with Modified Kaelble shift factor and where the data is acceptable if RMSE ≤ 2.25%. (Rowe, 2014b)

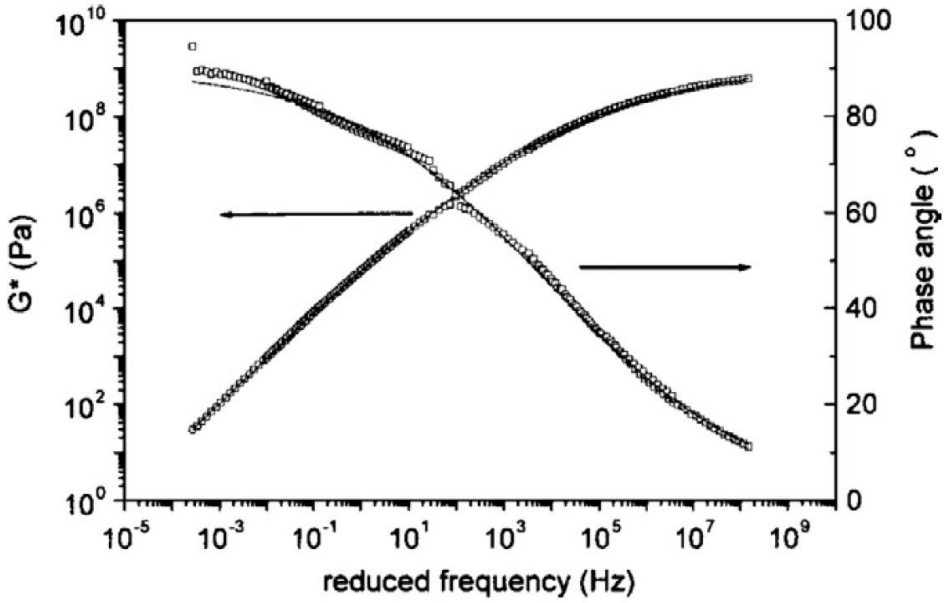

Figure 2-40: Modelling of the CAM model (Yusoff, Shaw, *et al.*, 2011)

The CA and CAM models were originally developed by Christensen and published by the Association of Asphalt Paving Technologists (AAPT), which describes binder master curves and works well for unmodified binders.

Binders and asphalt mixtures demonstrate different shapes of master curves. A master curve for a binder is successfully fitted by a hyperbolic function (CA and CAM), where a sigmoidal function is usually considered for an asphalt mixture. The sigmoidal model's upper and lower asymptotes relate to the aggregate and volumetric structure. The Standard Sigmoidal (SS) and Generalised Logistic Sigmoidal (GLS) models are used to accurately describe the master curve shape of an asphalt mixture. (Mensching, Rowe & Daniel, 2016)

The **Standard Sigmoidal (SS)** model was developed by the Belgium mathematician, Verhulst, in 1838. This model was adopted by the Asphalt Institute in 1982 and later introduced and used in the Mechanistic-Empirical Pavement Design Guide (MEPDG) in 2004. The SS model is a symmetrical four-parameter model that was developed specifically for asphalt mixtures. Figure 2-41 illustrates the definition of the SS model. (Alhaddad, 2015)

$$\log|G^*(\omega)| = min + \frac{\alpha}{1+e^{\beta+\gamma(\log\omega)}} \qquad (2\text{-}23)$$

Where,

min	*= Log equilibrium G*, lower horizontal asymptote (Log G_e)*
α	*= difference between the upper and lower horizontal asymptote value (Log G_g - Log G_e)*
ω	*= reduced frequency*
β	*= controls the horizontal position of the inflection point*
γ	*= slope of the curve*
β/γ	*= inflection point*

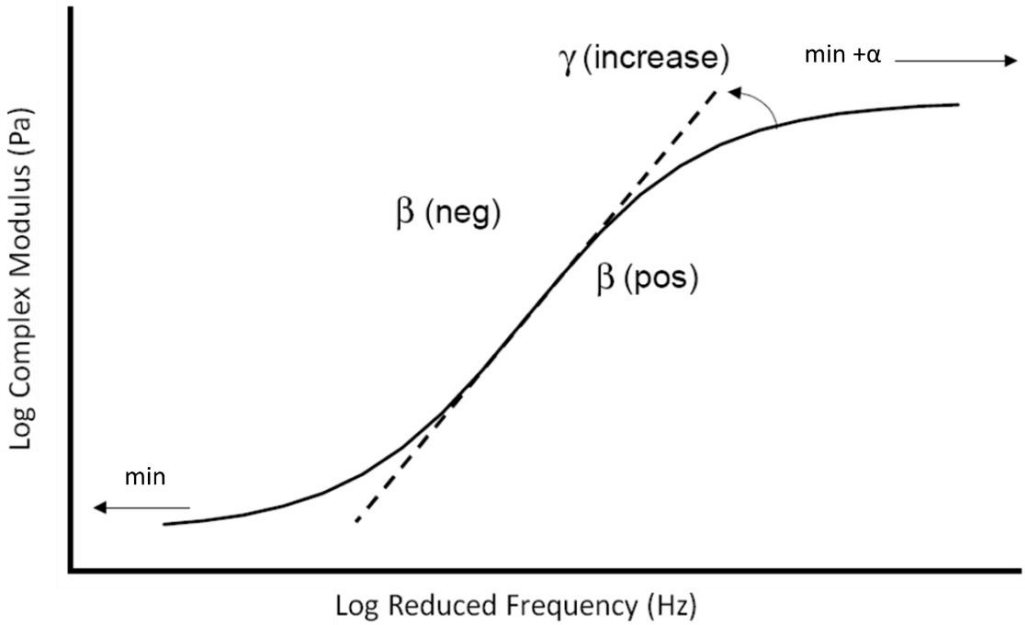

Figure 2-41: Definition of the Standard Sigmoidal model (Yusoff *et al.*, 2013)

However, between 1981 and 2005 the SS model was only used to model asphalt mixture but has since been modified to Equation 2-24 to also model unmodified and polymer-modified bituminous binders.

$$\log|G^*(\omega)| = min + \frac{max - min}{1 + e^{\beta + \gamma(\log \omega)}} \quad (2\text{-}24)$$

Where,

max = *maximum G*, upper horizontal asymptote, Log* G_g

Rowe (2009) developed a differential method to determine the phase angle at a certain time-temperature superposition. Equation 2-25 provides the phase angle function for the SS model:

$$\delta(\omega) = -90\alpha\gamma \frac{e^{\beta + \gamma(\log \omega)}}{\left[1 + e^{\beta + \gamma(\log \omega)}\right]^2} \quad (2\text{-}25)$$

Where,

α = *max – min or Log* G_g *– Log* G_e

The three fitting parameters (*min*, β and ɣ) are calculated by using the method of non-linear least square fit, being a numerical optimisation technique that was developed with the help of Microsoft Excel's Solver function. The β and ɣ defines the shape between the inflection point and the asymptotes (s-shape function parameters). The ɣ parameter has shown to be related to the width of the relaxation spectrum, where the standard value for ɣ is one (if ɣ < 1 the flatter the curve as shown in Figure 2-42). (Yusoff *et al.*, 2013) (Alhaddad, 2015) (Mensching *et al.*, 2016)

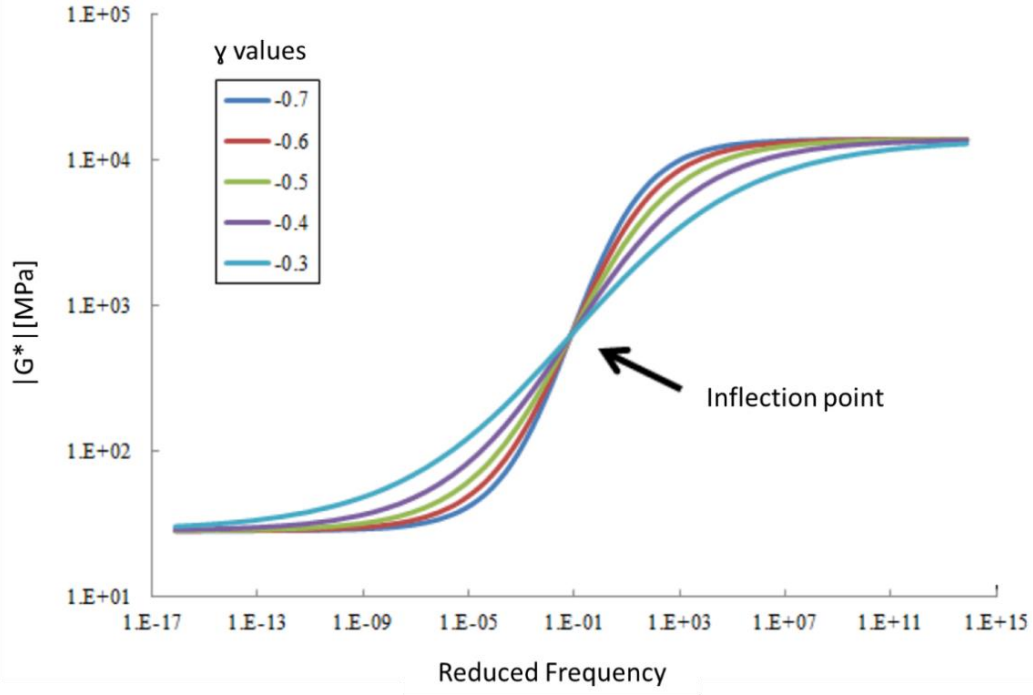

Figure 2-42: The SS model's |G*| graph with different ɣ values (Mensching *et al.*, 2016)

Since the G_g is 10^9 Pa for the SS model, which represents the upper asymptote, data at low temperatures and high frequencies are not required.

Yusoff et al. (2013) study on unmodified Middle Eastern, Russian and Venezuelan binders used the following reasonable initial values for modelling purposes: β = -1, *min* and ɣ =1.

Yusoff et al. (2013) study and Alhaddad's (2015) study on Iraqi asphalt observed that:

- the *min* values are all negative, which shows that the G* of asphalt is small at low frequencies and / or high temperatures;
- the ɣ, with or without ageing, does not influence the slope of the master curve from intermediate and high temperatures, due to the values being consistent; and
- the β values decreases with the presence of EVA and Styrene-Butadiene-Styrene (SBS) polymer in the bitumen and increases with age for unmodified binders.

According to the abovementioned findings it was concluded that although age did not influence the accuracy (Yusoff *et al.*, 2013), the SS model is unable to correlate the LVE rheological properties of highly modified bitumen.

In 2009 Rowe, Baumgardner & Sharrock recommended the generalisation of the Standard Sigmoidal model, called the **Generalised Logistic Sigmoidal (GLS)** or Richards Model to obtain a better fit of the master curve's non- symmetrical curve. The GLS model was developed by Richard in 1959, introducing an extra degree of freedom, allowing the inflection point to vary and forming a non-symmetrical sigmoid. (Yusoff, Chailleux, *et al.*, 2011) (Rowe, 2009)

$$\log|G^*(\omega)| = min + \frac{max-min}{\left[1+\lambda e^{\beta+\gamma(\log\omega)}\right]^{1/\lambda}} = \log G_e + \frac{\log G_g - \log G_e}{\left[1+\lambda e^{\beta+\gamma(\log\omega)}\right]^{1/\lambda}} \qquad (2\text{-}26)$$

$$\delta(\omega) = -90(max - min)\gamma \frac{e^{\beta+\gamma(\log\omega)}}{[1+\lambda e^{\beta+\gamma(\log\omega)}]^{\left(1+\frac{1}{\lambda}\right)}}$$
$$= -90\left(\log G_g - \log G_e\right)\gamma \frac{e^{\beta+\gamma(\log\omega)}}{[1+\lambda e^{\beta+\gamma(\log\omega)}]^{\left(1+\frac{1}{\lambda}\right)}} \quad (2\text{-}27)$$

Where,

λ = controls the height of the inflection point

Figure 2-43 shows how the additional parameter λ allows for a non-symmetrical shape of the G* graph. When $\lambda = 1$ the equation becomes the Standard Sigmoidal model and when λ trends to zero the equation becomes Gompertz. The Gompertz method was developed in 1825 and works well for highly modified binders. This additional parameter needs to be positive for the analysis as a negative value will not have an asymptote and will produce an unsatisfactory inflection point in the curve. (Rowe, Baumgardner & Sharrock, 2011)

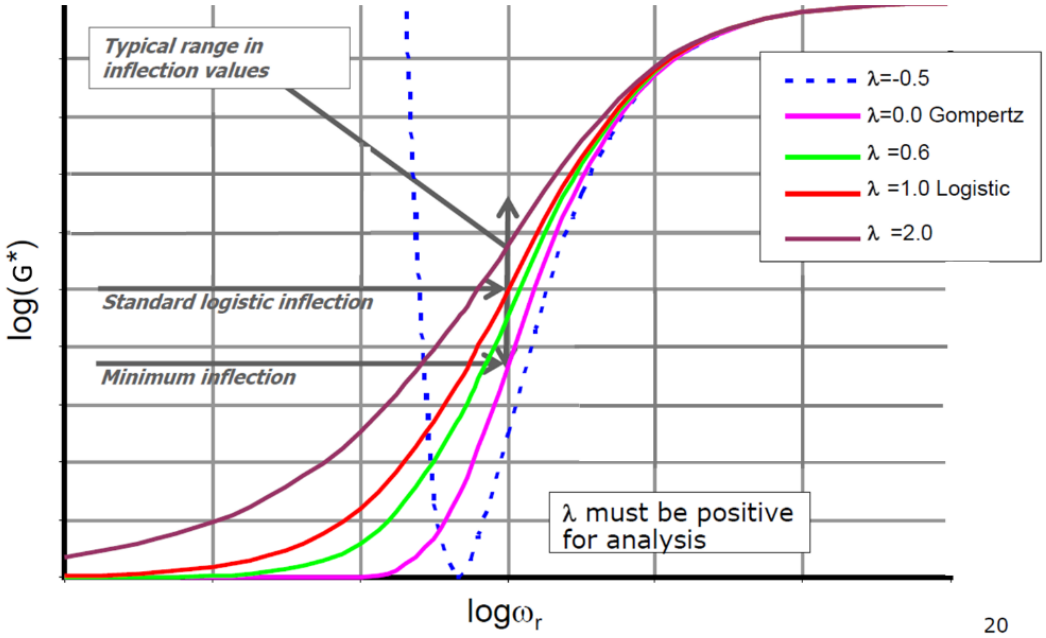

Figure 2-43: The GLS model's log G* graph with varies λ values (Rowe *et al.*, 2011)

Yusoff *et al*. (2013) modelled the G* graph by setting initial values of β, ɣ and λ to one and the *min* (lower asymptote) to zero, with a G_g fixed at 10^9Pa. Derived from findings it was found that the SS model is in line with the GLS model's observations. The addition to the GLS model's findings is that the parameter that makes a non-symmetrical analysis possible, λ, increases with age. If the SS model exhibits a non-symmetric behaviour, the GLS model will correlate better (Alhaddad, 2015).

However, the Generalised Logistic Sigmoidal (GLS) model is regarded to be a more comprehensive analysis tool for both asphalt mixtures and bituminous binders; the GLS model is still unable to predict highly modified bitumen. (Yusoff *et al.*, 2013) (Alhaddad, 2015)

If there is no structural re-arrangement over temperature and time of a bitumen, such as a phase change and the test being done within the LVE range of the binder, all empirical models generally seem to be able to describe the rheological behaviour of unmodified binders successfully, with the

GLS model being the front runner followed by SS, CAM and the CA models. All four of these models lack accuracy in respect of unaged polymer modified binders because of the presence of SBS and EVA.

Yusoff *et al*. (2013) also found that the GLS and SS models have outstanding experimental data correlation. When investigating the goodness-of-fit statistics, like the procedure of minimising the sum of square error (SSE), the GLS also generates the best fit, followed by SS, CAM and CA models. (Yusoff, Shaw, *et al.*, 2011) (Yusoff *et al.*, 2013)

Empirical modelling (CA, CAM, SS or GLS) is done to obtain the viscoelastic behaviour properties of the bituminous binder. The ageing ratio property in the proposed SATS 3208 (2018) Performance Grade (PG) Specifications for Bitumen in South Africa, Table 2-8, is the only property that is calculated by using the empirical modelling process. In short, the ageing ratio gives an indication of binder sensitivity to ageing, as discussed in Sections 2.8.5 and 3.5.2.

The rest of the properties as presented in Table 2-8 (excluding viscosity, storage ability and flash point), are calculated directly after rheometry testing (DSR and BBR), without going through the process of the empirical modelling.

2.8 Durability and Ageing Parameters

As a pavement ages, it will naturally crack and ravel over time.

Durability describes the ability of a binder to resist change in bitumen properties due to the effect of ageing, water and temperature variation for a particular traffic condition without deterioration and the ability to maintain satisfactory performance in-service. Glover, Davison, Domke, Ruan, Juristyarini, Knorr & Jung (2005) noted that although ageing leads to an increase in durability cracking, both fatigue and thermal, it also induces non-load cracking.

The main aim of the durability and ageing parameters listed hereunder are to evaluate in-service (temperature and time-related conditions) rheological properties: (Technical Guideline (TG) 1, 2019) (Hunter *et al.*, 2015) (Glover *et al.*, 2005)

- Glover and Glover-Rowe parameter (G-R);
- critical temperature difference (ΔT_c);
- viscoelastic transition (VET) stiffness and temperature;
- Rheological Index (R-value); and
- ageing ratios.

As mentioned in Section 2.7.4, the ageing ratio is the only property obtained from the SATS 3208, which is calculated by doing viscoelastic modelling. It is also important to note that viscoelastic modelling provides the opportunity to obtain other parameters / properties of bitumen such as G-R, VET (G^*_{VET} and T_{VET}) and Rheological Index, providing greater insight into the behaviour, performance and durability of the bitumen like the stiffness, relaxation, cracking and ageing susceptibility.

2.8.1 Glover and Glover-Rowe parameter

Glover *et al.* (2005) literature reports indicates that ductility of binders recovered from asphalt pavements correlates with cracking failure. Ductility measurement is a time and material consuming process and cannot be repeated as all materials are tested to failure.

Glover's initial parameter was based upon observation of low temperature ductility tests and the observation that these relate to non-load associated cracking. Glover considered a mechanical form (elongation model using a Maxwell element) for this test, involving springs and dashpots to describe the behaviour. From this it is evident that two rheological parameters are suggested to represent the extensional behaviour of asphalt binders, being the ratio of the dynamic viscosity to the storage modulus (η'/G') and the value of the storage modulus G'. The Glover parameter, also called the Glover viscosity function, is defined as: (Glover *et al.*, 2005)

$$Glover\ Parameter = \frac{G'}{\eta'/G'} \qquad (2\text{-}28)$$

Ductility at 15°C with an elongation rate of 1cm/min can be used to indicate durability, the η' and G' can be measured with a DSR at a frequency of 0.005 rad/s and 15°C. Glover proposed two limits for the Glover parameter, namely crack warning at $3 \cdot 10^{-3}$ MPa/s and crack limit at $9 \cdot 10^{-4}$ MPa/s, which correlate to ductility crack limits of 3 and 5 cm. (Glover *et al.*, 2005)

Glover *et al*. (2005) concluded that for unmodified binders the Glover parameter can serve as a surrogate for ductility, especially below a 10 cm ductility as can be seen in Figure 2-44. Accordingly, Glover *et al*. (2005) evaluated polymer modified binders and found that the ductility versus Glover parameter correlation improves when similar binder types are grouped (Figure 2-45).

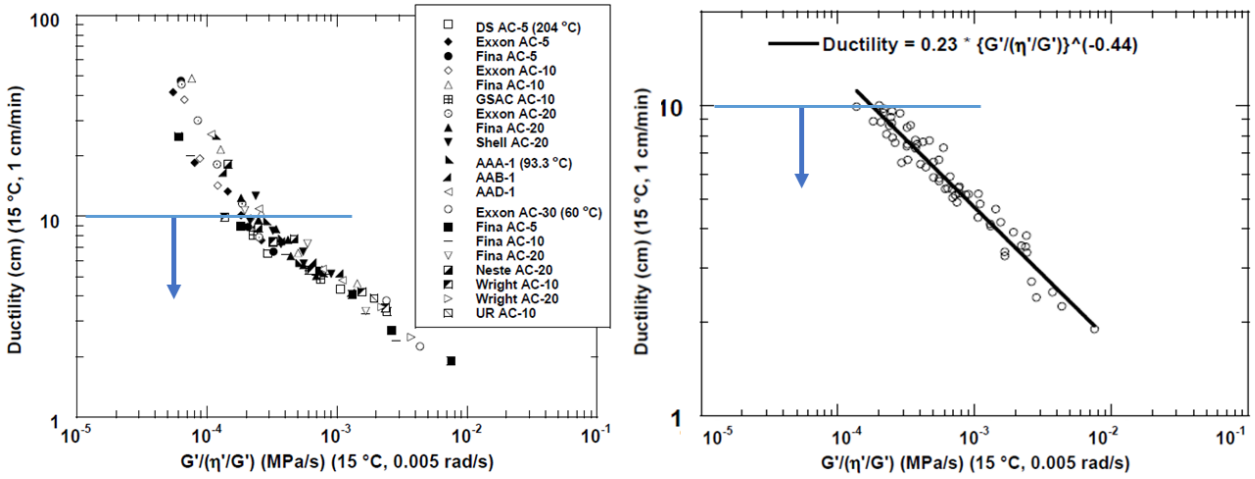

Figure 2-44: Ductility versus Glover parameter correlation for aged unmodified binders (Glover *et al.*, 2005)

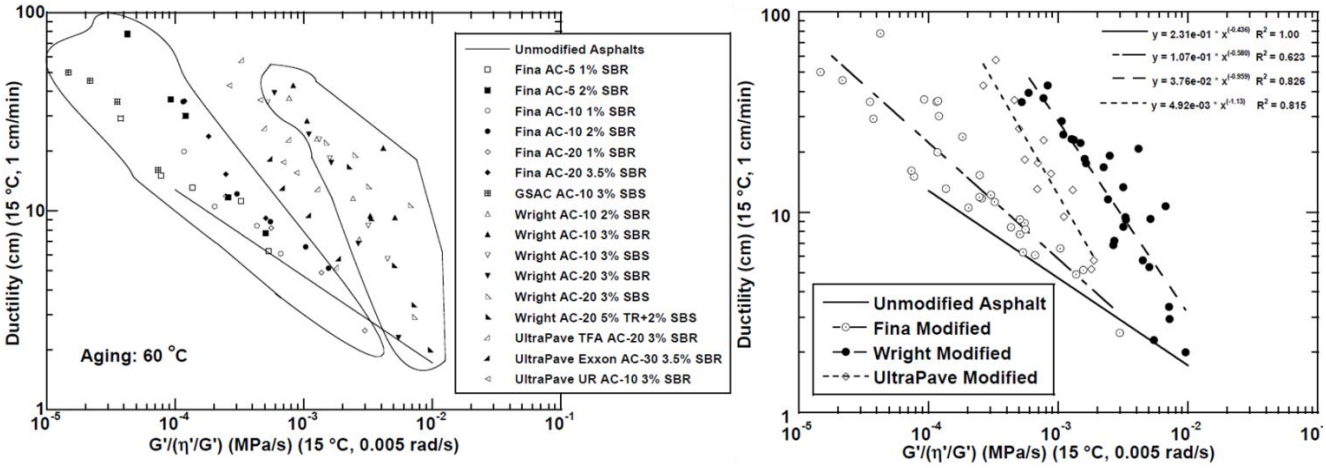

Figure 2-45: Ductility versus Glover parameter correlation for modified binders (Glover *et al.*, 2005)

Rowe, King & Anderson (2014) simplified the Glover parameter to only be described by G* and δ as follows:

$$\eta' = \frac{G''}{\omega} \text{ and } G' = \frac{G''}{\tan\delta}$$

hence

$$\frac{\eta'}{G'} = \frac{1}{\omega}\frac{G''}{G'} = \frac{\tan\delta}{\omega}$$

and

$$\frac{G'}{\eta'/G'} = \frac{G'}{\left(\frac{\tan\delta}{\omega}\right)} = \frac{G'\omega}{\tan\delta}$$

Thus, in the simplest format:

$$\frac{G'\omega}{\tan\delta} = \frac{G^*\cos\delta}{\tan\delta}\omega = \frac{G^*(\cos\delta)^2}{\sin\delta}\omega$$

With this test tested at a constant frequency, the ω falls away, which conclude to the Glover-Rowe parameter (G-R):

$$G - R = \frac{G^*(\cos\delta)^2}{\sin\delta} \qquad (2\text{-}29)$$

A limiting value of $9{\cdot}10^{-4}$ MPa/s crack limit at 0.005 rad/s was initially proposed for the onset of cracking, noting that when expressed in the G-R parameter format that the warning value becomes 180 kPa. A second value is suggested by Anderson for the development of significant cracking at 600 kPa. Thus, both these values 180 and 600 kPa are equivalent to 5 and 3 cm ductility at 15°C (Rowe, et al., 2013)

Since the G-R parameter is in terms of G* and the phase angle, ductility-based failure planes can be plotted in a Black Space diagram (G* versus δ), as per Figure 2-46, in order to monitor the effect of ageing on the binder. The Black Space diagram compares the stiffness (G*) and relaxation

properties (δ) of a binder without the need of the mathematical principle of time-temperature superposition, where Mensching *et al.* (2015) mentioned that different areas in the Black Space diagram might be related to different types of failure:

- Damage onset at G-R ≥ 180 kPa, where frequency is 0.005 rad/s and temperature 15°C;
- Significant cracking at G-R ≥ 600 kPa, where frequency is 0.005 rad/s and temperature 15°C;
- Fatigue cracking at G*sin δ ≤ 5 MPa, where frequency is 10 rad/s and temperatures varies; and
- Thermal cracking at G-R ≤ 184 MPa, where frequency is 0.01667 rad/s and temperatures varies.

Note that these limits may change depending upon location, climate and type of cracking.

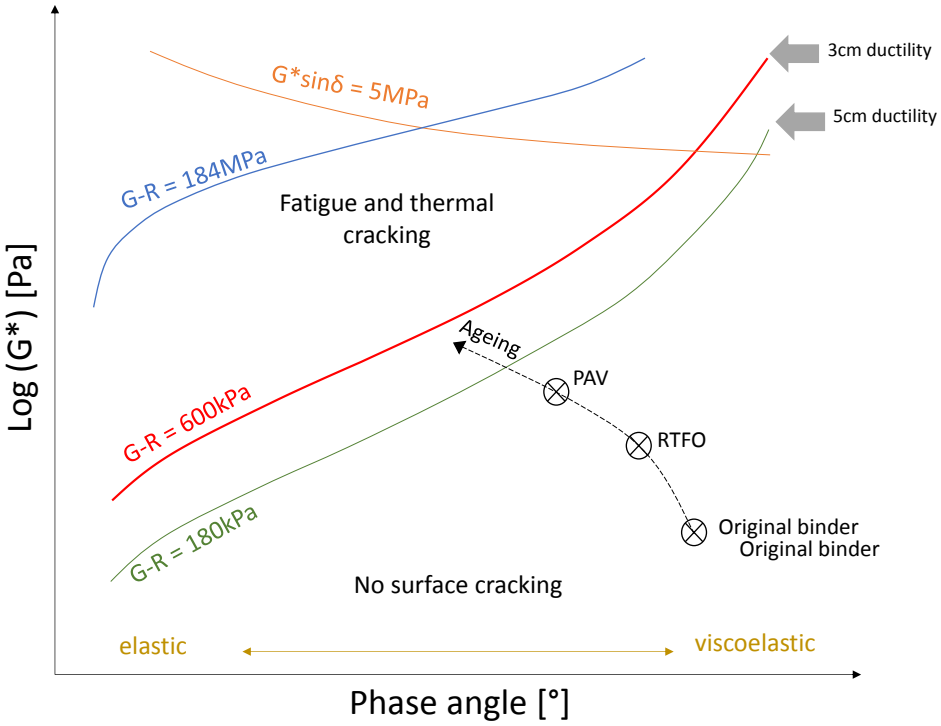

Figure 2-46: Ageing of binders in the ductility-based failure planes (adapted from Rowe, King & Anderson, 2014)

2.8.2 Critical temperature difference

Rowe *et al.* (2014) concluded that critical temperature difference (ΔT_c) and the G-R parameter are essentially describing similar behaviours, quantifying the loss of relaxation properties and concluding its susceptibility to low temperature durability cracking as the binder ages. The difference in critical low temperatures can be computed in accordance with ASTM D7643 and AASHTO PP78-16 standards: (King *et al.*, 2011)

$$\Delta T_C = T_{c,S(60)} - T_{c,m(60)} \quad (2\text{-}30)$$

With

$$T_{c,S(60)} = T_1 + \left[\frac{\log 300 - \log S(60)_1}{\log S(60)_1 - \log S(60)_2}(T_1 - T_2)\right] - 10 \quad (2\text{-}31)$$

$$T_{c,m(60)} = T_1 + \left[\frac{0.3 - m(60)_1}{m(60)_1 - m(60)_2}(T_1 - T_2)\right] - 10 \quad (2\text{-}32)$$

Where,

ΔT_c = *critical low temperature difference*

$T_{S(60)}$ = *stiffness critical temperature at 60 seconds*

$T_{m(60)}$ = *relaxation critical temperature at 60 seconds*

The stiffness (S) and relaxation (m) of the binder is defined in Section 2.6.3.2, where Equation 2-31 and 2-32 shows certain limitations and which should be considered when applied, as contained in the SATS 3208 , being S(60) ≤ 300 MPa and m(60) ≥ 0.3.

The ΔT_c indicates the difference in low temperature grade between stiffness and relaxation with BBR, where the binder is S-controlled or m-controlled. Binder is S-controlled when $T_{c,S(60)}$ is greater than $T_{c,m(60)}$, thus $\Delta T_c > 0$ and m-controlled when $\Delta T_c < 0$ (negative value). According to the SATS 3208 it is required that $\Delta T_c > -5°C$.

It is also evident that there is a relationship between the G-R parameter (DSR) and ΔT_c parameter (BBR), where both measure the stiffness (G or S) and relaxation (δ or m) at intermediate and low temperatures, respectively. The AAPT paper from King *et al.* (2011) and Rowe *et al.* (2011) recommends two minimum thresholds for ΔT_c at -2.5°C for cracking warning and -5°C as a cracking limit, as shown in Figure 2-47.

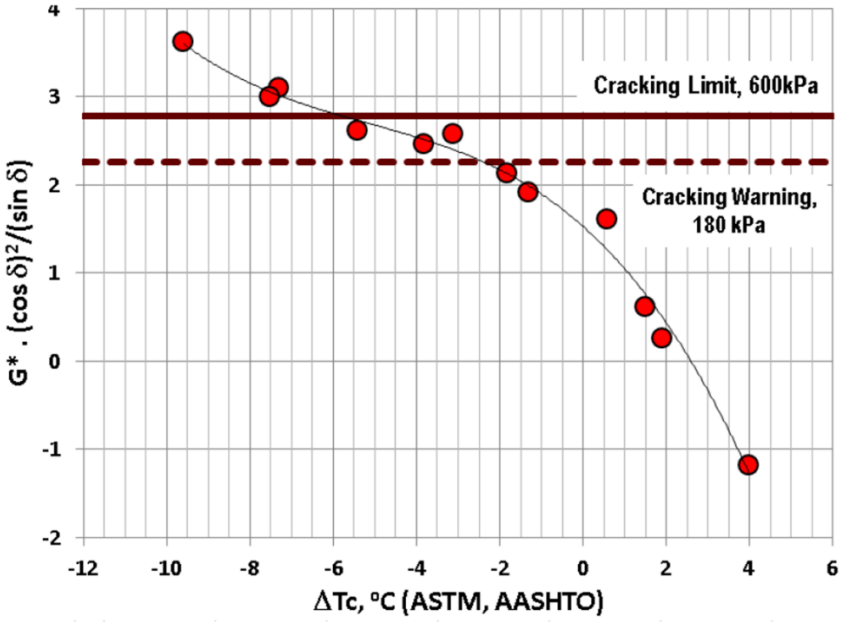

Figure 2-47: Relationship between the G-R and ΔT_c parameter (King *et al.*, 2011)

The critical temperature difference (ΔT_c) concept is linked to ductility, viscosity function, R-value, Black Space parameter and the shape of the BBR master curve. In 2014, Rowe converted the low temperature specification (S and m) to link with G* and δ values in order to allow the Black Space method to be more robust, where S(60) ≤ 300 MPa and m(60) ≥ 0.3 correspond to G* ≤ 111 MPa and δ ≥ 26.2°, respectively. This lead to the G-R low temperature limit of 184 MPa, as shown in Figure 2-48 (Rowe, 2014a)

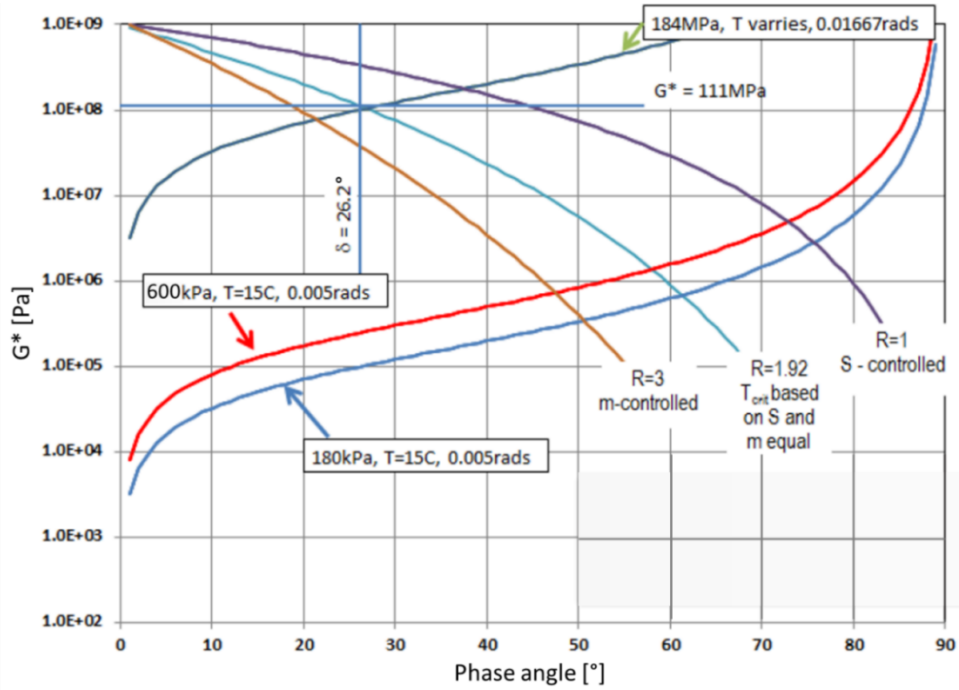

Figure 2-48: Extending the S and m values to the G-R concept (Rowe, 2014a)

2.8.3 Viscoelastic transition (VET) stiffness and temperature

The viscoelastic transition (VET) concept was originally developed by French researchers. They noted that a phase angle that equals 45° is related to surface cracking and observed a relationship between binder properties and fatigue cracking using 7.8 Hz, but was adopted by the UK specifications to 0.4 Hz. (Rowe, 2014a)

The viscoelastic transition temperature (T_{VET}) is based on the concept of G' = G'' when expressed as a function of temperature, i.e. $\delta = 45°$ and quantifies the ability of an unaged or aged binder to dissipate stress, confirming binder's susceptibility to cracking at a frequency of 0.4 Hz. It has been reported by Widyatmoko, Heslop & Elliott (2005) that a higher penetration grade binder (softer binder) has a lower T_{VET} than a lower penetration grade binder (harder binder), making the higher penetration grade binder more viscous and resistance to cracking at low temperatures. (Airey, Choi, Collop & Elliott, 2004)

Widyatmoko, Elliott, Heslop, and Williams took a step forward in 2002 and introduced a new parameter G^*_{VET}, complex shear modulus at T_{VET}, to assess the ageing of binders.

Figure 2-49 illustrates the trend between T_{VET} and G^*_{VET}, whereas the binder ages the T_{VET} increase and G^*_{VET} reduces, generally giving a poorer performance. All binders were tested at original (unaged) and RTFO, with the UK binders 50pen (penetration) and 10pen being tested at High Pressure Ageing test (HiPAT), which is PAV at 65 hours and 85°C. (Widyatmoko *et al.*, 2005)

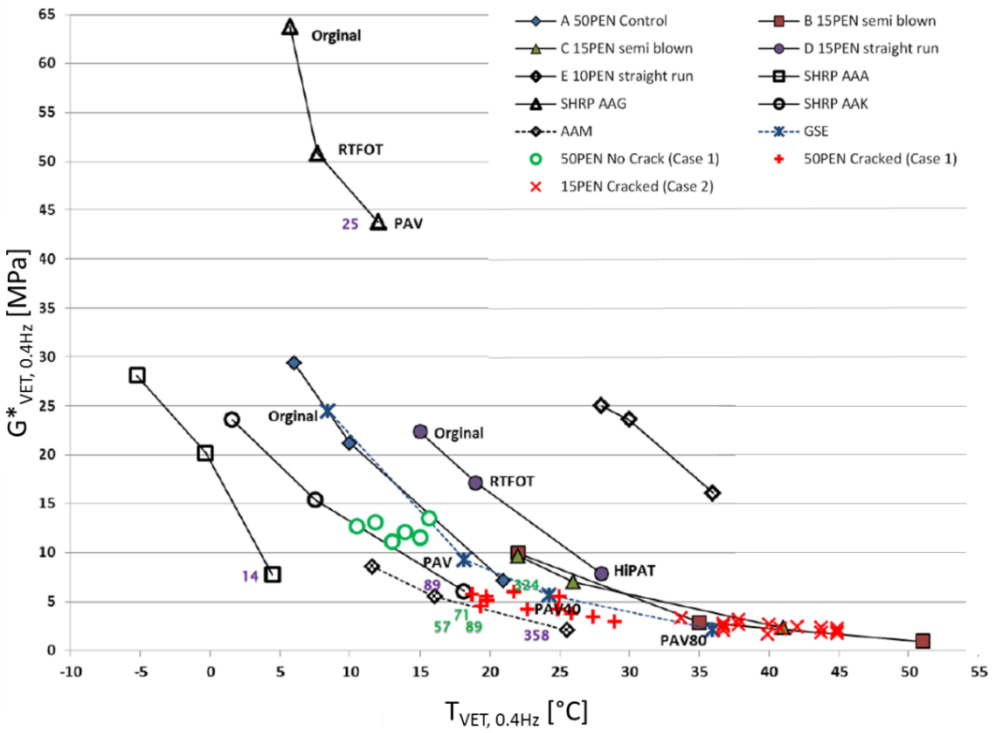

Figure 2-49: VET concept with age (Rowe, 2014a)

It is important to note that the VET criteria will differ for different binder grades, where Widyatmoko *et al.* (2005) proposed a tentative specification at 0.4 Hz to minimise crack susceptibility of binders:

- 15 penetration grade bitumen: $T_{VET} < 35°C$ and $G^*_{VET} > 5$ MPa
- 50 penetration grade bitumen: $T_{VET} < 20°C$ and $G^*_{VET} > 10$ MPa

G-R and VET can be regarded to be interrelated, with the VET criteria being grade dependent. G-R parameter can be plotted within the VET space and explains VET cracking parameter, where the VET cracking approach is related to the R-value, hardness susceptibility, temperature susceptibility, stiffness properties and relaxation properties. (Rowe, 2014a)

There is also an interrelationship between CAM and VET, when the complex shear modulus equals 10^9 Pa and the CAM model is shifted with the Modified Kaelble equation as shown in the equations below: (Rowe, 2014a)

$$T_{VET} = T_d + \chi\left(\frac{C_2}{1-|\chi|}\right) \quad (2\text{-}33)$$

$$G^*_{VET} = G_g\left(2^{\frac{-w}{v}}\right) \quad (2\text{-}34)$$

Where,

$$\chi = \frac{T_{ref}-T_d}{C_2+|T_{ref}-T_d|} - \frac{\log\omega_C - \log\omega_{VET}}{C_1} \quad (2\text{-}35)$$

2.8.4 Rheological Index

There are two ways of obtaining the R-value, being Equation 2-17 or from the master curve, being the difference between the G_g and G* at ω_C (where δ = 45°), as discussed in Section 2.7.3.

The Rheological Index gives a good indication of the change in the material's behaviour with ageing whilst field performance shows that cracking is related to the R-value. In the Black Space diagram, the G-R damage zones (Figure 2-46) can be replaced with the R-value as a potential damage parameter, as illustrated in Figure 2-50. A range of R-values between 2.3 and 2.7 might predict onset and spread of damage. (Rowe *et al.*, 2014)

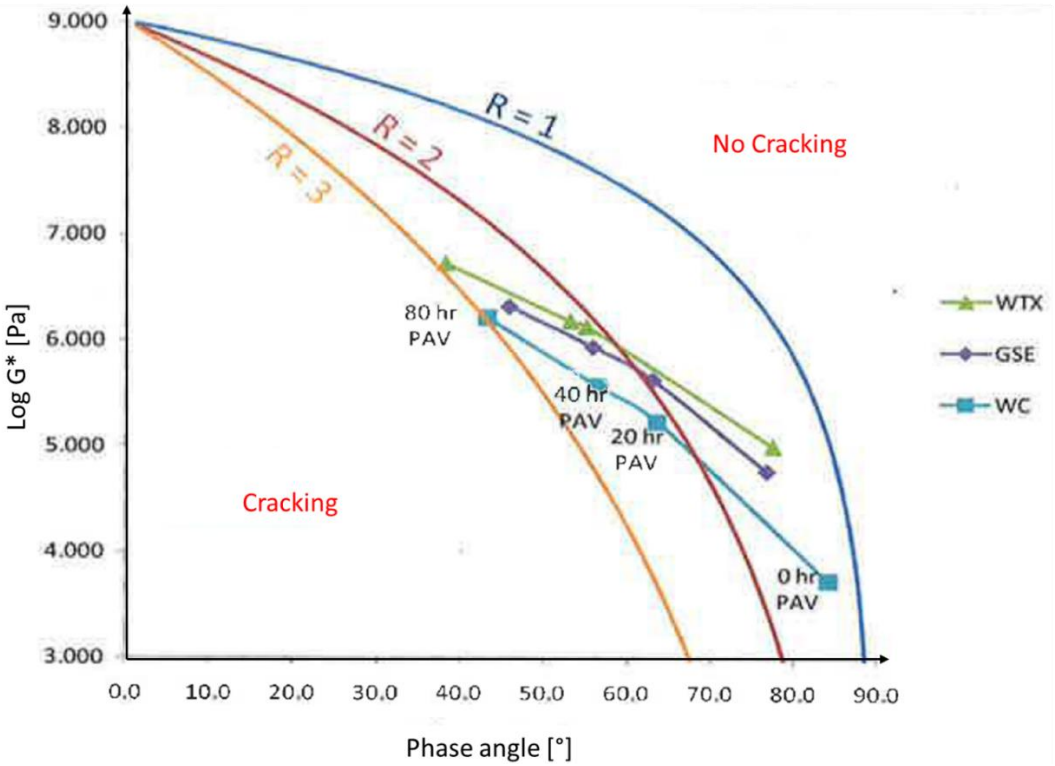

Figure 2-50: Using R-value as damage parameter for ageing in Black Space (Rowe *et al.*, 2014)

The R-value and ω_c are only expressed reliable when the data is in a range from 10^5 to 10^9 Pa. If the R-value < 3 (most typical binder) then the G-R critical values are all in the range captured by LVE analysis, which suggests limits on interrelationship of > 10^5Pa. R-value relate to stiffness and relaxation, where a low R-value is equal to S-controlled and a high value m-controlled.

This demonstrates and makes it evident that the R-value is related to the parameters ω_C, VET, G-R and that phase angle = 45°, providing information regarding the relaxation spectra and the chemical composition of the binder. (Rowe, 2014a) Table 2-11 shows different R-values calculated with specified frequency, temperature and glassy modulus.

Table 2-11: Various R-values (Rowe, 2014a)

	R-values
10 rad/s, 15°C, G_g = 10^9 Pa	2.15
10 rad/s, 25°C, G_g = 10^9 Pa	2.19
10 rad/s, 15°C, G_g = calculated	2.69
10 rad/s, 25°C, G_g = calculated	2.61
All the data	2.47
Reduced data	2.71

2.8.5 Ageing Ratios

Bituminous binders age primarily due to two distinct mechanisms, i.e. *volatilisation* of the light oils present in the bitumen and *oxidation* by reacting with the oxygen in the environment. Ageing can generally be placed into two categories, namely short- and long-term ageing. (Hunter *et al.*, 2015)

The most convenient way to look at rheological behaviour as the binder ages is the use of the Black Space diagrams (G* versus δ), as can be seen in Figure 2-51 showing that as the binder ages the Black Space diagram moves to the left and it decreases in phase angle. (King *et al.*, 2011)

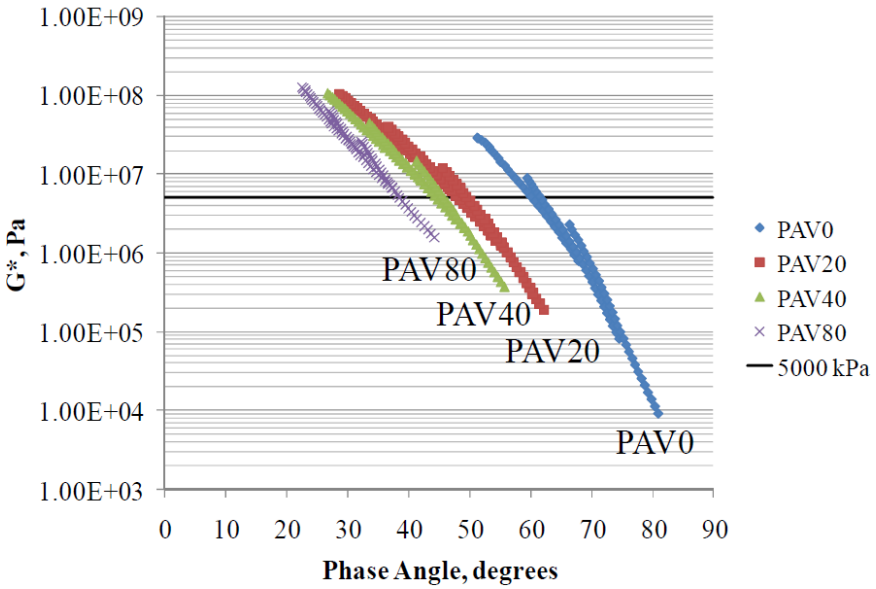

Figure 2-51: Black Space plot of Western Canadian PG64-28 binder with age (King *et al.*, 2011)

The ageing ratio measures rheological change and is normally expressed as the difference between the original (unaged) and the aged properties exhibited over time. The ageing ratio provides an indication of the sensitivity of the binder to short- (after RTFO) and long-term ageing (after RTFO and PAV), being the rate at which the properties deteriorate.

The ageing ratios are determined relative to the stiffness, G*, of a binder with the increase of ageing at intermediate temperatures and a frequency of 10 rad/s:

$$Short\ term\ ageing\ index\ = \frac{G^*_{RTFO}}{G^*_{Original}} \quad (2\text{-}36)$$

$$Long\ term\ ageing\ index\ = \frac{G^*_{PAV}}{G^*_{Original}} \quad (2\text{-}37)$$

As binder ages the R-value increases and the crossover frequency reduces, where rejuvenation should produce an opposite effect, as shown in Figure 2-52.

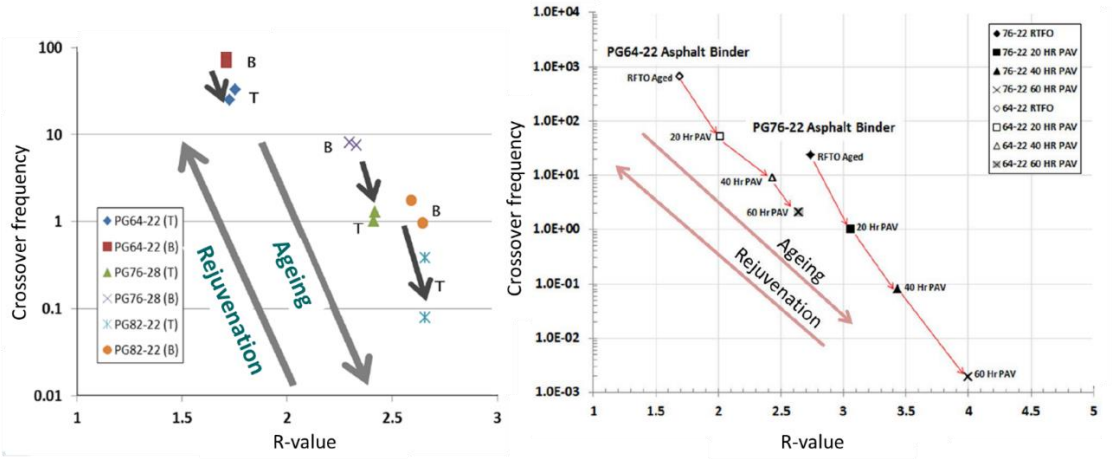

Figure 2-52: Effect of ageing on ω_c and R-value (Rowe, 2014a)

2.9 Summary

At present there are no guidelines or any specifications that can be used for seal surfacing in South Africa, causing major concern, inconsistency and undue surface failures. Hence the industry needs for the development and formulation of appropriate specifications which considers performance graded binders as opposed to penetration grade binders, covering all binders (modified and unmodified) and applications (asphalt and seals) for material behaviour over the entire performance spectrum (wider range of temperatures and loading frequencies).

The first step in this direction was accomplished in 2018 with the publication of the SATS 3208 Performance Grade (PG) Specification for Bitumen as interim temporary partial solution. Much work still needs to be done to have an all-inclusive and compressive specification of which seal surfacing is also an outstanding matter.

To contribute to the SATS 3208 (2018) this thesis aims to investigate and address identified shortcomings in relation to empirical testing, by providing reliable research data in order to include specifications for seal performance characteristics:

- understanding the behaviour of bitumen better;
- enabling to use of bitumen in the best possible way in pavements;
- ensuring an effective pavement life, which is safe for road users; and
- minimising failure mechanisms within pavement surfaces.

The most effective, appropriate and applicable test methods and modelling equations as identified in this Literature Chapter will be used to achieve this thesis's objectives and identify any further shortcomings.

Previous research confirmed that ageing of seal binders over a period of time decreases the performance and durability of the material that can also lead to failure within seals, such as cracking (cohesive failure) and ravelling (adhesive failure). The ageing ratio parameter in the SATS 3208 (2018) provides an indication of the sensitivity of the binder in relation to short- and long-term ageing, being the rate at which the properties deteriorate.

Other parameters will also be applied, such as the Glover-Rowe (G-R), viscoelastic transition (VET) and Rheological Index to validate binder ageing susceptibility.

Chapter 3: Research Materials and Methods

3.1 Introduction

In order to address the concerns and research objective as set out in Sections 1.2 and 1.3, seal binders in its original, in-service and aged (RTFO and PAV) state will be researched in this study. The focus is to define and compare seal binder's rheological performance properties with the SATS 3208 Performance Grade (PG) Specifications for Bitumen in South Africa (2018).

The most effective, appropriate and applicable test methods and modelling equations as identified in Chapter 2 will be used to achieve this thesis's objectives and identify any further shortcomings.

The effective, appropriate and applicable test methods and modelling equations as discussed in Chapter 2 are used as basis and point of departure to determine seal performance over time.

3.2 Experimental Design

The experimental design is presented in a schematic flow chart (Figure 3-1), illustrating the steps required to accomplish the research objectives set out in Section 1.3. The experimental design consists of three categories as discussed in the mentioned subsections, namely:

- Material Obtained and Selected (Section 3.3): The various material sources and regions, retrieval of in-service seal samples and to obtain related original binders.
- Test Methods and Material Preparation (Section 3.4): The extraction and recovery methods to retrieve seal samples; and Rolling Thin Film Oven (RTFO) and Pressure Ageing Vessel (PAV) ageing methods for original binders, including sample preparation for Dynamic Shear Rheometer (DSR) testing.
- Viscoelastic Modelling and Data Analysis (Section 3.5): The analysis of DSR data with Rhea Software, the viscoelastic modelling of the analysed DSR data and then analysing its durability parameters.

In recent years the PG Specification (SATS 3208) has become increasingly popular to classify bituminous binders in pavements, given the inadequacies of the Penetration Grade Specification (South African National Standards (SANS) 4001, 2016).

As currently contained in the SATS 3208, the prescribed USA (ASTM) and Europe (EN) standards will be used in conjunction with SA SANS, TG1 and CSIR standards.

The specific standard used for each procedure followed in the experimental design, Figure 3-1, is defined in each of the sections mentioned above.

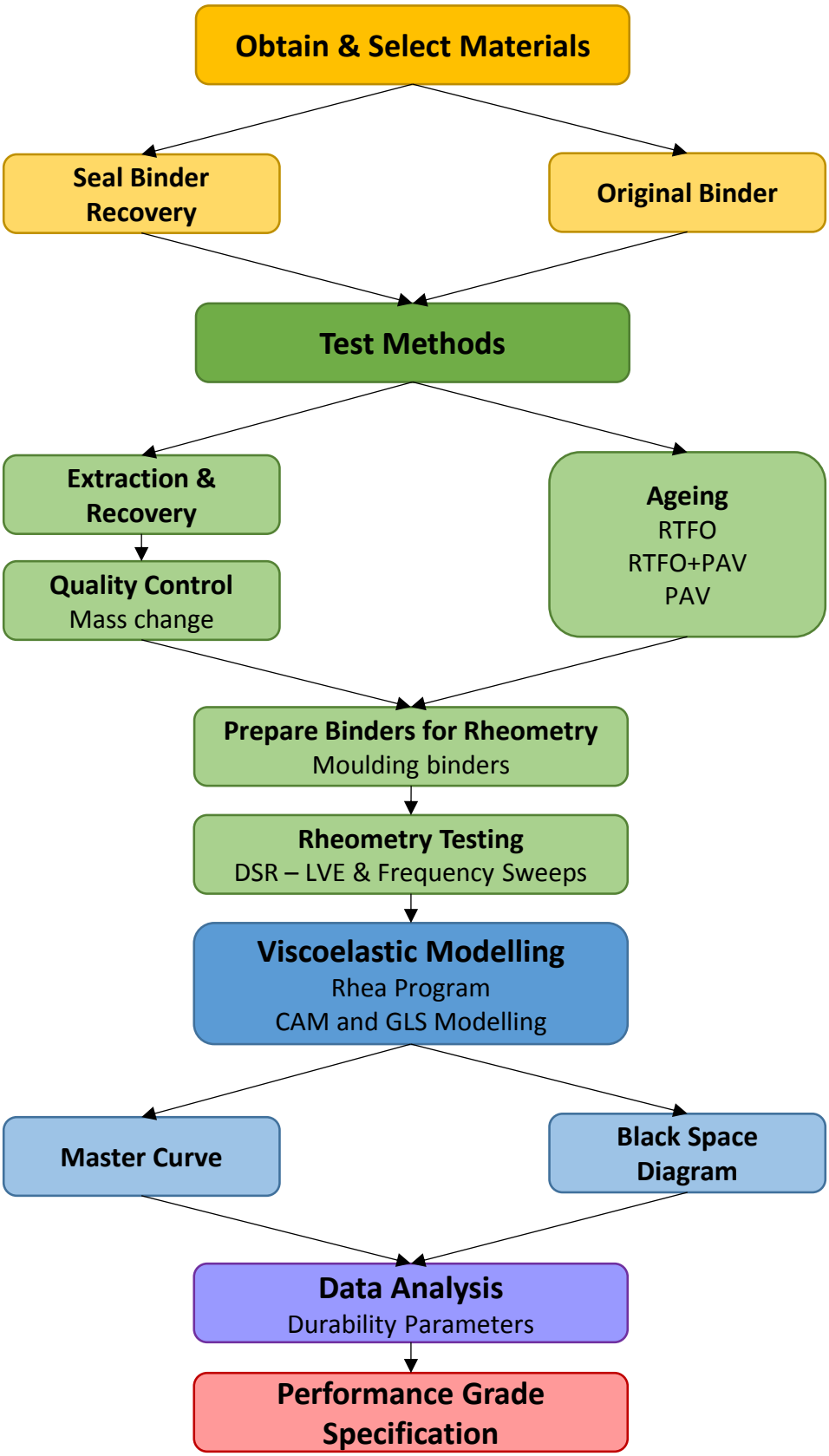

Figure 3-1: Experimental Design flow chart

3.3 Material Obtained and Selected

The bituminous binder used in this study was selected by taking into account what has already been studied and what was available.

Goosen (2018) studied retrieved single and double seals with binder types 70/100 and S-E1, whilst Engelbrecht (2018) studied the most common seal binders by ageing the binders from their original form, namely 70/100, S-E1 and S-E2.

In this study 32 retrieved seal samples and 6 original binders were sourced by Van Zyl (2018b) as part of Van Zyl's ongoing PhD research. Of which only 14 retrieved seal samples and 6 original binders were selected to conduct this study, based on the following criteria:

- Sample surface age and performance grade: Construction and retrieved date must be known to compute the age of each road section that was retrieved, by investigating age deterioration for the performance grade specification purposes.
- Sample Seal Structure: Cape seal (S4) and multiple seal (M).
- Sample Binder Type: Conventional binders are cationic (CAT) 65 % tack, CAT 65 % tack + CAT 65 % fog, 80/100 + CAT 65 % fog, 80/100 and slurry for Cape seals that is equal to anionic 60 %. All of the mentioned conventional (unmodified) binders shall revert back to 70/100 penetration bitumen. Modified binders shall either be S-E1, S-E1 + fog or SC-E2.
    - Unmodified binders 70/100 penetration grade bitumen is obtained from the refining process of crude oil and has a penetration value that lies between 70 and 100.
    - S-E1 is a hot applied elastomer modified seal surface binder.
    - SC-E2 is an emulsion elastomer modified seal surface binder.
- Sample Provincial Regions: Western Cape (WC), Eastern Cape (EC), Free State (FS), Limpopo and KwaZulu- Natal (KZN)
- Sample Road Types: Divisional Road (DR), Main Road (MR), Regional Road (R) and National Road (N)

Table 3-1 summaries the retrieved and original seal binder samples selected. Figure 3-2 shows the two forms of retrieved samples obtained as well as the original binders stored in steel containers. It is important to note that prior to retrieval of such sections the seal samples have not been subjected to any additional conditions (traffic, extreme weather or testing) that could influence the integrity of the binders within the retrieved seal samples.

This study's retrieved seal samples were retrieved by Van Zyl, Gerber and Lombard.

The method that was used to retrieve these seal samples from the field was based on the resin casting process developed by Gerber (2014) as shown in Figure 3-3.

A concrete saw was used to make dimension cuts (marked out desired dimensions) for a suitable seal sample in the road. The surfacing seal and base course was sawed approximately 150 mm deep or as deep as the concrete cutter blade allowed. The saw dust in the dimension cuts were cleaned by a high pressure air hose, before filled with quickset resin, to form a protective cast around

the sample. After the quickset resin casting was dry, a second extraction cut was made along the outside perimeter of the resin casket (2 cm apart). Material surrounding the sample was carefully excavated, making the retrieving of the in-situ seal sample from the road at the base-subbase interface easier. (Gerber, 2014) (Roelofse, 2014)

Table 3-1: Retrieved and Original seal binders selected for investigation

Road	Km	Seal Type	Binder Type	Province	Construction Date	Retrieved Date	Age (years)	Original Binder	Failure
DR1398	1	S4(19)	70/100	WC	1989	2011	22		Agg Loss & Croc
MR23	17	S4(19)		WC	2008	2011	3		Agg Loss
MR174	9	S4(19)		WC	2002	2011	9		Agg Loss & Croc
R56/7	5.6	S4	S-E1	EC	Feb-2017	Jan-2018	0.92	√	
N8/11	40.8	S4		EC	Sep-2015	Jan-2018	2.33	√	
N2/16	71.5	M(20/7/7)		FS	Mar-2017	Jan-2018	0.83	√	
N6/4	8	M(19/6/6)	S-E1 + fog	EC	2002	2011	9		Agg Loss
N10/2	11	M(19/6/6)		EC	2005	2011	6		Agg Loss
N1/29	79.8	M(19/6/6)		Limpopo	2002	2011	9		Agg Loss
N1/29	102.6	M(19/6/6)		Limpopo	2006	2011	5		Agg Loss
N2/31	59.6	M(19/6/6)		KZN	2005	2011	6		Agg Loss
R61/6	88.05	S4	SC-E2	EC	Jul-2018	Jan-2018	0.5	√	
R61/7	2.72	S4		EC	Jul-2018	Jan-2018	0.5	√	
R61/8	51.01	S4		EC	Feb-2018	Jan-2018	0.08	√	

(a) 300 x 300mm slab (b) Dimensions vary in bags (c) Steel containers

Figure 3-2: Retrieved and original seal samples

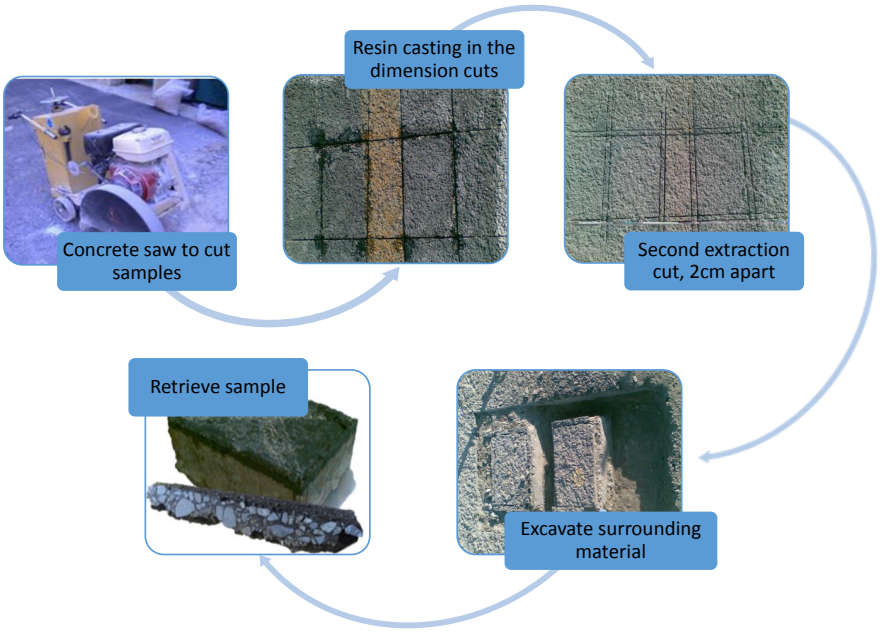

Figure 3-3: Field sample retrieving process (adapted from Gerber, 2014 and Roelofse, 2014)

3.4 Test Methods and Material Preparation

The material testing and preparation was conducted in either the Pavement Laboratory of Stellenbosch University Civil Engineering Faculty or that of Much Asphalt, based on availability of required testing equipment.

3.4.1 Storage and handling temperatures of bitumen

Bitumen can be reheated or maintained at elevated temperatures for a considerable time when it is handled properly, without affecting its properties. Mistreatment, by way of overheating or using conditions which promote oxidation can adversely affect the bitumen properties and influence the long-term performance of the bitumen. Depending on the hardness (grade) of the bitumen the range of temperature is between 140°C to over 200°C. (Morgan *et al.*, 1995)

In this study, original and recovered binders were heated to approximately 150°C for conventional binders and approximately 170°C for modified binders, as it is stiffer and needs higher temperatures to be able to physically handle the binder. The age of the binder also plays a role in the handling temperature, as older binders are stiffer.

3.4.2 Solubility and Recovery

To test only the bituminous binder of the retrieved road sample, a two-step process was followed as discussed in Section 2.6.1. The solubilisation includes the extraction and centrifugal procedures, in accordance with SANS 3001-AS20 (2011) and for the recovery process the EN-12697-3 (2013) was followed.

Due to the environmental and safety hazards involved (toxic and volatile chemicals) the toluene solvent originally selected had to be changed to trichloroethylene (TCE) solvent.

Toluene (C_7H_8) was originally selected as the preferred solvent, as it had no corrosive chemicals, with no severe health hazards and is easily obtainable. However, as research continued it was noted

that De Jonghe, Van den Bergh, Verheyen, Schoeters, Vuye & Van Leugenhagen (2005) from the Netherlands identified that toluene solvent is not used in the centrifuge as it is likely to cause an explosion. For similar reasons Mikhailenko & Baaj (2017) indicated that toluene is not used in the centrifuge extraction method in laboratories over US, Canada and Europe.

Accordingly, the solvent was changed to TCE as the solvent to be used further in this study. Trichloroethylene (C_2HCl_3) as can be seen in Table 2-10 is used the most for extraction and recovery procedures in laboratories, even when it:

- has the highest volatile chemical percentage of all the solvents;
- has corrosive chemical concerns; and
- is difficult and expensive to obtain (imported from China).

The equipment selected for the solubilisation (extraction and centrifugal) and recovery was based on the Mikhailenko & Baaj (2017) survey (Table 2-10) and SANS 3001-AS20 (2011), being:

- Solvent Extraction: Soak retrieved sample in trichloroethylene or toluene solvent.
- Centrifugal Separation: Filtration (0.25, 0.075 and 0.063 mm sieves) to remove large aggregate and centrifuge to remove all the fines from the binder-solvent solution.
- Recovery: Rotary evaporator apparatus (Heidolph Laborota 4003) used to recover binder.

The extraction of solvent procedure as shown in Figure 3-4 was applied. In this procedure the retrieved seal sample is preheated to a maximum of 110°C for 30 min, making fragmentation of the sample easier. Depending on the sample size, the trichloroethylene solvent volume added to the fragmented sample to be submerged varied between 1500 to 2500 ml. This excluded the solvent used to wash the aggregate during the centrifugal process. In this process the submerged sample is soaked and left over-night (less than 24 hours) to dissolve the binder, where after it is centrifuged and recovered the next day.

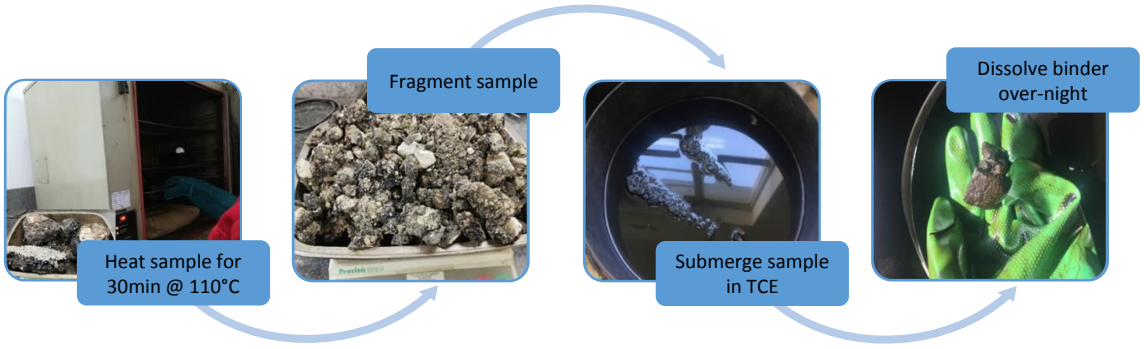

Figure 3-4: Extraction procedure

Figure 3-5 provides a schematic procedure diagram for the centrifugation process that was applied. The centrifuge machine is setup in a fume tight cupboard that has an extraction fan unit to ensure safe and sufficient removal of fumes.

Three sieves were assembled on top of the feed funnel of the centrifuge, with the 0.25 mm and 0.075 mm sieves protecting the 0.063 mm sieve, where the binder-solvents needs to pass through into the rotating metal cup, gathering all the fines. The aggregate on top of each sieve is washed and mixed until the solvents runs out colourless at the outlet drainpipe of the centrifuge into a suitable container.

After the entire sample passes through the 0.063 mm sieve, the collected binder-solvent solution (with the aggregate removed) is re-centrifuged for a 2nd time through only the 0.063 mm sieve into the feed funnel. When doing this it is important to adjust the feed funnel outlet tap that goes into the rotating metal cup to flow at a slower rate in order to ensure sufficient removal of fines.

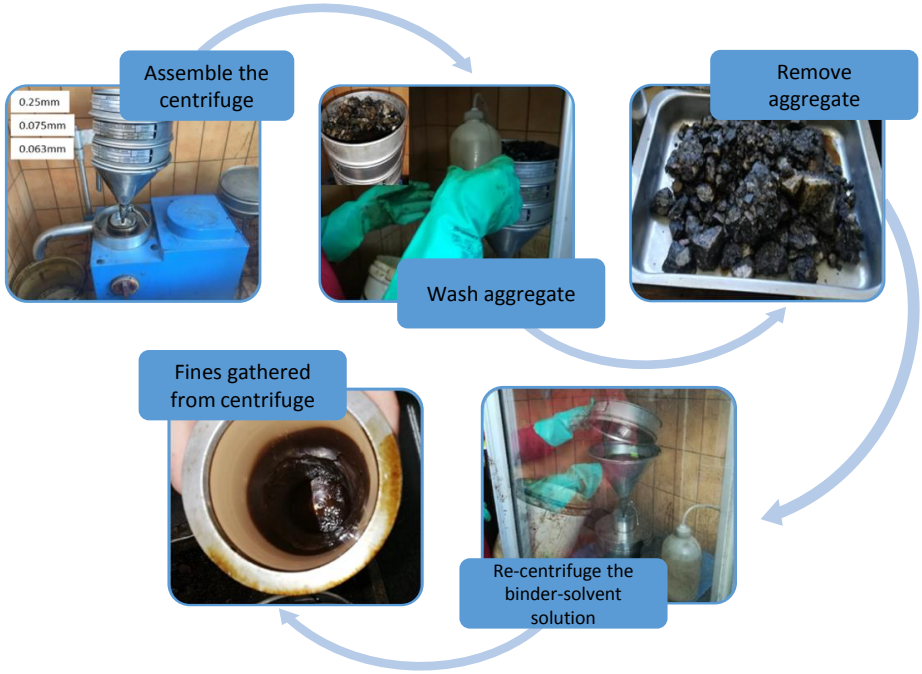

Figure 3-5: Centrifugation procedure

When the fine minerals in the rotating metal cup is substantial, exceeding 50g, a further re-centrifuging is needed using a new rotating metal cup.

Table 3-2 shows the fines results of the retrieved road section samples that were centrifuged in this study, with only three samples marginally exceeding the 50g fines threshold. Hence re-centrifuging was not needed, moving on to the recovery process.

Table 3-2: Retrieved road sections centrifuge fines

Road	Km	Binder Type	Fines from centrifuge (g)
DR1398	1	70/100	47.9
MR23	17		50.6
MR174	9		50.7
R56/7	5.6	S-E1	49.4
N8/11	40.8		50.2
N2/16	71.5		44.7
N6/4	8	S-E1 + fog	44.7
N10/2	11		44
N1/29	79.8		49.6
N1/29	102.6		48.2
N2/31	59.6		39.9
R61/6	88.05	SC-E2	43.8
R61/7	2.72		44.2
R61/8	51.01		44.3

The recovery process was done with the use of a rotary evaporator apparatus. As mentioned above, the solvent used for the extraction and recovery process had to be changed from toluene to trichloroethylene (TCE) due to safety and environmental concerns.

Table 3-3 shows the two solvents' specification in relation to the Rotary Evaporator procedure applied in this study. Recovery temperatures (T_1, T_2, and T_3) were allowed to differ with approximately 5°C, with recovery pressures P_1 at approximately 5 kPa and P_2 at approximately 0.5 kPa.

Table 3-3: Specifications of two solvents (European Standards (EN) -12697-3, 2013)

Solvent				First Phase		Second Phase		Extra Temp.
Type	Chemical Formula	Name	Boiling Point (°C)	Temp. T_1 (°C)	Pressure P_1 (kPa)	Temp. T_2 (°C)	Pressure P_2 (kPa)	Temp. T_3 (°C)
Aromatic hydrocarbon	C_7H_8	Toluene	110,6	110	40	160	2,0	185
Chlorinated hydrocarbons	C_2HCl_3	Trichloroethylene	87,0	90	40	160	2,0	185

The rotary evaporator apparatus was setup in a fume tight cupboard, with an extraction fan unit to ensure safe and sufficient removal of fumes.

Figure 3-6 illustrates the rotary evaporator apparatus that had two water inlets, one going through the filter and one going into the distiller itself. The binder-solvent solution (in the plastic container) was obtained after the centrifugal process, going through the delivery tube into the rotating evaporating flask. During this process the rotating evaporating flask rotates in a hot silicon oil bath, which is heated to temperature T1, allowing the solvent in the mixture to evaporate, with the vapes cooling down and condensate into the receiving flask.

Figure 3-6: Rotary evaporator with vacuum pump

The following recovery process (rotary evaporator) was applied in accordance with EN-12697-3 (2013):

1. Preheat the bath to temperature T_1.
2. Transfer the seal binder solution into evaporation flask.
    a. Lower the evaporating flask into the T_1 heated silicon oil bath.
    b. Set the vacuum pressure to P_1.
    c. Start rotating the evaporating flask at 75 rpm (revolutions per minute).

d. Start the vacuuming of the binder-solvent solution from the container to the evaporating flask, by opening the inlet valve.

3. When the entire binder-solvent solution has passed through, into the evaporating flask, then close the inlet valve and raise the temperature to T_2.

4. If there is bubbling of the bitumen in the evaporating flask, stop before the bath research temperature T_2:

    a. If YES -- lower pressure immediately to P_2.

    b. If NO -- gradually lower the pressure to P_2, and if the bubbling stops within 10 min of temperature T_2 reached.

        - If YES -- do step 4a.
        - If NO -- increase the temperature to T_3.

5. Maintain T_2, P_2 and the rotation at 75 rpm for 10 min, after bubbling of bitumen in the evaporating flask stopped.

6. Raise the evaporating flask from the bath and wipe the outside clean in order to remove the flask from the rotatory evaporator and to prepare the binder sample.

In order to minimise heating of the recovered binder which could compromise sample properties the number of heating, duration thereof and increasing temperatures were kept to a minimum by pouring approximately 25g of binder into a 150ml glass container. This allowed 25g recovered binders only to be heated once before rheometry testing, as shown in Figure 3-7.

Figure 3-7: Recovered bituminous binder sample preparation

The centrifugal and recovery procedure for this study on retrieved road section samples took between two to four hours, depending on the mass of the sample. Quality control was applied on the mass change of the recovered bituminous binder, by monitoring the solvent residue. This was done by placing some recovered binder in a 110°C oven for an hour, to identify if there was still any solvent residue left in the recovered binder, which may affect the binder properties.

3.4.3 Artificial Ageing Procedure

As discussed in Section 2.6.2, the Rolling Thin Film Oven (RTFO) simulates plant ageing (mixing, storage, transportation and placement), whilst the Pressure Ageing Vessel (PAV) simulates ageing during in-service life. These two ageing methods were done in laboratories and are called short- and long-term artificial ageing of original bituminous binders. The artificially aged results were compared to the field data (recovered binders) of this study.

It is important to note that RTFO ageing for seal binder is not included in the American standards (ASTM), as seal binders are not subjected to plant mixing after production. Although seal binders do not go through plant ageing, standardisation RTFO ageing applies to all pavement structures as included in SATS 3208. For this reason, in industry all binders from all surfacing structures (seals and asphalt) will be aged with RTFO prior to PAV ageing.

As only seal binders were investigated in this study, both age conditioning levels were tested. The first one being only the PAV ageing (in-service ageing) of the original binder, as seal binders do not go through the plant ageing process and the second conditioning level being the industry's artificial ageing of RTFO followed by PAV (plant and in field ageing). Both the ageing conditioning levels are compared in this study.

The following equipment was used for artificial ageing:

- RTFO ageing: Scientific Manufacturing Corporation RTFO apparatus.
- PAV ageing: PAV3 and Vacuum Degassing Oven from ATS (Applied Test System INC.).

The RTFO ageing procedure for this study was followed by using the ASTM D2872 (2004) for unmodified binders and TG1 (2015) for modified binders, as the two procedures differ. These two methods are summarised in Table 3-4.

Table 3-4: RTFO ageing procedure

Unmodified binder (ASTM D2872)	Modified binder (TG-1)
• Preheat oven to operating temperature of 163 ± 0.5 °C for minimum of 16 hours prior to testing • Pour 35 ± 0.5 g of sample in glass containers • Pre-coat cylindrical surface of the container • Cool sample for minimum of 60 min and maximum of 180 min • Rotate the samples in oven with air flow for 85 min • Test residue within 72 hours of performing RTFO	• Preheat oven to operating temperature of 163 ± 0.5 °C for 2 hours prior to testing • Pour 40 g of sample in metal containers • Cool sample to room temperature (18-25°C) • Stationary (without rotation and air flow) in oven for 30 min • Rotate the samples in oven with air flow for 60 min • Test residue within 24 hours of performing RTFO

Only the TG1 "Method MB-3: Modified RTFO Test" was used as all six original road section binder samples were modified binders. Figure 3-8 show visuals of the RTFO modified procedure applied.

(a) RTFO machine (b) Metal container with roller (c) RTFO setup

Figure 3-8: RTFO modified binder ageing

The PAV procedure was applied as per ASTM D6521 (2008), where PAV was done on original binders and RTFO aged binders. The PAV procedure for this study was only applied at 40 hours (PAV2) and 80 hours (PAV4).

Figure 3-9 illustrates the long-term ageing apparatus that was used for this study, with Figure 3-10 providing a visual diagram of the long-term ageing procedure that was followed.

Figure 3-9: Long-term ageing apparatus

The aged modified binder was collected from all the RTFO metal containers (Figure 3-8b) into a single container and then mixed to ensure homogeneity, before placing 50g of aged binder into each standard stainless-steel pan for the PAV process. The original binders obtained from these steel containers (Figure 3-2c) were also heated and stirred in order to homogenise the sample before pouring it into the standard stainless-steel pans.

The 50g stainless steel pan samples were then loaded into the sample rack and placed inside an unpressurised PAV chamber that was preheated to 110°C. The chamber is closed and tightened with bolts to ensure that there is no variation in pressure. When the air-tight PAV chamber reaches 110°C, 2.1 MPa dry air pressure is applied and maintained for 40 hours for PAV2 and 80 hours for PAV4.

At the end of PAV testing (after 40 and 80 hours) the pressure was released gradually, to avoid bubbling and foaming of the pan samples. The pan samples were then immediately transferred from the PAV chamber to a separate preheated 163°C oven for 15 min and then scraped into specific single containers so that the binder's depth is between 15 mm and 40 mm, ready for the Vacuum Degassing Oven (VDO). The VDO is used to remove any entrapped air bubbles in the binder, which may affect further testing and results.

The binders in the specific VDO single containers were then placed inside the VDO chamber, which was preheated to 170°C. The samples were heated for 20 min at 170°C before a vacuum absolute pressure of 15 ± 2.5 kPa was applied and maintained for 30 min. After degassing, 25g of binder samples was then poured into 150 ml glass containers, ready to be moulded for rheometry testing.

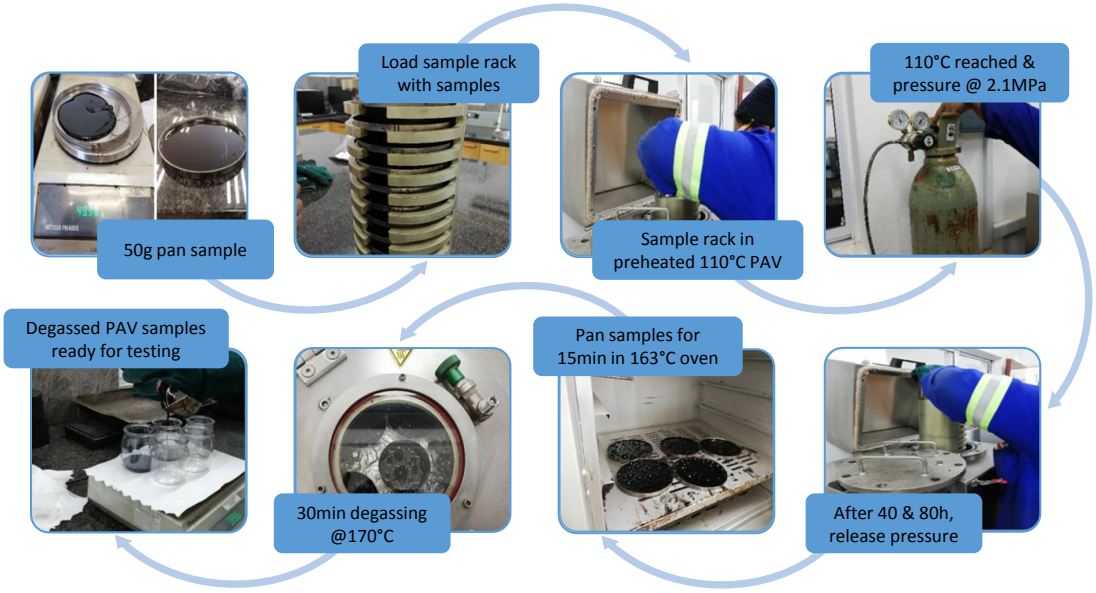

Figure 3-10: PAV and Degassing procedure

3.4.4 DSR Moulds

The Dynamic Shear Rheometer's most common setup was used in this study. This entailed the use of a parallel plate (PP) apparatus of 8 mm and 25 mm diameter. To make DSR testing easier, silicone elastomer moulds (8 mm and 25 mm) were prepared for the binders.

The moulds were fabricated by mixing silicone elastomer with 10% silicone activator (catalyst), poured into 8 mm and 25 mm moulds and left to dry overnight. Thereafter the prepared bituminous binders, after recovery and ageing, were heated to allow pouring of enough bituminous binder to fill the moulds. Moulded binders were then left to cool to room temperature, before removing the binder sample from the mould, to be tested in the DSR.

Figure 3-11 shows the DSR moulding procedure.

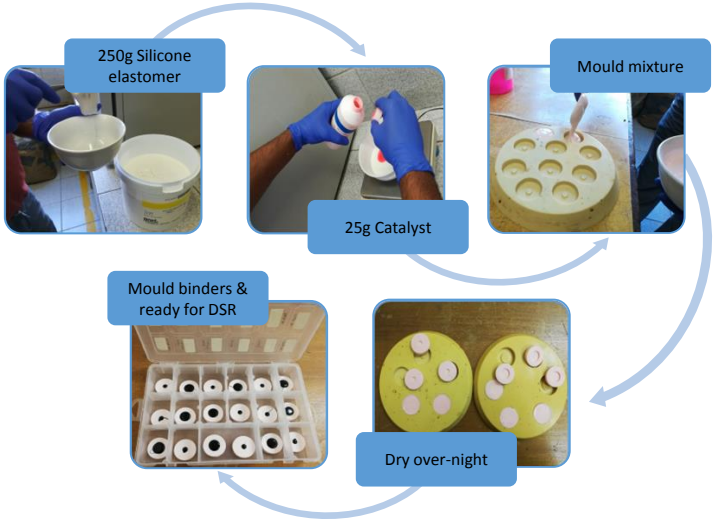

Figure 3-11: Moulding procedure

3.4.5 DSR test

Due to time constraints only the DSR test was used for rheometry testing purposes, notwithstanding various other testing methods available as can be seen in Figure 3-12, namely Rotational Viscometer (RV), Bending Beam Rheometer (BBR) and Direct Tension Tester (DTT).

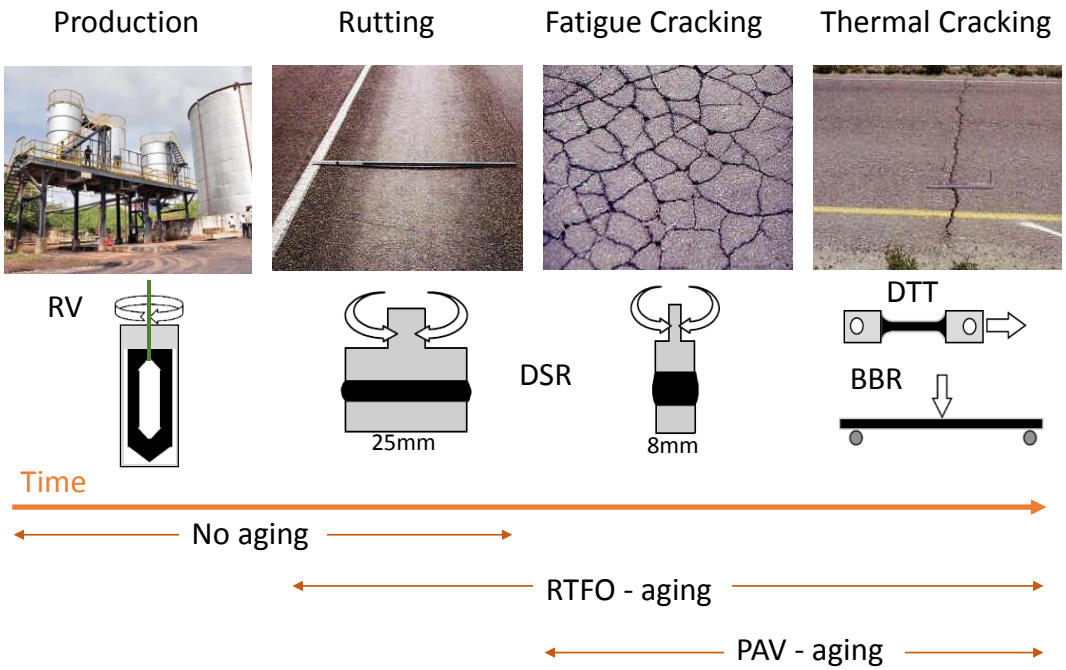

Figure 3-12: Testing that can be done (adapted from Bahia, 2007 and D'Angelo, 2013)

As discussed in Section 2.6.3.1, DSR is used to conduct strain sweeps (LVE range) and frequency sweeps. This testing procedure was followed as per ASTM D7175 (2008) with the DSR equipment used shown in Figure 3-13:

- DSR device used: Anton Paar Modular Compactor Rheometer 302 with parallel plates (8 mm and 25 mm), compressor and cooling unit.
- Computer with Software program used: Rheo Compass, the navigation tool for rheology, version 1.21.825.

The DSR apparatus was prepared by setting the compressor at 5 bar, the cooling unit at 5°C, initialising the DSR parallel plates (8 mm with 2 mm gap and 25 mm with 1 mm gap) and setting the zero gap for the 8 mm PP at 20°C and the 25 mm PP at 50°C. The DSR parallel plate was then heated to 60°C to ensure sufficient bonding between the test plate and the binder sample from the silicone elastomer mould. Trimming of the sample is essential in order to ensure that only the binder sample is tested, providing accurate and reliable results.

The DSR test temperature range for the 8 mm PP is 35, 25, 15 and 5°C; and for the 25 mm PP 35, 45, 60 and 70°C.

The linear viscoelastic (LVE) range for each binder was obtained by conducting strain sweeps between 0.01-10% strain and 10 rad/s frequency. The temperatures at which the strain sweep was tested differed according to the plate geometry, 15°C for 8 mm to 45°C for 25 mm.

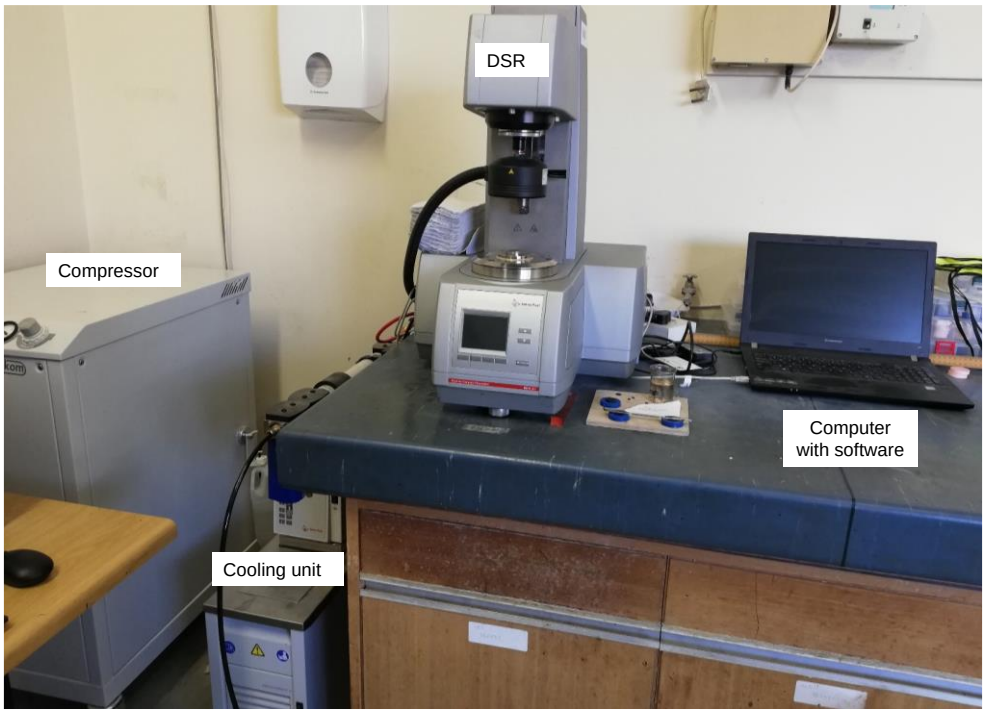

Figure 3-13: DSR equipment

These temperatures were chosen as the lowest temperature is the more critical temperature, as it is more elastic and therefore more prone to breaking. It is also important to note that it is possible that the lowest temperature may fall outside of the plate's tolerance accuracy, as it was observed in the work of Goosen (2018) and Engelbrecht (2018) that the strain sweep for 25 mm binder sample at the lowest temperature, in their case 5°C, resulted into complex shear modulus (G*) values greater than 10^6 Pa. Values greater than 10^6 Pa are technically too high for the 25 mm, meaning it is too stiff and cannot ensure accurate results.

Figure 3-14 shows Engelbrecht' s (2018) 70/100 binder's strain sweep results of the 8 mm plate at 10°C, giving unexpected results.

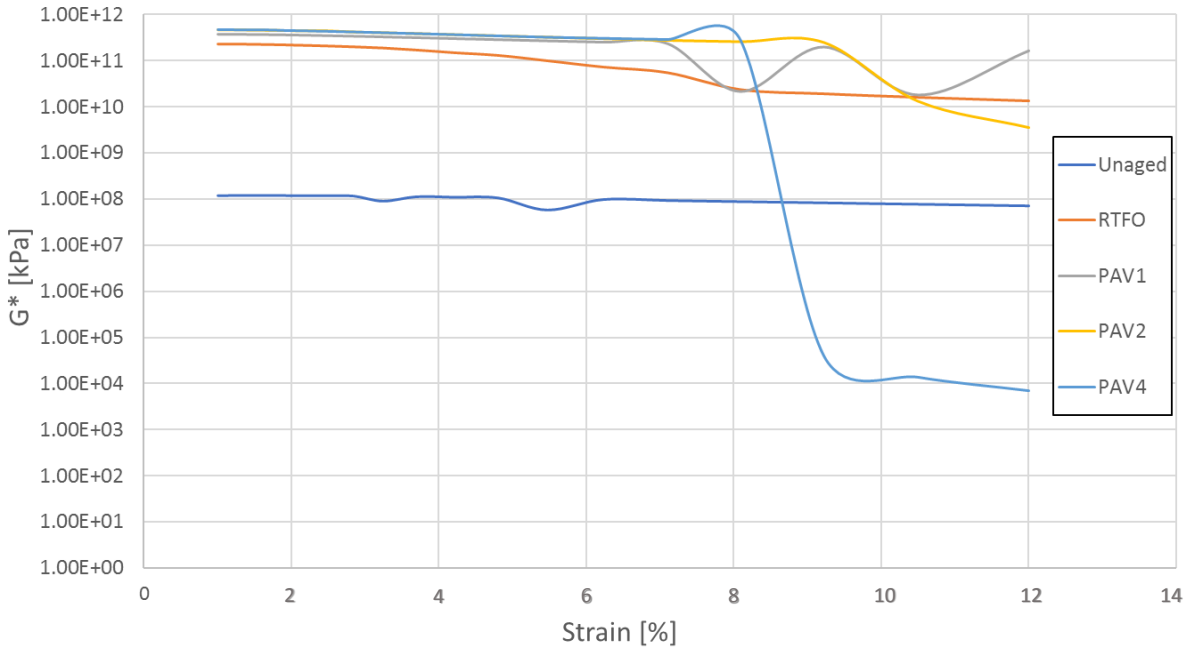

Figure 3-14: 70/100 strain sweeps (Engelbrecht, 2018)

For this reason, as illustrated in Figure 3-14 above, it was decided to use the second lowest temperature range for 8 mm and 25 mm as the lowest temperature range is likely to fall outside the test machine's capabilities.

The LVE limit is defined from the strain sweep results, as the maximum complex modulus is reduced to 95%, as discussed in Section 2.6.3.1. When the LVE strain limit is less than 1%, then that percentage strain is used for the frequency sweeps, otherwise 1% is applied.

The frequency sweeps within LVE range were tested at each of the test range temperatures (5, 15, 25, 35, 45, 60 and 70°C), at a frequency range of 0.251 to 25.1 rad/s and strain obtained from the strain sweep.

Table 3-5 summarises the strain and frequency sweep testing conditions. Note that the 35°C temperature data overlap for the 8 mm and 25 mm PP, ensuring correlation between the two data sets (8 mm and 25 mm).

Table 3-5: DSR testing conditions

	Strain Sweep		Frequency Sweep						
Parallel plate (mm)	8	25	8			8 & 25	25		
Temperatures (°C)	15	45	5	15	25	35	45	60	70
Frequency (rad/s)	10		0.251-25.1						
Strain (%)	0.01-10		if < 1%, use value as is, otherwise use 1% (from strain sweep data)						

3.5 Viscoelastic Modelling and Data Analysis

As bituminous binder behaves linear viscoelastic when exposed to stress or strain over time, the objective of viscoelastic modelling and data analysis is to determine the performance and behaviour of seal binders over a range of temperatures and frequencies. In order to achieve this, modelling was limited and simplified to the LVE range, which enables data to use the time-temperature superposition principle (TTSP).

For this purpose, the data obtained from the DSR testing (frequency sweeps within LVE range) was used, modelled and analysed to interpret the rheological property trends such as durability parameters in terms of ageing.

3.5.1 Master curves and Black Space diagrams

Empirical equation modelling is used to plot master curves and Black Space diagrams individually, as discussed in Section 2.7.3. In order to complete such viscoelastic modelling, the following is required:

- DSR data: Frequency sweeps (at 5, 15, 25, 35, 45, 60 and 70°C) was analysed with Abatech RHEA software version P16-040, where only one 35°C data set (overlapping temperature) from the 25 mm or the 8 mm results was selected, as follow:
    - if the binder's average complex shear modulus (G*) at 35°C are greater than 10^5 Pa, then the PP 8 mm 35°C data is used; and
    - if average G* at 35°C are equal to or less than 10^5 Pa, then then PP 25 mm 35°C data is used.

- Glass transition and reference temperatures: Abatech RHEA software gives a recommended glass transition temperature (T_g) for bituminous binders depending on the temperature range that is used, which for this study was -20°C (Baglieri, Dalmazzo, Barazia, Tabatabaee & Bahia, 2012). For this study 25 °C was selected as the reference temperature (T_{ref}), as it is within the SATS 3208 (2018) intermediate temperature range of 22, 28 and 34°C. A temperature that one can easily relate to.

- Shifting procedure (factors and model): Abatech RHEA software makes use of the Gordon and Shaw (1994) free-shifting method, where a pairwise free-shift is completed for G', G'' and G*. Figure 3-15 shows an example of G* pairwise shift to T_{ref} with a log shift factor (α_T) for each temperature. Modified Kaelble is ranked first regarding its ability to provide a tremendous fit to the experimental data, due to its lowest RMSE, as discussed in Section 2.7.3. The Modified Kaelble model is then fitted to the G* shift factors, determining the model parameters (C_1, C_2 and defining temperature, T_d). The data obtained with the Abatech RHEA software is already shifted.

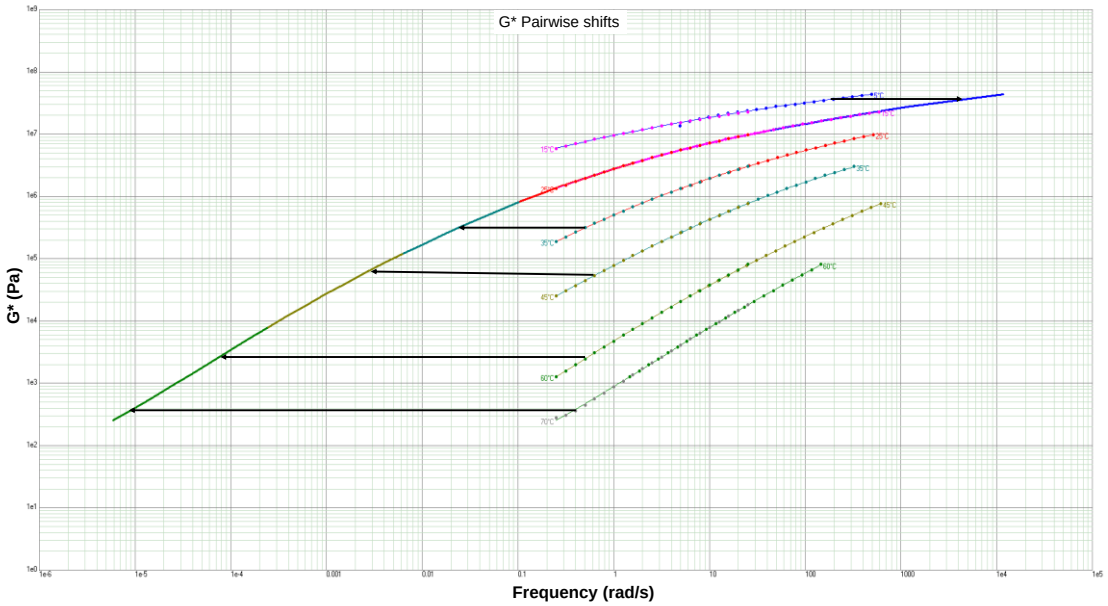

Figure 3-15: G* pairwise shift and Modified Kaelble model

- Fit G* and δ empirical models: The Christensen - Anderson - Marasteanu (CAM) and Generalised Logistic Sigmoidal (GLS) models were fitted to all binder master curves and Black Space diagrams.

  CAM models are only fitted for G* data greater than 10^5 Pa as it has been shown by various researchers to provide good results. GLS models were fitted to G* data that is greater than 10^4 Pa, as the model starts to deviate, when G* < 10^4 Pa, from observed / measured material behaviour of this study. Figure 3-16 shows an example of this GLS model's deviation with all the data, thus using G* > 10^4 Pa data for GLS.

  The initial CAM and GLS values for the model parameters for this study are stated in Table 3-6. The crossover frequency (ω_c) was calculated from the shifted data where the phase angle (δ) is equal to 45°, thus tan δ = 1. The rest of the model parameters were solved in MS Excel to minimise the RMSE (Equation 3-6) of fit, thus minimising the model errors.

Table 3-6: Initial values for the model parameters

CAM		GLS	
G_g	10^9 Pa	G_e	1 Pa
w	-1	G_g	10^9 Pa
v	0.2	β	-1
ω_c	calculated	ɣ	-1
		λ	0.001

The empirical model (CAM and GLS) equations for this study had to be modified, as the Solver function in MS Excel struggled to solve negative values. In Table 3-6 expected negative values from certain model parameters can be seen. For this reason, to only solve positive values, the following modelling equations were used:

Modified Kaelble:

$$\log \alpha_T = -C_1 \left(\frac{T - T_d}{C_2 + |T - T_d|} - \frac{T_{ref} - T_d}{C_2 + |T_{ref} - T_d|} \right) \tag{3.1}$$

CAM:

$$|G^*(\omega)| = G_g \left[1 + \left(\frac{\omega_c}{\omega} \right)^v \right]^{-\frac{w}{v}} \tag{3-2}$$

$$\delta(\omega) = \frac{90w}{1 + \left(\frac{\omega}{\omega_c} \right)^v} \tag{3-3}$$

GLS:

$$\log|G^*(\omega)| = \log G_e + \frac{\log G_g - \log G_e}{\left[1 + \lambda e^{-\beta - \gamma(\log \omega)} \right]^{1/\lambda}} \tag{3-4}$$

$$\delta(\omega) = -90\left(\log G_g - \log G_e\right)(-\gamma) \frac{e^{-\beta - \gamma(\log \omega)}}{\left[1 + \lambda e^{-\beta - \gamma(\log \omega)} \right]^{\left(1 + \frac{1}{\lambda}\right)}} \tag{3-5}$$

As mentioned above, the Root Mean Square Error (RMSE) was used to solve certain model parameters to minimise the models error fit:

$$RMSE\ (\%) = \sqrt{\frac{\Sigma\left(\frac{X_{model} - X_{data}}{X_{data}} \right)^2}{n}} \tag{3-6}$$

Where,

n = *number of data points*

x_{data} = *measured values from Abatech RHEA*

x_{model} = *predicted values from model fit*

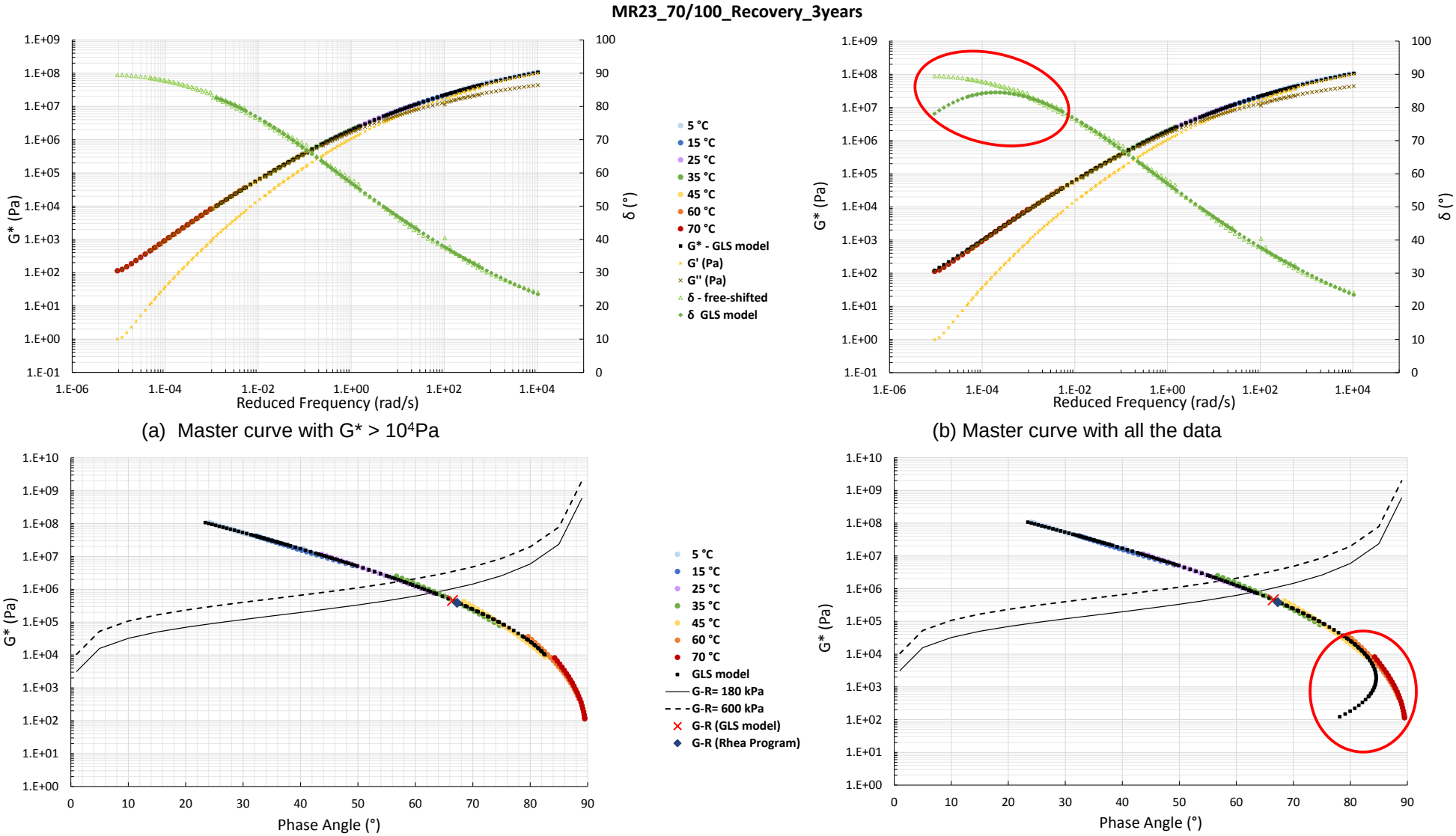

(a) Master curve with G* > 10^4Pa

(b) Master curve with all the data

(c) Black Space with G* > 10^4Pa

(d) Black Space with all the data

Figure 3-16: GLS model optimised for fit

3.5.2 Durability and Ageing Parameters

The aim of durability and ageing parameters is to evaluate in-service rheological properties of seal binders, as discussed in Section 2.8.

The durability and ageing parameters were obtained and calculated after completing viscoelastic modelling of the CAM and GLS for each binder. The model suitability was judged on a binder to binder basis (including ageing of binders), as no specific model has been applied universally. Consequently, the durability and ageing parameters for each binder were computed through the suitable model (CAM or GLS) that was selected, by observing which model gives the minimum RMSE fit percentage and if the G-R parameter fits onto the selected modelled data.

The following procedure was used in this study to compute each durability and ageing parameter:

- Glover-Rowe (G-R) parameter: It measures the ductility of a binder at 15°C to interpret binder cracking and ageing. The G-R parameter was calculated from suitable model (CAM or GLS) data at 0.005 rad/s frequency that was shifted with the temperature 15°C shift factor (ω_r), as it needs to be calculated at 15°C. Complex shear modulus (G*) and phase angle (δ) was computed with the suitable model's equations. G-R parameter's limits 180 kPa for onset cracking and 600 kPa for significant cracking were used.

$$G - R = \frac{G^*_{model}(\cos \delta_{model})^2}{\sin \delta_{model}} \quad (3\text{-}7)$$

- Critical low temperature difference (ΔT_c): It quantifies the loss of relaxation properties and temperature susceptibility to low temperature cracking as the binder ages from the BBR. The ΔT_c was not computed as this study does not include BBR testing.

- Viscoelastic transition (VET) parameters: G^*_{VET} and T_{VET} were calculated where the angular frequency (ω) and crossover frequency (ω_c) equals 2.513 rad/s (i.e. 0.4 Hz). T_{VET} was calculated using the Modified Kaelble by shifting T_{ref} to T_{VET}, as shown in Figure 3-17. First the difference between $\log(\omega_c)$ and log(2.513) was computed to determine the log shift, $\log(\alpha_T)$. The shift factor was then substituted in Equation 3.1 and used to solve T_{VET}. G_{VET} was calculated from the suitable model at frequency where the $\omega = \omega_c = 2.513$ rad/s is shifted to the corresponding T_{VET}. Basically G^*_{VET} is calculated at T_{VET} and ω_c, because both crossover frequency and VET is at $\delta = 45°$.

$$\log \omega_c - \log 2.513 = \log \alpha_T = -C_1 \left(\frac{T_{VET} - T_d}{C_2 + |T_{VET} - T_d|} - \frac{T_{ref} - T_d}{C_2 + |T_{ref} - T_d|} \right) \quad (3\text{-}8)$$

As discussed in Section 2.8.3, VET parameter equations were developed for the CAM model by Rowe (2014a). For this reason, the T_{VET} equation of the CAM model was used if the suitable model was the CAM model.

$$T_{VET} = T_d + \chi \left(\frac{C_2}{1 - |\chi|} \right) \quad (3\text{-}9)$$

Where,

$$\chi = \frac{T_{ref} - T_d}{C_2 + |T_{ref} - T_d|} - \frac{\log \omega_C - \log \omega_{VET}}{C_1} \quad (3\text{-}10)$$

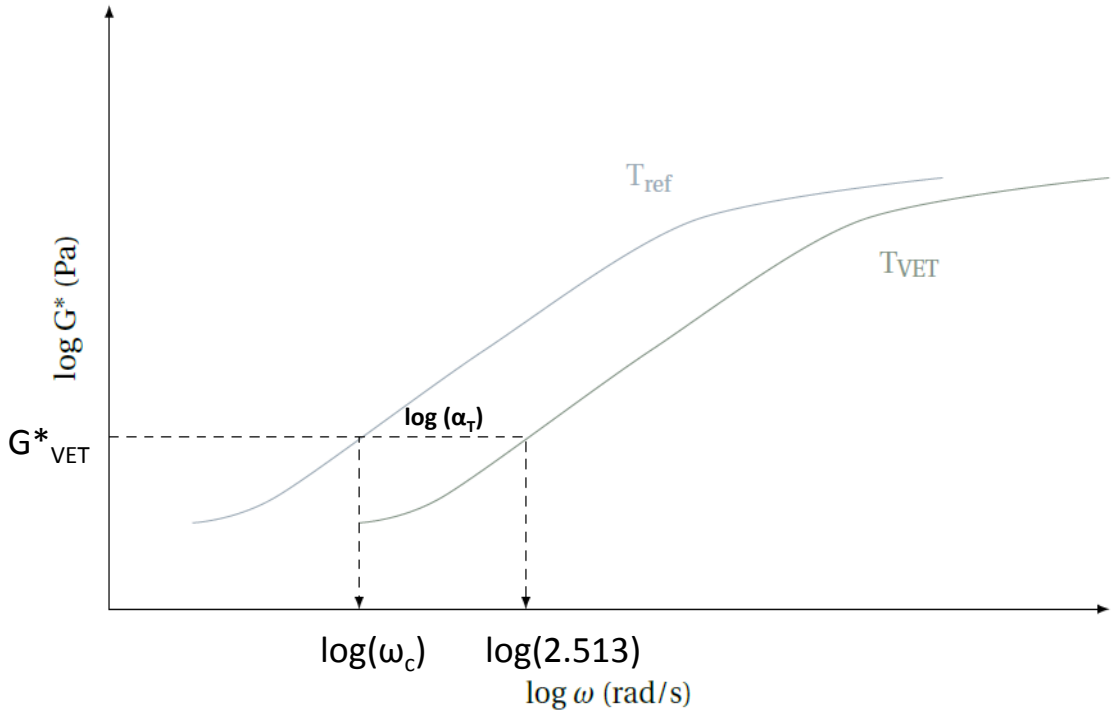

Figure 3-17: Schematic illustration of computing VET parameters (adapted from Goosen, 2018)

- Rheological Index (R-value): As discussed in Section 2.8.4, the field performance of binder shows that cracking is related to R-value and shows a good indication of material behaviour change with age. For this study the R-value was calculated in terms of model suitability and can be obtained by the difference between the upper limit of G* (glass modulus) and the G* at the ω_c:

$$R = \log G_{g_{(model)}} - \log G^*_{(model)} \quad (3\text{-}11)$$

- Ageing ratio: From SABITA (2017), South African Performance Grade Bitumen Specification, ageing ratios are calculated at the intermediate temperature (T_{int}) and 10 rad/s. The ageing ratio gives an indication of the sensitivity of the binder to ageing. To calculate T_{int}, the BBR data is used to compute the T_{min} as per Equation 3-12.

$$T_{int} = \frac{(T_{max}+T_{min})}{2} + 4 \quad (3\text{-}12)$$

However, as this study does not include BBR data, the above procedure cannot be used to calculate the ageing ratios. Goosen (2018) verified in terms of ageing, that G-R parameter at 15°C and 0.005 rad/s can evaluate binder ageing in a similar manner as G* at the intermediate temperature and 10 rad/s. Figure 3-18 illustrates that it gives a good correlation. Therefore, for this study ageing ratios were calculated in terms of G-R at 15°C and 0.005 rad/s for the suitable model:

$$Short\ term\ ageing\ index = \frac{G-R_{RTFO}}{G-R_{Original}},\ Long\ term\ ageing\ index = \frac{G-R_{PAV}}{G-R_{Original}} \quad (3\text{-}13)$$

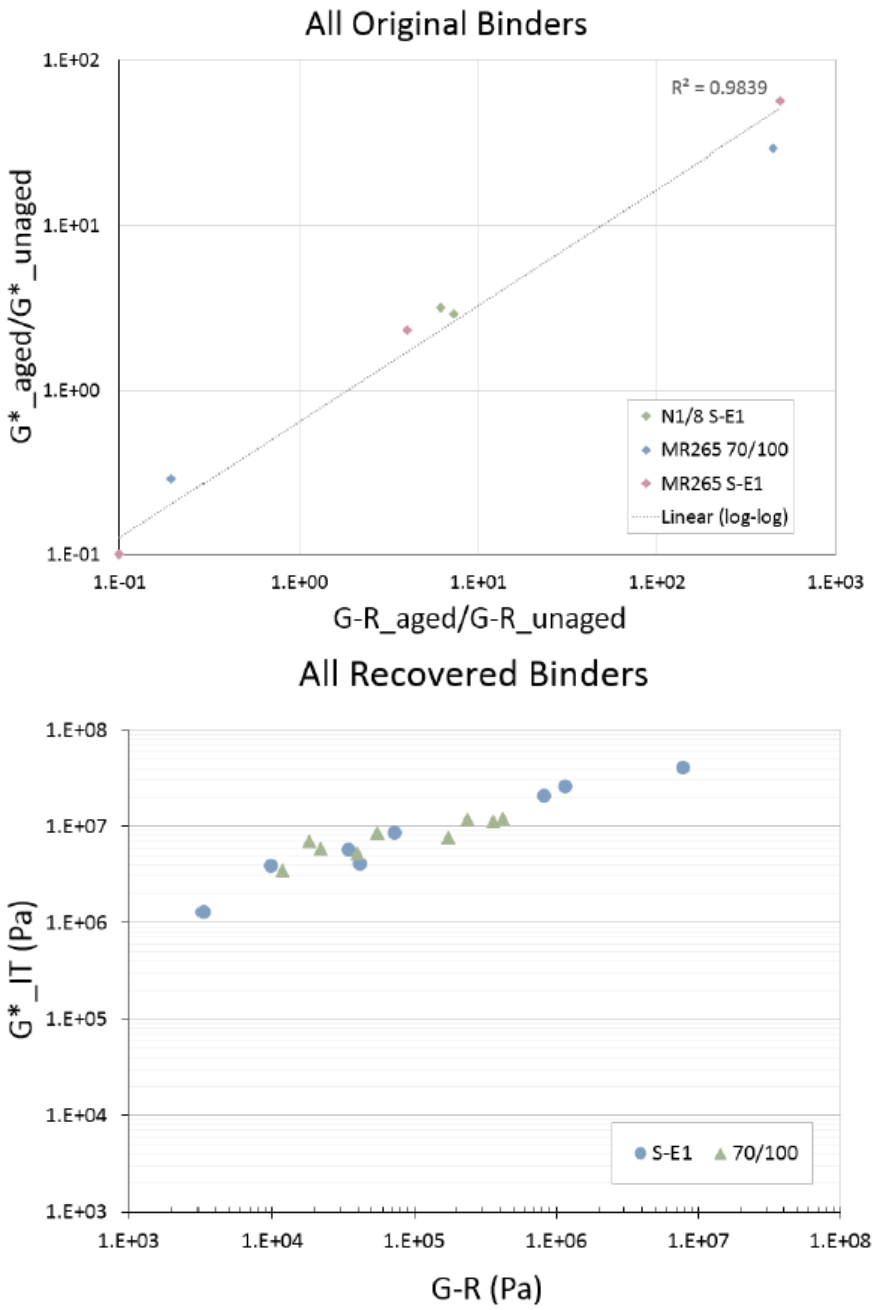

Figure 3-18: Correlation between $G^*_{TINT, 10rad/s}$ and $G\text{-}R_{15°C, 0.005rad/s}$ (Goosen, 2018)

3.6 Summary

The specific standard used for each procedure that was followed in the experimental design was provided and discussed in each section.

The bituminous binder used in this study was mainly selected by taking into account what has already been studied and what was available. In consideration of the seal structure, binder type and the origin from where binder samples were sourced broadens the intelligence and applicability in relation to the performance behaviour of seal binders in South Africa.

The durability and ageing parameters computed from the empirical modelling will be used to evaluate in-service performance and ageing susceptibility of seal binders. These performance properties of seal binders will contribute to the proposed SATS 3208 Performance Grade (PG) Specification for Bitumen in South Africa.

Chapter 4: Test Results and Findings

4.1 Introduction

The results of this study are analysed, interpreted and discussed in this chapter.

For this study on performance grade specifications, the objective is particularly aimed at rheological performance of seals in South Africa based on binder ageing considerations in order to:

- gain a better understanding of the durability aspects that are connected to the ageing performance of seal binders in South Africa, as it ages;
- make a meaningful contribution to the formulation of a comprehensive PG specification for SA bituminous binders with respect to seals only; and to
- determine the key rheological considerations impacting on the transition from a Penetration-Viscosity Specification to a Performance Grade Specification.

Table 4-1 outlines what will be covered in this chapter.

Table 4-1: Outline of the interpretation and discussion of the results

	Description	Results & Discussion	Objectives
Solubilisation & Recovery	Retrieve in-service seals binder	4.2	Effectiveness of the solubilisation and recovery process
Rheometry testing (DSR)	Obtain LVE limit from strain sweeps, followed by frequency sweeps	4.3	Evaluate performance development according to SATS 3208
Modelling	Model with established models		
○ Shift factor	Obtain shift factor for each temperature from Abatech RHEA, using the Modified Kaelble equation	4.4.1	
○ Master curves & Black Space diagram before modelling	Measured behaviour of seal binders	4.4.2	
○ Empirical modelling and selecting Suitable model	Use empirical models, CAM and GLS, to model viscoelastic behaviour of seal binders	4.4.3 & 4.5	To identify suitable models on a binder to binder basis, including ageing of binders
Durability parameters	Obtain durability parameters (G-R, VET, R-value and ageing ratio) from Master curves and Black Space diagrams	4.6	Interpret durability parameters to understand behaviour of seal binders
Summary of findings		4.7	

4.2 Solubilisation and Recovery

As discussed in Section 3.4.2, the toluene solvent originally used for the solubilisation and recovery process was replaced with trichloroethylene (TCE). The necessary quality control was applied on the entire solubilisation and recovery process by heating the binder for 1 hour at 110°C. Mass change of recovered binder was monitored, to identify if there was any solvent residue within the recovered binder after recovery. Table 4-2 confirms that for all the retrieved seal samples that was recovered, it does not matter what solvent was used as there was no mass change in the binder.

It is also evident from Table 4-2, that TCE recovered higher percentages of binder (between 3-5%) from the retrieved seal samples than toluene, thus producing more seal binder to be tested.

Table 4-2: Mass change of binder and % binder recovered from retrieved samples

Road	Km	Binder Type	Age (years)	Solvent	Mass change of binder after recovery	% binder recovered from retrieved sample
DR1398	1	70/100	22	Toluene	0.00%	2.996%
MR23	17		3	Toluene	0.00%	2.863%
MR174	9		9	Toluene	0.00%	2.558%
R56/7	5.6	S-E1	0.92	TCE	0.00%	5.514%
N8/11	40.8		2.33	TCE	0.00%	5.037%
N2/16	71.5		0.83	TCE	0.00%	4.056%
N6/4	8	S-E1 + fog	9	TCE	0.00%	3.180%
N10/2	11		6	TCE	0.00%	4.202%
N1/29	79.8		9	Toluene	0.00%	1.934%
N1/29	102.6		5	TCE	0.00%	3.641%
N2/31	59.6		6	Toluene	0.00%	2.243%
R61/6	88.05	SC-E2	0.5	TCE	0.00%	3.825%
R61/7	2.72		0.5	TCE	0.00%	3.817%
R61/8	51.01		0.08	TCE	0.00%	4.471%

4.3 DSR Rheometry Testing

Table 4-3 summarises each binder's, recovered and artificially aged (RTFO, PAV2, PAV4, RTFO+PAV2 and RTFO+PAV4) DSR performance, with an upper LVE limit strain used to obtain required stiffness isotherms (frequency sweeps), necessary to analyse the specific binder's performance behaviour.

In Table 4-3 it is noted that only one recovered binder (N1/29_79.8km) at 25 mm PP and 8 mm PP yielded a lower upper LVE limit of 0.5% shear strain, in comparison to the rest that has an upper LVE limit of 1% shear strain. The same recovered sample also yielded the highest G* average strain sweep results, as can be seen in Table 4-4 where the stiffness increases above $5 \cdot 10^6$ Pa and therefore is the hardest and stiffest seal binder in this study.

Table 4-3: DSR parallel plate upper LVE strain for frequency sweeps

				Recovered		Artificial ageing	
Road	Km	Binder Type	Retrieved Age (years)	25 mm	8 mm	25 mm	8 mm
DR1398	1	70/100	22	1%	1%	1%	1%
MR23	17		3	1%	1%	1%	1%
MR174	9		9	1%	1%	1%	1%
R56/7	5.6	S-E1	0.92	1%	1%	1%	1%
N8/11	40.8		2.33	1%	1%	1%	1%
N2/16	71.5		0.83	1%	1%	1%	1%
N6/4	8	S-E1 + fog	9	1%	1%	1%	1%
N10/2	11		6	1%	1%	1%	1%
N1/29	79.8		9	0.5%	0.5%	1%	1%
N1/29	102.6		5	1%	1%	1%	1%
N2/31	59.6		6	1%	1%	1%	1%
R61/6	88.05	SC-E2	0.5	1%	1%	1%	1%
R61/7	2.72		0.5	1%	1%	1%	1%
R61/8	51.01		0.08	1%	1%	1%	1%

Figure 4-1 displays typical strain sweep test results, where the blue data shows a binder with a smaller LVE range than the green data.

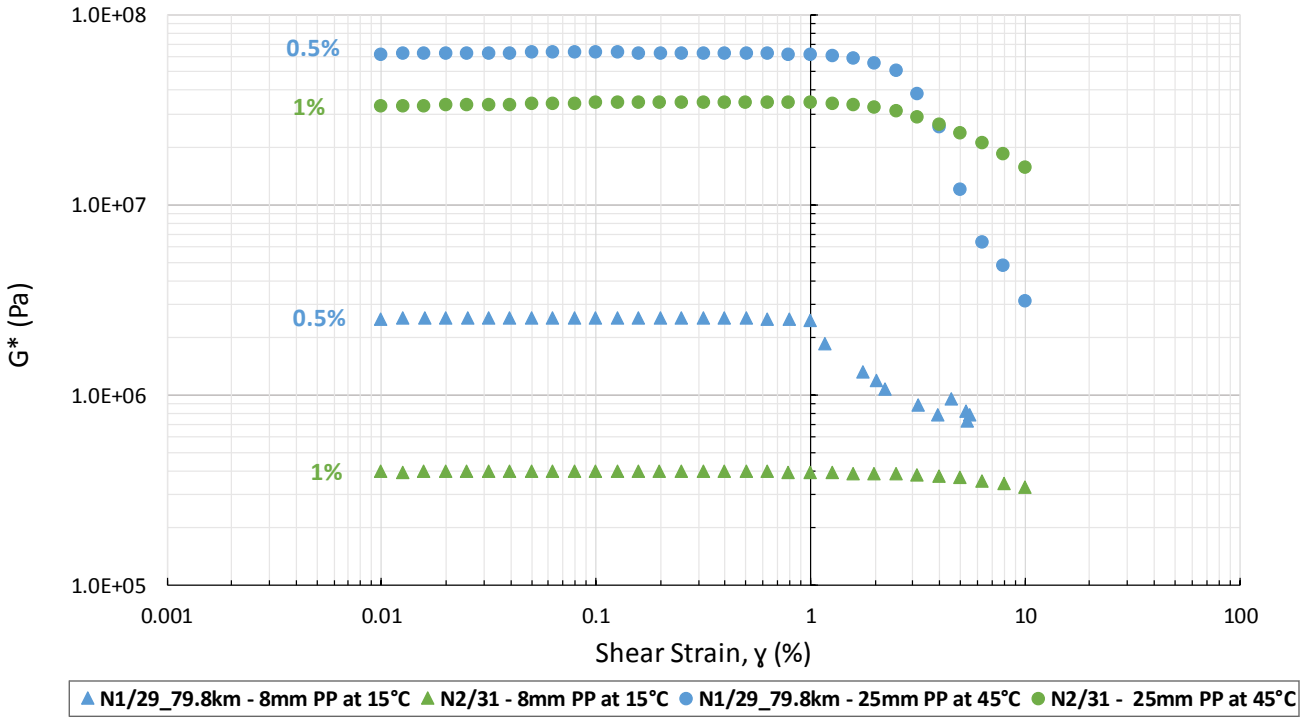

Figure 4-1: DSR strain sweeps of binders with higher and lower upper LVE limits

Table 4-4 displays a typical DSR frequency sweep output of a single temperature isotherm.

Figure 4-2 provides an example of a binder's isotherms data that is obtained with the frequency sweep test, when only one 35°C (overlapping temperature) isotherm is selected from the 25 mm PP or 8 mm PP geometry modelling. The 35°C isotherm was selected in compliance with the SATS 3208 (2018) standard. When the average stiffness (G*) is greater than 10^5 Pa then the 8 mm PP isotherm data is used. Alternatively, when the opposite, G* ≤ 10^5 Pa, then the 25 mm PP isotherm data is used.

For this study, 6 x 25 mm PP and 41 x 8 mm PP 35°C isotherm data recordings were considered for further modelling, where most of the binder's average G* at 35°C is above 10^5Pa, leading to harder / stiffer binders at 35°C.

Table 4-4: DSR frequency sweep output for one temperature

Test: N1/29_79.8km_S-E1+fog_Recovered_9y - 8mm_0.5%strain Result: FS 35										
Point No.	Temp. [°C]	ω [rad/s]	G' [Pa]	G'' [Pa]	Loss Factor	ɣ [%]	τ [Pa]	Torque [mN·m]	δ [°]	G* [Pa]
1	35	0.251	8.52E+05	1.05E+06	1.23	0.5	6767.8	0.68	50.99	1.35E+06
2	35	0.316	1.01E+06	1.20E+06	1.19	0.5	7843	0.79	49.87	1.57E+06
3	35	0.398	1.18E+06	1.35E+06	1.14	0.5	8999	0.91	48.83	1.80E+06
4	35	0.501	1.38E+06	1.52E+06	1.1	0.5	10256	1.03	47.85	2.05E+06
5	35	0.63	1.59E+06	1.70E+06	1.07	0.5	11616	1.17	46.93	2.32E+06
6	35	0.794	1.82E+06	1.89E+06	1.04	0.5	13132	1.32	46.03	2.63E+06
7	35	0.999	2.08E+06	2.10E+06	1.01	0.5	14782	1.49	45.17	2.96E+06
8	35	1.26	2.37E+06	2.32E+06	0.977	0.5	16587	1.67	44.34	3.32E+06

Point No.	Temp. [°C]	ω [rad/s]	G' [Pa]	G'' [Pa]	Loss Factor	ɣ [%]	τ [Pa]	Torque [mN·m]	δ [°]	G* [Pa]
9	35	1.58	2.69E+06	2.56E+06	0.95	0.5	18561	1.87	43.53	3.71E+06
10	35	1.99	3.05E+06	2.81E+06	0.924	0.5	20733	2.09	42.74	4.15E+06
11	35	2.51	3.44E+06	3.09E+06	0.9	0.5	23110	2.33	41.97	4.62E+06
12	35	3.16	3.86E+06	3.39E+06	0.876	0.5	25695	2.59	41.23	5.14E+06
13	35	3.98	4.33E+06	3.70E+06	0.854	0.5	28506	2.87	40.51	5.70E+06
14	35	5.01	4.85E+06	4.04E+06	0.833	0.5	31550	3.17	39.8	6.31E+06
15	35	6.3	5.41E+06	4.40E+06	0.813	0.5	34861	3.51	39.12	6.97E+06
16	35	7.94	6.02E+06	4.78E+06	0.794	0.5	38466	3.87	38.46	7.69E+06
17	35	9.99	6.69E+06	5.19E+06	0.776	0.5	42365	4.26	37.81	8.47E+06
18	35	12.6	7.42E+06	5.63E+06	0.759	0.5	46581	4.69	37.18	9.31E+06
19	35	15.8	8.21E+06	6.09E+06	0.742	0.5	51124	5.14	36.57	1.02E+07
20	35	19.9	9.06E+06	6.58E+06	0.726	0.5	56004	5.64	35.98	1.12E+07
21	35	25.1	9.99E+06	7.10E+06	0.711	0.5	61270	6.17	35.4	1.23E+07
									Avg.	5.42E+06

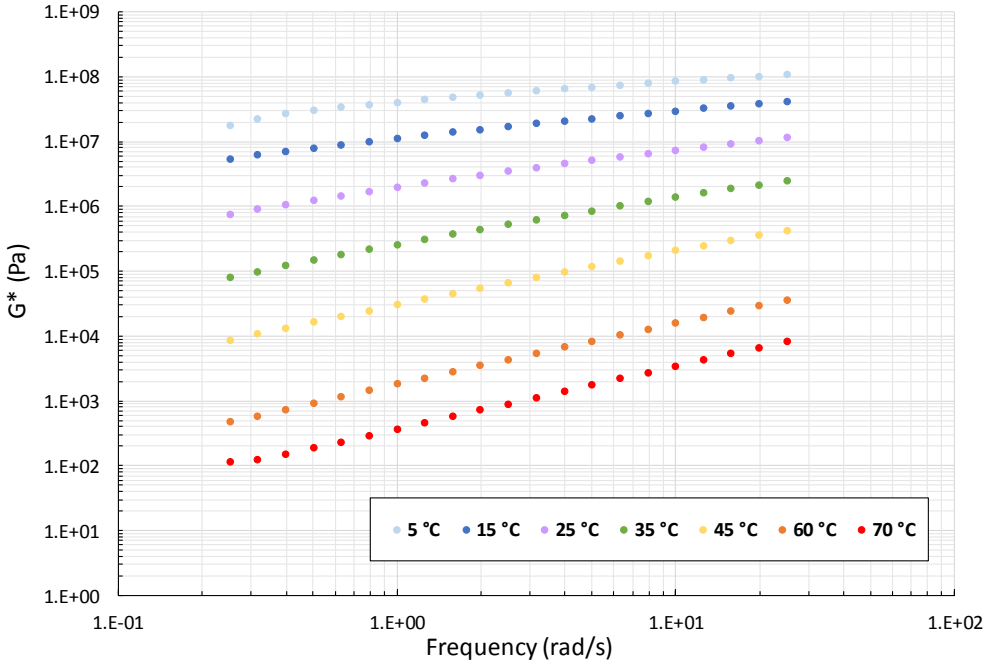

Figure 4-2: MR23_70/100_Recovery_3years DSR isotherm data

4.4 Modelling

Artificial ageing is not directly related to pavement life, where RTFO simulate in-plant ageing during mixing and PAV in-field ageing, where PAV is generally accepted to be between 0-3 years. This is a very broad interval as bitumen will age differently depending on the climatic and environmental factors.

Due to this broad spectrum of artificial ageing versus in-service ageing, some of the aged binder data will be plotted in name intervals, i.e. unaged, RTFO, RTFO+PAV2, RTFO+PAV4, PAV2, PAV4. This is done in order to be able to compare and discuss the results and to ultimately better understand the durability behavioural aspects in respect to ageing of seal binders in SA.

Note that during the modelling of the binders, binder R61/6_SC-E2 was the only original binder that was artificially aged by only PAV2 and PAV4 due to not having enough original binder to conduct RTFO artificial ageing.

4.4.1 Shift Factor

The first ranked shift factor model was Modified Kaelble due to its ability to provide an exceptionally good fit to the experimental data, yielding the lowest RMSE. This was discussed in Section 2.7.3 and also confirmed with the Abatech RHEA software.

Figure 4-3 provides an example plot of the free-shifting of Gordon and Shaw, and the Modified Kaelble that was used to describe the shift of each isotherm to reference temperature, T_{ref} = 25°C, to construct the master curves and Black Space diagrams for each binder.

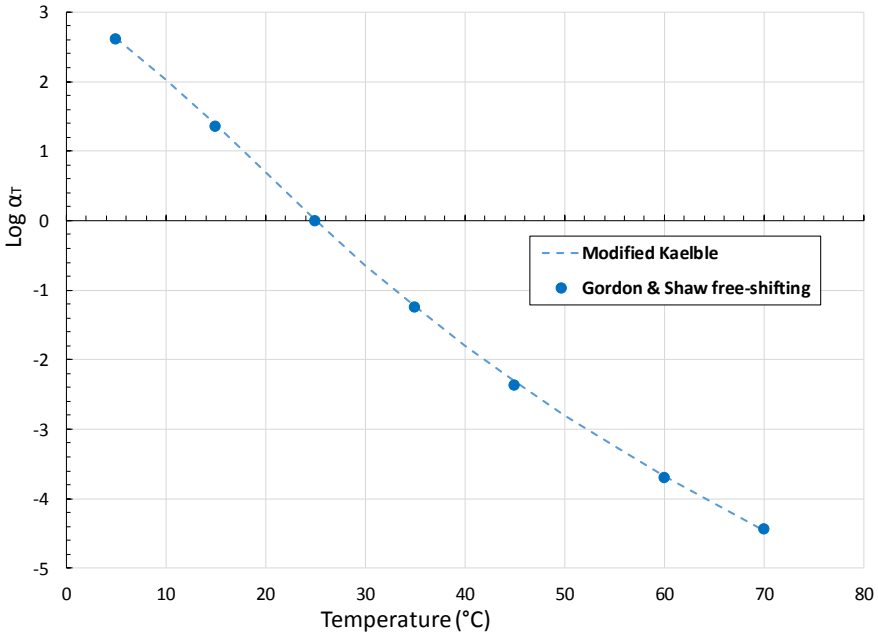

Figure 4-3: Typical Modified Kaelble shift equation plot

Table 4-5 summarises this study's shift factors for each binder, where the Root Mean Square Error (RMSE) of Log α_T for most of the binder ranges between 0 - 5%, with two outliers of 14.35% and 23.05% for a SC-E2 binder at RTFO+PAV4 and PAV4 respectively.

Table 4-5: Synthesis of Abatech RHEA Modified Kaelble shift parameters at T_{ref} = 25°C

Binder	Modified Kaelble			
	C_1	C_2	T_d	RMSE in Log α_T
Original binders with artificial ageing				
N8/11_S-E1_ORIG	11.788	86.40	20	3.40%
N8/11_S-E1_RTFO	15.493	115.40	20	2.87%
N8/11_S-E1_RTFO+PAV2	18.382	129.90	22	5.64%
N8/11_S-E1_RTFO+PAV4	22.934	164.10	20	1.40%
N8/11_S-E1_PAV2	17.303	124.50	20	3.42%
N8/11_S-E1_PAV4	18.799	131.40	22	5.03%
N2/16_S-E1_ORIG	13.113	103.40	20	3.87%
N2/16_S-E1_RTFO	15.018	118.40	17	0.76%
N2/16_S-E1_RTFO+PAV2	16.777	124.10	20	3.62%
N2/16_S-E1_RTFO+PAV4	19.863	145.60	20	3.85%
N2/16_S-E1_PAV2	16.486	123.20	20	3.22%
N2/16_S-E1_PAV4	19.522	142.50	21	4.69%

Binder	Modified Kaelble			
	C_1	C_2	T_d	RMSE in Log α_T
Original binders with artificial ageing				
R56/7_S-E1_ORIG	10.515	71.50	20	4.47%
R56/7_S-E1_RTFO	11.564	79.00	20	3.42%
R56/7_S-E1_RTFO+PAV2	14.764	99.40	20	1.69%
R56/7_S-E1_RTFO+PAV4	17.675	115.80	20	1.01%
R56/7_S-E1_PAV2	14.287	95.70	20	1.48%
R56/7_S-E1_PAV4	16.864	113.10	20	1.65%
R61/6_SC-E2_ORIG	10.084	73.30	22	5.83%
R61/6_SC-E2_PAV2	16.249	120.10	20	3.54%
R61/6_SC-E2_PAV4	19.166	122.80	25	23.05%
R61/7_SC-E2_ORIG	12.168	94.80	18	3.86%
R61/7_SC-E2_RTFO	14.219	108.80	18	1.73%
R61/7_SC-E2_RTFO+PAV2	17.798	132.60	20	1.03%
R61/7_SC-E2_RTFO+PAV4	17.584	113.30	26	14.35%
R61/7_SC-E2_PAV2	15.297	112.40	20	2.56%
R61/7_SC-E2_PAV4	20.192	149.90	20	2.43%
R61/8_SC-E2_ORIG	13.555	104.00	16	1.73%
R61/8_SC-E2_RTFO	14.525	112.80	17	2.29%
R61/8_SC-E2_RTFO+PAV2	18.496	139.40	20	2.55%
R61/8_SC-E2_RTFO+PAV4	20.277	147.60	21	2.33%
R61/8_SC-E2_PAV2	17.323	133.40	18	1.66%
R61/8_SC-E2_PAV4	19.221	144.60	20	2.78%
Recovered binders				
N8/11_S-E1_2y4m	17.096	120.10	20	2.65%
N2/16_S-E1_10m	18.526	131.50	18	2.88%
R56/7_S-E1_11m	16.447	113.10	18	1.74%
R61/6_SC-E2_6m	15.770	119.70	18	2.85%
R61/7_SC-E2_6m	14.642	107.80	20	2.59%
R61/8_SC-E2_1m	15.400	116.20	18	2.08%
DR1398_70/100_22y	19.950	136.80	20	2.04%
MR23_70/100_3y	17.995	124.70	20	2.70%
MR174_70/100_9y	16.918	121.40	20	1.86%
N1/29(79.8km)_S-E1+fog_9y	27.179	189.00	17	3.81%
N1/29(102.6km)_S-E1+fog_5y	21.216	149.20	20	2.97%
N2/31_S-E1+fog_6y	21.576	150.30	20	4.16%
N6/4_S-E1+fog_9y	24.125	173.50	18	0.79%
N10/2_S-E1+fog_6y	18.645	137.60	18	1.74%

The Modified Kaelble shift plot for each binder is included in **Appendix A**.

4.4.2 Master Curves and Black Space Diagrams before modelling

The master curves and Black Space diagrams that describes the measured material behaviour was done with the use of Abatech RHEA software, before empirical modelling was applied, as discussed in Section 4.4.3.

The effect of ageing on binders can be illustrated in both master curves and / or Black Space diagrams.

Glassy Modulus: From the applicable literature discussion in Section 2.7.4 about the glassy modulus (G_g), the combined master curves in **Appendix B**, including Figure 4-4, the following is evident:

- The industry's expected glassy modulus, G_g, range is between $0.6 \cdot 10^9$ Pa and 10^9 Pa.

- This study strives to converge the measured glassy modulus of the binder between $0.6 \cdot 10^8$ Pa and 10^8 Pa. The reason for this is temperature range for the master curves and Black Space diagrams are between 5 and 70°C, with T_{ref} = 25°C, as only DSR testing was done.
    - The G_g ranges for this study and the industry differs due to BBR data not being included in this study.
- If BBR data was combined with DSR data (temperature ranges will be -36 to 70°C). The master curves would then have extended to higher frequencies and lower temperatures, resulting in the industry's G_g range. Thus, data in this regard are not seen as problematic.
- The measured material behaviour's G_g is an important consideration, as it shows the upper limit value of G* (stiffness) of a binder at low temperatures and high frequencies.

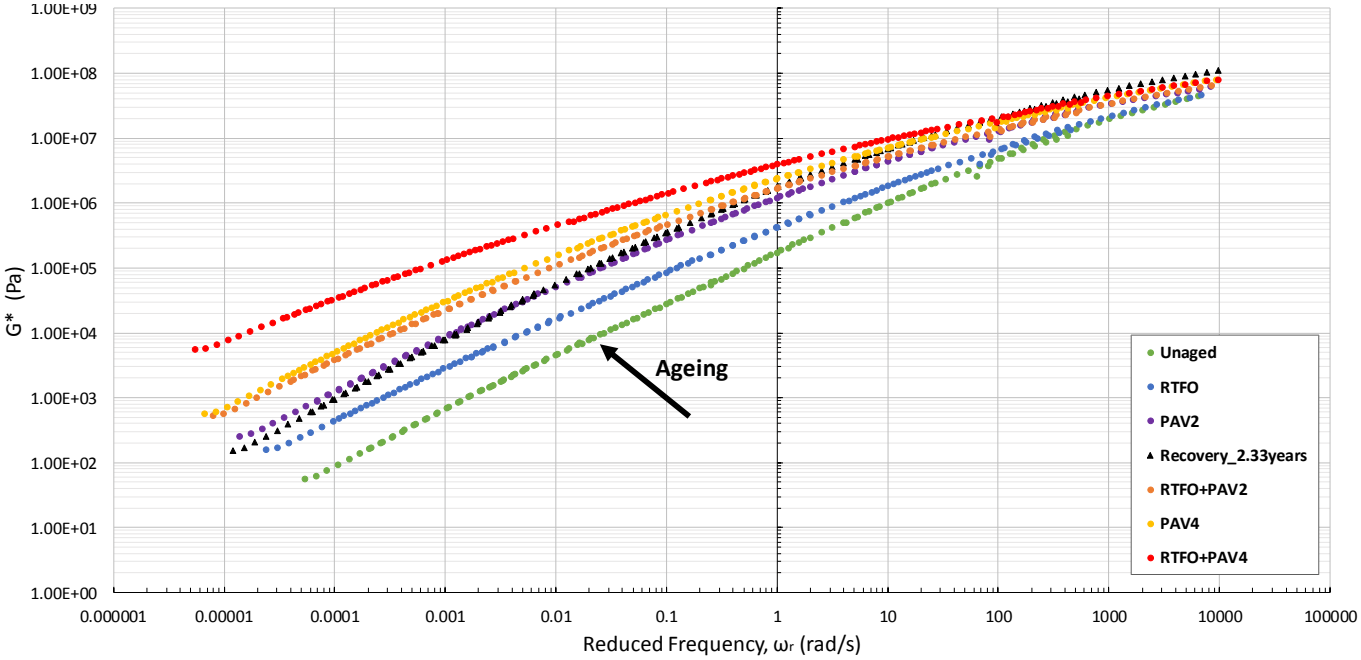

Figure 4-4: Combined master curves for N8/11_S-E1

Ageing: The combined master curves in **Appendix B**, including Figures 4-4 and 4-5 indicate how variations of temperatures, oxidation and volatilisation influence a binder (ageing the binder), with the following being observed:

- As a binder ages the stiffer (harder) the binder becomes, resulting in a loss of relaxation properties of the binder and leading to failure mechanisms such as surface cracking. From literature, surface cracking commonly occurs in Cape seals due to overstressing of surfacing layer, ageing of binder and the loss of elasticity, where 8 out of 14 road section samples for this study is Cape seal samples.
- All master curves of this study flatten (slope decrease) with age.
- The magnitude of the effect of ageing on binders (from unaged to artificial RTFO+PAV4) were indicated by observing the G* values at frequency 0.005 rad/s. The sample in Figure 4-4 showed G* values at 0.005 rad/s with 2.63 kPa for unaged and 353.44 kPa for RTFO+PAV4, demonstrating the loss in relaxation properties.
- The artificial (short- and long-term) ageing master curves of all the binders can clearly be distinguished, except for the SC-E2 binder of road R61/8 (Figure 4-5), where the RTFO and

unaged plot showed the same ageing and behavioural trend, as well as the RTFO+PAV2 and PAV4 plot.

- The study data, as mentioned above, thus confirms that ageing of binders has a major effect on the performance behaviour of seal binders in-service.

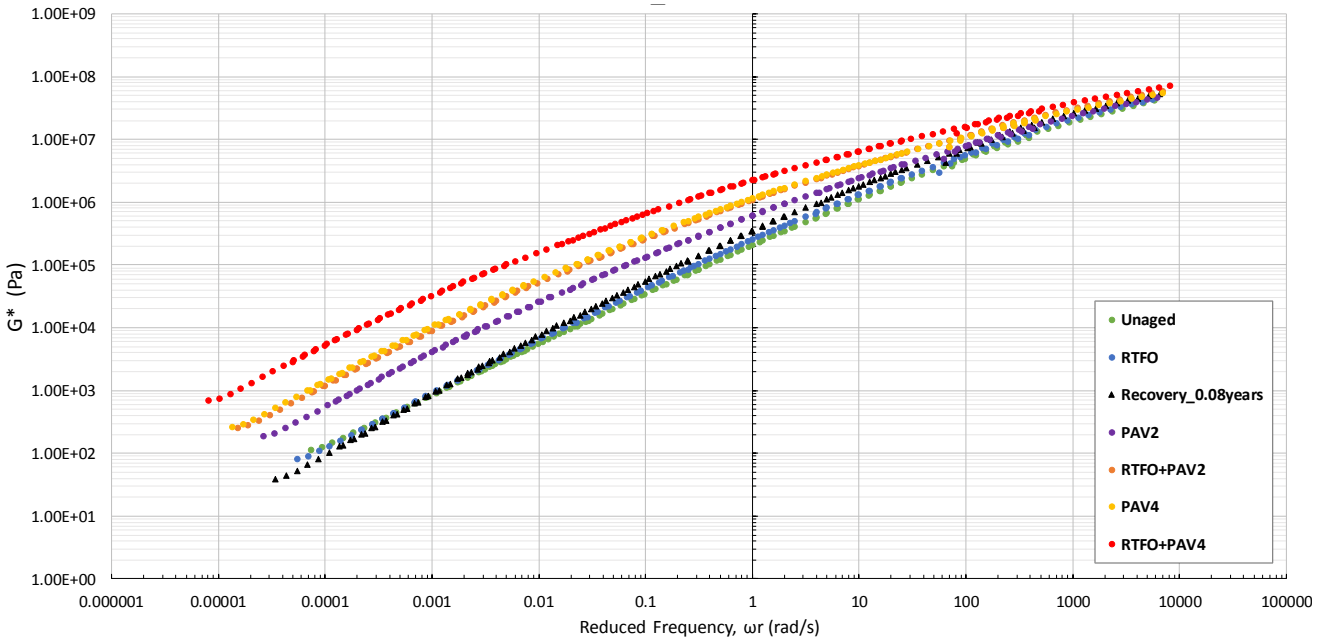

Figure 4-5: Combined master curves R61/8_SC-E2

Artificial vs In-Service Ageing: The binders' recovered master curves were plotted with the artificial combined master curves (**Appendix B**), in an attempt to obtain an indication of how many years' artificial ageing (RTFO and PAV) presents versus in-service ageing.

- The three SC-E2 binders, two at 6 months and one at 1 month old, showed to be between the RTFO and PAV2 artificially aged master curve plot.
- However, the three S-E1 binders (age 10 months, 11 months and 2 years 4 months) did not display any consistency, showing the following:
    - the 2 years 4 months old binder (N8/11) being between PAV2 and RTFO+PAV2;
    - the 11 months (R56/7) between PAV2 and RTFO+PAV2; and
    - the 10 months (N2/16) between RTFO+PAV2 and PAV4.
- To predict an ageing rate based on this study's results for artificial ageing was found to be impossible. This is because the generally accepted interval for PAV, 0-3 years, being a very broad interval as every bituminous binder will age differently in terms of:
    - environmental conditions (temperature, relative humidity (RH), rainfall);
    - orientation of the road (to the north or to the south);
    - traffic types, traffic frequency and traffic severity conditions;
    - position of the layer in the paving structure;

- type of coating (asphalt versus seal);
- volumetric properties (voids) that will increase accessibility of oxygen and water;
- binding properties (classification, film thickness, composition, chemical constituents, polymers); and
- the manufacturing temperature and construction temperature of bituminous binders.

The Black Space diagrams has proven to be very resourcefulness as it clearly identifies when a binder is modified (added modifiers like polymers) or not; and gives a much better understanding of bituminous binders behaviour (linking binder properties to in-services behaviour) by plotting its rheological parameters, G-R and R-value, on a Black Space diagram.

Modifiers: From the literature discussion in Section 2.2.4.1 about polymer elastomer modifiers and the combined Black Space diagrams in **Appendix B**, including Figure 4-6, the following is evident:

- Figure 4-6 confirmed the literature that polymer elastomer modifiers increase the elasticity and strength properties of a binder. It shows that modified binder graph moves to the left of the unmodified binder, indicating less viscous and more elastic behaviour for the modified binder, showing the influence of modification of a binder.
- Bitumen at high temperatures tends to be in a viscous state, but when adding polymer modifier, it reduces temperature susceptibility and moves the modified binder to a more elastic state. However, polymers can still melt at high temperature depending on the type of polymer used, where the modified binder will again lean towards a more viscous state / behaviour.

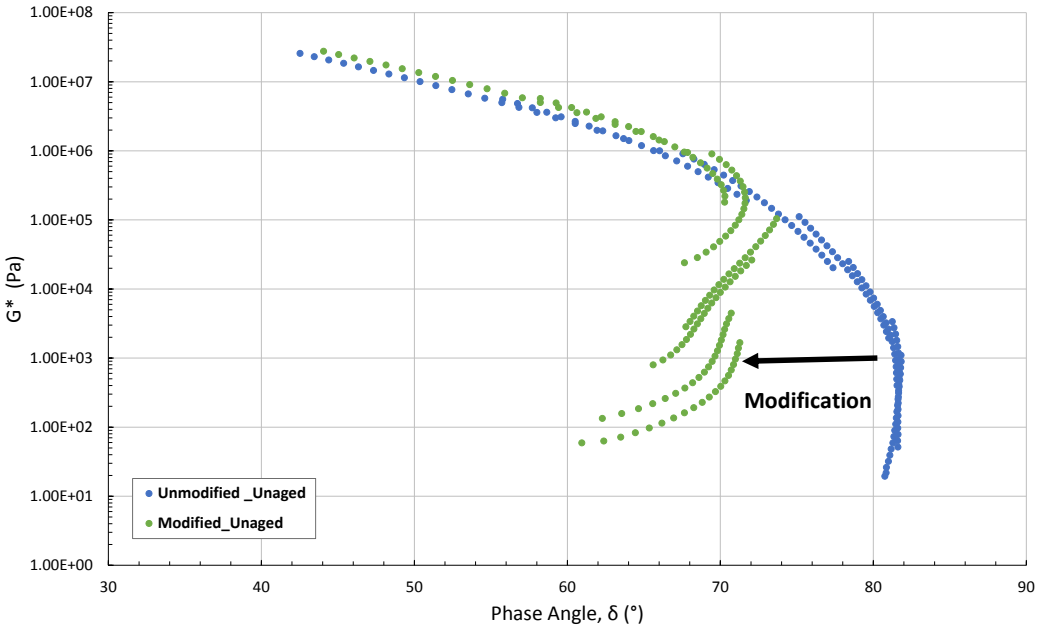

Figure 4-6: Modification of unaged binder's Black Space diagrams

Ageing effect on modifiers: Figure 4-7 was obtained from Engelbrecht (2018) thesis, to show / explain the difference in combined Black Space diagrams for unmodified (70/100) and modified binders (only studies binders S-E1 and SC-E2), as ageing of binders effect the modification of binders. The following was observed:

- The Black Space diagram shows a decrease in stiffness as the temperature and phase angle increases, which is common for unmodified binder behaviour.
- Note that Engelbrecht' s (2018) work, Figure 4-7, includes BBR and DSR data that ranges from -30 and 70 °C at T_{ref} = 15°C.
- The unmodified binder's combined Black Space diagrams (Figure 4-7) converge at both elastic and viscous states, where the phase angle (δ) is equal to 7° and 90° respectively.
- The δ for the unmodified binder reduced for each isotherm as it aged (less viscous), whilst the stiffness reduced which increased the ductility of the binder to elongate under traffic without cracking.
- Figure 4-8 shows the influence of ageing on modified binders. It is noted that S-E1 and 70/100 binders exhibits similar behaviour at low temperatures (less viscous behaviour as it ages), but at the viscous state (high temperatures and phase angles) the Black Space diagram for S-E1 binder does not converge, but becomes more viscous with age.
    - This behaviour is caused by the modifiers within the S-E1 binder, which dominated the behaviour at high temperatures and high phase angles.
    - From all the combined Black Space diagrams it is noted that most of the unaged and RTFO binders have an inflection point in the Black Space diagram at lower phase angle, where the graph moves to a more elastic state (Figure 4-8) at higher temperatures.
    - This indicates that the polymer in unaged and RTFO binders still contributes to the elasticity properties of the binder.
- However, for long-term artificial ageing the polymer provides an increased viscous component and a reduced sign of modification, thus showing that polymer degrades / melts away (no effective modifier left) at higher temperatures, as the binder ages.

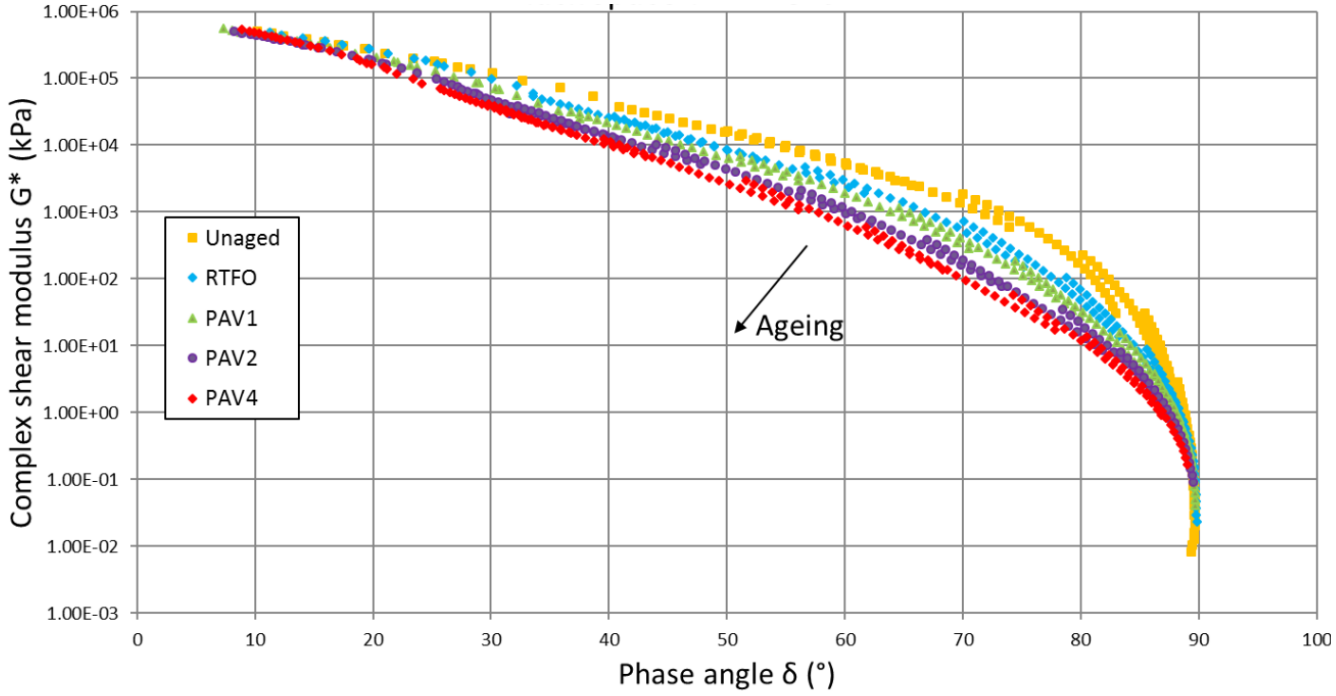

Figure 4-7: Combined Black Space diagrams for artificially aged 70/100 binder, T_{ref} = 15°C
(Engelbrecht, 2018)

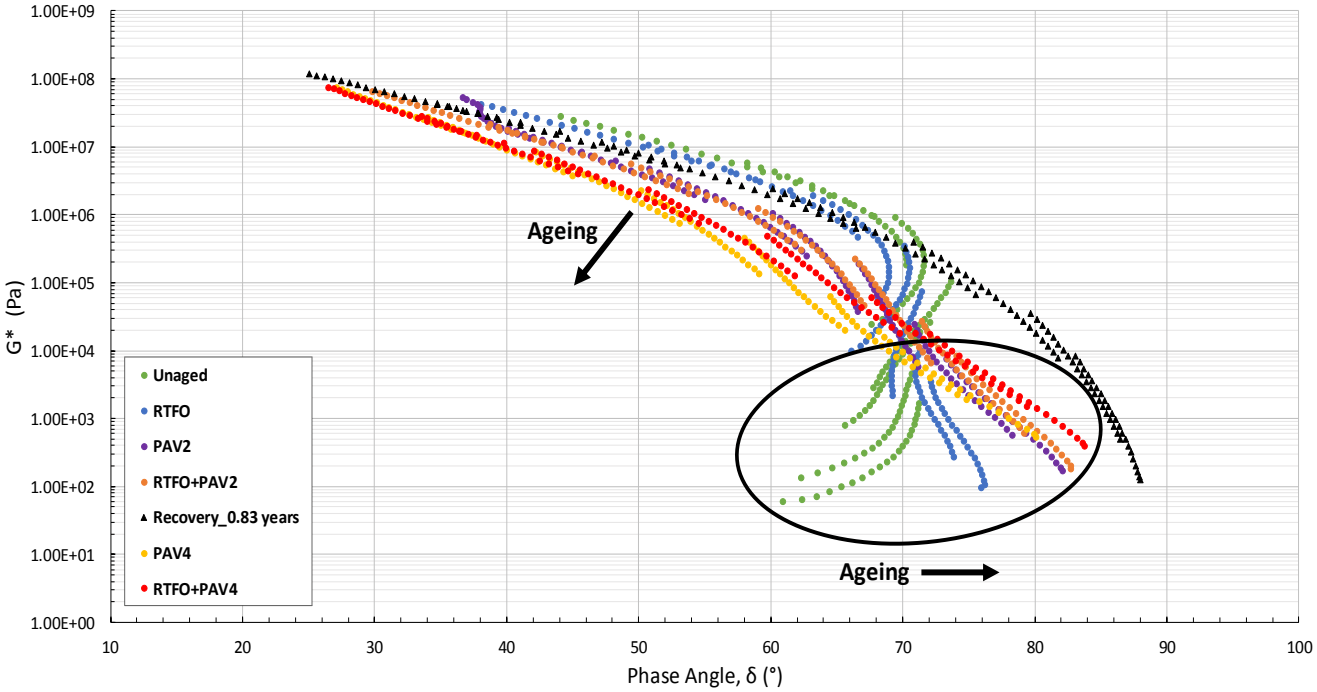

Figure 4-8: Combined Black Space diagrams N2/16_S-E1, T_{ref} = 25°C

4.4.3 Empirical models

This section deals with the appropriateness of fit between the measured data (from Abatech RHEA) and both the empirical models CAM and GLS for all seal binders of this study,

4.4.3.1 Christensen - Anderson - Marasteanu (CAM) model

The CAM model produced Black Space diagrams (G* versus δ) and master curves for stiffness and phase angle (G* versus reduced frequency, ω_r, and δ versus ω_r). For all the seal binders, the CAM model was fitted and plotted to data where G* > 10^5 Pa, with reference temperature, T_{ref} = 25°C.

Table 4-6 summaries the CAM model parameters for each binder while pointing out the binders that exceed RMSE value of 2.25%.

Table 4-6: Summary of CAM model parameters at T_{ref} = 25°C

Binder	Parameters	ω_c (rad/s)	G_g (Pa)	$\|w\|$	v	Σ RMSE
Original binders with artificial ageing						
N8/11_S-E1_ORIG	G*	751.277	3.55E+09	1.113	0.143	0.391%
	δ	751.277		1.022	0.200	1.823%
N8/11_S-E1_RTFO	G*	145.520	4.56E+09	1.041	0.114	0.290%
	δ	145.520		1.005	0.142	1.867%
N8/11_S-E1_RTFO+PAV2	G*	2.553	1.46E+09	0.999	0.110	0.203%
	δ	2.553		1.009	0.115	1.800%
N8/11_S-E1_RTFO+PAV4	G*	0.045	2.21E+09	0.964	0.086	0.154%
	δ	0.045		0.986	0.089	1.554%
N8/11_S-E1_PAV2	G*	15.543	5.41E+08	1.009	0.153	0.212%
	δ	15.543		1.037	0.124	4.517%
N8/11_S-E1_PAV4	G*	1.575	9.32E+08	1.006	0.121	0.210%
	δ	1.575		1.019	0.123	2.041%
N2/16_S-E1_ORIG	G*	3752.426	7.10E+10	1.206	0.106	0.532%
	δ	3752.426		1.002	0.215	2.415%
N2/16_S-E1_RTFO	G*	861.774	8.01E+09	1.128	0.128	0.407%
	δ	861.774		1.020	0.189	2.459%

Binder	Parameters	ω_c (rad/s)	G_g (Pa)	$\lvert w \rvert$	v	Σ RMSE
Original binders with artificial ageing						
N2/16_S-E1_RTFO+PAV2	G*	82.845	1.20E+09	0.996	0.145	0.234%
	δ	82.845		0.981	0.161	1.602%
N2/16_S-E1_RTFO+PAV4	G*	5.514	1.04E+09	1.015	0.128	0.216%
	δ	5.514		1.022	0.132	1.716%
N2/16_S-E1_PAV2	G*	64.542	7.59E+08	1.018	0.154	0.249%
	δ	64.542		1.046	0.131	3.171%
N2/16_S-E1_PAV4	G*	4.850	1.66E+09	1.011	0.115	0.196%
	δ	4.850		1.016	0.121	1.581%
R56/7_S-E1_ORIG	G*	2451.258	1.01E+10	1.192	0.138	0.555%
	δ	2451.258		1.010	0.247	1.475%
R56/7_S-E1_RTFO	G*	621.097	3.91E+09	1.121	0.143	0.414%
	δ	621.097		1.022	0.205	1.512%
R56/7_S-E1_RTFO+PAV2	G*	25.222	1.10E+09	1.037	0.141	0.274%
	δ	25.222		1.021	0.153	1.576%
R56/7_S-E1_RTFO+PAV4	G*	2.358	8.88E+08	1.023	0.128	0.256%
	δ	2.358		1.023	0.129	2.078%
R56/7_S-E1_PAV2	G*	124.505	6.01E+08	0.957	0.172	0.292%
	δ	124.505		0.961	0.161	3.716%
R56/7_S-E1_PAV4	G*	10.824	9.25E+08	1.030	0.137	0.257%
	δ	10.824		1.025	0.143	1.780%
R61/6_SC-E2_ORIG	G*	2055.135	2.26E+09	1.104	0.156	0.427%
	δ	2055.135		1.003	0.227	1.215%
R61/6_SC-E2_PAV2	G*	87.226	9.82E+08	1.006	0.149	0.261%
	δ	87.226		0.994	0.155	2.159%
R61/6_SC-E2_PAV4	G*	2.594	1.60E+09	1.010	0.111	0.222%
	δ	2.594		1.019	0.118	2.958%
R61/7_SC-E2_ORIG	G*	2689.781	5.42E+09	1.139	0.141	0.475%
	δ	2689.781		0.997	0.221	1.199%
R61/7_SC-E2_RTFO	G*	408.538	2.84E+09	1.082	0.138	0.329%
	δ	408.538		1.020	0.178	1.253%
R61/7_SC-E2_RTFO+PAV2	G*	6.501	1.05E+09	1.029	0.124	0.231%
	δ	6.501		1.031	0.128	1.955%
R61/7_SC-E2_RTFO+PAV4	G*	0.480	8.62E+08	1.024	0.115	0.246%
	δ	0.480		1.034	0.115	3.585%
R61/7_SC-E2_PAV2	G*	87.176	8.71E+08	1.002	0.149	0.279%
	δ	87.176		0.998	0.148	2.540%
R61/7_SC-E2_PAV4	G*	3.950	1.32E+09	1.010	0.117	0.213%
	δ	3.950		1.011	0.119	1.606%
R61/8_SC-E2_ORIG	G*	596.837	4.03E+09	1.092	0.133	0.330%
	δ	596.837		1.016	0.174	1.727%
R61/8_SC-E2_RTFO	G*	442.192	3.30E+09	1.080	0.135	0.320%
	δ	442.192		1.016	0.171	1.302%
R61/8_SC-E2_RTFO+PAV2	G*	10.089	1.78E+09	1.027	0.115	0.215%
	δ	10.089		1.026	0.123	1.602%
R61/8_SC-E2_RTFO+PAV4	G*	0.785	1.24E+09	1.019	0.109	0.201%
	δ	0.785		1.027	0.110	2.259%
R61/8_SC-E2_PAV2	G*	70.705	2.42E+09	1.005	0.118	0.239%
	δ	70.705		0.985	0.134	1.363%
R61/8_SC-E2_PAV4	G*	6.084	1.22E+09	1.027	0.118	0.220%
	δ	6.084		1.029	0.122	1.816%
Recovered binders						
N8/11_S-E1_2y4m	G*	20.228	6.39E+08	1.034	0.172	0.243%
	δ	20.228		1.032	0.174	2.046%
N2/16_S-E1_10m	G*	31.154	5.66E+08	1.030	0.189	0.254%
	δ	31.154		1.033	0.188	2.141%
R56/7_S-E1_11m	G*	116.215	6.84E+08	0.985	0.183	0.290%
	δ	116.215		0.967	0.197	2.280%
R61/6_SC-E2_6m	G*	222.795	1.36E+09	1.062	0.151	0.302%
	δ	222.795		1.022	0.178	1.433%

Binder	Parameters	ω_c (rad/s)	G_g (Pa)	$\|w\|$	v	Σ RMSE
Recovered binders						
R61/7_SC-E2_6m	G*	168.208	9.32E+08	1.049	0.166	0.283%
	δ	168.208		1.018	0.189	1.613%
R61/8-SCE2-1m	G*	236.460	1.19E+09	1.067	0.160	0.309%
	δ	236.460		1.023	0.189	1.464%
DR1398_70/100_22y	G*	2.431	3.73E+08	1.029	0.171	0.261%
	δ	2.431		1.037	0.156	4.334%
MR23_70/100_3y	G*	13.341	4.73E+08	1.040	0.180	0.252%
	δ	13.341		1.042	0.176	2.852%
MR174_70/100_9y	G*	19.408	5.40E+08	1.034	0.167	0.233%
	δ	19.408		1.036	0.163	3.029%
N1/29(79.8km)_S-E1+fog_9y	G*	0.052	3.40E+08	1.008	0.147	0.175%
	δ	0.052		0.992	0.110	13.252%
N1/29(102.6km)_S-E1+fog_5y	G*	2.897	4.27E+08	1.019	0.152	0.243%
	δ	2.897		1.028	0.141	4.116%
N2/31_S-E1+fog_6y	G*	5.624	5.06E+08	1.015	0.172	0.244%
	δ	5.624		1.026	0.160	3.699%
N6/4_S-E1+fog_9y	G*	1.206	3.73E+08	1.008	0.151	0.192%
	δ	1.206		1.033	0.112	8.367%
N10/2_S-E1+fog_6y	G*	25.221	5.25E+08	1.026	0.176	0.236%
	δ	25.221		1.035	0.165	3.271%

The crossover frequency, ωc, for each binder was determined individually and not solved per model, thus the ωc for each binder is the same for both CAM and GLS models.

The specific temperature isotherm data, where the phase angle equals 45° was used to calculate the Log ω_c, as illustrated in Figure 4-9.

For all the original and RTFO aged binders, including most of the recovered binder that is only months old, the 5°C isotherm data was used to calculate ωc. The oldest recovered 70/100 binder, at 22 years (DR1398), fell within the 25°C isotherm range, where the stiffest binder (N1/29_79.8km) is within the 35°C isotherm range.

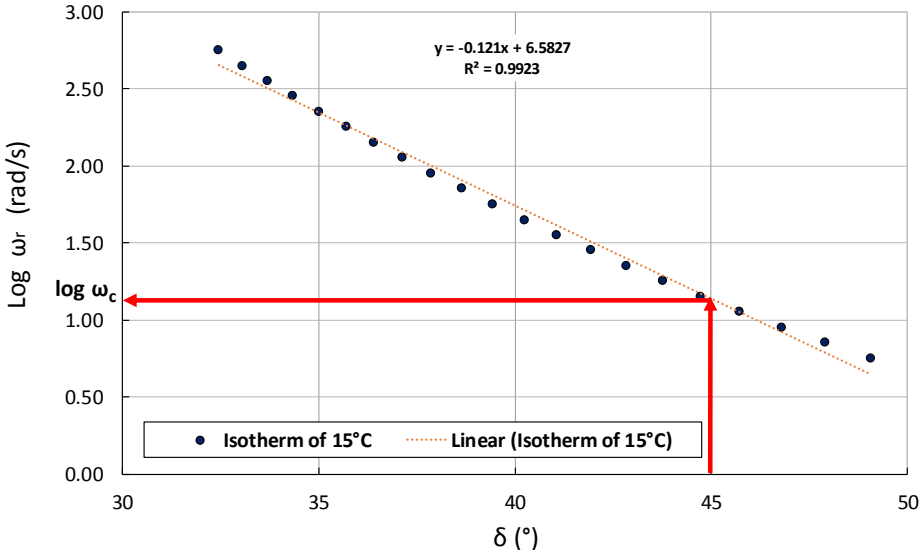

Figure 4-9: Determination of the crossover frequency, ω_c

As discussed in Section 2.7.4 regarding CAM, it is expected that for unmodified binders the R-value will increase with age as the gradient of the G* master curve flattens. The ω_c as well as one of the fitting parameters v should both decrease with age, while the w fitting parameter reduces with modification.

The ω_c and fitting parameter v trends discussed in the literature are confirmed by this study's artificial and recovered binders data, as can be seen in Figures 4-11 and 4-12 for both G* and δ CAM model parameters. It is however important to note that the fitting parameter w showed a decease for the G* model and an increase for the δ model with age.

It is therefore evident that crossover frequency has a greater relationship with age, than the other parameters. Thus, the average values for v, w and G_g parameters were computed as 0.153, 1.028 and $2.53 \cdot 10^9$ Pa individually for this study.

It is also noted that the glassy modulus, G_g, average for the CAM model of $2.53 \cdot 10^9$ Pa was close to (with in the same range) the literature assumption of 10^9 Pa for G_g.

The CAM model data is acceptable if the RMSE ≤ 2.25%. From Table 4-6 and Figure 4-10 it is evident that the CAM model performs satisfactory for all G* occurrences. But not as well for δ where there was nine artificially aged and nine recovered binders above the mentioned limitation, which showed an extreme outlier of 13.252% RMSE for the stiffest binder (N1/29_79.8km).

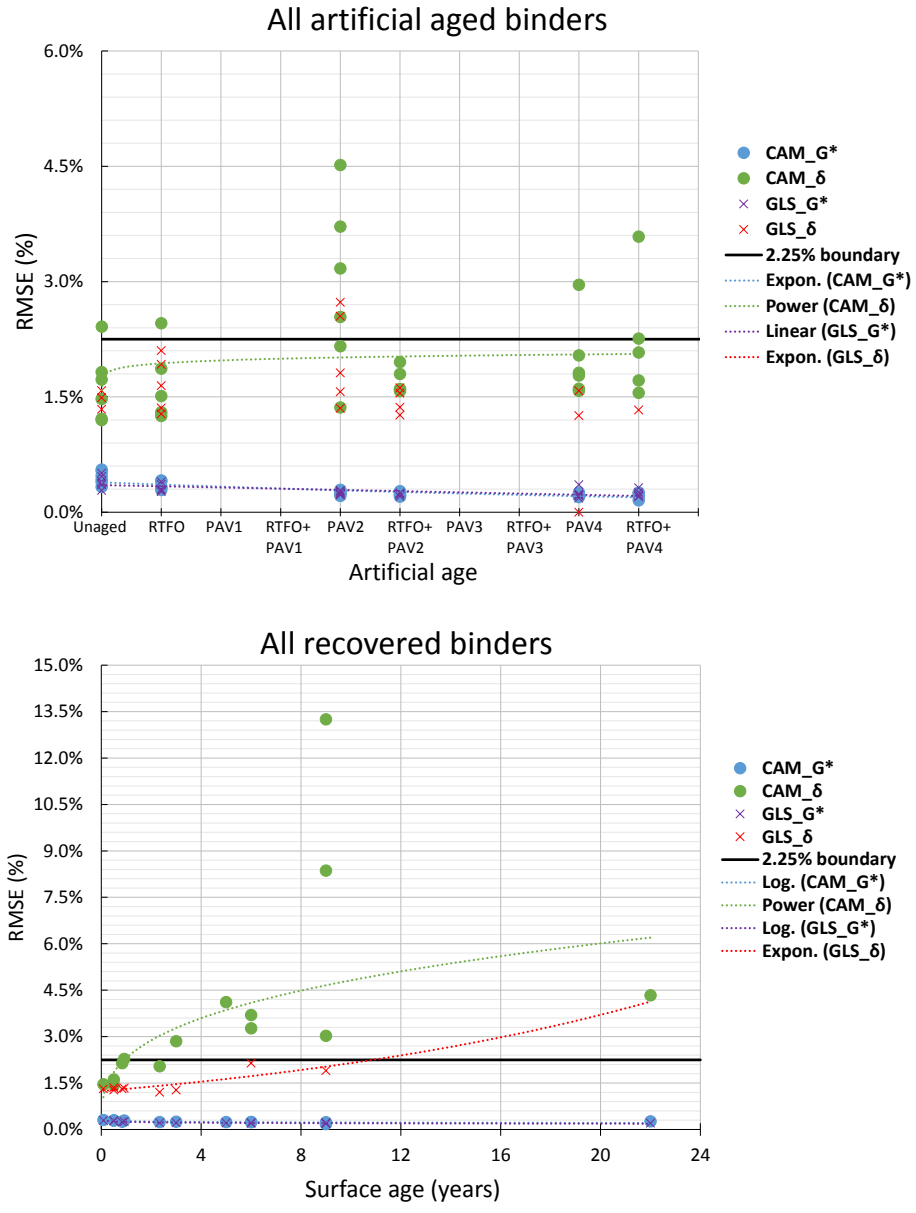

Figure 4-10: RMSE (%) with age for the CAM and GLS models

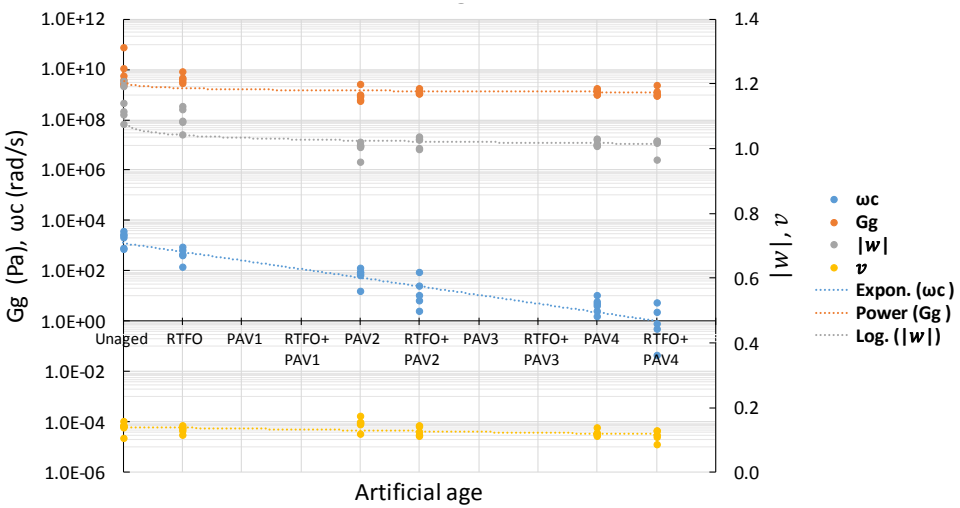

(a) G* model parameters

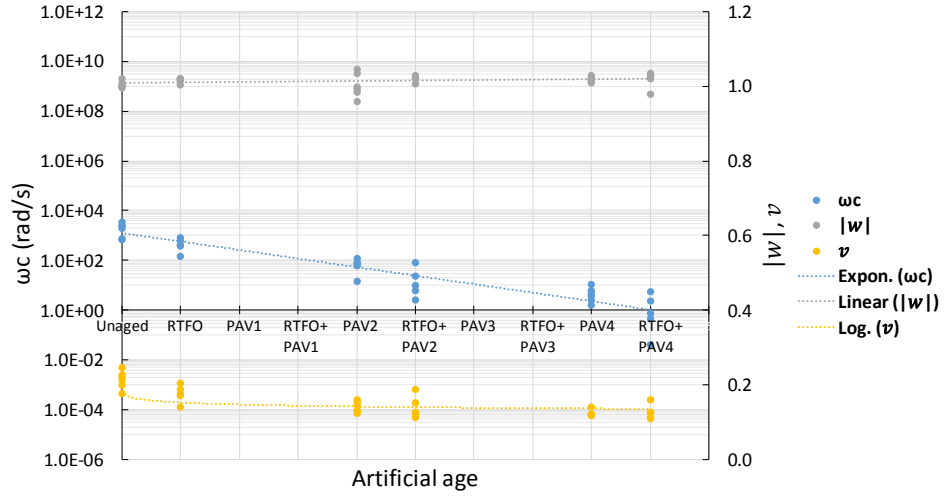

(b) δ model parameters

Figure 4-11: CAM model parameters of artificially aged binders

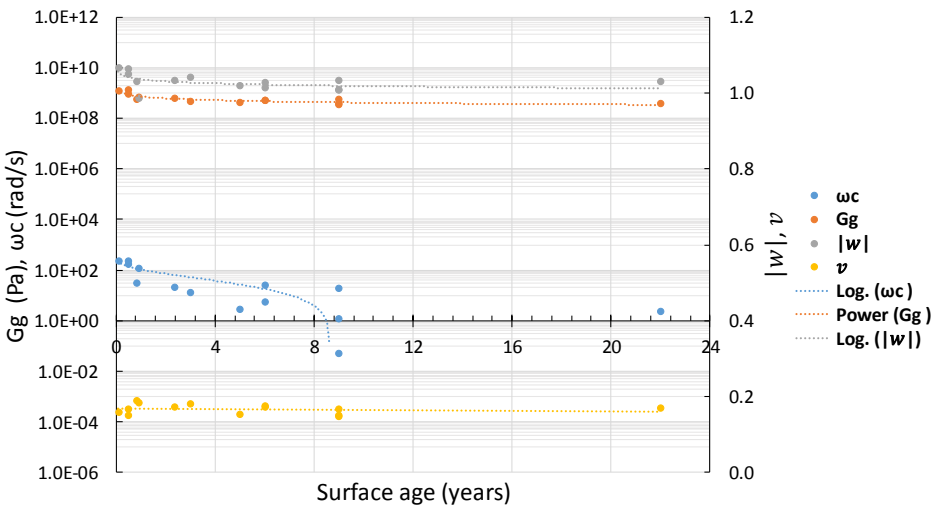

(a) G* model parameters

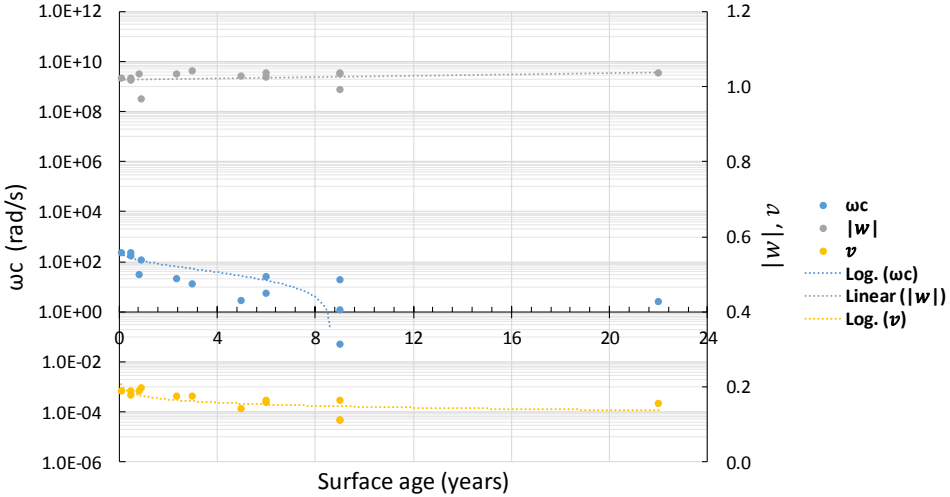

(b) δ model parameters

Figure 4-12: CAM model parameters of recovered binders

It is also important to analyse inspection when modelled data is compared to measured data and not only to explore the RMSE variable.

The CAM model through inspection accurately predicted the binder behaviour for G* > 10^5 Pa, where it fits the stiffness and phase angle master curves thoroughly. Figures 4-13 and 4-14 shows an example of the CAM model's correlation (R^2) between the modelled and measured data, with its summary contained in **Appendix C**.

For all the lesser aged binders (unaged, RTFO, 6 and 1 months recovered), as well as R61/7_SC-E2_PAV2, the G* associated with the G-R parameter were below the 10^5 Pa acceptable CAM model limit. For this reason, the CAM model was not regarded suitable for these few binders to determine the G-R parameter.

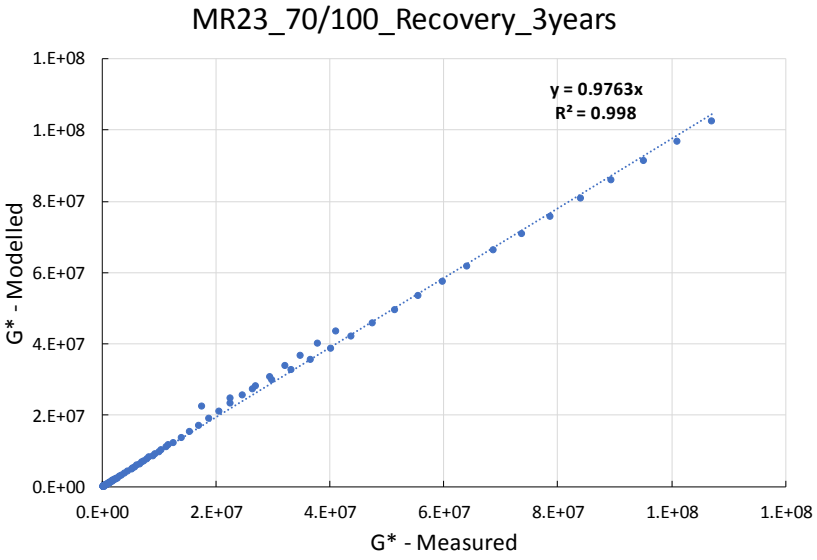

Figure 4-13: CAM G* data correlation, G* > 10^5 Pa

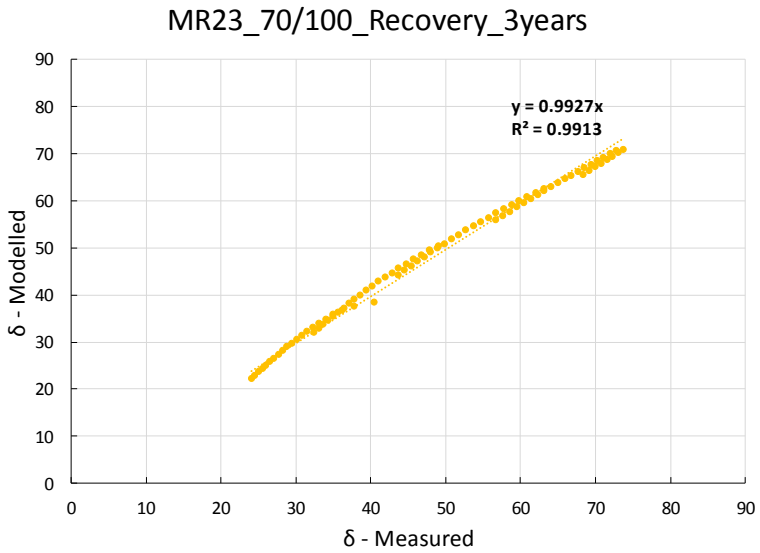

Figure 4-14: CAM δ data correlation, G* > 10^5 Pa

Figures 4-15 and 4-16 shows the final result after modelling with the CAM model, in order to obtain the master curves and Black Space diagrams of binders. These figures include binders with and without G-R parameter on the binder's modelled Black Space diagram.

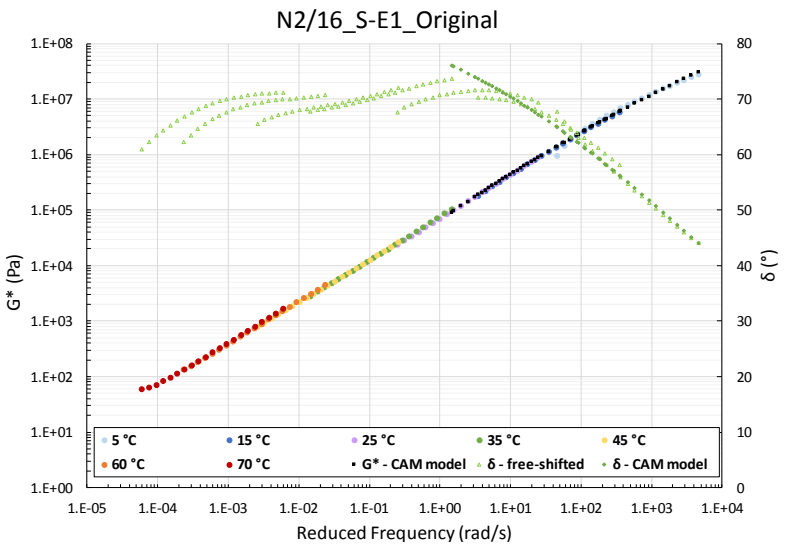

(a) G-R parameter not on Black Space Diagram

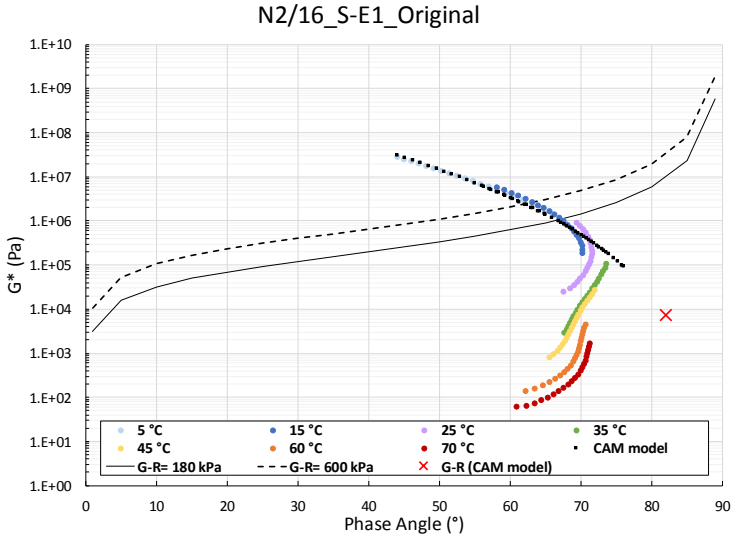

(a) G-R parameter not on Black Space Diagram

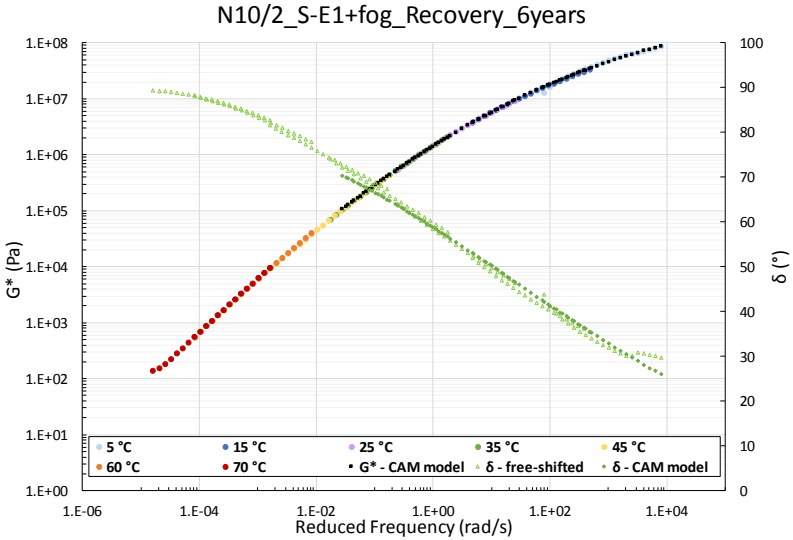

(b) G-R parameter on Black Space Diagram

Figure 4-15: CAM model G* and master curves

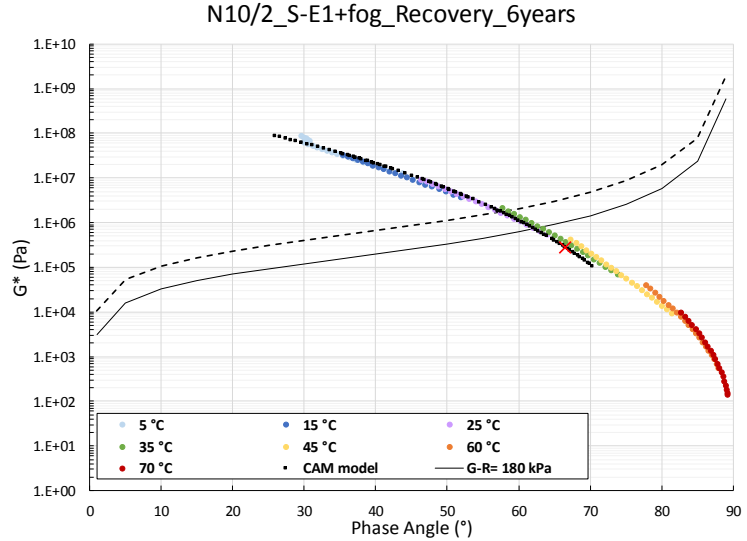

(b) G-R parameter on Black Space Diagram

Figure 4-16: CAM model Black Space diagrams

4.4.3.2 Generalised Logistic Sigmoidal (GLS) model

The GLS model produces Black Space diagrams (G* versus δ) and master curves for stiffness and phase angle (G* versus ω_r, and δ versus ω_r).

It was observed in this study that the GLS model starts to deviate from measured material behaviour data when G* is less than 10^4 Pa. For this reason, the GLS model were only fitted and plotted to data where G* > 10^4 Pa, with reference temperature, T_{ref} = 25°C.

Table 4-7 summaries the GLS model parameters for each binder while pointing out the binders that exceed RMSE value of 2.25% and binders that could not be solved with the GLS model.

Table 4-7: Summary of GLS model at T_{ref} = 25°C

Binder	Parameters	G_e (Pa)	G_g (Pa)	|β|	|γ|	λ	Σ RMSE
Original binders with artificial ageing							
N8/11_S-E1_ORIG	G*	3.970	1.62E+10	0.318	0.231	0.001	0.356%
	δ	2.394	1.22E+07	0.200	0.330	0.001	1.582%
N8/11_S-E1_RTFO	G*	2.281	8.21E+09	0.517	0.211	0.001	0.268%
	δ	1.783	2.12E+08	0.507	0.253	0.001	1.922%
N8/11_S-E1_RTFO+PAV2	G*	1.202	1.63E+09	0.926	0.218	0.001	0.206%
	δ	0.013	2.34E+09	1.108	0.199	0.001	1.549%
N8/11_S-E1_RTFO+PAV4	G*	1.295	1.73E+09	1.073	0.189	0.001	0.206%
	δ	0.000	2.11E+09	1.121	0.182	0.001	No Solve
N8/11_S-E1_PAV2	G*	1.188	1.54E+09	0.873	0.241	0.001	0.224%
	δ	0.000	2.09E+09	0.831	0.215	0.001	No Solve
N8/11_S-E1_PAV4	G*	1.162	1.15E+09	1.037	0.232	0.001	0.214%
	δ	0.000	2.09E+09	1.084	0.213	0.001	No Solve
N2/16_S-E1_ORIG	G*	19.777	9.60E+10	0.000	0.220	0.001	0.467%
	δ	2.027	0.00E+00	0.037	0.261	0.001	No Solve
N2/16_S-E1_RTFO	G*	9.220	4.45E+10	0.204	0.216	0.001	0.396%
	δ	2.336	1.19E+07	0.163	0.321	0.001	2.103%
N2/16_S-E1_RTFO+PAV2	G*	1.477	3.71E+09	0.704	0.229	0.001	0.233%
	δ	1.831	1.70E+08	0.653	0.268	0.001	1.617%
N2/16_S-E1_RTFO+PAV4	G*	1.203	1.67E+09	0.925	0.231	0.001	0.201%
	δ	0.000	2.08E+09	1.010	0.224	0.001	No Solve
N2/16_S-E1_PAV2	G*	1.471	3.42E+09	0.682	0.230	0.001	0.283%
	δ	0.505	1.53E+09	0.673	0.228	0.001	2.731%
N2/16_S-E1_PAV4	G*	1.330	2.65E+09	0.859	0.214	0.001	0.184%
	δ	0.424	1.63E+09	0.923	0.217	0.001	1.580%
R56/7_S-E1_ORIG	G*	6.249	3.07E+10	0.148	0.241	0.001	0.509%
	δ	2.010	0.00E+00	0.210	0.293	0.001	No Solve
R56/7_S-E1_RTFO	G*	2.330	8.98E+09	0.415	0.245	0.001	0.364%
	δ	2.223	4.92E+07	0.342	0.316	0.001	1.647%
R56/7_S-E1_RTFO+PAV2	G*	1.218	2.11E+09	0.813	0.242	0.001	0.249%
	δ	1.421	5.51E+08	0.810	0.259	0.001	1.264%
R56/7_S-E1_RTFO+PAV4	G*	1.170	1.35E+09	1.004	0.235	0.001	0.228%
	δ	0.061	2.14E+09	1.151	0.221	0.001	1.331%
R56/7_S-E1_PAV2	G*	1.210	2.03E+09	0.776	0.249	0.001	0.272%
	δ	0.475	1.57E+09	0.815	0.244	0.001	2.550%
R56/7_S-E1_PAV4	G*	1.162	1.59E+09	0.891	0.242	0.001	0.233%
	δ	0.723	1.30E+09	0.935	0.244	0.001	1.256%
R61/6_SC-E2_ORIG	G*	3.659	1.18E+10	0.240	0.241	0.001	0.377%
	δ	2.200	0.00E+00	0.230	0.314	0.001	No Solve
R61/6_SC-E2_PAV2	G*	1.233	2.24E+09	0.734	0.243	0.001	0.245%
	δ	0.300	1.77E+09	0.819	0.240	0.001	1.567%
R61/6_SC-E2_PAV4	G*	1.050	1.14E+09	0.993	0.235	0.001	0.358%
	δ	0.000	2.09E+09	1.060	0.224	0.001	No Solve

Binder	Parameters	G_e (Pa)	G_g (Pa)	|β|	|ɣ|	λ	Σ RMSE
Original binders with artificial ageing							
R61/7_SC-E2_ORIG	G*	3.411	1.31E+10	0.221	0.243	0.001	0.401%
	δ	1.845	1.00E+08	0.209	0.304	0.001	1.339%
R61/7_SC-E2_RTFO	G*	1.730	4.88E+09	0.499	0.243	0.001	0.299%
	δ	1.625	3.73E+08	0.497	0.276	0.001	1.357%
R61/7_SC-E2_RTFO+PAV2	G*	1.027	1.31E+09	0.902	0.236	0.001	0.247%
	δ	0.000	2.15E+09	0.974	0.222	0.001	No Solve
R61/7_SC-E2_RTFO+PAV4	G*	1.137	7.28E+08	1.134	0.241	0.001	0.318%
	δ	0.000	2.11E+09	1.215	0.220	0.001	No Solve
R61/7_SC-E2_PAV2	G*	1.219	2.07E+09	0.731	0.243	0.001	0.256%
	δ	0.140	1.97E+09	0.828	0.230	0.001	1.813%
R61/7_SC-E2_PAV4	G*	1.192	1.68E+09	0.914	0.223	0.001	0.217%
	δ	0.000	2.68E+09	1.195	0.196	0.001	No Solve
R61/8_SC-E2_ORIG	G*	8.248	7.66E+09	0.338	0.241	0.001	0.282%
	δ	2.187	4.06E+07	0.290	0.295	0.001	1.489%
R61/8_SC-E2_RTFO	G*	2.114	6.79E+09	0.464	0.236	0.001	0.282%
	δ	1.924	1.53E+08	0.416	0.279	0.001	1.279%
R61/8_SC-E2_RTFO+PAV2	G*	1.205	1.89E+09	0.830	0.227	0.001	0.234%
	δ	0.001	3.62E+09	1.131	0.198	0.001	1.365%
R61/8_SC-E2_RTFO+PAV4	G*	1.148	1.10E+09	1.029	0.226	0.001	0.258%
	δ	0.000	2.09E+09	1.070	0.209	0.001	No Solve
R61/8_SC-E2_PAV2	G*	1.397	3.23E+09	0.676	0.221	0.001	0.232%
	δ	0.151	1.97E+09	0.800	0.217	0.001	1.353%
R61/8_SC-E2_PAV4	G*	1.141	1.38E+09	0.878	0.230	0.001	0.236%
	δ	0.000	2.17E+09	0.940	0.215	0.001	No Solve
Recovered binders							
N8/11_S-E1_2y4m	G*	1.165	1.64E+09	0.933	0.266	0.001	0.213%
	δ	1.542	4.29E+08	0.904	0.284	0.001	1.204%
N2/16_S-E1_10m	G*	1.181	1.78E+09	0.917	0.273	0.001	0.242%
	δ	1.770	2.30E+08	0.853	0.300	0.001	1.311%
R56/7_S-E1_11m	G*	1.207	2.13E+09	0.801	0.263	0.001	0.256%
	δ	1.785	2.19E+08	0.755	0.294	0.001	1.333%
R61/6_SC-E2_6m	G*	1.283	2.66E+09	0.609	0.254	0.001	0.285%
	δ	1.057	9.43E+08	0.652	0.270	0.001	1.277%
R61/7_SC-E2_6m	G*	1.260	2.41E+09	0.668	0.260	0.001	0.273%
	δ	1.443	5.40E+08	0.678	0.284	0.001	1.354%
R61/8-SCE2-1m	G*	1.305	2.78E+09	0.610	0.259	0.001	0.290%
	δ	1.551	4.39E+08	0.608	0.286	0.001	1.315%
DR1398_70/100_22y	G*	1.117	6.95E+08	1.201	0.280	0.001	0.202%
	δ	0.000	2.10E+09	1.272	0.260	0.001	No Solve
MR23_70/100_3y	G*	1.112	1.09E+09	1.006	0.279	0.001	0.220%
	δ	0.900	1.12E+09	1.040	0.281	0.001	1.275%
MR174_70/100_9y	G*	1.118	1.24E+09	0.920	0.265	0.001	0.217%
	δ	0.211	1.88E+09	1.027	0.256	0.001	1.903%
N1/29(79.8km)_S-E1+fog_9y	G*	1.237	5.10E+08	1.537	0.261	0.001	0.199%
	δ	0.000	2.16E+09	1.542	0.217	0.001	No Solve
N1/29(102.6km)_S-E1+fog_5y	G*	1.102	7.08E+08	1.111	0.264	0.001	0.212%
	δ	0.000	2.09E+09	1.173	0.243	0.001	No Solve
N2/31_S-E1+fog_6y	G*	1.152	1.16E+09	1.105	0.269	0.001	0.197%
	δ	0.256	1.83E+09	1.172	0.257	0.001	2.141%
N6/4_S-E1+fog_9y	G*	1.127	6.29E+08	1.203	0.261	0.001	0.192%
	δ	0.000	2.08E+09	1.084	0.222	0.001	No Solve
N10/2_S-E1+fog_6y	G*	1.130	1.37E+09	0.918	0.268	0.001	0.218%
	δ	0.000	2.08E+09	0.996	0.255	0.001	No Solve

As discussed in Section 2.7.4, Figure 2-41 shows and confirms how the GLS model parameters affects the form of the G* master curve. Where the β, ɣ and λ parameters define the shape between

the inflection point and the asymptotes, ɣ gives the slope of the G* master curve at the inflection point, β controls the horizontal position of the inflection point, while the λ controls the vertical position of the inflection point.

Accordingly, it is expected that the slope of the G* master curve will flatten with age and that asymmetry of the curve will increase, thus ɣ will decrease. Consequently, β is expected to increase with age. It was also found in literature that the additional non-symmetrical parameter, λ, increases with age.

The following trends were observed in this study's GLS model parameters (Figures 4-17 and 4-18):

- The literature trend was confirmed by inspection that while the frequency of the inflection point decreases the β value increases with age.
- The slope of the δ master curve, parameter ɣ, shows decreases for both artificially aged and recovered binders, with the exception of the recovered G* master curve where a slight increase in age was observed. An average value of 0.252 was obtained for the slope parameters of the GLS model, ranging between 0.20 and 0.33.
- The non-symmetrical parameter, λ, trend was in contrast with this study as a slight decline in age where observed for both artificially aged and recovered binders (G* and δ model parameters). All the λ values were in the region of the initial value of 0.001, which aligns with literature as it is close to the Gompertz method (λ = 0.0) and worked well for highly modified binders.
- The glassy modulus, G_g, deceased with age for the G* model parameters while it reduced for the δ model parameters. The average glassy modulus for all the binders was $3.22 \cdot 10^9$ Pa, which is in the same order size mentioned in literature, a fixed value of 10^9 Pa.
- The equilibrium complex shear modulus, G_e, decreased with age for both artificially aged and recovered binders (G* and δ model parameters).

Table 4-7 and Figure 4-12 also shows that the GLS model's RMSE percentages for all the binders. There was no specific RMSE limit stated in literature for the GLS model. Thus, the CAM model's RMSE ≤ 2.25% limit was also used for the GLS model in this study.

Data shows that there is only two δ RMSE percentages that are above the 2.25% line, both being S-E1 binders that were artificially aged to PAV2 (highest value of 2.731%), which is much less than the CAM model's RMSE's values above 2.25%. Although the RMSE results for GLS were excellent, it could not solve 18 binders' δ material behaviour data, where the CAM model fitted to all the binders measured behaviour.

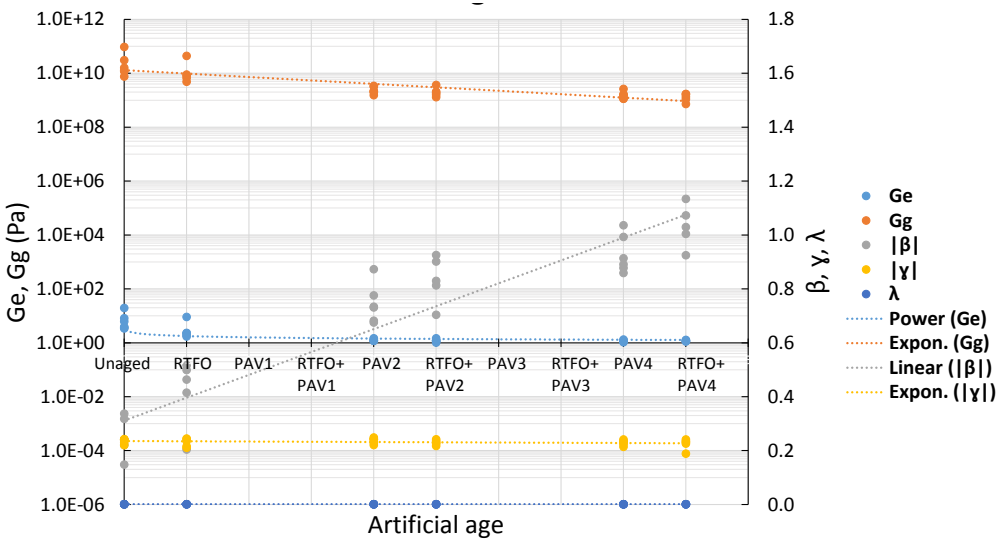

(a) G* model parameters

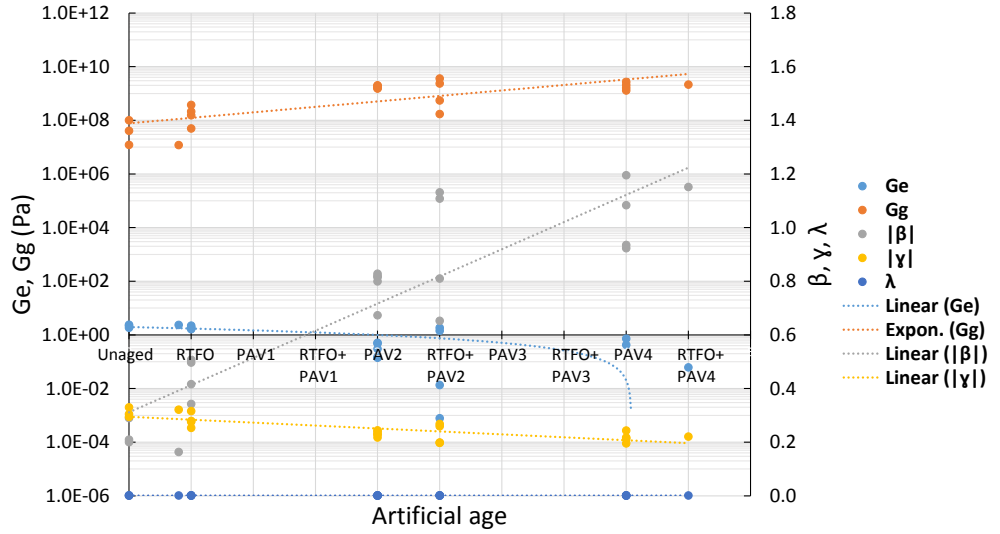

(b) δ model parameters

Figure 4-17: GLS model parameters of artificially aged binders

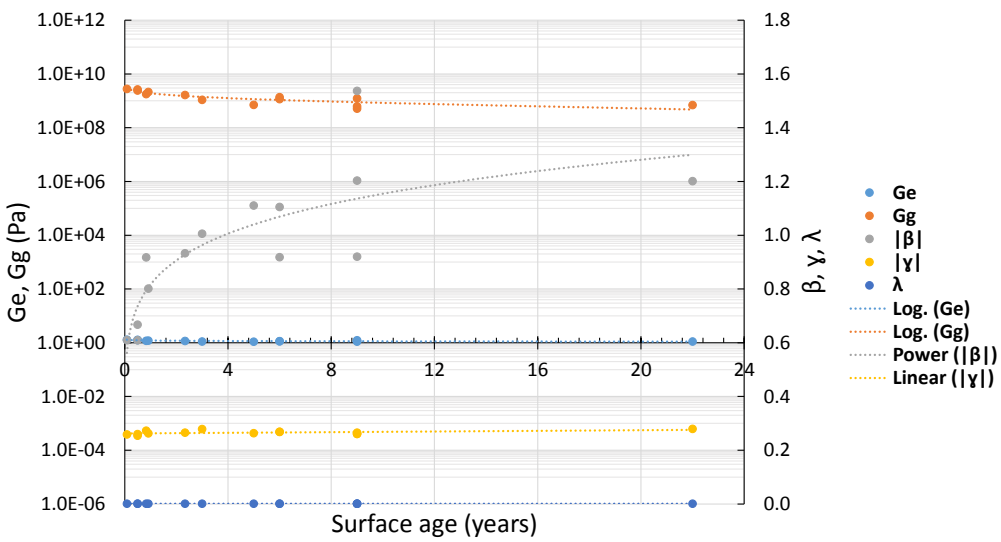

(a) G* model parameters

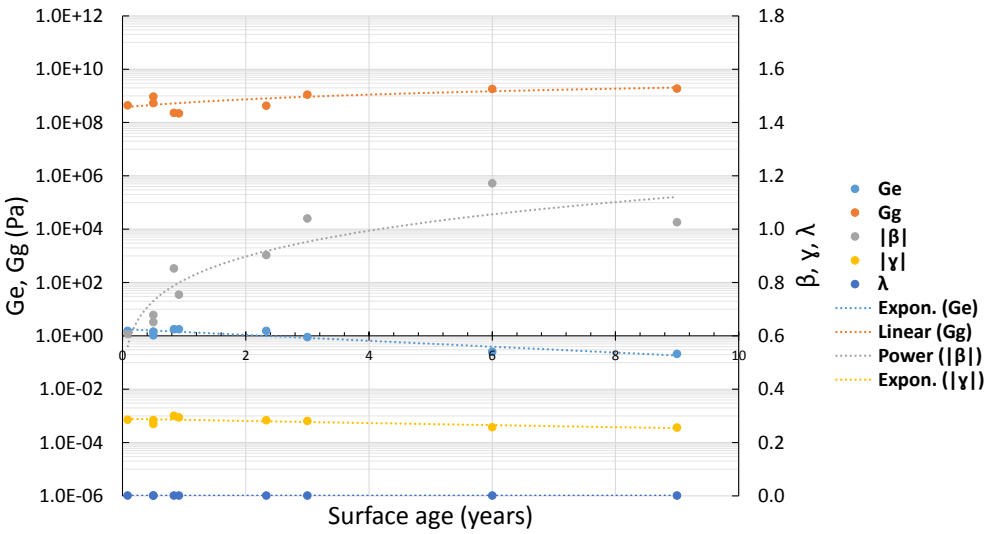

(b) δ model parameters

Figure 4-18: GLS model parameters of recovered binders

Figures 4-19 and 4-20 shows the GLS model's correlation (R^2) between the modelled and measured data, with its summary contained in **Appendix C**.

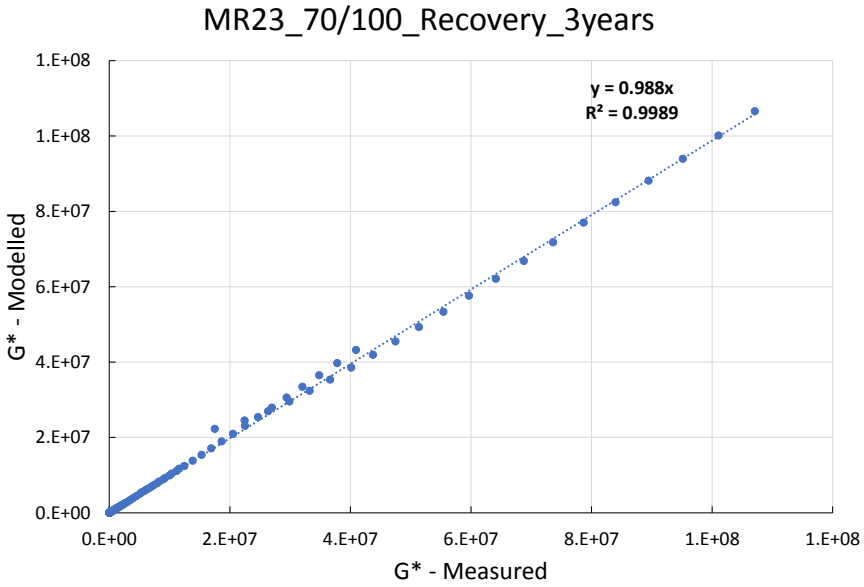

Figure 4-19: GLS G* data correlation, G* > 10^4 Pa

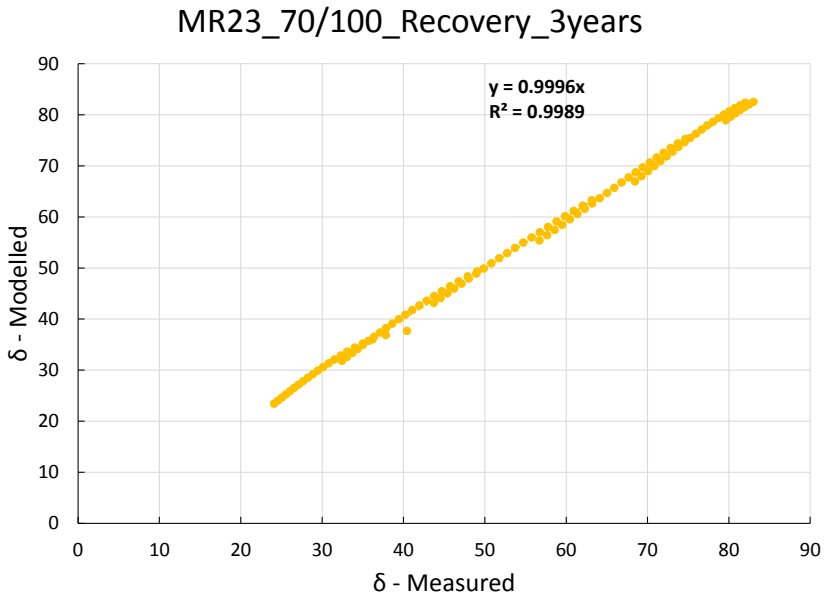

Figure 4-20: GLS δ data correlation, G* > 10^4 Pa

Figures 4-21 and 4-22 shows the end result after modelling with the GLS model, needed to obtain the master curves and Black Space diagrams of binders. These figures include binders with and without G-R parameter on the binder's modelled Black Space diagram.

Appendix A (modelling) shows that binder R61/7_SC-E2_Original is the only binder where the G* of 8.07·103 Pa (associated with the G-R parameter) was below the 104 Pa GLS acceptable limit for this study. For this reason, the GLS model was not regarded suitable for the R61/7_SC-E2_Original binder to determine the G-R parameter.

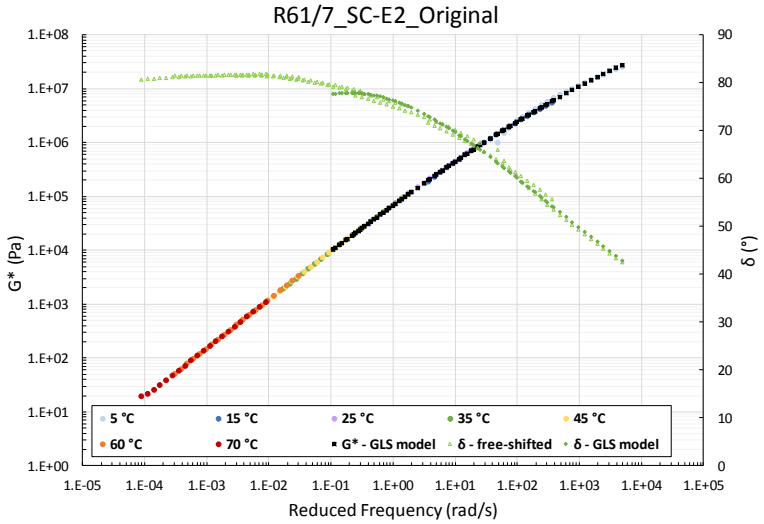

(a) G-R parameter not on Black Space Diagram

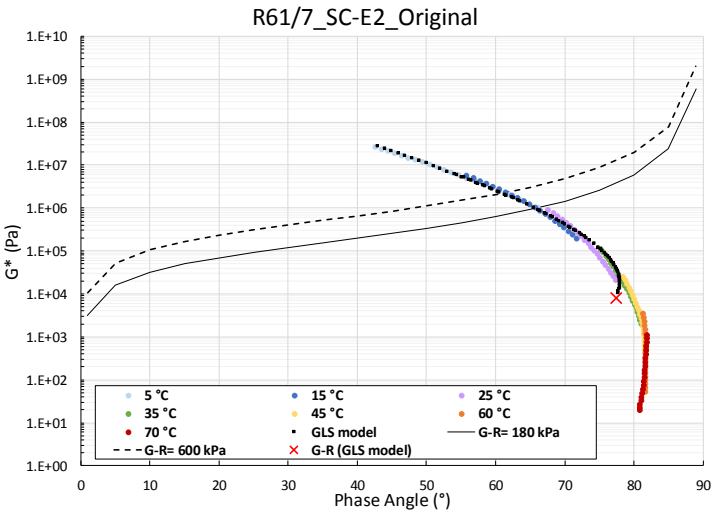

(a) G-R parameter not on Black Space Diagram

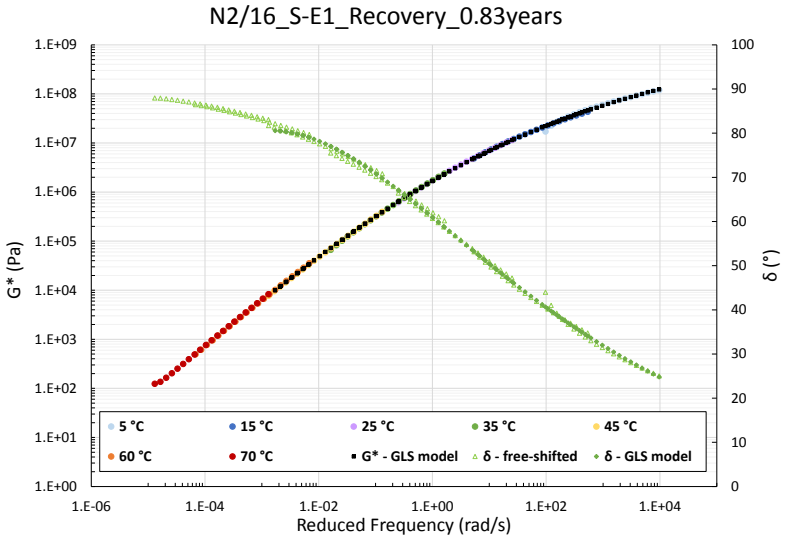

(b) G-R parameter on Black Space Diagram

Figure 4-21: GLS model G* and master curves

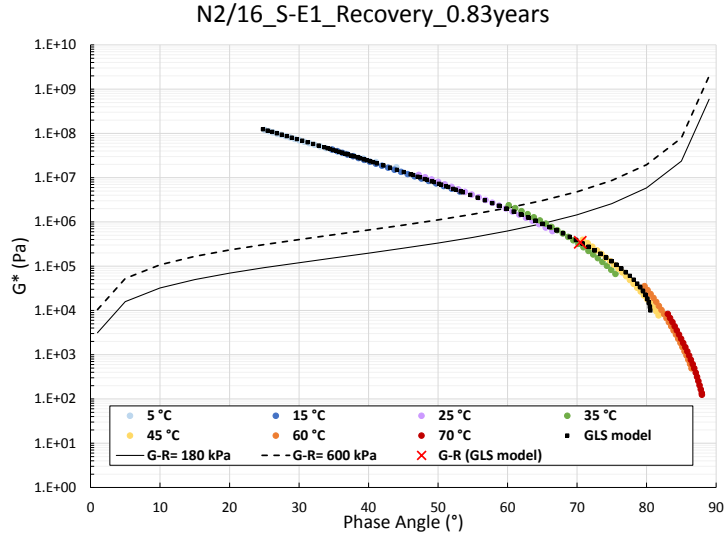

(b) G-R parameter on Black Space Diagram

Figure 4-22: GLS model Black Space diagram

4.5 Suitable model

After modelling the measured behaviour of all the binders with the CAM and GLS models, a suitable model was identified on a binder-to-binder basis, including ageing of binders, in order to ensure that all binder data delivers results and don't become unusable.

The following suitability criteria were used to select an appropriate model:

- First the suitable model was selected by taking into account the best RMSE percentage, which meant that the model best fits the measured behaviour of the binder;
- It was also important to take into consideration that the G-R parameter of the binder needs to fall on top of the binder's modelled Black Space diagram, ensuring that data can be used to calculate the G-R parameter.

There were six binders in the best fit model (lowest RMSE percentage), where the G-R parameter did not fall on top of the modelled Black Space diagram. In such a case the other model was used, provided it could be solved, if not, such a binder's G-R parameter could not be used for further analysis.

Table 4-8 shows the suitable model for each binder (binder-to-binder basis). Each binder's isotherm graph, Modified Kaelble shift factor information, modelled master curve and Black Space diagram are included in **Appendix A**.

Table 4-8: Suitable model on binder to binder basis

Binder		Σ RMSE		Binder		Σ RMSE	
		CAM	GLS			CAM	GLS
Original binders with artificial ageing							
N8/11_S-E1_ORIG	G*		0.356%	R61/7_SC-E2_ORIG	G*		0.401%
	δ		1.582%		δ		1.339%
N8/11_S-E1_RTFO	G*		0.268%	R61/7_SC-E2_RTFO	G*		0.299%
	δ		1.922%		δ		1.357%
N8/11_S-E1_RTFO+PAV2	G*		0.206%	R61/7_SC-E2_RTFO+PAV2	G*	0.231%	
	δ		1.549%		δ	1.955%	
N8/11_S-E1_RTFO+PAV4	G*	0.154%		R61/7_SC-E2_RTFO+PAV4	G*	0.246%	
	δ	1.554%			δ	3.585%	
N8/11_S-E1_PAV2	G*	0.212%		R61/7_SC-E2_PAV2	G*		0.256%
	δ	4.517%			δ		1.813%
N8/11_S-E1_PAV4	G*	0.210%		R61/7_SC-E2_PAV4	G*	0.213%	
	δ	2.041%			δ	1.606%	
N2/16_S-E1_ORIG	G*	0.532%		R61/8_SC-E2_ORIG	G*		0.282%
	δ	2.415%			δ		1.489%
N2/16_S-E1_RTFO	G*		0.396%	R61/8_SC-E2_RTFO	G*		0.282%
	δ		2.103%		δ		1.279%
N2/16_S-E1_RTFO+PAV2	G*	0.234%		R61/8_SC-E2_RTFO+PAV2	G*		0.234%
	δ	1.602%			δ		1.365%
N2/16_S-E1_RTFO+PAV4	G*	0.216%		R61/8_SC-E2_RTFO+PAV4	G*	0.201%	
	δ	1.716%			δ	2.259%	
N2/16_S-E1_PAV2	G*		0.283%	R61/8_SC-E2_PAV2	G*		0.232%
	δ		2.731%		δ		1.353%
N2/16_S-E1_PAV4	G*		0.184%	R61/8_SC-E2_PAV4	G*	0.220%	
	δ		1.580%		δ	1.816%	
R56/7_S-E1_ORIG	G*	0.555%		R61/6_SC-E2_ORIG	G*	0.427%	
	δ	1.475%			δ	1.215%	
R56/7_S-E1_RTFO	G*		0.364%	R61/6_SC-E2_PAV2	G*		0.245%
	δ		1.647%		δ		1.567%

Binder		Σ RMSE		Binder		Σ RMSE	
		CAM	GLS			CAM	GLS
Original binders with artificial ageing							
R56/7_S-E1_RTFO+PAV2	G*		0.249%	R61/6_SC-E2_PAV4	G*	0.222%	
	δ		1.264%		δ	2.958%	
R56/7_S-E1_RTFO+PAV4	G*		0.228%				
	δ		1.331%				
R56/7_S-E1_PAV2	G*		0.272%				
	δ		2.550%				
R56/7_S-E1_PAV4	G*		0.233%				
	δ		1.256%				
Recovered binders							
N8/11_S-E1_2y4m	G*		0.213%	MR23_70/100_4y	G*		0.220%
	δ		1.204%		δ		1.275%
N2/16_S-E1_10m	G*		0.242%	MR174_70/100_10y	G*		0.217%
	δ		1.311%		δ		1.903%
R56/7_S-E1_11m	G*		0.256%	N1/29(79.8km)_S-E1+fog_9y	G*	0.175%	
	δ		1.333%		δ	13.252%	
R61/6_SC-E2_6m	G*		0.285%	N1/29(102.6km)_S-E1+fog_5y	G*	0.243%	
	δ		1.277%		δ	4.116%	
R61/7_SC-E2_6m	G*		0.273%	N2/31_S-E1+fog_6y	G*		0.197%
	δ		1.354%		δ		2.141%
R61/8-SCE2-1m	G*		0.290%	N6/4_S-E1+fog_9y	G*	0.192%	
	δ		1.315%		δ	8.367%	
DR1398_70/100_23y	G*	0.261%		N10/2_S-E1+fog_6y	G*	0.236%	
	δ	4.334%			δ	3.271%	

The abovementioned table shows that up to 60% of all the binders were suitable to the GLS model, with overall only 12 binders (δ data) exceeding the RMSE acceptability limit of 2.25%.

4.6 Durability and Ageing Parameters

Both durability and ageing parameters for each binder was determined according to its suitability of the CAM or GLS, as determined and listed in Section 4.5. Throughout this section, both the ageing conditioning levels (with and without RTFO ageing) will be compared, to obtain if there is a substantial difference between seal RTFO and seal RTFO+PAV artificial ageing. The objective is to understand how ageing aspects of seal binder influences the behaviour.

4.6.1 Glover-Rowe (G-R) Parameter

The Glover-Rowe (G-R) parameter was calculated with its suitable model per binder, as shown in Table 4-9. This was done at temperature 15°C and 0.005 rad/s frequency.

It should be noted that four of the binders (N2/16_S-E1_Original, R56/7_S-E1_Original, R61/6_SC-E2_Original and R61/7_SC-E2_Original) were not included in Table 4-9, as there G-R data are unusable for further analysis. Table 4-9 shows that the G-R parameter increased with age, while G* increased and the phase angle decreased, except for the N2/16_S-E1 artificially aged binder at PAV4 and RTFO+PAV4.

Table 4-9: G-R parameter and associated G* and δ for all the binders

Binder	Suitable Model	G-R (Pa)	G* (Pa)	δ (°)
Original binders with artificial ageing				
N8/11_S-E1_ORIG	GLS	2.59E+03	2.73E+04	72.468
N8/11_S-E1_RTFO	GLS	1.57E+04	8.42E+04	65.664
N8/11_S-E1_PAV2	CAM	7.86E+04	2.84E+05	60.581
N8/11_S-E1_RTFO+PAV2	GLS	2.14E+05	4.95E+05	53.809
N8/11_S-E1_PAV4	CAM	3.25E+05	7.20E+05	53.100
N8/11_S-E1_RTFO+PAV4	CAM	1.19E+06	1.48E+06	42.527
N2/16_S-E1_RTFO	GLS	3.22E+03	2.56E+04	69.891
N2/16_S-E1_PAV2	GLS	2.42E+04	1.31E+05	65.749
N2/16_S-E1_RTFO+PAV2	CAM	2.97E+04	1.64E+05	65.986
N2/16_S-E1_PAV4	GLS	1.62E+05	4.37E+05	56.319
N2/16_S-E1_RTFO+PAV4	CAM	1.47E+05	4.36E+05	57.757
R56/7_S-E1_RTFO	GLS	1.97E+03	3.62E+04	76.687
R56/7_S-E1_PAV2	GLS	3.41E+04	1.92E+05	66.204
R56/7_S-E1_RTFO+PAV2	GLS	5.58E+04	2.62E+05	64.048
R56/7_S-E1_PAV4	GLS	1.03E+05	3.73E+05	60.596
R56/7_S-E1_RTFO+PAV4	GLS	3.10E+05	7.43E+05	54.404
R61/6_SC-E2_PAV2	GLS	2.07E+04	1.29E+05	67.370
R61/6_SC-E2_PAV4	CAM	2.56E+05	5.88E+05	53.709
R61/7_SC-E2_RTFO	GLS	2.52E+03	3.53E+04	74.802
R61/7_SC-E2_PAV2	GLS	2.07E+04	1.22E+05	66.735
R61/7_SC-E2_RTFO+PAV2	CAM	9.20E+04	2.88E+05	58.551
R61/7_SC-E2_PAV4	CAM	1.65E+05	4.18E+05	55.226
R61/7_SC-E2_RTFO+PAV4	CAM	4.88E+05	9.09E+05	50.060
R61/8_SC-E2_ORIG	GLS	3.31E+03	2.90E+04	70.812
R61/8_SC-E2_RTFO	GLS	3.31E+03	3.53E+04	72.574
R61/8_SC-E2_PAV2	GLS	2.62E+04	1.18E+05	63.492
R61/8_SC-E2_RTFO+PAV2	GLS	7.11E+04	2.44E+05	59.892
R61/8_SC-E2_PAV4	CAM	9.16E+04	2.72E+05	57.754
R61/8_SC-E2_RTFO+PAV4	CAM	3.28E+05	6.52E+05	51.241
Recovered binders				
N8/11_S-E1_2y4m	GLS	6.44E+04	3.91E+05	67.092
N2/16_S-E1_10m	GLS	4.12E+04	3.47E+05	70.460
R56/7_S-E1_11m	GLS	2.21E+04	2.02E+05	71.228
R61/6_SC-E2_6m	GLS	3.38E+03	4.96E+04	75.134
R61/7_SC-E2_6m	GLS	4.89E+03	7.42E+04	75.376
R61/8_SC-E2_1m	GLS	2.82E+03	5.01E+04	76.470
DR1398_70/100_22y	CAM	3.63E+05	1.04E+06	57.227
MR23_70/100_3y	GLS	7.90E+04	4.55E+05	66.473
MR174_70/100_9y	GLS	4.97E+04	2.86E+05	66.481
N1/29(79.8km)_S-E1+fog_9y	CAM	3.56E+06	4.42E+06	42.492
N1/29(102.6km)_S-E1+fog_5y	CAM	2.44E+05	6.69E+05	56.506
N2/31_S-E1+fog_6y	GLS	2.56E+05	9.10E+05	60.357
N6/4_S-E1+fog_9y	CAM	4.60E+05	9.94E+05	52.648
N10/2_S-E1+fog_6y	CAM	4.77E+04	2.76E+05	66.540

Figure 4-23 shows the recovered binders' G-R parameters plotted in Black Space, noting the following:

- All recovered binders showed the same trend by decreasing in phase angle and increasing in G*. Thus, implying that the binders gain a larger elastic component as it aged, becoming more brittle and stiff.
- The G-R parameter limits are 180 kPa for onset cracking and 600 kPa for significant cracking correlating with 5 and 3 cm ductility at 15°C. Figure 4-23 showed that the ductility of the binders reduced with age, whilst increasing in G-R value, making the binders susceptible to cracking (ductile fracture).The stiffest sample (N1/29_79.8km) with an age of 9 years had the

least resistance to cracking as it exceeded both cracking G-R limits, with the highest G-R value of 3560 kPa.

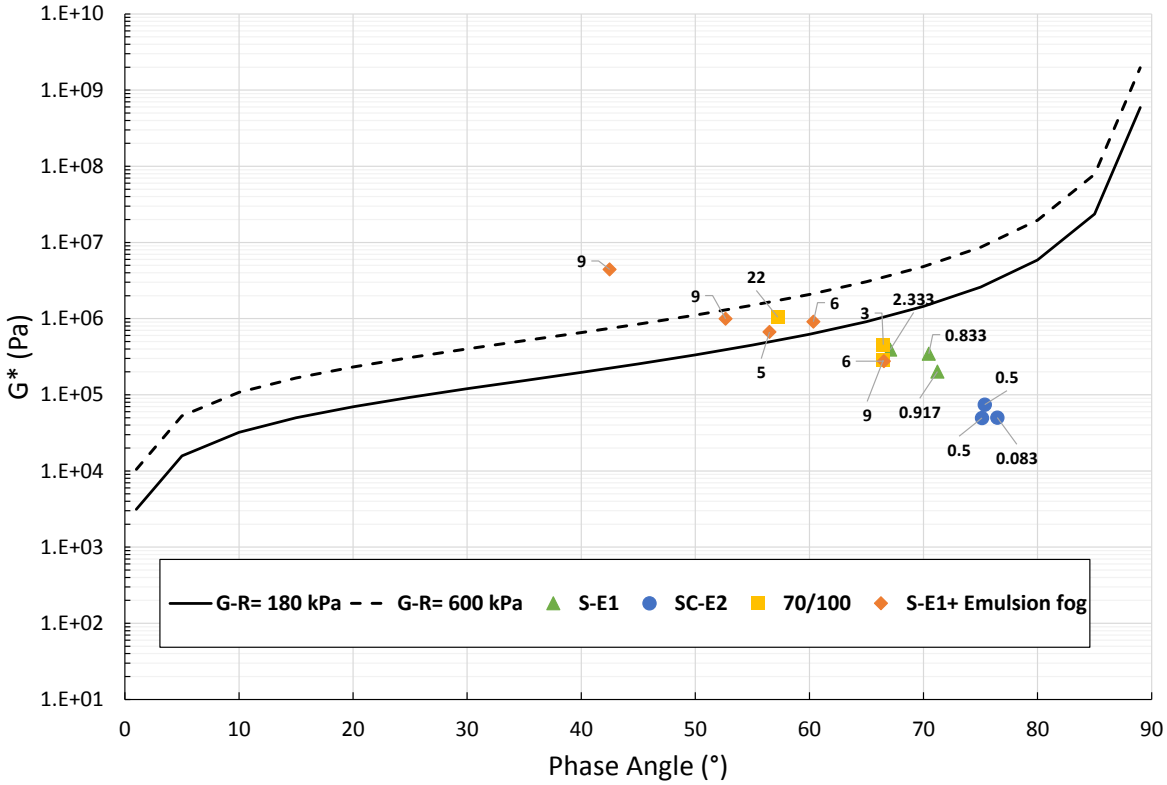

Figure 4-23: G-R parameter for all recovered binders

Figure 4-24 shows the artificially aged binders' G-R parameters plotted in Black Space, noting the following:

- It shows the effect of binder reacting with the oxygen in the environment, making the binder more elastic, brittle and stiff.
- The G-R value and associated G* increased with artificial ageing at 15°C and 0.005 rad/s.
- Only the N8/11_S-E1 artificially aged at RTFO+PAV4 exceeded the significant cracking limit (G-R = 600 kPa) and shows fatigue and thermal cracking, with a G-R value of 1190kPa.
- Of the 6 artificially aged samples, 5 entered the onset cracking zone (exceeding the 180 kPa G-R limit) with N8/11_S-E1 already being in the significant cracking zone. Whilst the N2/16_S-E1 artificially aged sample was the only sample that did not enter the onset cracking zone, with a maximum value of 162 kPa for PAV4 ageing.
- The figure also shows that ductility decreased, and G-R increased with age, similar to that for recovered samples, indicating vulnerability of cracking.
- The figure further shows that the unaged and RTFO aged binder graph bends more, whilst the long-termed aged binder graph becomes straighter. This indicates that the polymer in the modifier at long-term aged no longer influences the binder's elasticity properties, in comparison to short-term aged where there is still active polymer influencing behaviour.
- From Engelbrecht's (2018) work, it is noted that the unmodified (70/100) artificially aged samples' G-R values are spaced out more consistently than that for modified binders (S-E1 and S-E2). This study's modified binders (S-E1 and SC-E2) also showed inconsistent spaced G-R values, due to the modification of binders varying too much.

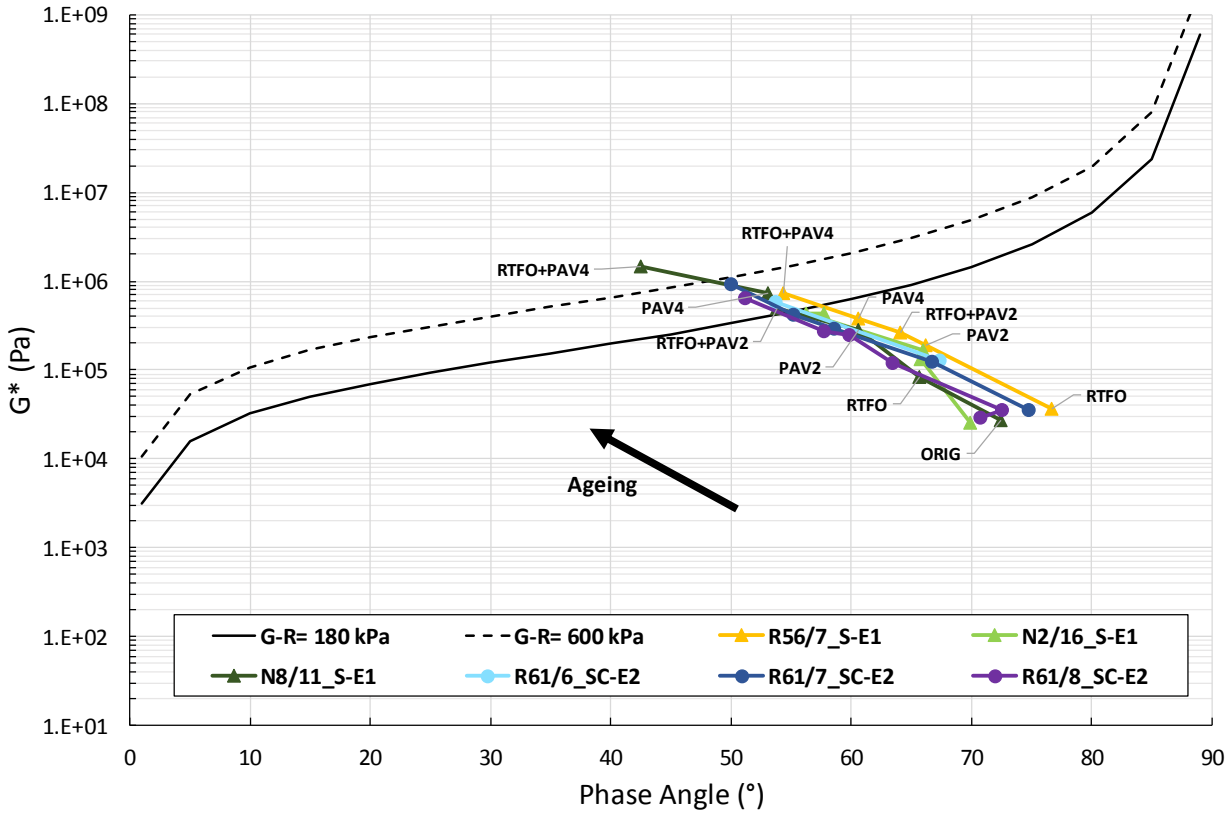

Figure 4-24: Artificially aged binder's G-R values in Black Space

Figures 4-25 and 4-26 distinguishes between unmodified and modified recovered binder deterioration of G-R values with age.

- Figure 4-25 shows a reasonably consistent trend regarding the correlation between G-R and surface ageing, yielding correlation for unmodified and modified binders.
    - This is significant as the G-R onset cracking limit is reached at 6 and 12 years for modified and unmodified binders respectively.
    - Only 5 of the 14 recovered binders showed cracking, where 4 of them are multiple modified seals with an emulsion fog and one unmodified, being the oldest sample.
    - Results showed that the Limpopo multiple modified seal's ductility (stiffest sample of all samples) was largely affected, as it crossed both G-R limits.
- Figure 4-26 shows Goosen's (2018) recovered binder results, also showing a reasonable consistent trend regarding the correlation between G-R and surface ageing for both unmodified and modified binders.
    - The G-R onset cracking limit is reached at 8 and 19 years for modified and unmodified binders respectively.
- As no visual assessment was conducted in this study (Figure 4-25), it is concluded from literature that for both Figures 4-25 and 4-26 the binders below G-R = 180 kPa will experience no cracking. Cracking will start when binder's G-R exceed 180 kPa.
    - Based on this conclusion, it is evident that after 6 years a visual assessment will be recommended to determine possible early deterioration of the pavement.

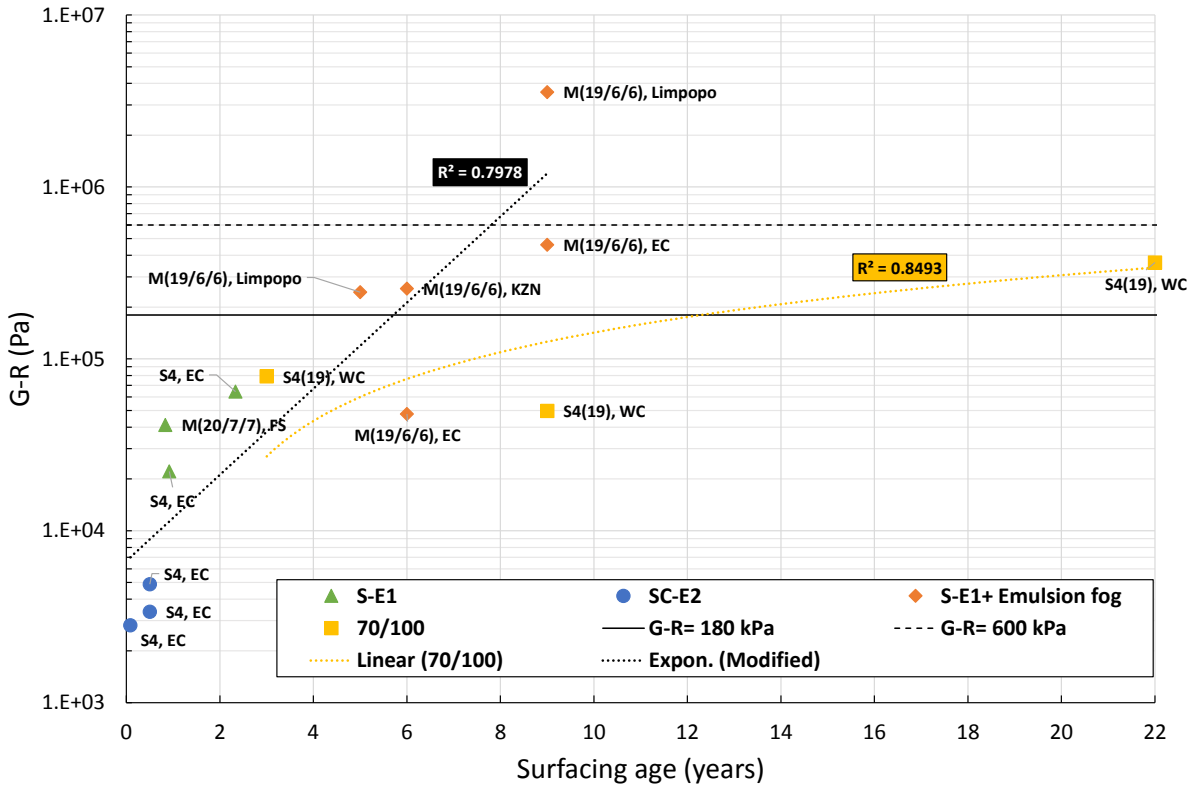

Figure 4-25: Recovered binder's G-R values with age, seal type and province

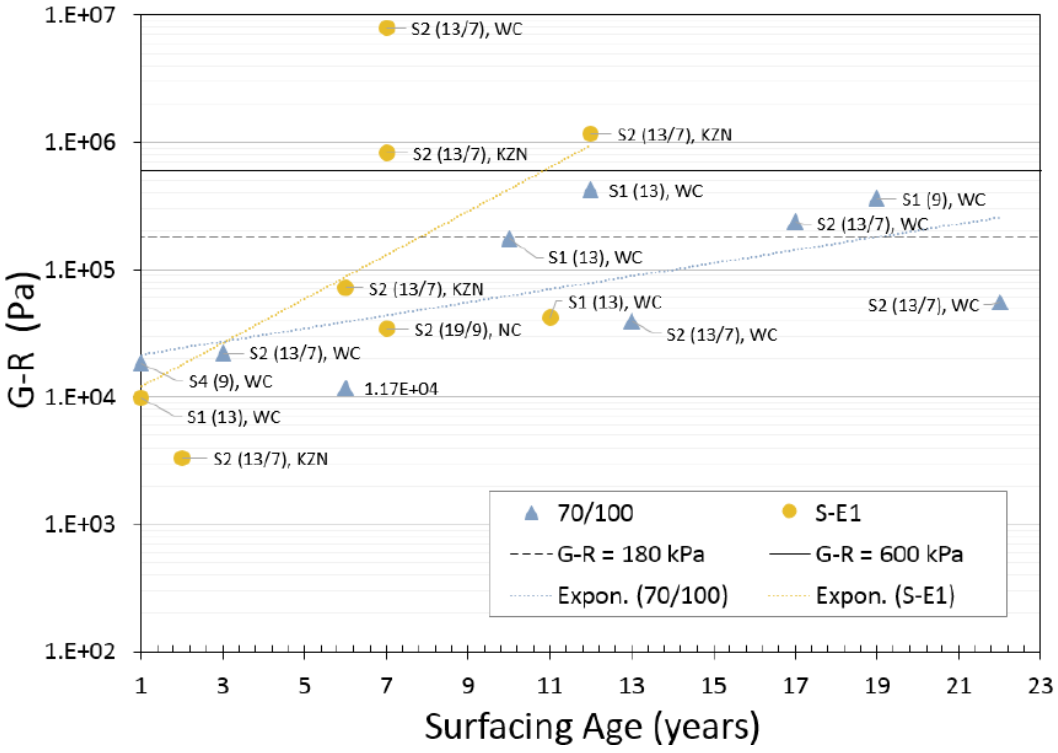

Figure 4-26: Goosen's recovered binder's G-R values with age, seal type and province (Goosen, 2018)

Figure 4-27 shows Goosen's (2018) work on comparing performance parameters to in-field cracking visual assessments. Note the G-R limits of 80 kPa and 1500 kPa. It is evident that most of the aggregate loss observed occurred below G-R = 600 kPa.

Moisture damage is a failure mechanism that causes loss of adhesive strength in seals, thus constituting aggregate loss. This may also lead to fractures that are in form of cracking. Thus aggregate loss is an indication of deterioration that may lead to complete failure of the pavement.

This result shows that the required period to do a visual assessment (identifying deterioration of pavement) can be extended to 8 year. Figures 4-25 and 4-26 shows a correlation trend at G-R = 600 kPa, as Figure 4-27 shows only cracking with values above G-R = 790 kPa.

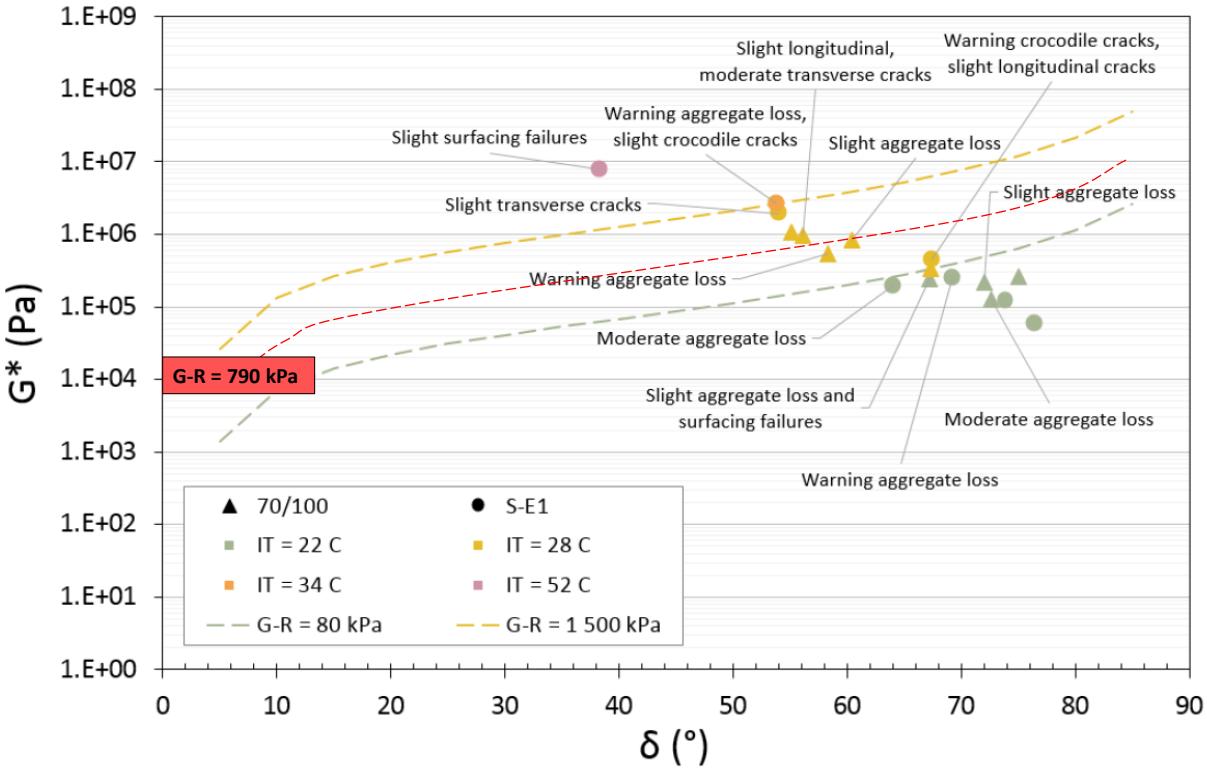

Figure 4-27: Recovered binders' G-R correlation with field performance (adapted from Goosen, 2018)

4.6.2 Viscoelastic transition (VET) stiffness and temperature

The viscoelastic transition (VET) stiffness and temperature are other parameters that can also be used to define susceptibility to different forms of cracking.

Table 4-10 shows the VET parameters' results for all the binders. T_{VET} was calculated from the Modified Kaelble shift equation and G^*_{VET} from the suitable model at T_{VET} and ω_c as discussed in methodology in Section 3.5.2.

Table 4-10: VET stiffness and temperature parameters for all the binders at 15°C and 0.005 rad/s

Binder	Suitable Model	G^*_{VET} (Pa)	T_{VET} (°C)	G-R (Pa)
Original binders with artificial ageing				
N8/11_S-E1_ORIG	GLS	1.60E+07	4.114	2.59E+03
N8/11_S-E1_RTFO	GLS	8.08E+06	11.013	1.57E+04
N8/11_S-E1_PAV2	CAM	5.52E+06	19.107	7.86E+04
N8/11_S-E1_RTFO+PAV2	GLS	2.73E+06	24.950	2.14E+05
N8/11_S-E1_PAV4	CAM	2.95E+06	26.501	3.25E+05
N8/11_S-E1_RTFO+PAV4	CAM	9.54E+05	39.446	1.19E+06
N2/16_S-E1_ORIG	CAM	2.71E+07	-5.197	1.40E+02
N2/16_S-E1_RTFO	GLS	1.78E+07	3.033	3.22E+03

Binder	Suitable Model	G*$_{VET}$ (Pa)	T$_{VET}$ (°C)	G-R (Pa)
Original binders with artificial ageing				
N2/16_S-E1_PAV2	GLS	7.56E+06	13.992	2.42E+04
N2/16_S-E1_RTFO+PAV2	CAM	1.02E+07	13.227	2.97E+04
N2/16_S-E1_PAV4	GLS	3.77E+06	22.830	1.62E+05
N2/16_S-E1_RTFO+PAV4	CAM	4.20E+06	22.371	1.47E+05
R56/7_S-E1_ORIG	CAM	2.58E+07	-0.041	1.25E+02
R56/7_S-E1_RTFO	GLS	1.73E+07	6.342	1.97E+03
R56/7_S-E1_PAV2	GLS	1.26E+07	12.909	3.41E+04
R56/7_S-E1_RTFO+PAV2	GLS	6.68E+06	17.977	5.58E+04
R56/7_S-E1_PAV4	GLS	5.06E+06	20.538	1.03E+05
R56/7_S-E1_RTFO+PAV4	GLS	3.53E+06	25.198	3.10E+05
R61/6_SC-E2_ORIG	CAM	1.69E+07	-2.369	1.96E+02
R61/6_SC-E2_PAV2	GLS	9.00E+06	13.032	2.07E+04
R61/6_SC-E2_PAV4	CAM	2.91E+06	24.912	2.56E+05
R61/7_SC-E2_ORIG	GLS	1.99E+07	-2.841	3.98E+02
R61/7_SC-E2_RTFO	GLS	1.23E+07	6.572	2.52E+03
R61/7_SC-E2_PAV2	GLS	8.31E+06	13.067	2.07E+04
R61/7_SC-E2_RTFO+PAV2	CAM	3.29E+06	21.767	9.20E+04
R61/7_SC-E2_PAV4	CAM	3.25E+06	23.459	1.65E+05
R61/7_SC-E2_RTFO+PAV4	CAM	1.85E+06	29.765	4.88E+05
R61/8_SC-E2_ORIG	GLS	1.38E+07	5.006	3.31E+03
R61/8_SC-E2_RTFO	GLS	1.29E+07	6.067	3.31E+03
R61/8_SC-E2_PAV2	GLS	6.66E+06	13.333	2.62E+04
R61/8_SC-E2_RTFO+PAV2	GLS	3.80E+06	20.278	7.11E+04
R61/8_SC-E2_PAV4	CAM	3.01E+06	21.971	9.16E+04
R61/8_SC-E2_RTFO+PAV4	CAM	1.95E+06	28.981	3.28E+05
Recovered binders				
N8/11_S-E1_2y4m	GLS	9.86E+06	18.417	6.44E+04
N2/16_S-E1_10m	GLS	1.28E+07	16.877	4.12E+04
R56/7_S-E1_11m	GLS	1.61E+07	12.924	2.21E+04
R61/6_SC-E2_6m	GLS	1.03E+07	9.231	3.38E+03
R61/7_SC-E2_6m	GLS	1.16E+07	10.581	4.89E+03
R61/8_SC-E2_1m	GLS	1.17E+07	9.075	2.82E+03
DR1398_70/100_22y	CAM	5.74E+06	25.107	3.63E+05
MR23_70/100_3y	GLS	8.52E+06	19.783	7.90E+04
MR174_70/100_9y	GLS	7.31E+06	18.411	4.97E+04
N1/29(79.8km)_S-E1+fog_9y	CAM	2.90E+06	38.635	3.56E+06
N1/29(102.6km)_S-E1+fog_5y	CAM	4.14E+06	24.538	2.44E+05
N2/31_S-E1+fog_6y	GLS	8.51E+06	22.441	2.56E+05
N6/4_S-E1+fog_9y	CAM	3.69E+06	27.518	4.60E+05
N10/2_S-E1+fog_6y	CAM	9.16E+06	17.266	4.77E+04

Figures 4-28, 4-29 and 4-30 shows the correlation between the VET parameters for artificially aged and recovered binders, plotting it with age and G-R, noting the following:

- Figures 4-29(a) and 4-30(a) shows that the viscoelastic transition stiffness (G*$_{VET}$) decreased with age, whilst the viscoelastic transition temperature (T$_{VET}$) increased with age, confirming literature in Section 2.8.3. This indicates poor performance of binders in-service.

- Figure 4-28 represents the artificially aged samples. It also shows behaviour corresponding with literature as per Section 2.8.3 for most of the samples.

- It was only the N8/11_S-E1 (RTFO+PAV2 and PAV4) and N2/16_S-E1 (PAV2, RTFO+PAV2, PAV4 and RTFO+PAV4) that showed some differences, which also shows in Table 4-10.
- The N2/16_S-E1 sample showed the best resistance to cracking, by having the highest G^*_{VET} and lowest T_{VET} values.

- Both the G-R parameter and the VET parameters define cracking susceptibility, with the relationship between the two evaluated in Figures 4-29(b) and 2-30(b).
  - Both artificially aged and recovered binders showed a good relationship between the G-R and the VET parameters, with a correlation that can be rounded up to one for both G^*_{VET} and T_{VET}.
  - The G^*_{VET} reduced slightly and T_{VET} increased with an increase in G-R value. The decrease in G^*_{VET} and increase in both T_{VET} and G-R values indicates the growth in cracking vulnerability.

- Note that these relationships and correlations in Figures 4-29 and 4-30 are noted without investigation of binder modification.

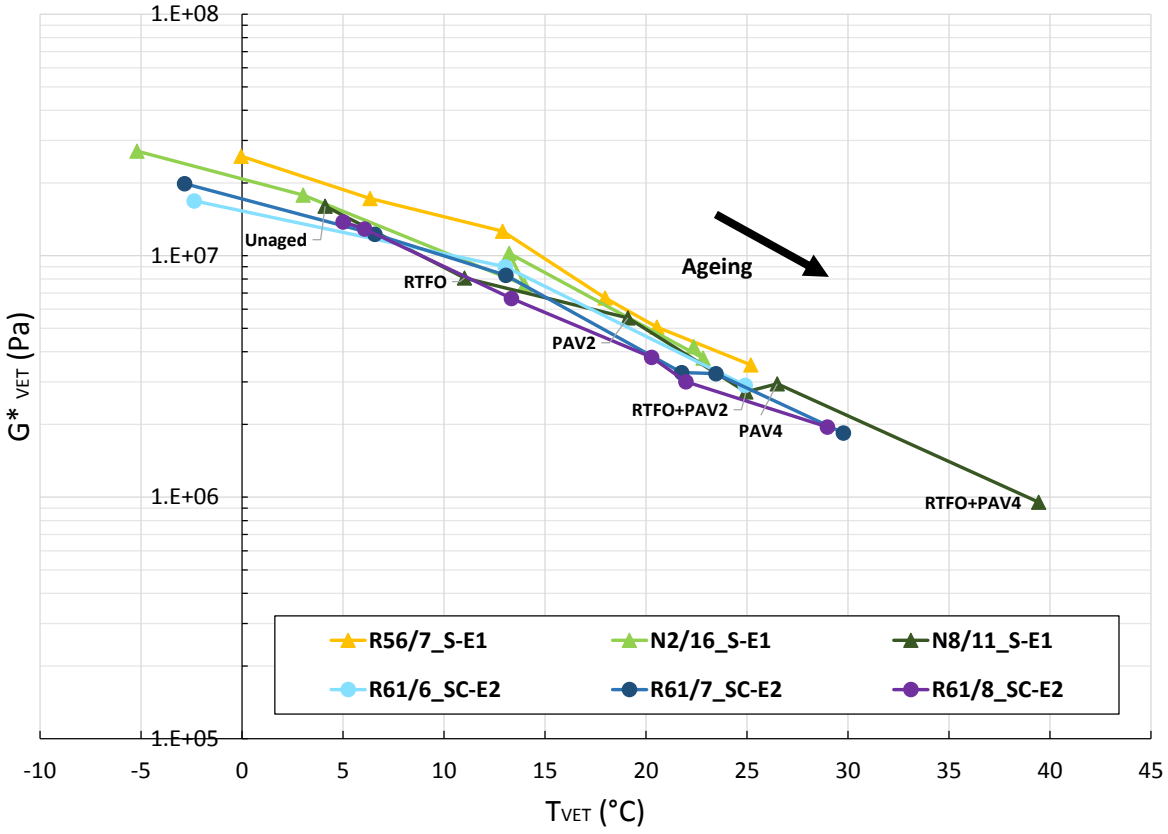

Figure 4-28: VET parameters correlation with artificial ageing

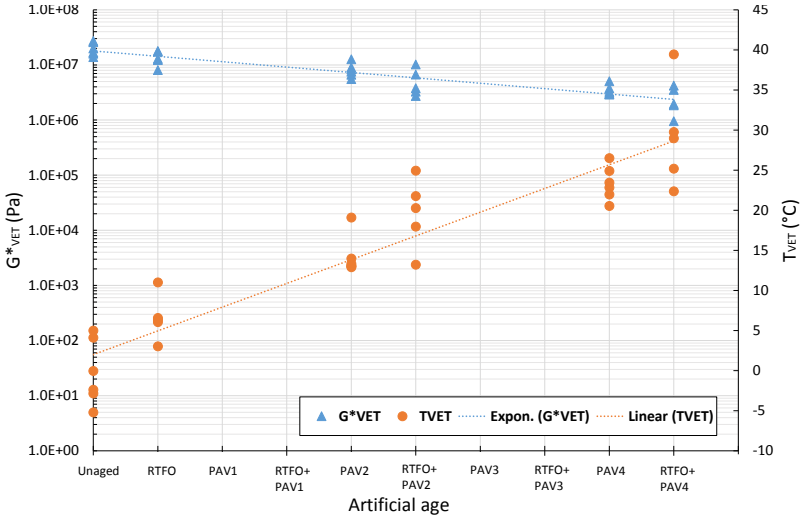

(a) VET parameters with artificial ageing

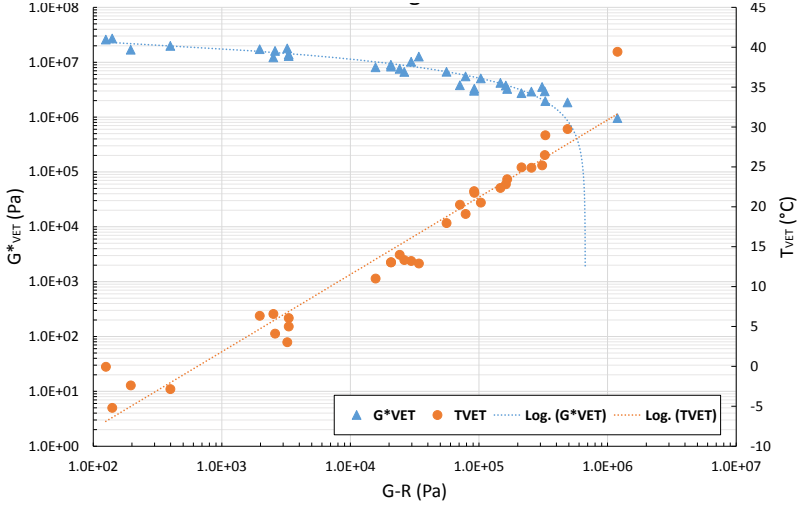

(b) Relationship between VET and G-R

Figure 4-29: Development of VET for artificially aged binders

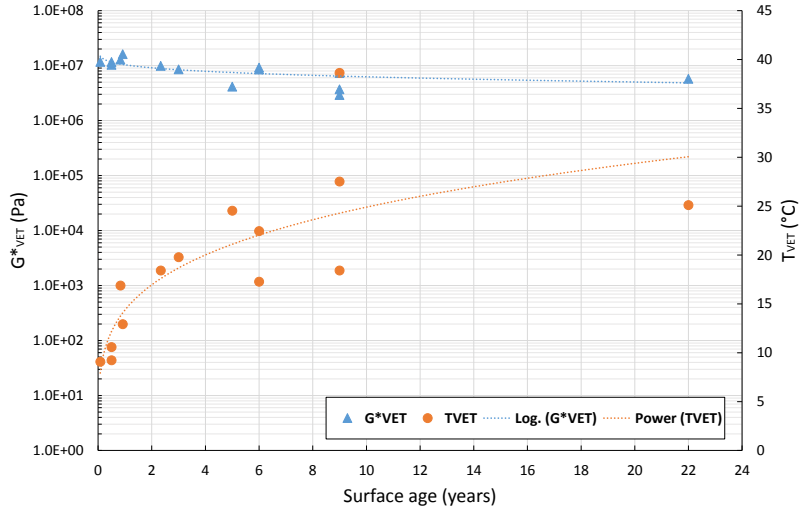

(a) VET parameter with recovered surface ageing

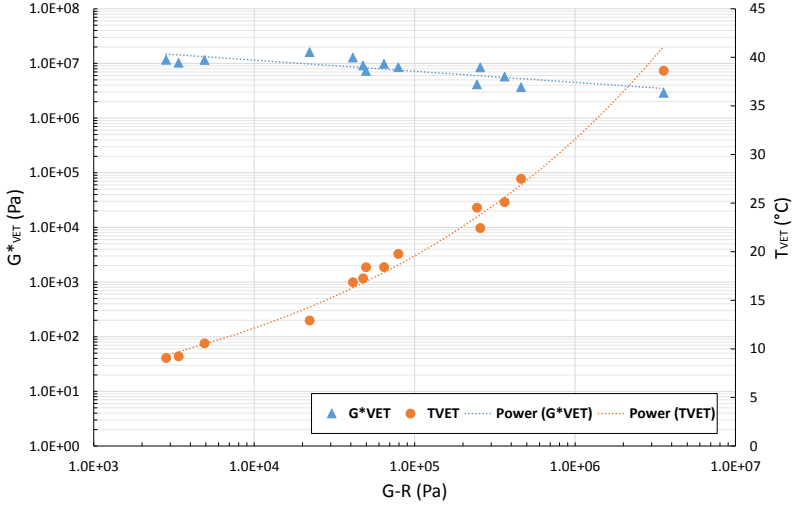

(b) Relationship between VET and G-R

Figure 4-30: Development of VET for recovered binders

Figures 4-31, 4-32 and 4-33 shows the VET parameters' correlation with modification and the cracking rate thereof, noting the following:

- Figures 4-31 and 4-33 shows a reasonably consistent trend regarding the correlation between G^*_{VET} and T_{VET}, yielding correlation unmodified and modified binders.
- Figure 4-32 shows Goosen's (2018) recovered binder results, also showing a reasonable consistent trend regarding the correlation between the two VET parameters for both unmodified and modified binders.
- Widyatmoko, Heslop and Elliott (2005) proposed a tentative specification for two unmodified binders (15 pen and 50 pen), to minimise crack susceptibility of binders. They reported that a higher penetration grade binder will decrease the T_{VET} limit and increase the G^*_{VET} limit, with 50 pen grade binder specification of $T_{VET} < 20°C$ and $G^*_{VET} > 10^7$ Pa.
    - Figure 4-31 shows that the three unmodified recovered binders (70/100) have poor resistance to cracking, with a $G^*_{VET} < 10^7$ Pa and T_{VET} between 18°C and 25°C.
- Figures 4-31 and 4-33 also shows the difference in cracking rate for both unmodified and modified binders, where modified binders (both recovered and artificially aged) generated a more rapid rate to cracking than unmodified binders, due to having the lowest G^*_{VET} and highest T_{VET} values.

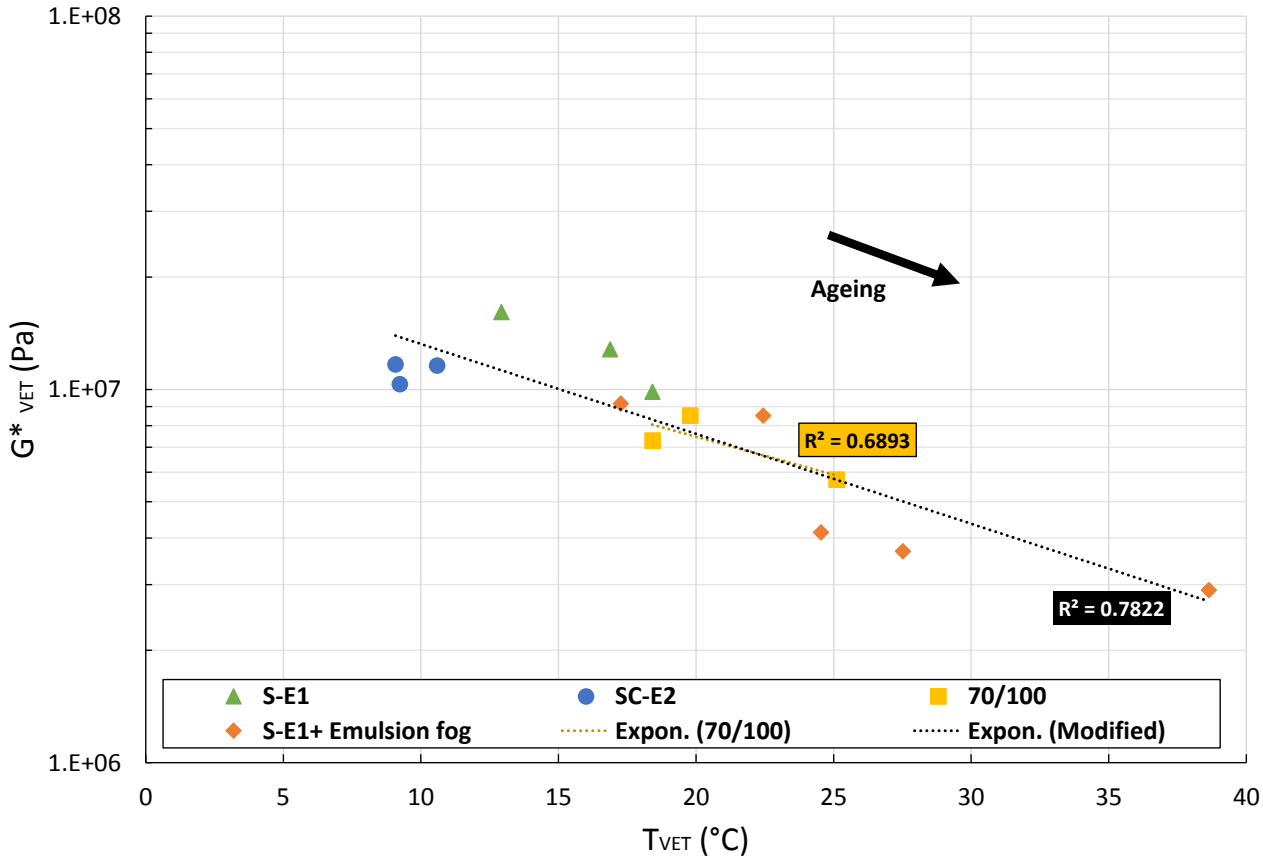

Figure 4-31: G^*_{VET} and T_{VET} correlation for recovered binders

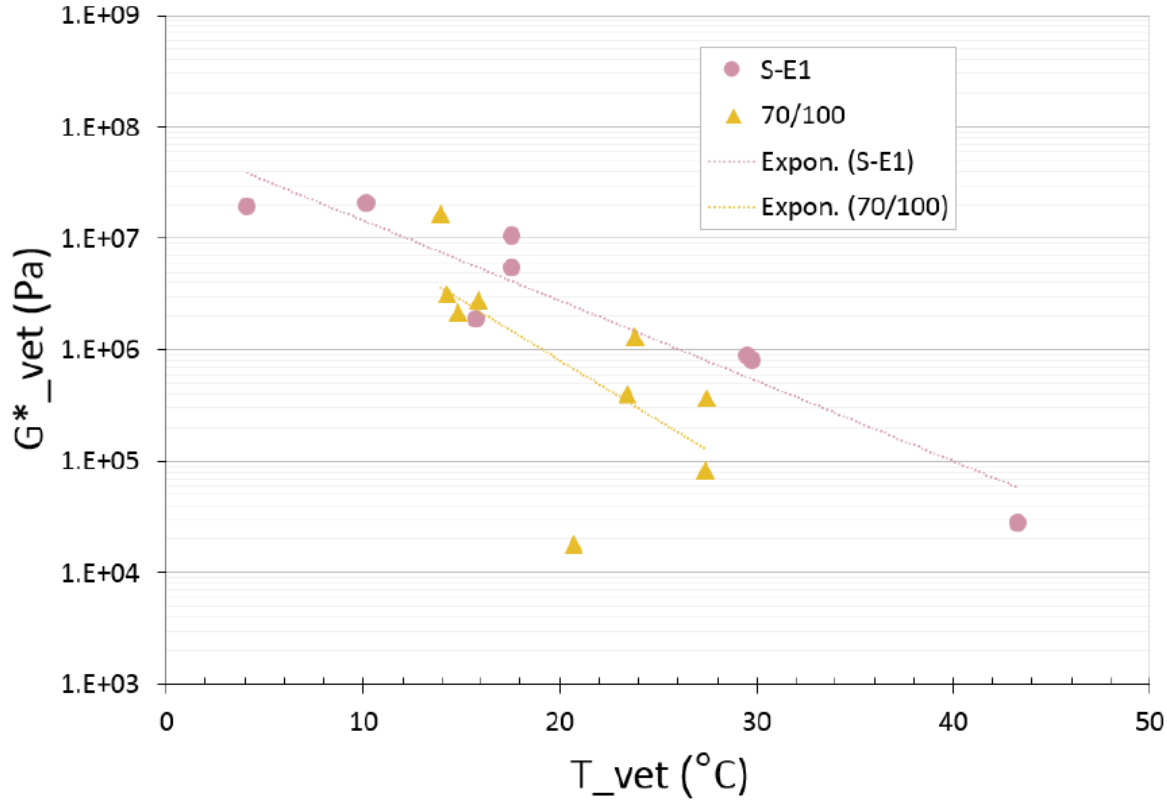

Figure 4-32: Goosen's recovered binder's VET parameters correlation (Goosen, 2018)

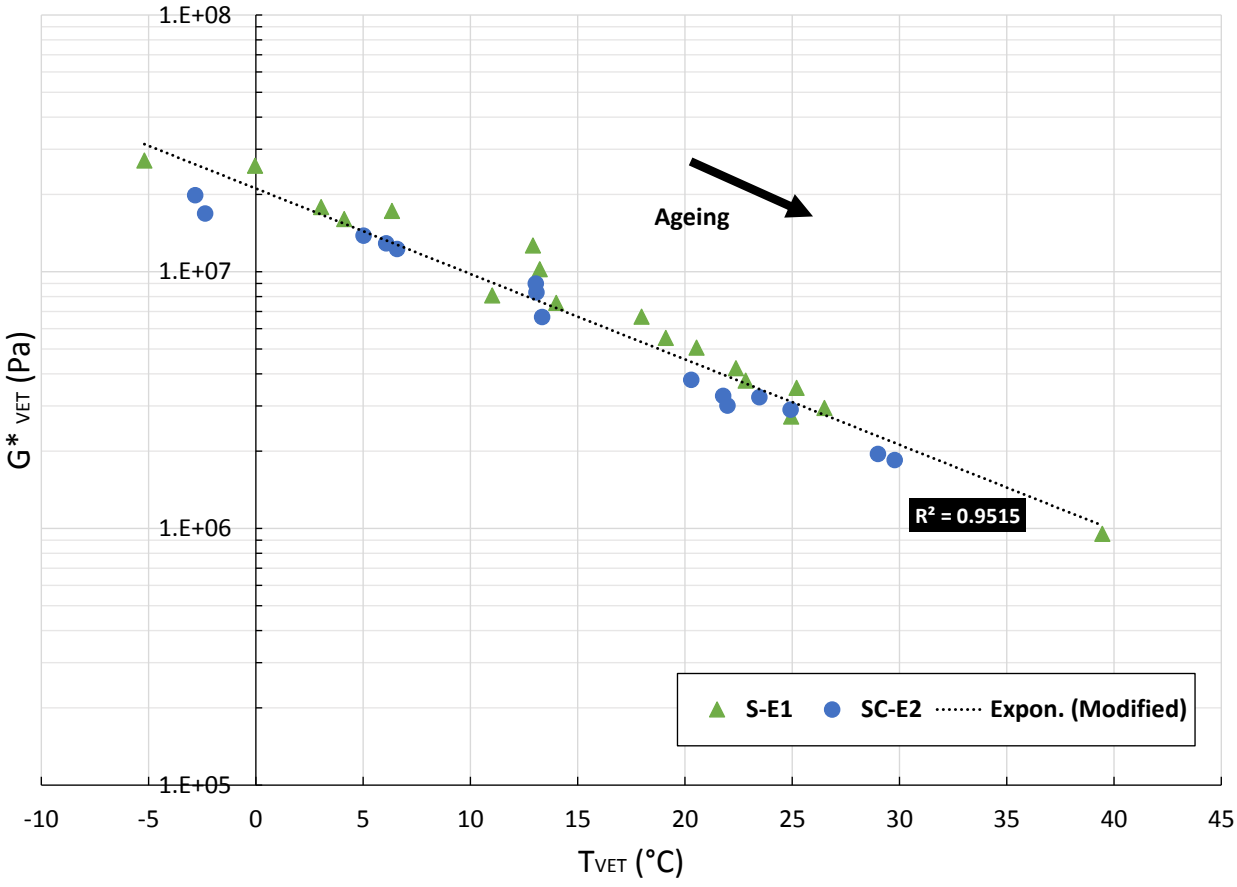

Figure 4-33: G^*_{VET} and T_{VET} correlation for artificially aged binders

Figure 4-34 shows Goosen's (2018) work on comparing performance parameters to in-field cracking visual assessments.

As discussed the decrease in G^*_{VET} and increase in T_{VET} with an increase in both G-R and ageing of binder, indicate poor performance and growth in cracking vulnerability. Figure 4-34 confirms how the severity of failure mechanisms increase with decrease in G^*_{VET} and increase in T_{VET}.

Further investigation is required on SA seals, regarding the VET influence on aggregate loss before performance limits can be proposed for performance specifications.

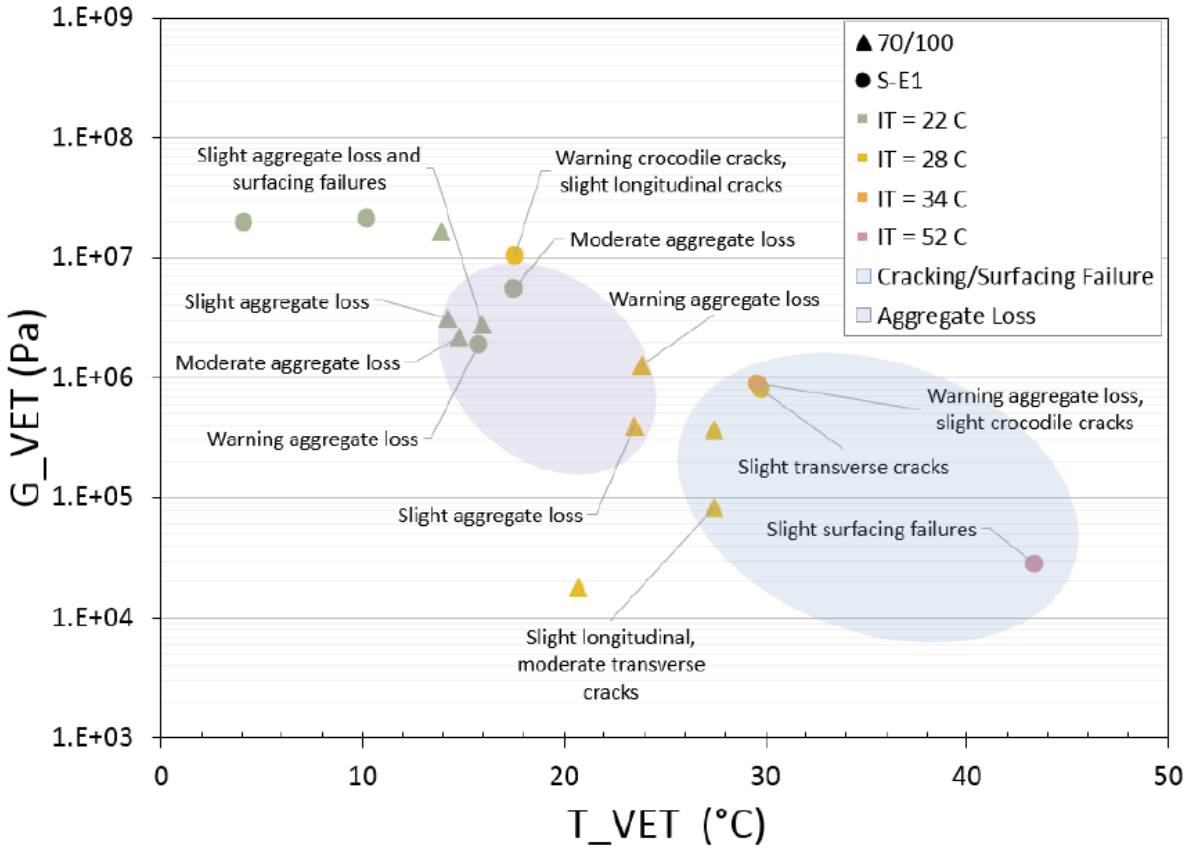

Figure 4-34: Recovered binders' VET parameters correlation with field performance (Goosen, 2018)

4.6.3 Rheological Index

The literature in Section 2.8.4 indicated that cracking is related to the Rheological Index (R-value) and can replace the G-R damage zones in the Black Space, as illustrated in Figure 2-50.

Table 4-11 shows the Rheological Index values and ω_c for all the binders investigated.

Table 4-11: Rheological Index and crossover frequency values

Binder	Suitable Model	R-value	ω_c (rad/s)
Original binders with artificial ageing			
N8/11_S-E1_ORIG	GLS	3.004	751.277
N8/11_S-E1_RTFO	GLS	3.007	145.520
N8/11_S-E1_PAV2	CAM	1.991	15.543
N8/11_S-E1_RTFO+PAV2	GLS	2.777	2.553
N8/11_S-E1_PAV4	CAM	2.500	1.575
N8/11_S-E1_RTFO+PAV4	CAM	3.366	0.045
N2/16_S-E1_ORIG	CAM	3.418	3752.426
N2/16_S-E1_RTFO	GLS	3.397	861.774

Binder	Suitable Model	R-value	ω_c (rad/s)
Original binders with artificial ageing			
N2/16_S-E1_PAV2	GLS	2.655	64.542
N2/16_S-E1_RTFO+PAV2	CAM	2.070	82.845
N2/16_S-E1_PAV4	GLS	2.847	4.850
N2/16_S-E1_RTFO+PAV4	CAM	2.394	5.514
R56/7_S-E1_ORIG	CAM	2.593	2451.258
R56/7_S-E1_RTFO	GLS	2.716	621.097
R56/7_S-E1_PAV2	GLS	2.205	124.505
R56/7_S-E1_RTFO+PAV2	GLS	2.500	25.222
R56/7_S-E1_PAV4	GLS	2.498	10.824
R56/7_S-E1_RTFO+PAV4	GLS	2.584	2.358
R61/7_SC-E2_ORIG	GLS	2.818	2689.781
R61/7_SC-E2_RTFO	GLS	2.600	408.538
R61/7_SC-E2_PAV2	GLS	2.396	87.176
R61/7_SC-E2_RTFO+PAV2	CAM	2.506	6.501
R61/7_SC-E2_PAV4	CAM	2.609	3.950
R61/7_SC-E2_RTFO+PAV4	CAM	2.669	0.480
R61/8_SC-E2_ORIG	GLS	2.743	596.837
R61/8_SC-E2_RTFO	GLS	2.721	442.192
R61/8_SC-E2_PAV2	GLS	2.686	70.705
R61/8_SC-E2_RTFO+PAV2	GLS	2.697	10.089
R61/8_SC-E2_PAV4	CAM	2.617	6.084
R61/8_SC-E2_RTFO+PAV4	CAM	2.812	0.785
R61/6_SC-E2_ORIG	CAM	2.127	2055.135
R61/6_SC-E2_PAV2	GLS	2.396	87.226
R61/6_SC-E2_PAV4	CAM	2.742	2.594
Recovered binders			
N8/11_S-E1_2y4m	GLS	2.221	20.228
N2/16_S-E1_10m	GLS	2.142	31.154
R56/7_S-E1_11m	GLS	2.122	116.215
R61/6_SC-E2_6m	GLS	2.411	222.795
R61/7_SC-E2_6m	GLS	2.319	168.208
R61/8_SC-E2_1m	GLS	2.377	236.460
DR1398_70/100_22y	CAM	1.814	2.431
MR23_70/100_3y	GLS	2.109	13.341
MR174_70/100_9y	GLS	2.229	19.408
N1/29(79.8km)_S-E1+fog_9y	CAM	2.069	0.052
N1/29(102.6km)_S-E1+fog_5y	CAM	2.013	2.897
N2/31_S-E1+fog_6y	GLS	2.136	5.624
N6/4_S-E1+fog_9y	CAM	2.005	1.206
N10/2_S-E1+fog_6y	CAM	1.758	25.221

The literature in Section 2.8.5 and Figure 2-52, which indicates the R-value increases with age while the crossover frequency (ω_c) reduces, was compared with this study's R-value data (Figure 4-35) showing the following:

- The ω_c parameter shows a decrease with age, as discussed in Section 4.4.3.1
- Figure 4-35 shows no trend regarding the R-value for this study, as all the values range between 1.8 and 3.4, with no correlation between ageing.
- Rowe, King & Anderson (2014) identified a range for R-values that might predict cracking onset and crack spreading between 2.3 and 2.7.
    - Figure 4-35 shows that only modified binders exceeded the 2.7 R-value limit where the cracking will spread significantly.

- The N2/16_S-E1_Original binder shows the most cracking with the highest R-value of 3.418.
- The recovered binder N10/2_ S-E1+fog show the best resistance to cracking with an R-value of 1.758.

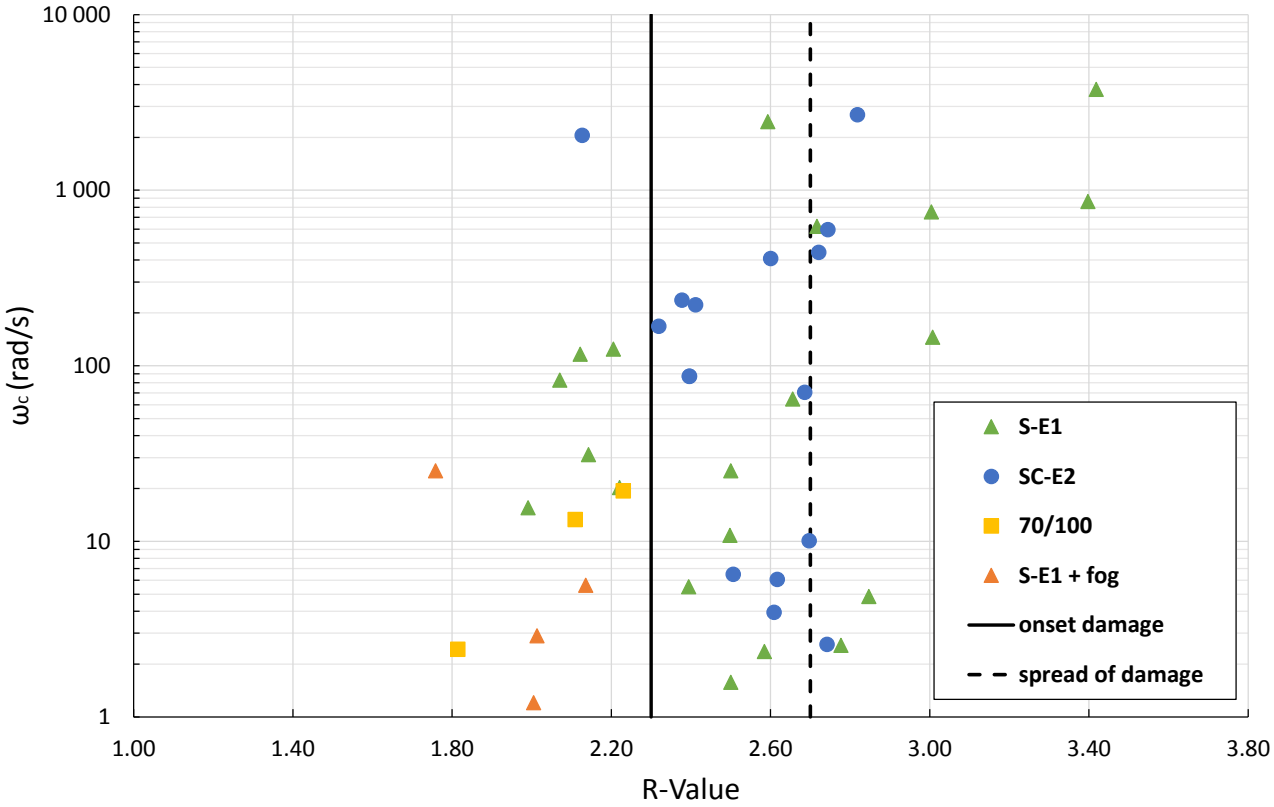

Figure 4-35: Cracking related to R-value for all binders

4.6.4 Ageing Ratio

Section 3.5.2, Figure 3-17 and Equation 3-13 explains the procedure followed to determine this study's ageing ratios.

This study's ageing ratios could not be compared to the proposed SATS 3208, as SATS 3208 calculates the ageing ratios at the intermediate temperature (T_{int}) that needs both BBR and DSR, where this study only investigates DSR.

Table 4-12 shows the binder's ageing ratios in terms of the G-R parameter, calculated at 15°C and 0.005 rad/s. Some binders' ageing ratios could not be calculated as the original material properties for the specific binder type is required, resulting in eight recovered binders' (70/100 and S-E1+fog binders) ageing ratios which could not be determined.

Table 4-12: Ageing ratios in terms of G-R parameters

Binder	Suitable Model	G-R (Pa)	Ageing Ratio
Original binders with artificial ageing			
N8/11_S-E1_ORIG	GLS	2.59E+03	1.00
N8/11_S-E1_RTFO	GLS	1.57E+04	6.05
N8/11_S-E1_PAV2	CAM	7.86E+04	30.28
N8/11_S-E1_RTFO+PAV2	GLS	2.14E+05	82.39
N8/11_S-E1_PAV4	CAM	3.25E+05	125.17
N8/11_S-E1_RTFO+PAV4	CAM	1.19E+06	459.52

Binder	Suitable Model	G-R (Pa)	Ageing Ratio
Original binders with artificial ageing			
N2/16_S-E1_ORIG	CAM	1.40E+02	1.00
N2/16_S-E1_RTFO	GLS	3.22E+03	22.97
N2/16_S-E1_PAV2	GLS	2.42E+04	172.15
N2/16_S-E1_RTFO+PAV2	CAM	2.97E+04	211.64
N2/16_S-E1_PAV4	GLS	1.62E+05	1150.70
N2/16_S-E1_RTFO+PAV4	CAM	1.47E+05	1043.96
R56/7_S-E1_ORIG	CAM	1.25E+02	1.00
R56/7_S-E1_RTFO	GLS	1.97E+03	15.73
R56/7_S-E1_PAV2	GLS	3.41E+04	272.04
R56/7_S-E1_RTFO+PAV2	GLS	5.58E+04	445.77
R56/7_S-E1_PAV4	GLS	1.03E+05	824.17
R56/7_S-E1_RTFO+PAV4	GLS	3.10E+05	2471.43
R61/6_SC-E2_ORIG	CAM	1.96E+02	1.00
R61/6_SC-E2_PAV2	GLS	2.07E+04	105.68
R61/6_SC-E2_PAV4	CAM	2.56E+05	1306.78
R61/7_SC-E2_ORIG	GLS	3.98E+02	1.00
R61/7_SC-E2_RTFO	GLS	2.52E+03	6.33
R61/7_SC-E2_PAV2	GLS	2.07E+04	52.03
R61/7_SC-E2_RTFO+PAV2	CAM	9.20E+04	231.22
R61/7_SC-E2_PAV4	CAM	1.65E+05	416.04
R61/7_SC-E2_RTFO+PAV4	CAM	4.88E+05	1228.27
R61/8_SC-E2_ORIG	GLS	3.31E+03	1.00
R61/8_SC-E2_RTFO	GLS	3.31E+03	1.00
R61/8_SC-E2_PAV2	GLS	2.62E+04	7.92
R61/8_SC-E2_RTFO+PAV2	GLS	7.11E+04	21.45
R61/8_SC-E2_PAV4	CAM	9.16E+04	27.64
R61/8_SC-E2_RTFO+PAV4	CAM	3.28E+05	98.90
Recovered binders			
N8/11_S-E1_2y4m	GLS	6.44E+04	24.81
N2/16_S-E1_10m	GLS	4.12E+04	293.29
R56/7_S-E1_11m	GLS	2.21E+04	176.45
R61/6_SC-E2_6m	GLS	3.38E+03	17.29
R61/7_SC-E2_6m	GLS	4.89E+03	12.30
R61/8_SC-E2_1m	GLS	2.82E+03	0.85

Figures 4-36 and 4-37 show the development of ageing ratios with artificial ageing and surface ageing respectively, indicating the following:

- All the artificially aged binders' ageing ratios increased with age, following the same path in Figure 4-36. Note that binder R61/6_SC-E2 did not include RTFO ageing.

- The recovered binders in Figure 4-37 showed some variation, where the S-E1 binders decreased with age, whilst the SC-E2 binders increased with age similar to artificially aged binders.

- Goosen's (2018) and Engelbrecht's (2018) research shows that the binder type (modification) and manufacturer of the binder are some of the factors that effects the ageing rate of a seal, confirming literature.

    - The variation shown in Figures 4-36 and 4-37 are aligned with Goosen's (2018) and Engelbrecht's (2018) work, showing ageing ratios from different provinces (manufacturers):

        - Goosen (2018): 70/100, S-E1 and SC-E2 binders from Western Cape, Northern Cape and KwaZulu- Natal;

- Engelbrecht (2018): 70/100, S-E1 and S-E2 binders from Western Cape, Gauteng and KwaZulu- Natal; and
- This study: S-E1 and SC-E2 binders from Eastern Cape.

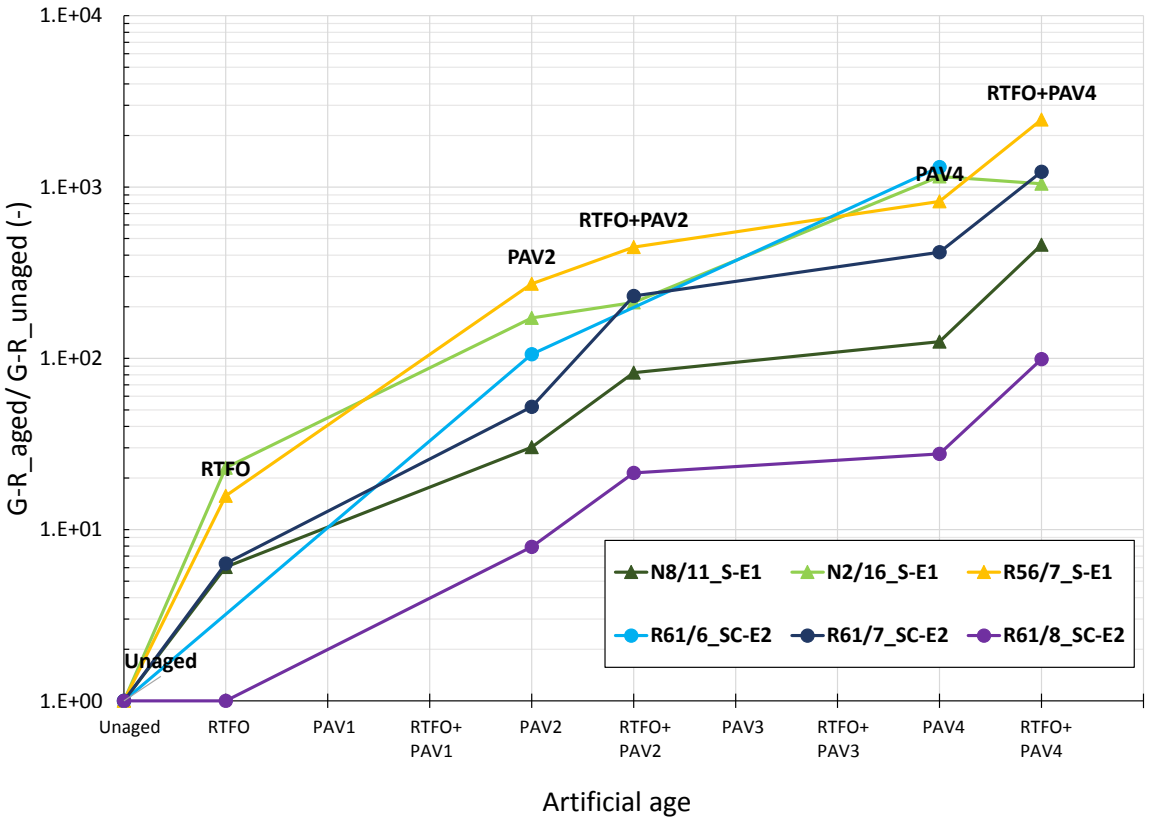

Figure 4-36: Ageing ratios (G-R) for all artificially aged binders

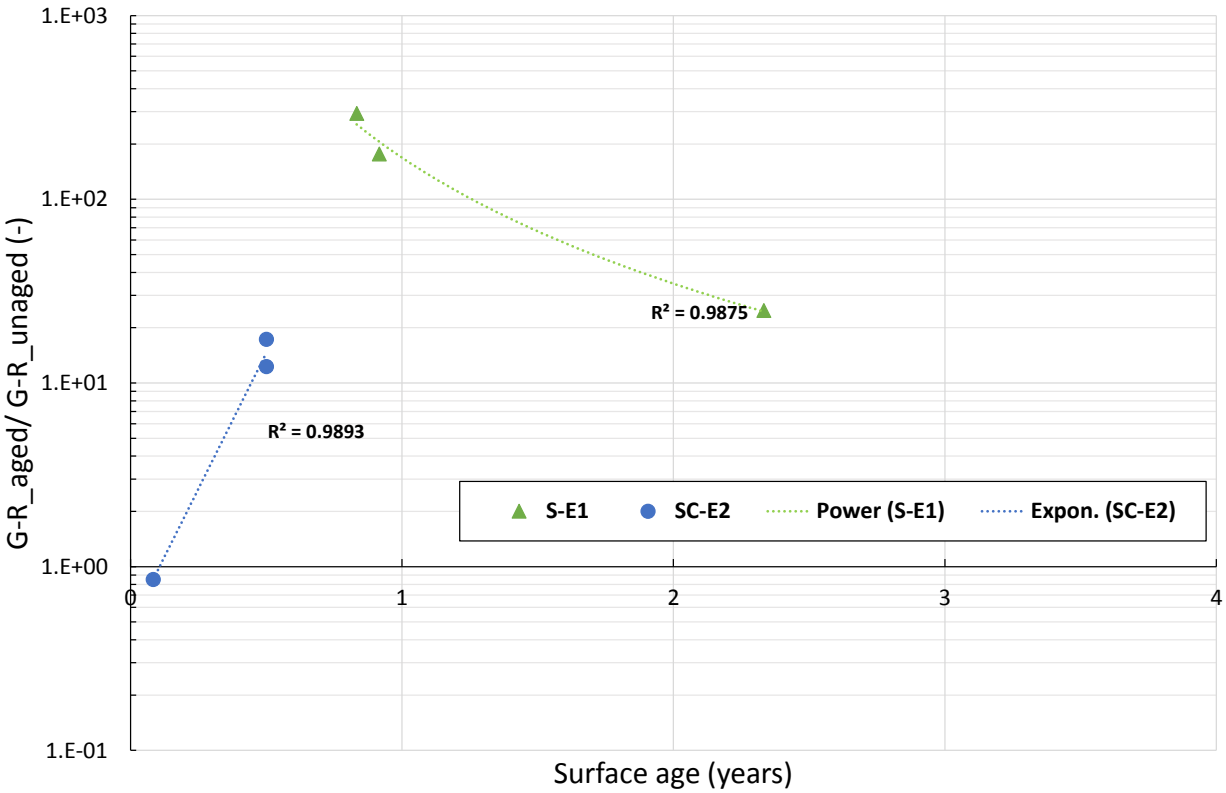

Figure 4-37: Ageing ratios (G-R) for S-E1 and SC-E2 recovered binders

4.7 Summary of Findings

With all objectives being met, the following findings are evident from the investigation results, thus far:

a) Both solvents toluene and trichloroethylene are very effective, with both leaving no solvent residue (0%) within recovered binders after recovery. Trichloroethylene is the preferred solvent as it does not pose the explosion hazards as toluene.

b) Researcher and Abatech RHEA software regard Modified Kaelble as the top ranked shift factor method to be used for pavement engineering investigations.

c) The master curves and Black Space diagrams show and confirm that an increase in temperature reduces the stiffness of binder, whilst the phase angle increases and frequency decreases, indicating that a binder will show a more viscous and less stiff behaviour at high temperatures.

d) It is shown by the combined master curves and the Black Space diagrams, that only have DSR data, strives and converges between $0.6 \cdot 10^8$ -10^8 Pa:

   - That should BBR have been conducted and the data thereof included in this study, the glassy modulus (G_g) would converge at between 0.6-1.5 GPa according to literature.

e) Of the two empirical models, CAM and GLS, GLS model provides better RMSE than CAM, overall providing a better fit to measured material behaviour, confirmed by:

   - Less binders modelled with the GLS model exceeded the 2.25% RMSE boundary for acceptability.
   - The RMSE for both CAM and GLS model reduced with age.

f) In order to ensure that all binder data delivers results and don't become unusable, modelling must be on a binder-to-binder basis.

g) The seal binder ageing assessment shows that master curves flatten (slope decrease) and stiffness of binder increases with age.

h) The Black Space diagrams shows when a binder is modified (added modifiers like polymers) or not, confirmed by:

   - The modified binders exhibited less viscous and more elastic behaviour at high temperatures than for unmodified binders, showing the influence of polymer (modifier) within the binder.
   - However, for long-term artificial ageing the polymer provides an increased viscous component and a reduced sign of modification, thus showing that polymer degrades / melts away (no effective modifier left) at higher temperatures, as the binder ages.

i) Data analysis of the crossover frequency (ω_c) showed that it reduces with age, while the associated G* at ω_c also reduces.

j) The calculation of ω_c showed that the 5 °C isotherm data was used for original (unaged), RTFO and younger recovered binders, whilst the oldest binder uses 25 °C isotherm data and the stiffest binder 35 °C isotherm.

k) The Glover-Rowe (G-R) parameter Black Space diagrams of this study show that it increased with artificial and surface ageing, thus confirming that ductility of the binder decreases.

l) The G-R results showed to contradict with the combined Black Space diagrams, as the Black Space showed that as the binder ages the G* reduces.

m) The Glover-Rowe (G-R) data showed to be very sensitive in terms of seal structure, modification and source of the binder, as the rate of binder deterioration (especially cracking) varied in these areas.

n) The G-R correlation with age and deterioration of pavement shows that after between 6-8 years of service a visual assessment is recommended to determine early failure mechanisms within the pavement.

o) The G-R parameter investigation showed that cracking only starts when G-R exceed 790 kPa.

p) Data analysis of viscoelastic transition (VET) parameters show that G^*_{VET} decreased and T_{VET} increased with artificial and surface ageing.

q) The VET parameters and G-R showed good correlation, as G^*_{VET} decreased and T_{VET} increased with increasing G-R values, indicating crack vulnerability, irrespective of modification.

r) Further investigation is required on SA seals, regarding the VET influence on aggregate loss before performance limits can be proposed for performance specifications.

s) The Rheological Index (R-value) of this study showed to have no correlation with age, being to the contrary of literature findings in Section 2.8.4.

t) Data analysis of ageing ratios ($G\text{-}R_{aged}/G\text{-}R_{unaged}$) showed an increase in artificial ageing, varying with binder type and binder sources.

Chapter 5: Conclusions and Recommendations

With the industries transition from Penetration Grade to Performance Grade (PG) specification, this study aims to investigate the rheological performance of seals in South Africa based on binder ageing considerations in order to:

- gain a better understanding of the durability aspects that are connected to the ageing performance of seal binders in South Africa;
- make a meaningful contribution to the formulation of a comprehensive PG specification for SA bituminous binders with respect to seals only; and to
- determine the key rheological considerations impacting on the transition from a Penetration-Viscosity Specification to a Performance Grade Specification.

5.1 Conclusions

5.1.1 Recovery and artificial ageing of seal binders

Objective 1 was achieved by characterising seal ageing in terms of PG specification by recovering 14 retrieved seal in-service samples according to EN-12697-3 (2013). The available original binders associated with the recovered binders were aged with both artificial conditioning levels (with and without RTFO) according to ASTM D2872 (2004), TG 1 (2019) and ASTM D6521 (2008).

Although the EN-12697-3 (2013) specification is flexible, it still lacks a recovery procedure for seal samples. This EN specification requires more detailed guidelines regarding the volume of solvent per sample size and soaking time during the solvent extraction procedure. This is important as hardening of the binder increased with long contact time with the solvent, which may result in inaccurate modelling of seal binder behaviour.

The ASTM D2872 (2004), TG 1 (2019) and ASTM D6521 (2008) specification codes are only for asphalt, hence lacking specifications for artificial ageing on seal binders.

5.1.2 DSR testing at intermediate temperatures

Objective 2 was achieved by evaluating the performance development of seal binders, by doing DSR testing in compliance with SATS 3208. The DSR testing was done at seven binder ages i.e. original (unaged), RTFO, PAV2, RTFO+PAV2, PAV4, RTFO+PAV4 and recovered surface age.

It is concluded that, even though the SATS 3208 recommend two strain levels (1% and 2%) for 8 mm and 25 mm PP respectively, the strain sweep test is still a necessity to determine the binder's linear viscoelastic (LVE) range before performing frequency sweeps, because all of this study's binders' upper LVE limit were computed to be 1% shear strain, except for one recovered binder, the stiffest binder, yielding a 0.5% shear strain upper LVE limit. Using predetermined percentages in this regard may fall outside the binder's LVE range and therefore resulting inaccurate binder behaviour results.

5.1.3 Modelling and identify suitable rheological indicators

Objectives 3 and 4 were achieved by analysing and modelling of test data and rheological parameters in order to determine binder properties in response to the ageing process of seals. This includes determining binder properties and identifying suitable rheological indicators and principles.

Over and above the findings identified and listed in Section 4.7 for this study, the following is concluded from the modelling and analysis of test data:

a) It is concluded based on this study's master curve results, that one cannot predict an ageing rate (how many years artificial ageing presents versus in-service ageing), as every bituminous binder will age differently.

b) The G-R parameter for this study was concluded to be the best rheological parameter to identify seal performance with age at intermediate temperatures, as the Rheological Index for this study showed no correlation to ageing and could not be replaced by the G-R damaging (cracking) zones.

c) Visual assessment on seal roads is recommended after 6-8 years of in-service to determine deterioration (failure mechanisms) of the pavement, based the G-R data findings of this study and others.

d) Further investigation is required on SA seals, regarding the VET influence on aggregate loss (failure mechanisms) before performance limits can be proposed for performance specifications.

e) Ageing influence the modification of seal binders. Long-term artificial ageing of polymer modified seal binder provides an increased viscous component, thus showing that the polymer degrades at high temperatures as the binder ages.

f) It was concluded that both BBR and DSR data are needed to compute the ageing ratios of binder, as the ageing ratios ($G\text{-}R_{aged}/G\text{-}R_{unaged}$) for this study showed great variability in terms of binder type and binder source.

g) The study concludes that the DSR testing can be used in a performance grade binder selection process, replacing the conventional Penetration Grade Specification. Rheological properties of binders based on DSR testing measure the effects of binder ageing on pavement performance. Consequently, DSR testing is a requirement for the transition from Penetration Grade Specification to a performance grade (PG) specification.

h) Overall it is concluded that BBR, DSR and MSCR testing (low, intermediate and high temperatures) is required to cover the entire performance spectrum of binder in-service in order to obtain a trustworthy and accurate representative behaviour of seal binders in-service.

5.2 Recommendations

The findings and conclusions of this study have provided much needed evidence to make a substantial contribution to improve, address, clarify and in some cases solve the challenges of the current SATS 3208 Performance Grade (PG) Specifications for Bitumen. Accordingly, the following is recommended:

a) The extraction and recovery procedure for seals be investigated in further research studies in detail, in order to provide more detailed intelligence on the solvent to be used in terms of binder type (modified or unmodified), the required soaking / exposure time based on surface

ageing and the influence that the solvent and soaking / exposure time has on the constitution and structure of the bitumen.

b) Pavement conditions including traffic speed, traffic volume and temperatures be included in the SATS 3208, as sufficient proof exists that the rate of binder deterioration (especially cracking) is sensitive to change in seal structure, modification and source of the binder.

c) A wider range of pavement structures (asphalt and seals) and binder types be investigated in further research studies in order to provide more detailed intelligence on what specifically determines or influences the variability of ageing rates.

d) As ageing is a fundamental principle that affects the performance of a pavement, which will lead to failure mechanisms within the pavement, continued research be conducted on pavement inspection data in order to compare in-service failure with the rheological analysis of the binder. Thus, ensuring a better understanding / indication of which properties best describe failure mechanisms of seal binders in order to compile robust compliance criteria for optimal seal binder selection.

e) Further research be conducted to investigate and gather more detailed intelligence on whether RTFO artificial ageing with PAV is really needed for seal binders, as seals does not go through in-plant ageing like asphalt binders, as this will reduce the testing time to conclude to the seal binder's viscoelastic behaviour.

f) Further research be conducted to investigate and gather more detailed intelligence on VET behaviour of binders for seals and asphalt in order to expand on the Widyatmoko, Heslop & Elliott's (2005) VET criteria, providing a wider range of modified and unmodified binders to minimise crack susceptibility of binders.

g) As the relationship between binder performance and related surface failure has been documented and well researched for asphalt, but less for seals, further research be conducted to investigate and gather more detailed intelligence on seals, especially doing repeat tests and analysis to gain comprehensive and accurate results so that seal binders' relationships can also be documented.

Reference List

Abrahams, M.S. 2015. Towards the Development of a Standard Test Protocol : Application of the MMLS3 for Evaluating the Performance of Surfacing Seals. MEng (Research) Thesis, University of Stellenbosch.

Airey, G.D., Rahimzadeh, B. & Collop, A.C. 2002. Viscoelastic linearity limits for bituminous materials. In Vol. 71. Association of Asphalt Paving Technologists (AAPT) *Performance Testing and Evaluation of Bituminous Materials*. 331–338.

Airey, G.D., Choi, Y.K., Collop, A.C. & Elliott, R.C. 2004. Rheological and fracture characteristics of low penetration grade bitumen. *Road Materials and Pavement Design*. 5:107–131.

Alhaddad, A.H.A. 2015. Construction of a Complex Shear Modulus Master Curve for Iraqi Asphalt Binder using a Modified Sigmoidal Fitting. *International Journal of Scientific and Technology Research*. 4(February 2015):682–690.

American Society for Testing and Materials (ASTM) D1856. 2009. Standard Test Method for Recovery of Asphalt From Solution by Abson Method 1. *Annual Book of American Society for Testing Materials Standards*. 9(226):1–5.

Anderson, D.A. & Marasteanu, M. 2010. Continuous Models for Characterizing Linear Viscoelastic Behavior of Asphalt Binders.

Anderson, D.A., Rowe, G.M. & Christensen, D. 2008. Historical and Current Rheological Binder Characterization vs. Binder Performance. *Petersen Conference*. 1–17.

Van Assen, E. & Rust, F.C. 1997. *Assessment of Binder Extraction Methodologies*. Pretoria.

ASTM D2872. 2004. Standard Test Method for Effect of Heat and Air on a Moving Film of Asphalt (Rolling Thin-Film Oven Test). *Annual Book of American Society for Testing Materials Standards*. 13(C):1–6.

ASTM D6521. 2008. Standard Practice for Accelerated Ageing of Asphalt Binder Using a Pressurized Ageing Vessel (PAV). *Annual Book of American Society for Testing Materials Standards*. (January):8–13.

ASTM D6648. 2008. Standard Test Method for Determining the Flexural Creep Stiffness of Asphalt Binder Using the Bending Beam Rheometer (BBR). *Annual Book of American Society for Testing Materials Standards*. 1–21.

ASTM D7175. 2008. Determining the Rheological Properties of Asphalt Binder Using a Dynamic Shear Rheometer. *Annual Book of American Society for Testing Materials Standards*. 1–16.

ASTM D7405. 2010. Standard Test Method for Multiple Stress Creep and Recovery (MSCR) of Asphalt Binder Using a Dynamic Shear Rheometer. *Annual Book of American Society for Testing Materials Standards*.

Australian Asphalt Pavement Association (AAPA). 2011. Study Tour 2011. *South Africa & CAPSA'11*. 5(September).

Baglieri, O., Dalmazzo, D., Barazia, M., Tabatabaee, H.A. & Bahia, H.U. 2012. Influence of Physical Hardening on the Low-Temperature Properties of Bitumen and Asphalt Mixtures. *Procedia - Social and Behavioral Sciences. SIIV - 5th International Congress - Sustainability of Road Infrastructures*. 53:504–513.

Bahia, H.U. 2007. Advanced Course on Bitumen Technology. *Stellenbosch University*.

Bahia, H.U., Jenkins, K. & Hanz, A. 2008. Performance Grading of Bitumen Emulsions. *Cost Effective High Performance Surfacings*. 1–13.

Blackrock Paving & Seal coating INC. 2019. *What is the difference between Asphalt and Chip Seal*. [Online], Available: https://www.blackrockpavingandsealcoating.com/what-is-the-difference-between-asphalt-and-chip-seal/.

Christensen, D.W. & Anderson, D.A. 1992. Interpretation of Dynamic Mechanical Test Data for Paving Grade Asphalt. *Journal of the Association of Asphalt Paving Technologists*. 61:67–116.

Committee for State Road Authorities. 1992. TMH 9: Pavement management systems: standard visual assessment manual for flexible pavements. *Technical Methods for Highways*.

D'Angelo, J. 2013. Superpave Asphalt Binders: Aging and what they mean to the specification. *Unpublished class notes. D'Angelo Consulting*.

Distin, T. 2008. Spray Sealing Practice in South Africa. In ARRB Group and Ltd and Authors *1st Sprayed Sealing Conference – cost effective high performance surfacings, Adelaide, Australia 2008*. 1–19.

Engelbrecht, F. 2018. Age-related performance of typical seal binders in South Africa. MEng (Research) Thesis, University of Stellenbosch.

Engelbrecht, F. 2019. The effect of ageing on bituminous seal binder rheology. In Sun City *12th Conference on Asphalt Pavements for Southern Africa*. 1–18.

European Standards (EN) -12697-3. 2013. Bituminous mixtures-Test methods for hot mix asphalt-Part 3: Bitumen recovery:Rotary evaporator. *European Standards*.

Forough, S.A., Nejad, F.M. & Khodaii, A. 2014. A comparative study of temperature shifting techniques for construction of relaxation modulus master curve of asphalt mixes. *Construction and Building Materials*. 53:74–82.

Gerber, J.A.K. 2014. *Review Report on the Development of a Mechanistic Seal Model. Improved Damage Models for Bituminous Materials (Part 2 - Thin Surfacings)*.

Gerber, J.A.K. 2016. Numerical modelling of performance and failure criteria for surfacing seals. PhD (Eng) Dissertation, University of Stellenbosch.

Glover, C.J., Davison, R.R., Domke, C.H., Ruan, Y., Juristyarini, P., Knorr, D.B. & Jung, S.H. 2005. Development of a New Method for Assessing Asphalt Binder Performance Durability. *Texas Transportation Institute*. 7(2).

Goosen, E. 2018. Rheological Performance Evaluation of Recovered Seal Binders in South Africa. MEng (Research) Thesis, University of Stellenbosch.

Gordon, G.V. & Shaw, M.T. 1994. *Computer Programs for Rheologists*. New York: Hanser Pub Inc.

Hagos, E.T. 2008. The effect of aging on binder properties of porous asphalt concrete. PhD (Eng) Dissertation, Delft University of Technology.

Hunter, R.N., Self, A. & Read, J. 2015. *Shell Bitumen Handbook*. 6th ed. ICE Publising.

De Jonghe, A.C.A., Van den Bergh, W., Verheyen, J., Schoeters, G., Vuye, C. & Van Leugenhagen, F. 2005. Onderzoek naar de compatibiliteit van bindmiddelen bij gebruik van asfaltpuingranulaat.

King, G.N., Anderson, R.M., Hanson, D.I. & Blankenship, P.B. 2011. Evaluation of the Relationship between Asphalt Binder Properties and Non-Load Related Cracking. *Asphalt Paving Technology*. 615–663.

Labi, S. & Sinha, K.C. 2003. Effectiveness of Highway Pavement Seal Coating Treatments. *Journal of Transportation Engineering*. 130(1):14–23.

Louw, K. 2016. Polymer-Modified Bitumen (PMB). *Unpublised class notes*.

Mensching, D.J., Rowe, G.M., Daniel, J.S. & Bennert, T. 2015. Exploring low temperature performance in Black Space. *Asphalt Paving Technology: Association of Asphalt Paving Technologists-Proceedings of the Technical Sessions*. 84(September):459–496.

Mensching, D.J., Rowe, G.M. & Daniel, J.S. 2016. A mixture-based Black Space parameter for low temperature performance of hot mix asphalt. *Asphalt Paving Technology: Association of Asphalt Paving Technologists-Proceedings of the Technical Sessions*. 85:611–640.

Mikhailenko, P. & Baaj, H. 2017. Survey of Current Asphalt Binder Extraction and Recovery Practices. *Testing and Modelling of Road and Embankment Materials*. (September).

Milne, T.I. 2004. Towards a performance related seal design method for bitumen and modified road seal binders. PhD (Eng) Dissertation, University of Stellenbosch.

Morgan, P., Mulder, A. & Bitumen, S. 1995. *The Shell Bitumen Industrial Handbook*. London: Shell Bitumen.

Mturi, G., O'Connell, J.O. & Zoorob, S.E. 2011. Investigating the Rheological Characters of South African Road Bitumens. *10th Conference on Asphalt Pavements for Southern Africa*. 149–187.

Mturi, G., Rippenaar, A., Hamraj, S., Naicker, S. & Husselman, S. 2015. *A Review Towards a National Bitumen Extraction-Recovery Method*.

Much Asphalt. 2013. Performance Grade Study Tour United States of America. *USA PG Study Tour*. (December).

Mukandila, E. 2015. Investigation of rheological response, cohesion and adhesion fatigue damage of bituminous road seal materials. Unpublished Draft PhD (Eng) Dissertation, University of Pretoria.

Nielsen, E. 2012. State of the Art – Recycling Polymer Modified Asphalt. *Report of RECYPMA Project*. 2(2):1–43.

RAHA Bitumen Co. 2016. *Bitumen Components*. [Online], Available: http://rahabitumen.com/bitumen-components/ [2019, April 11].

Roelofse, C.B. 2014. Influencing of slushing on granular materials. BEng (Project) Skripsie, University of Stellenbosch.

Rowe, G.M. 2009. Phase angle determination and interrelationships within bituminous materials. *Advanced Testing and Characterization of Bituminous Materials*. (1):43–52.

Rowe, G.M. 2014a. Interpretation in Rheological Parameters. In Laramie *51st Petersen Asphalt Research Conference*. 1–32.

Rowe, G.M. 2014b. Assessment of Parameters for Asphalt Cracking Using Linear Visco-Elastic Properties. *Innovations for Predicting Pavement Performance*.

Rowe, G.M. & Sharrock, M.J. 2011. Alternate Shift Factor Relationship for Describing Temperature Dependency of Viscoelastic Behavior of Asphalt Materials. *Transportation Research Record: Journal of the Transportation Research Board*. (1).

Rowe, G.M., Baumgardner, G. & Sharrock, M.J. 2009. Functional Forms for Master Curve Analysis of Bituminous Materials. In *Proceedings of 7th International RILEM Symposium ATCBM09 on Advanced Testing and Characterization of Bituminous Materials*. 81–91.

Rowe, G.M., Baumgardner, G. & Sharrock, M.J. 2011. Application of Rheological Models to Modified Binders. In Western Research Institute *48th Petersen Asphalt Research Conference*. 153-153–16.

Rowe, G.M., King, G.N. & Anderson, M. 2014. The influence of binder rheology on the cracking of asphalt mixes on airport and highway projects. *Journal of Testing and Evaluation*. 42(5):1–35.

Rowe, G.M., Jenkins, K. & Van de Ven, M. 2017. Ageing and Durability. *Unpublished class notes. Advanced Course on Binder Technology*. (April).

SABITA. 2011a. Manual 28: Best practice for the design and construction of slurry seals.

SABITA. 2011b. Manual 30: A guide to the selection of bituminous binders for road construction. 1–47.

SABITA. 2016. South African Performance Grade Bitumen Specification. Version 20.

SABITA. 2017. The Introduction of a Perfomance Grade Specification for Bituminous Binders. *TECHNICAL GUIDELINE*. (February):1–16.

SABITA. 2018. Design and Use of Asphalt in Road Pavements. *Sabita Manual 35/TRH 8*.

SABITA. 2019a. Sabita information sheet # 1 - Origin and use of bitumen. 0–1.

SABITA. 2019b. Sabita information sheet #3 -Spray seals. 20–21.

SANRAL. 2009. Flexible Pavements Road Pavement Repairs - Flexible Pavements. *Routine Road Maintenance Manual*. (2):1–28.

SANS 3001. 2011. Part AS20: Determining of the Soluble Binder Content and Particle Size Analysis of an Asphalt mix. *South African National Standard*.

SANS 4001. 2012. Civil engineering specifications Part BT2: Cutback bitumen. *South African National Standard*.

SANS 4001. 2014a. Civil engineering specifications Part BT3: Anionic bitumen road emulsion. *South African National Standard*.

SANS 4001. 2014b. Civil engineering specifications Part BT4: Cationic bitumen road emulsion. *South African National Standard*.

SANS 4001. 2014c. Civil engineering specifications Part BT5: Inverted bitumen road emulsion. *South African National Standard*.

SAPEM. 2014a. South African Pavement Engineering Manual Chapter 13: Quality Management. (January).

SAPEM. 2014b. South African Pavement Engineering Manual Chapter 14: Post-Construction. (October).

Shaw, M.T. & MacKnight, W.J. 2005. *Introduction to polymer viscoelasticity*. 3rd ed. Hoboken, N.J. : Wiley-Interscience.

South African National Roads Agency Limited (SANRAL). 2007. TRH 3: Design and Construction of Surfacing Seals. *Technical Recommendations for Highways*. (May).

South African National Standards (SANS) 4001. 2016. Civil engineering specifications Part BT1 : Penetration grade bitumen.

South African Pavement Engineering Manual (SAPEM). 2013. South African Pavement Engineering Manual Chapter: 2 Pavement Composition and Behaviour. (January).

South African Technical Specification (SATS) 3208. 2018. Performance grade bitumen (Draft). *SABS Standards Division Technical Specification*.

Southern African Bitumen Association (SABITA). 2014. Manual 2: Bituminous binders for road construction and maintenance. 6.

Technical Guideline (TG) 1. 2019. The Use of Modified Bituminous Binders in Road Construction. *SABITA*. 4(January).

Thermal Analysis Instruments. 2019. Rheology: Theory and Applications. *Journal of Fluid Mechanics*. 5(4):652–653.

Van de Ven, M., Jenkins, K. & Bredenhann, S. 2004. State of the Art Review. *of PG binder testing with Focus on rheology using DSR equipment*. 1–21.

Van de Ven, M., Rowe, G.M. & Jenkins, K. 2017. Welcome and Introduction. *Unpublished class notes. Advanced Course on Binder Technology*.

Vijaykumar, A. 2012. Validation of surface Performance-Graded Specification for surface treatment binders. MEng (Research) Thesis, Texas A&M University.

Widyatmoko, I., Heslop, M.W. & Elliott, R.C. 2005. Viscous to Elastic Transition Temperature and the In Situ Performance of Bituminous and Asphaltic Materials. *Journal of the Institute of Asphalt Technology*. (14):3–7.

Yusoff, N.I. 2012. Modelling the Linear Viscoelastic Rheological Properties of Bituminous Binders. PhD (Eng) Dissertation, University of Nottingham.

Yusoff, N.I., Shaw, M.T. & Airey, G.D. 2011. Modelling the linear viscoelastic rheological properties of bituminous binders. *Construction and Building Materials*. 25(5):2171–2189.

Yusoff, N.I., Chailleux, E. & Airey, G.D. 2011. A Comparative Study of the Influence of Shift Factor Equations on Master Curve Construction. *ISSN Int. J. Pavement Res. Technol. International Journal of Pavement Research and Technology*. 4(6):324–336.

Yusoff, N.I., Jakarni, F.M., Nguyen, V.H., Hainin, M.R. & Airey, G.D. 2013. Modelling the rheological properties of bituminous binders using mathematical equations. *Construction and Building Materials*. 40:174–188.

Van Zyl, G. 2018a. Design of Surface Treatment. *Unpublised class notes*.

Van Zyl, G. 2018b. Unpublished. PhD (Eng) Dissertation, University Stellenbosch.

Van Zyl, G. & Jenkins, K. 2015. Overview of Long Term Evolution. In Sun City: Mycube Asset Management Systems and University of Stellenbosch *Conference on Asphalt Pavements for Southern Africa*. 1–13.

Appendix A: Modelling

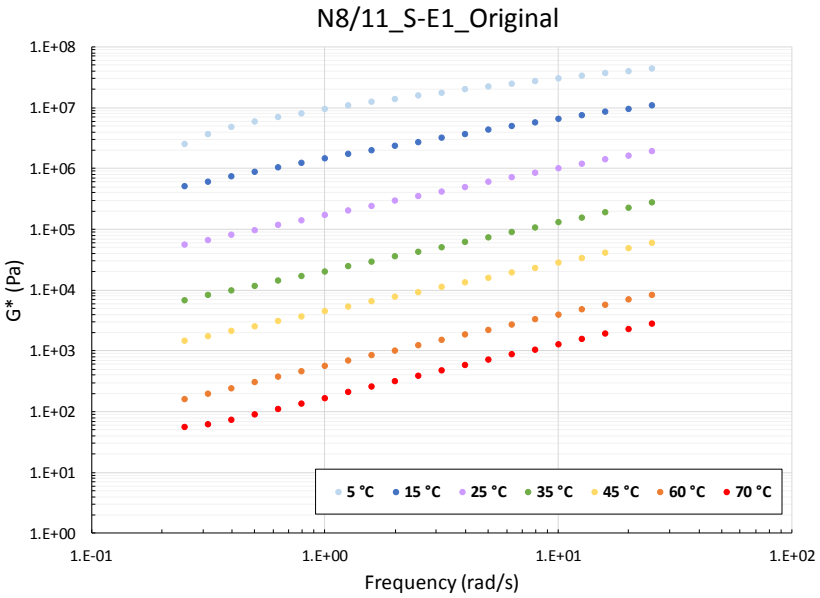

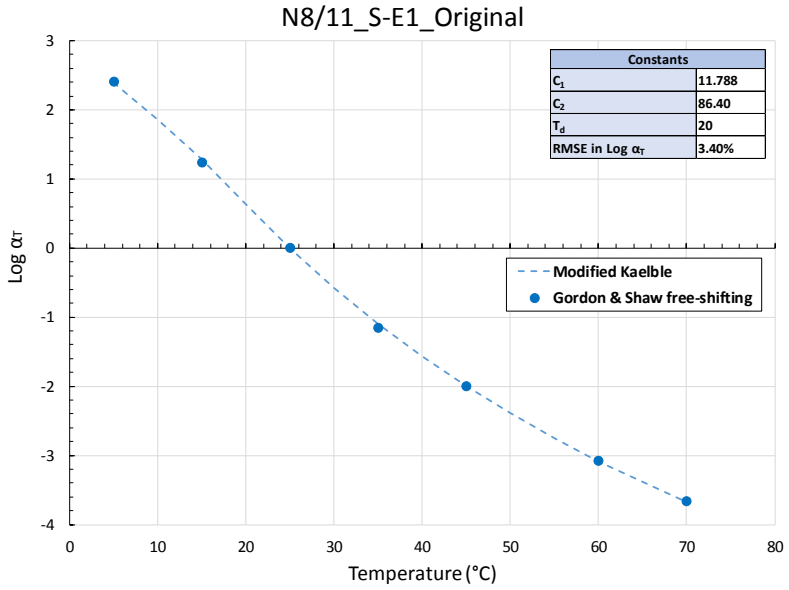

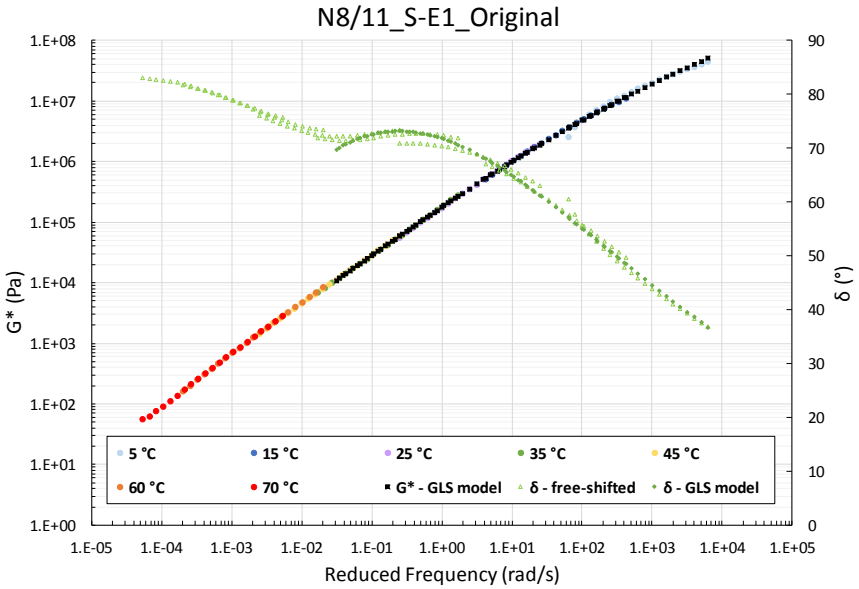

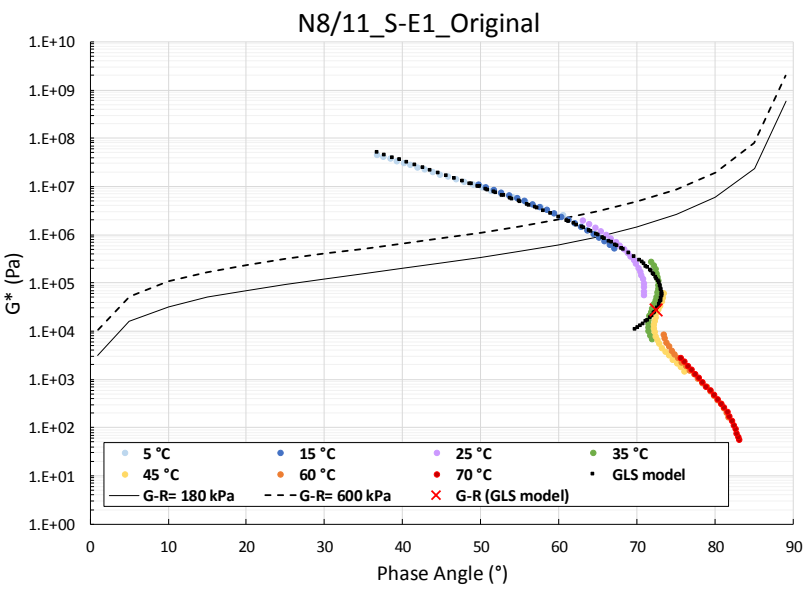

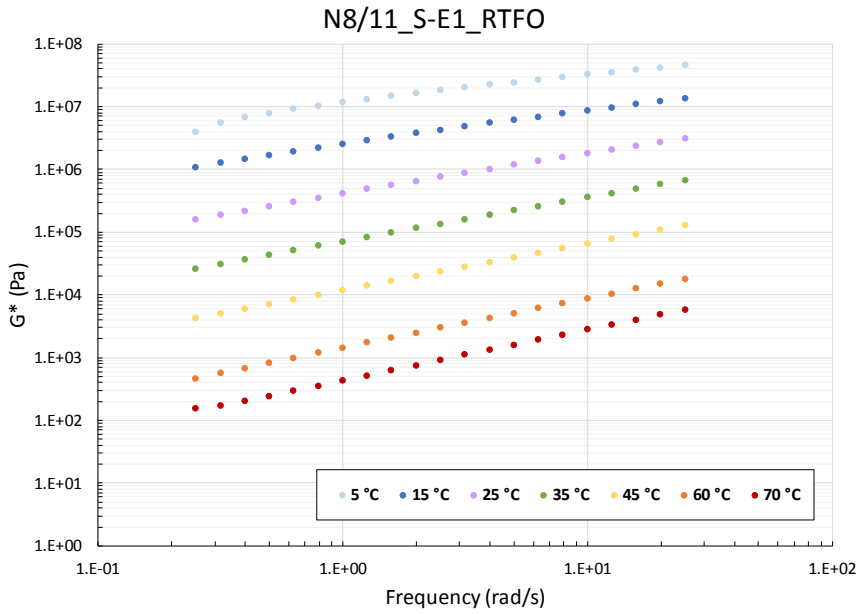

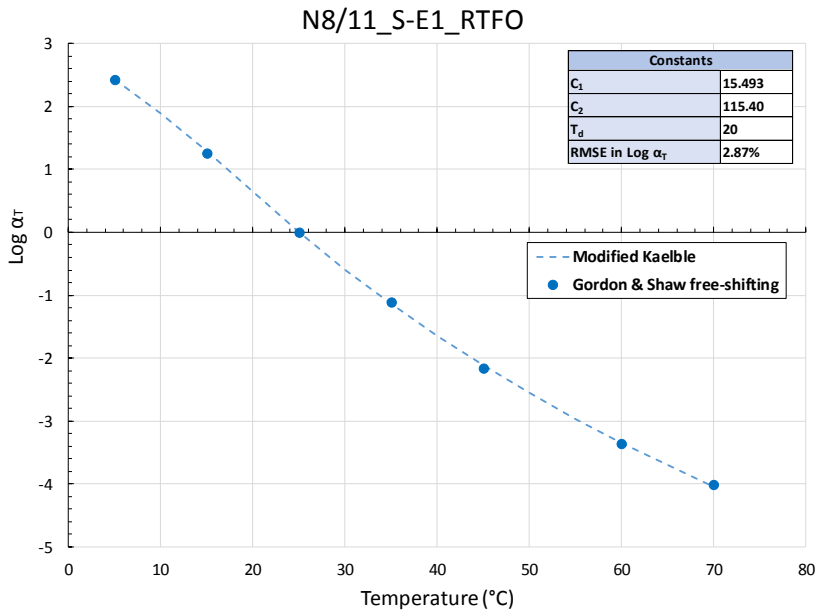

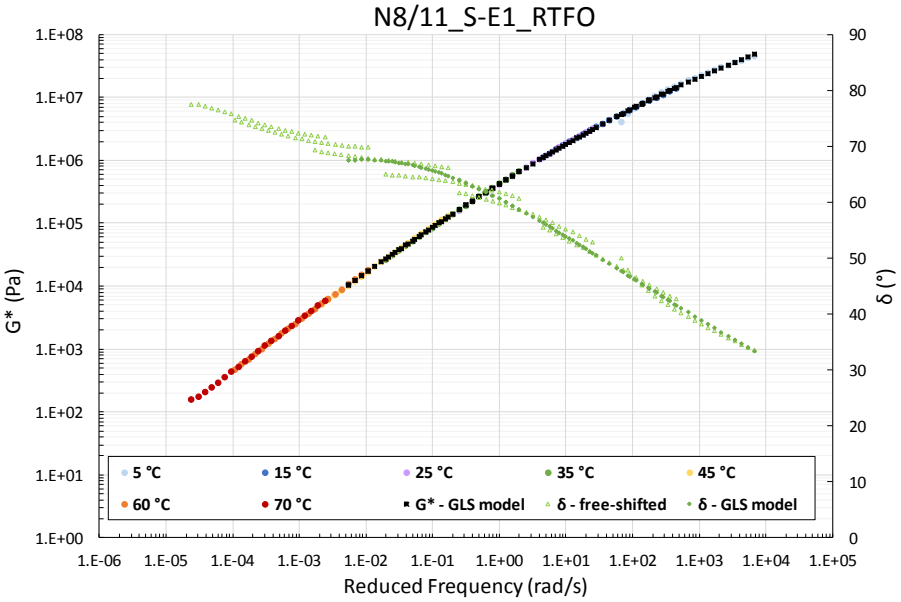

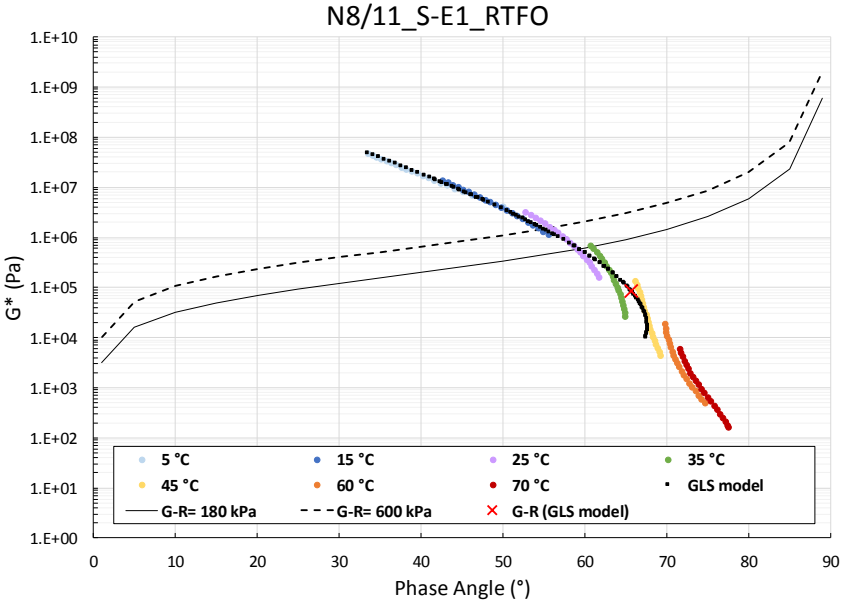

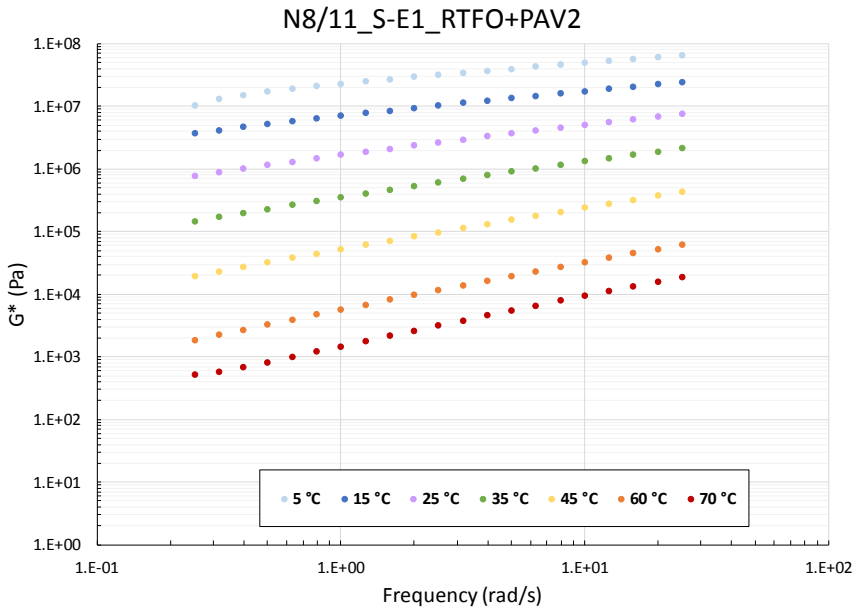

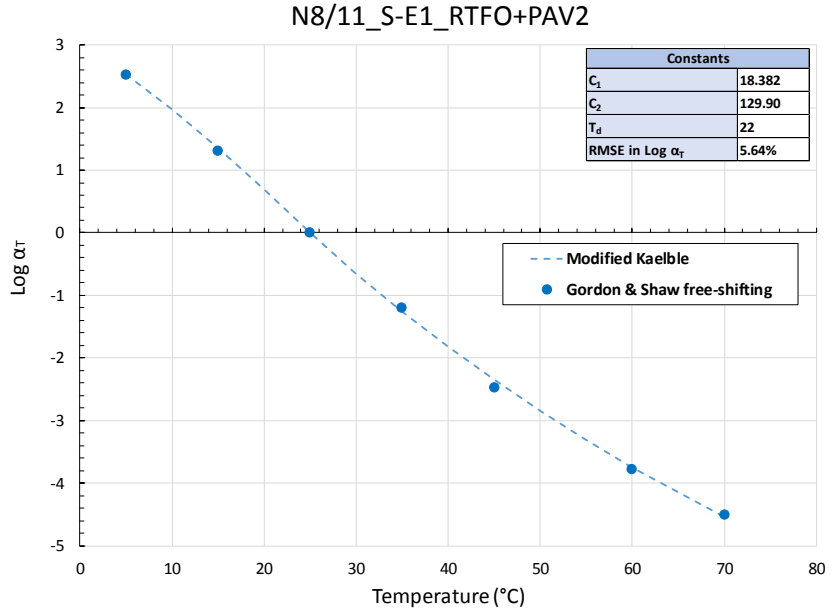

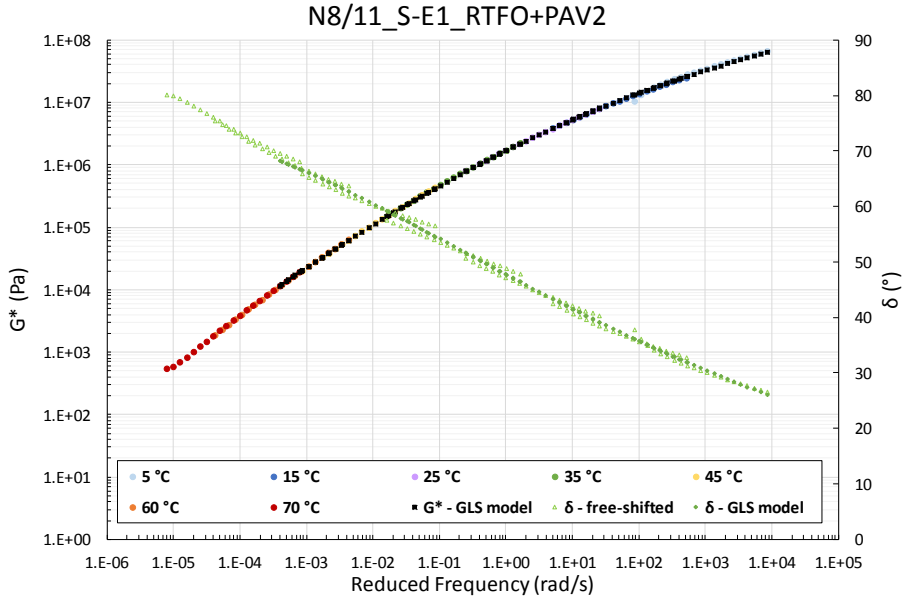

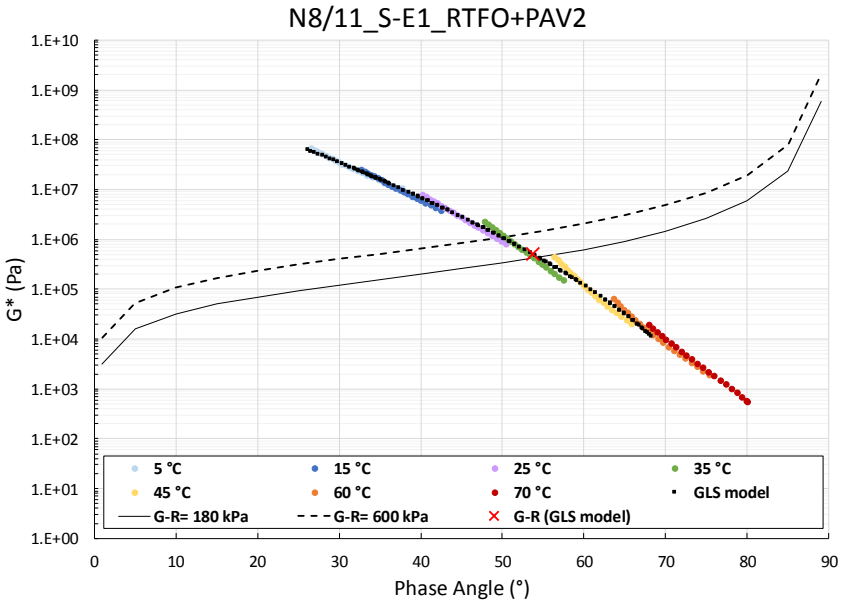

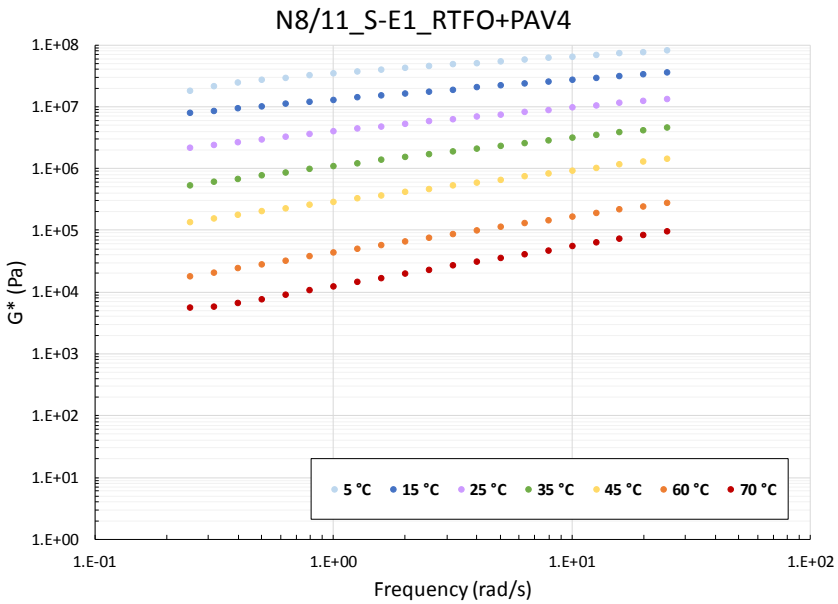

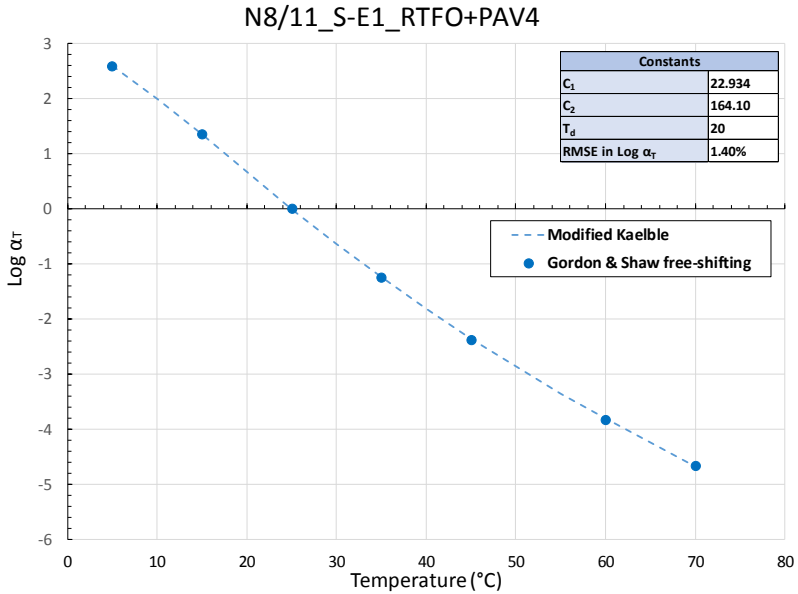

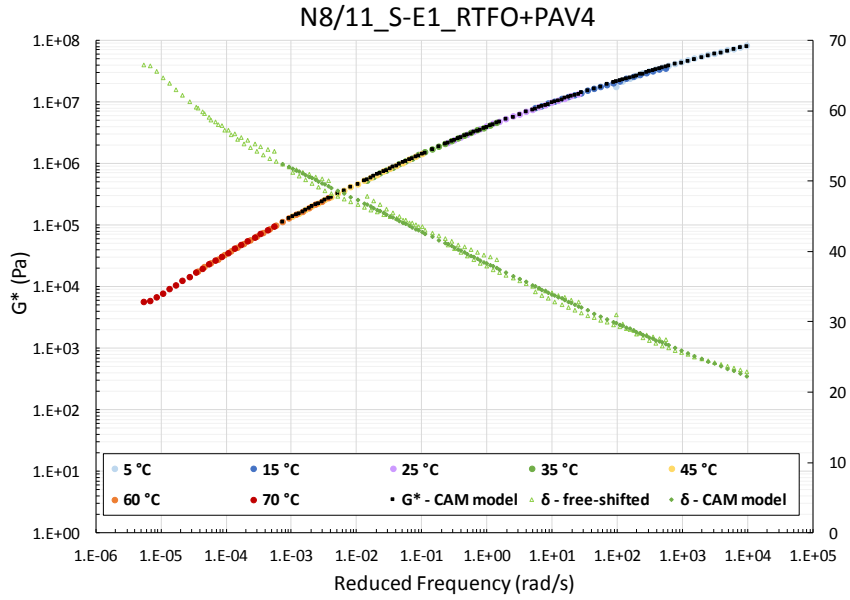

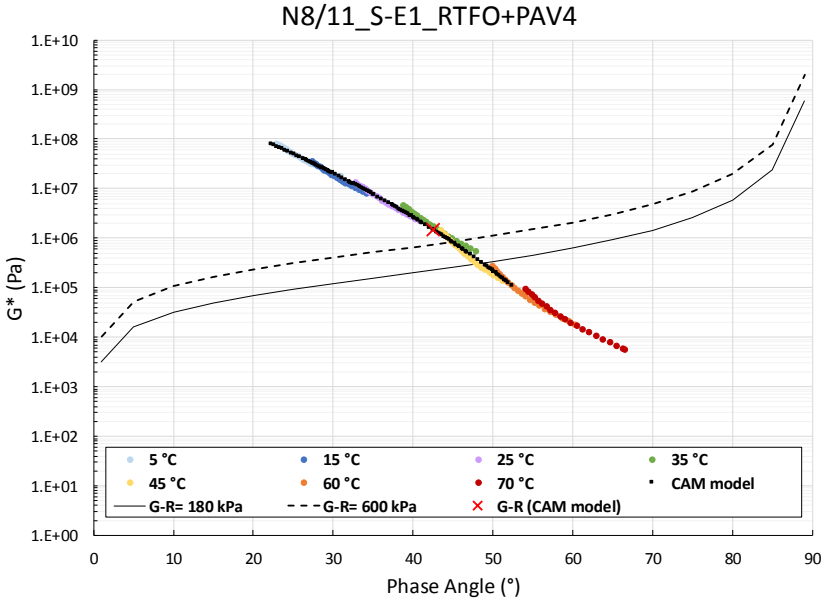

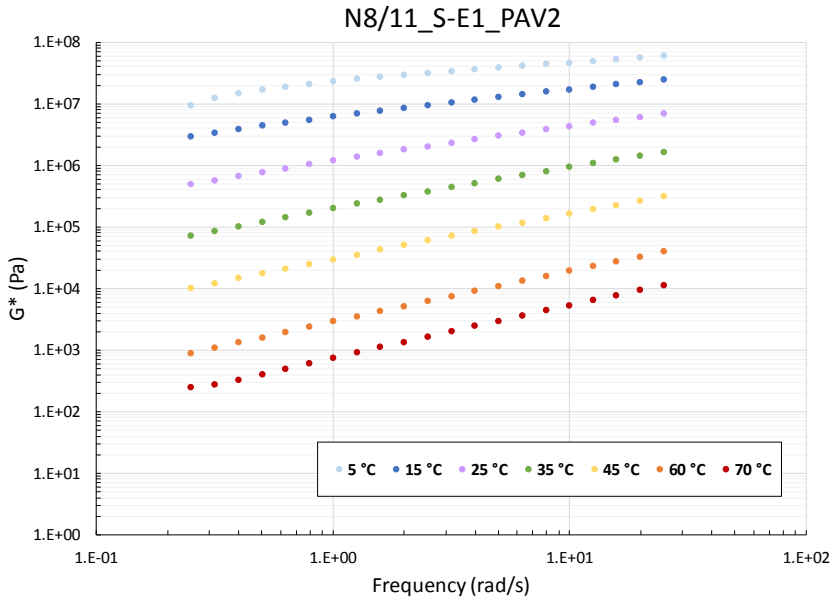

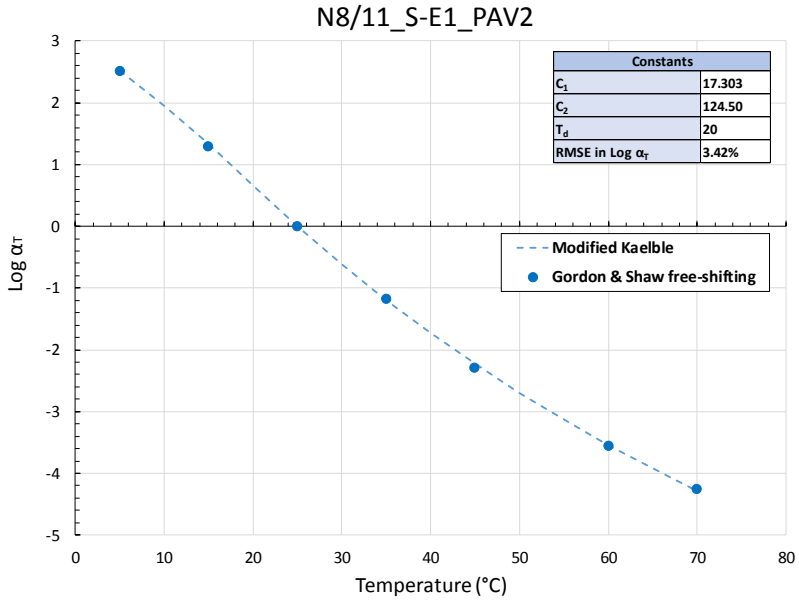

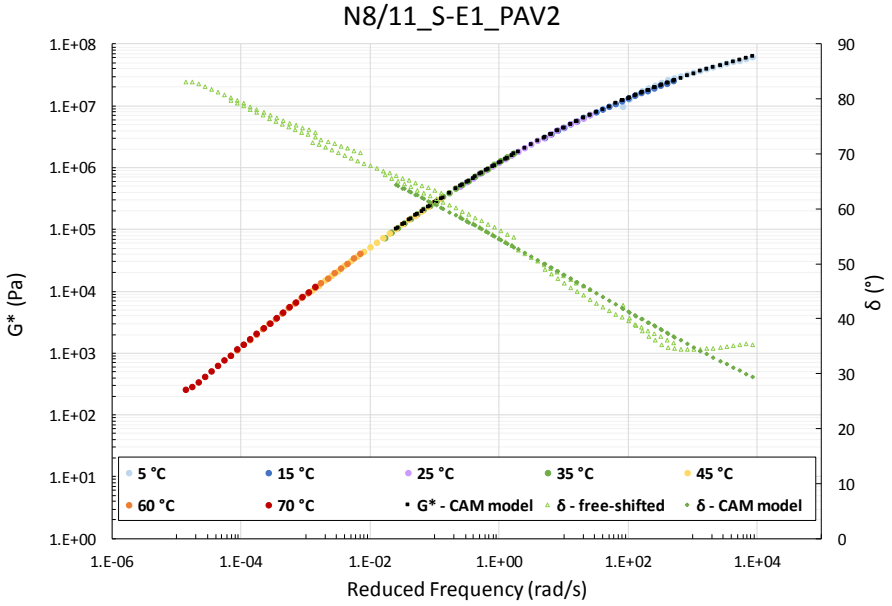

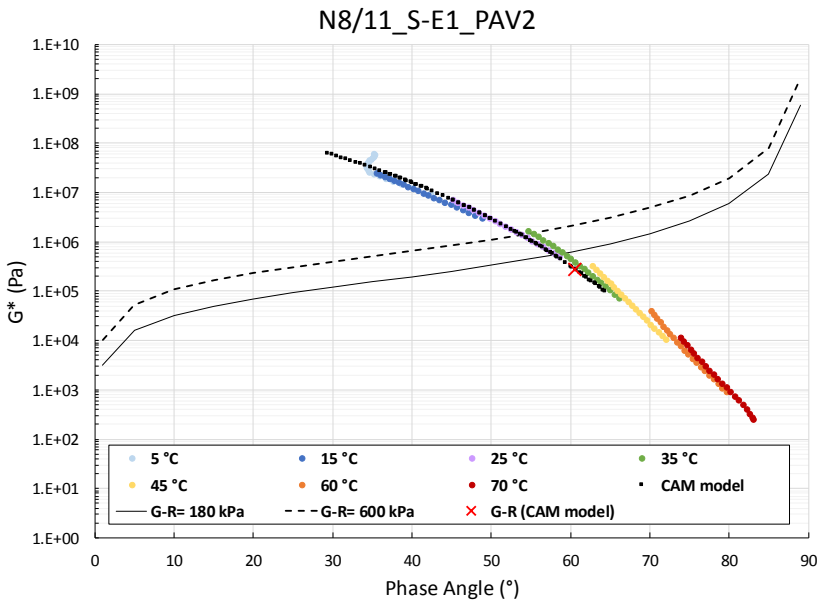

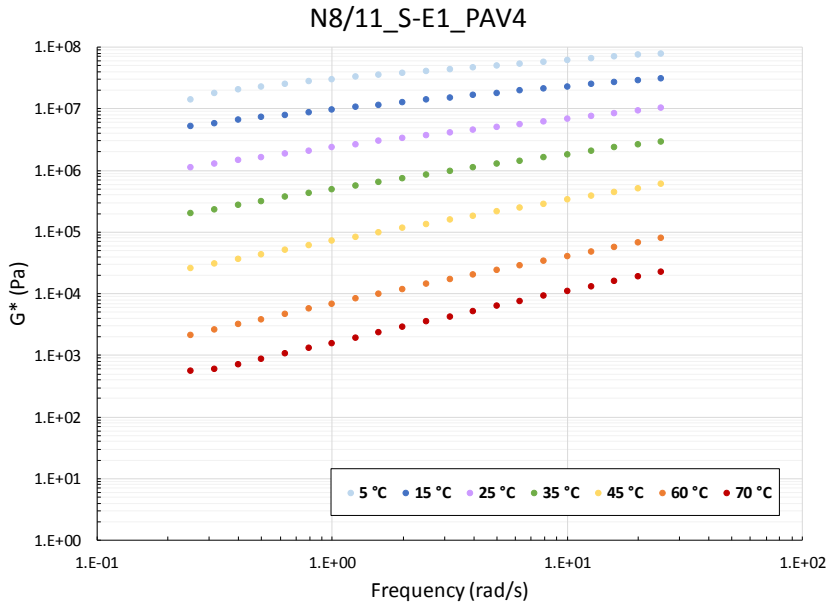

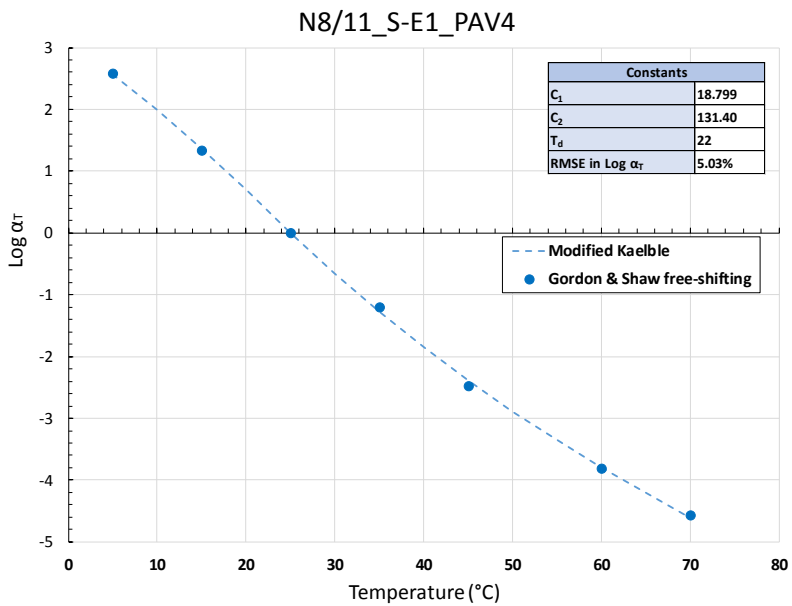

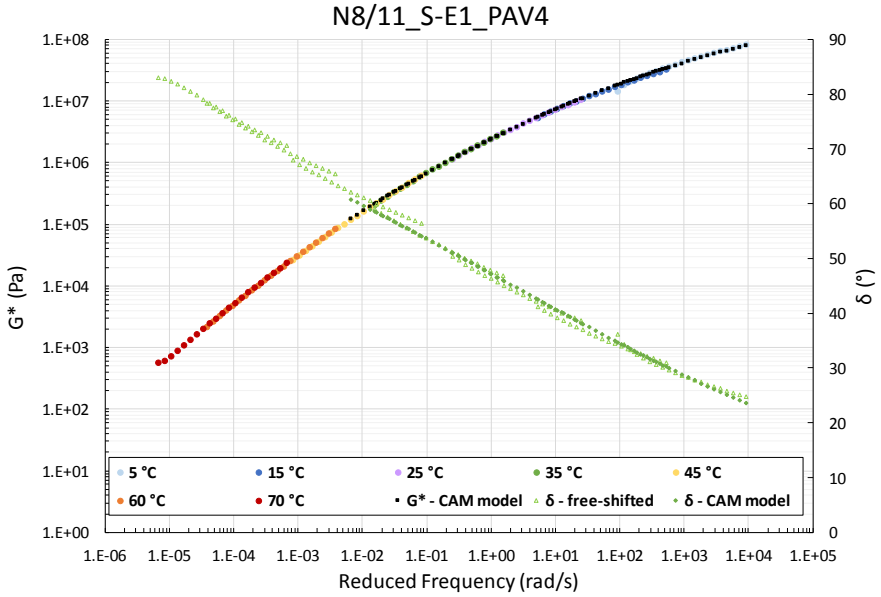

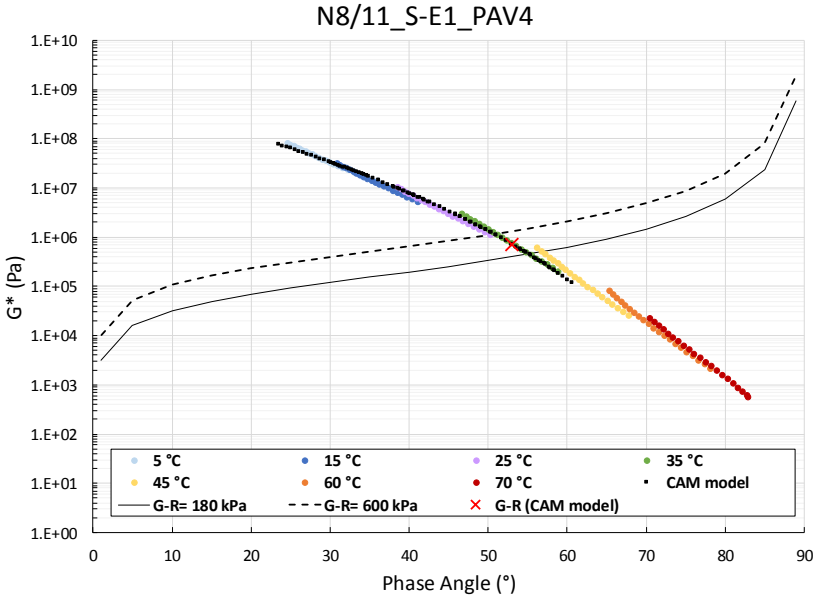

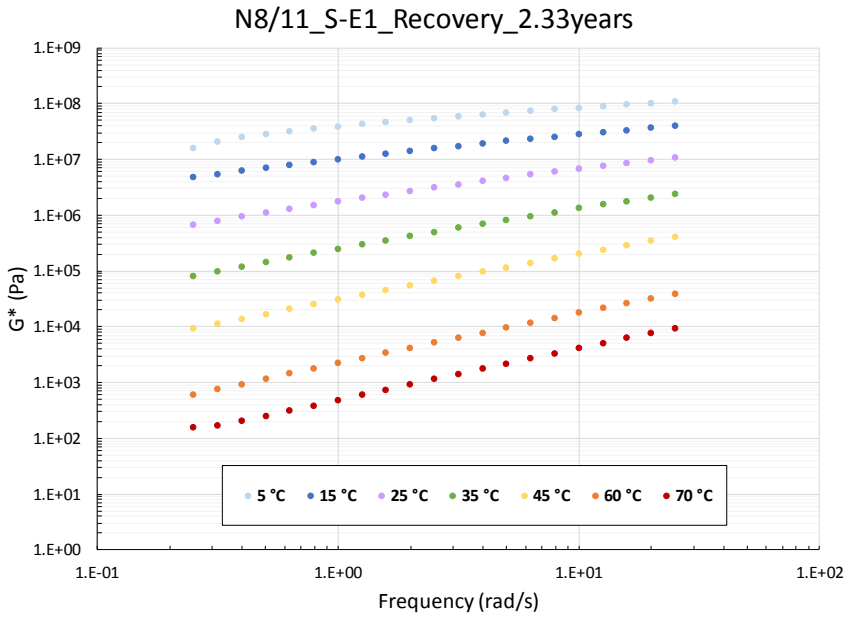

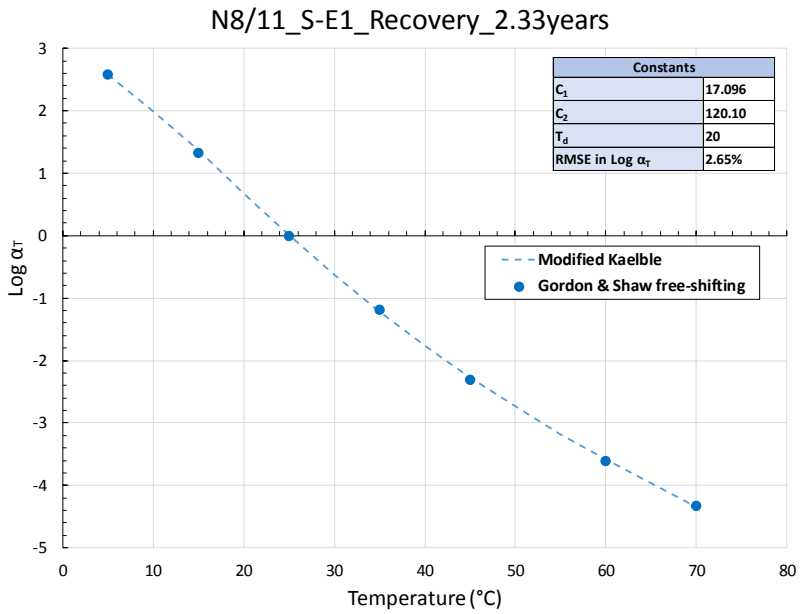

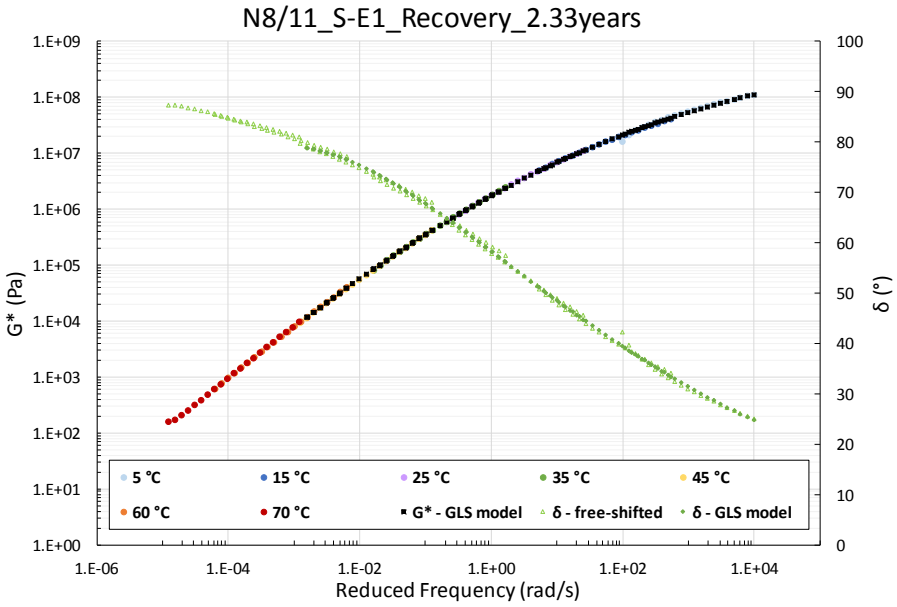

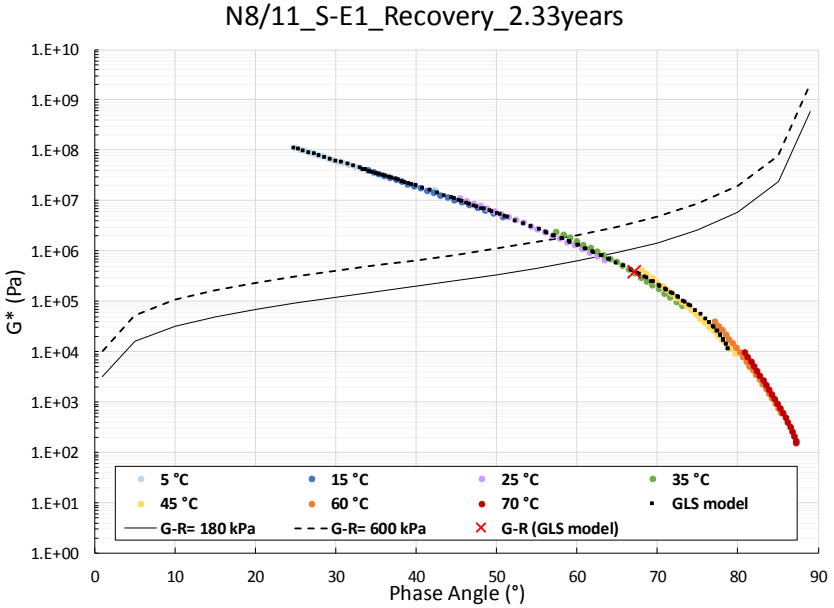

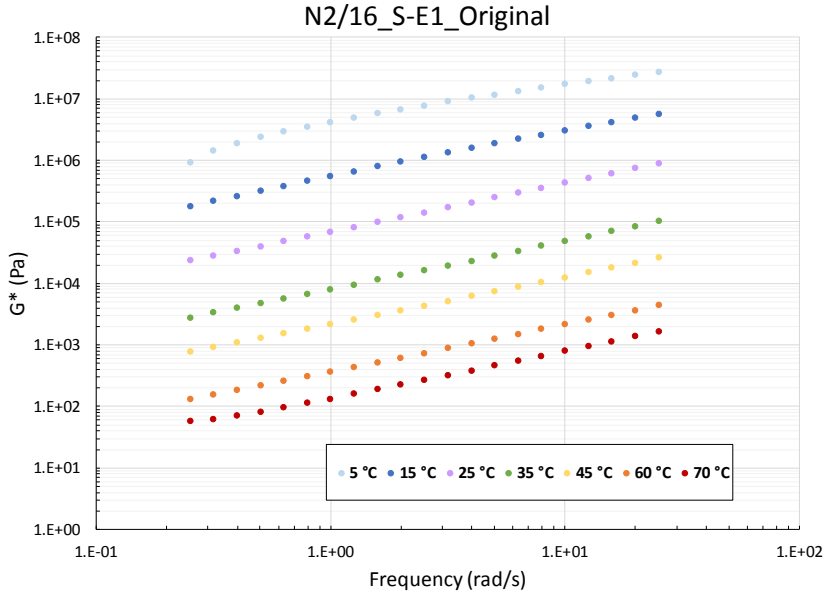

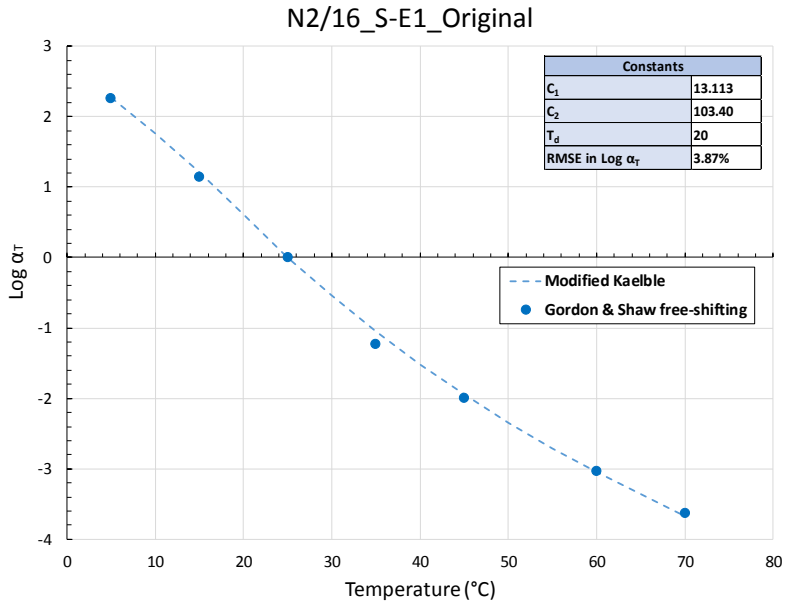

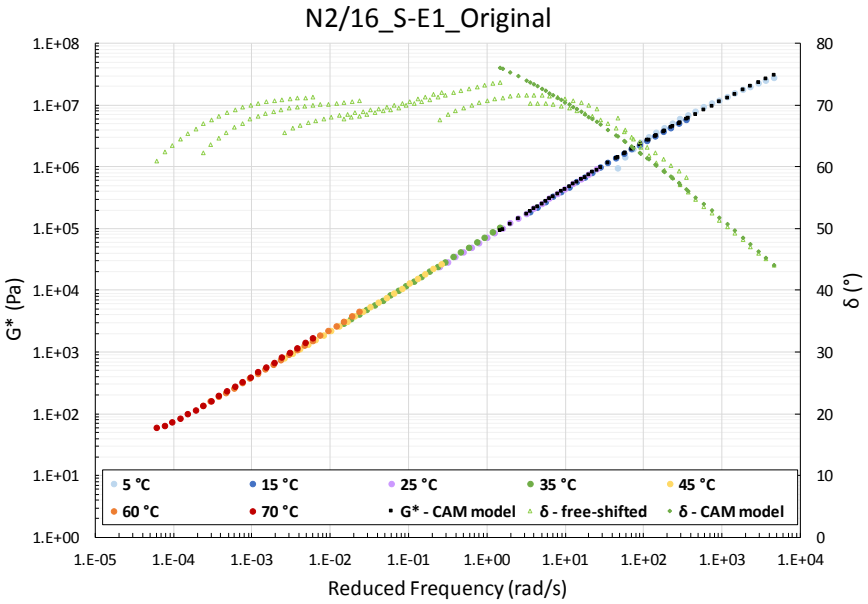

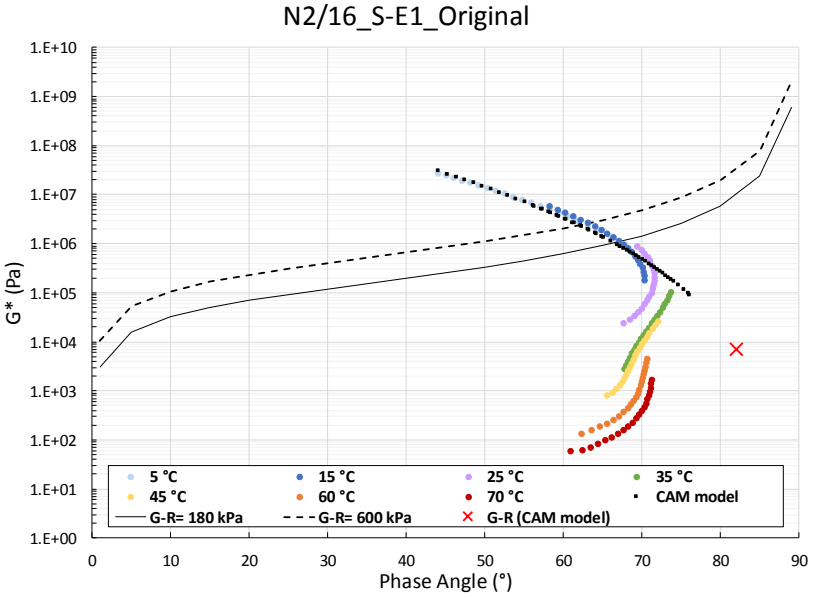

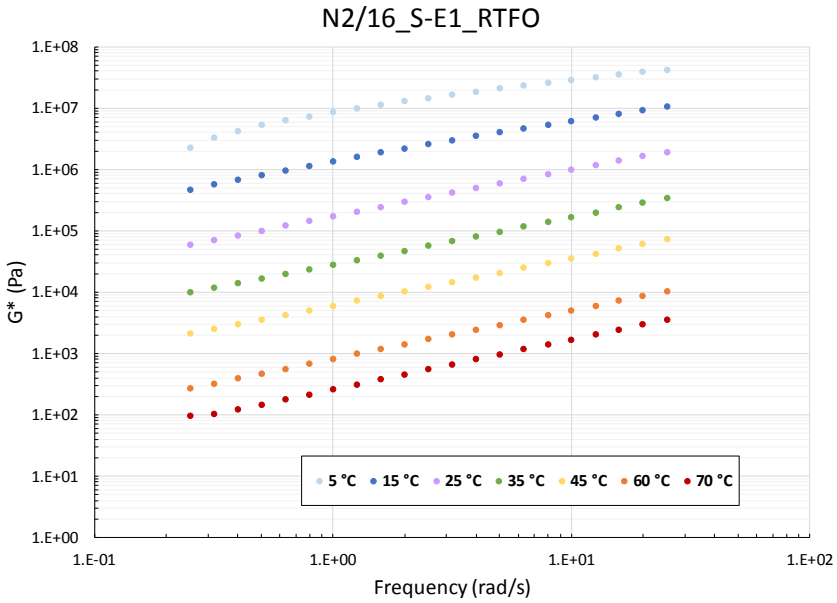

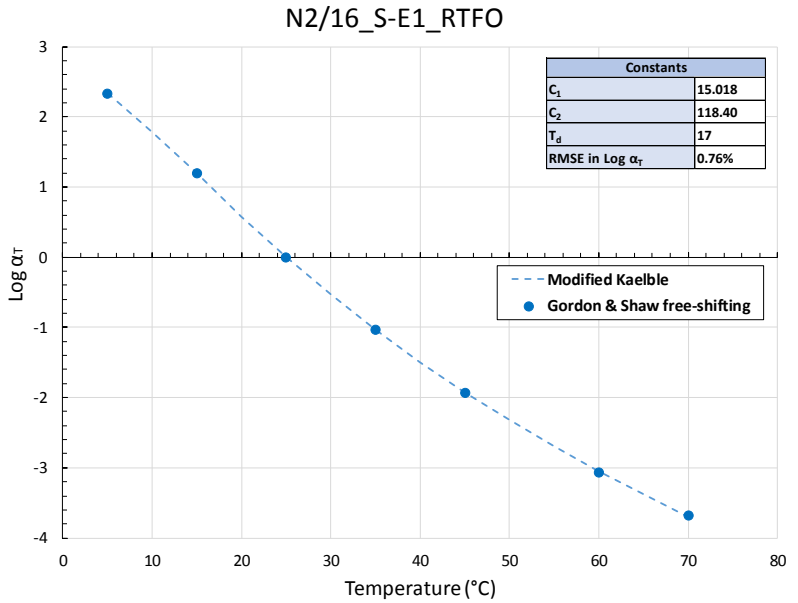

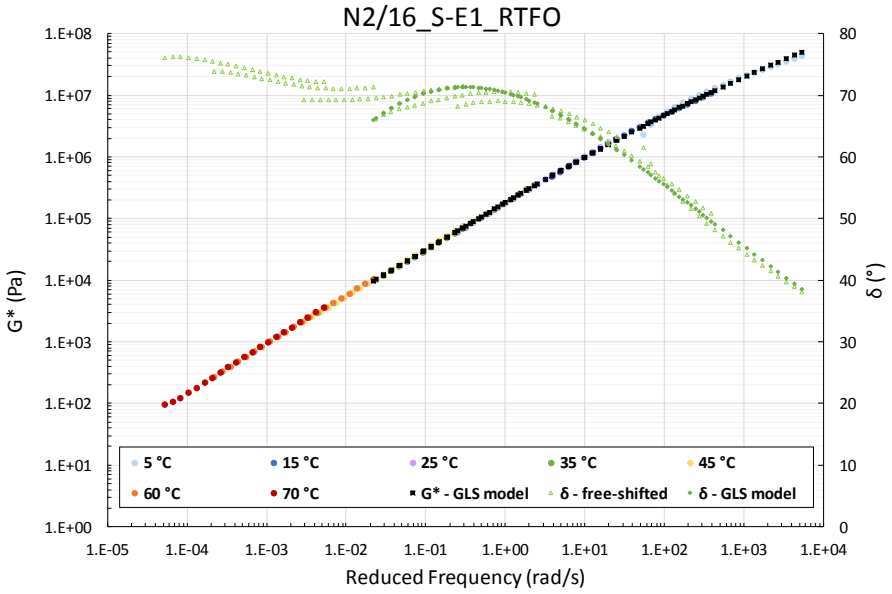

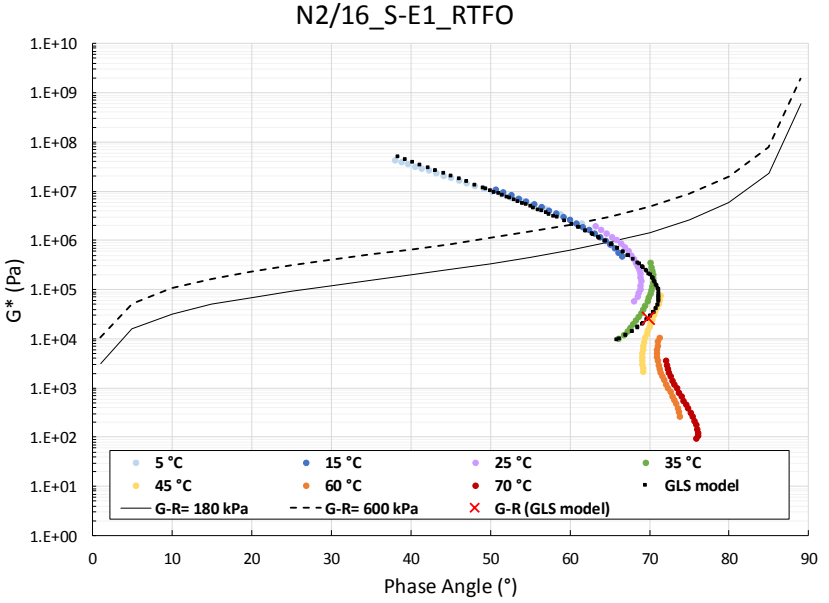

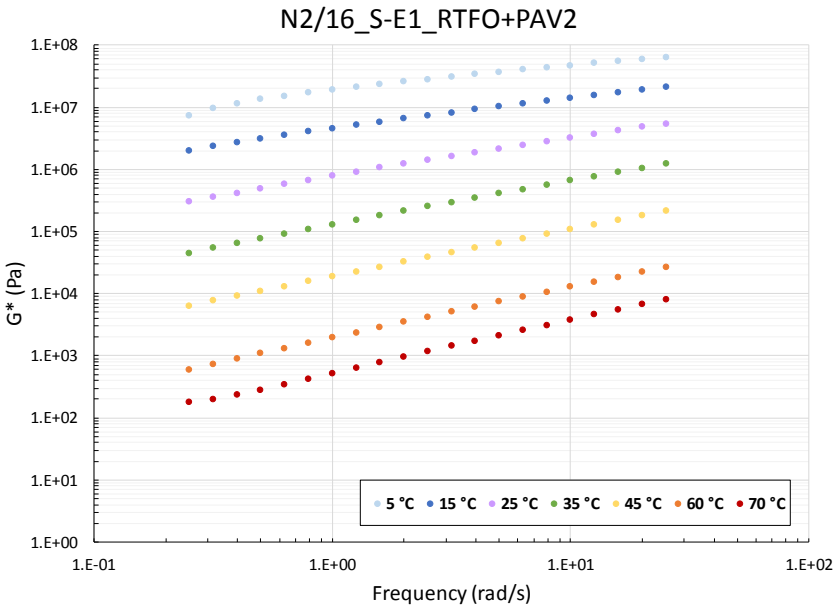

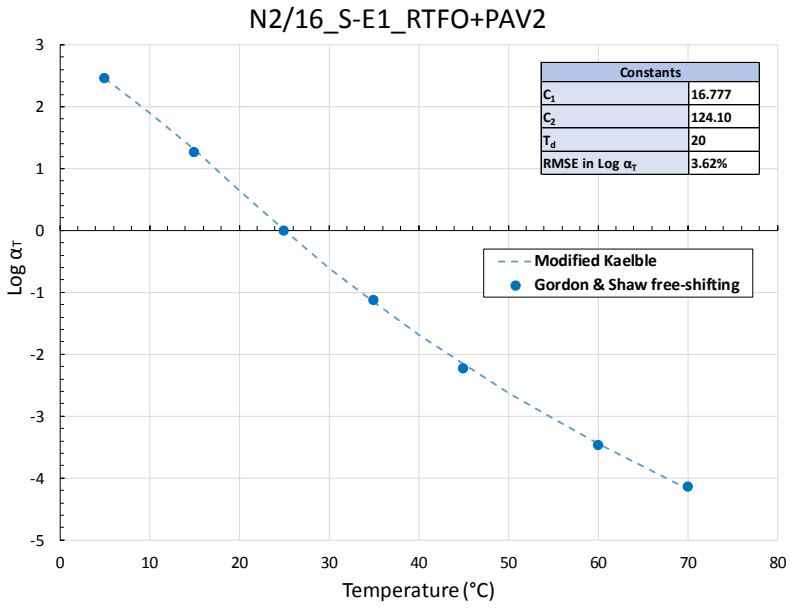

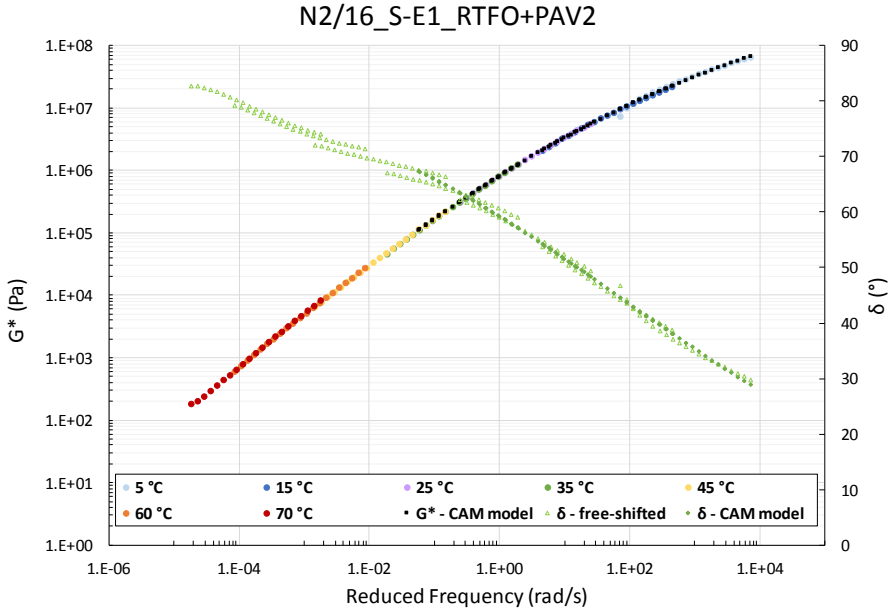

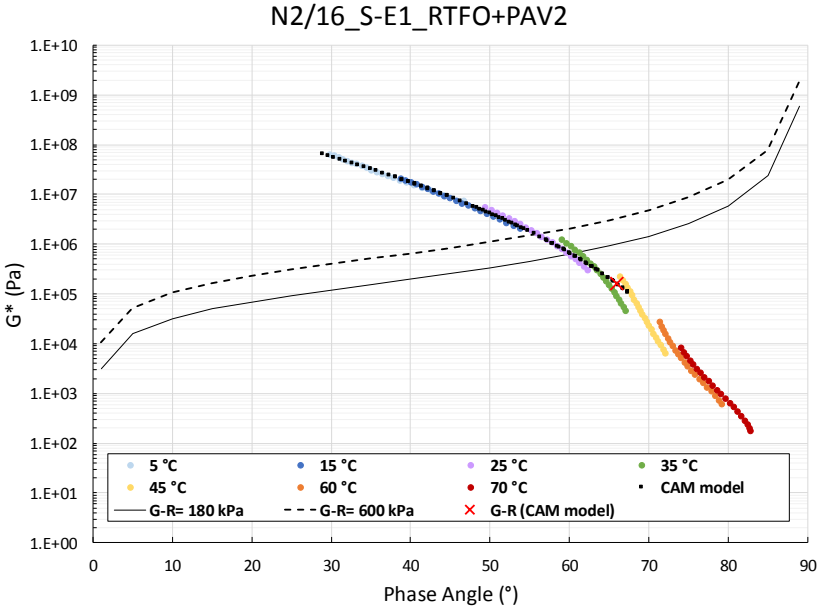

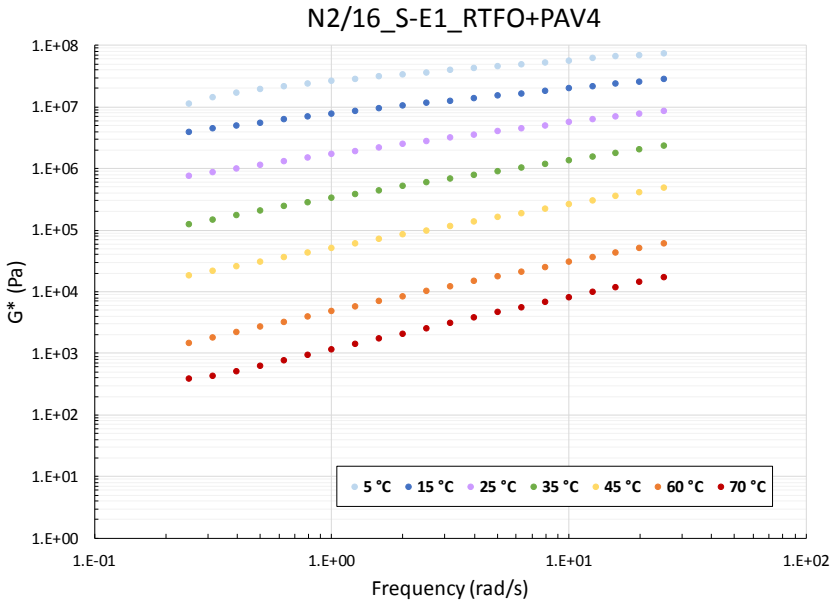

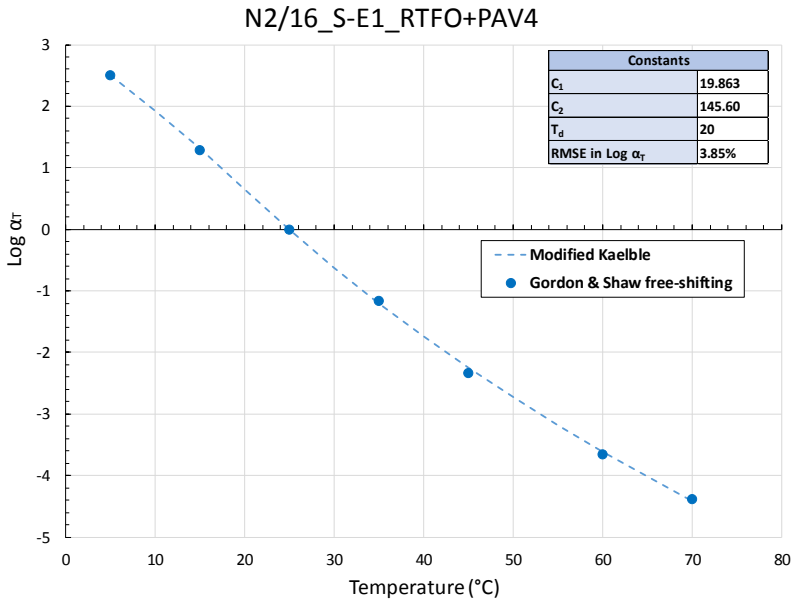

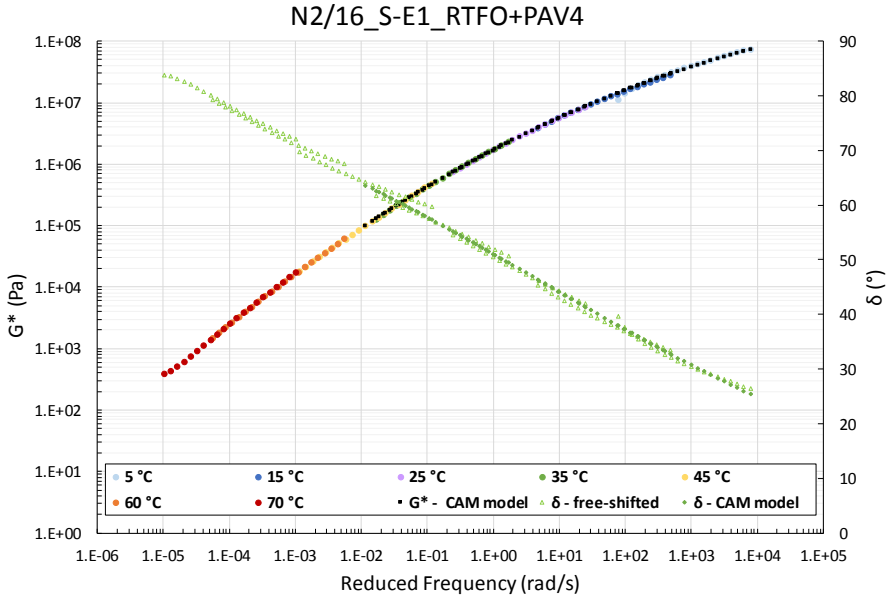

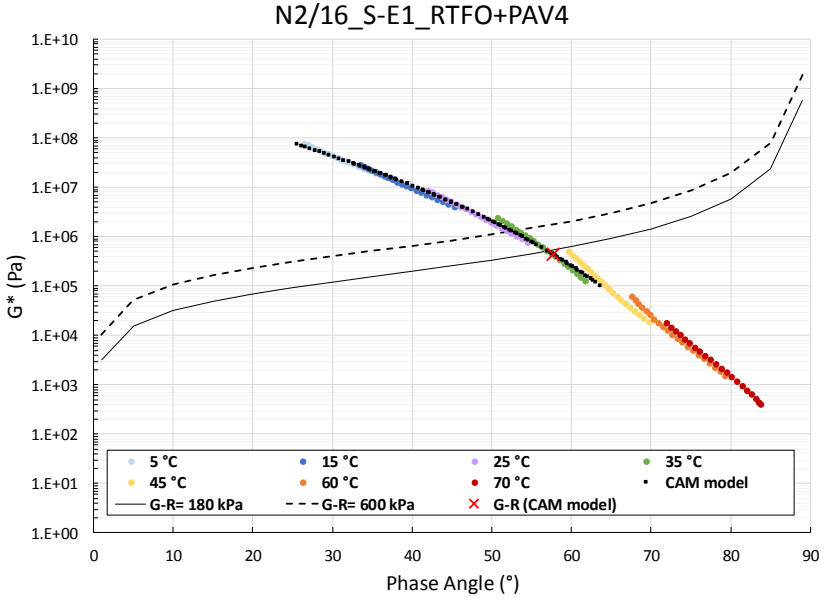

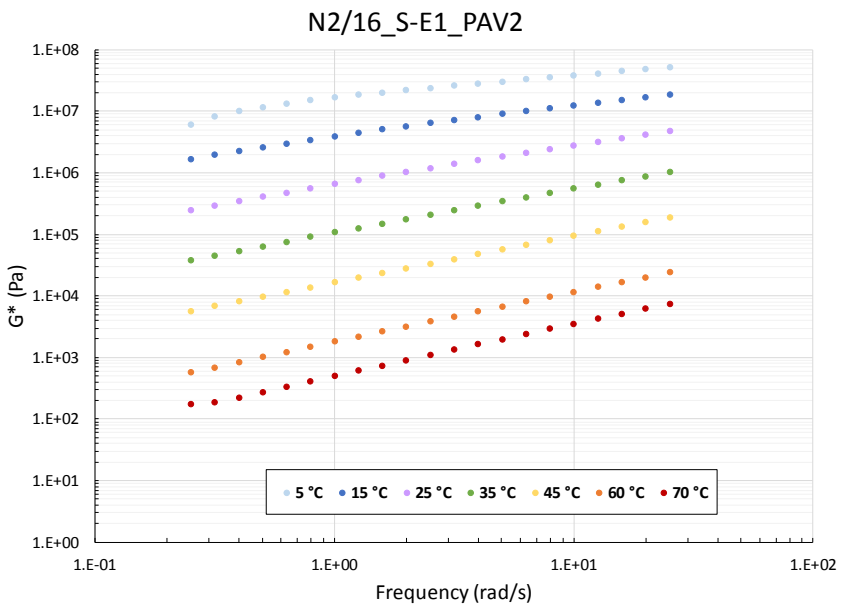

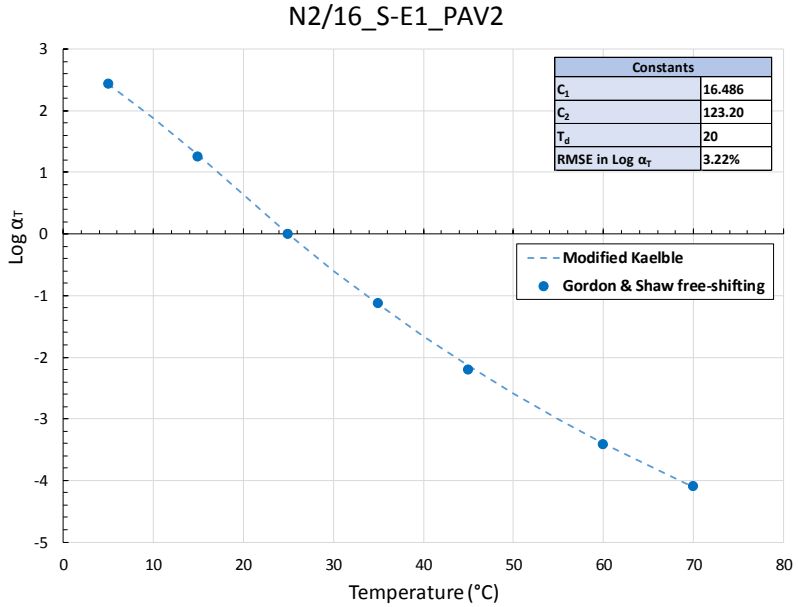

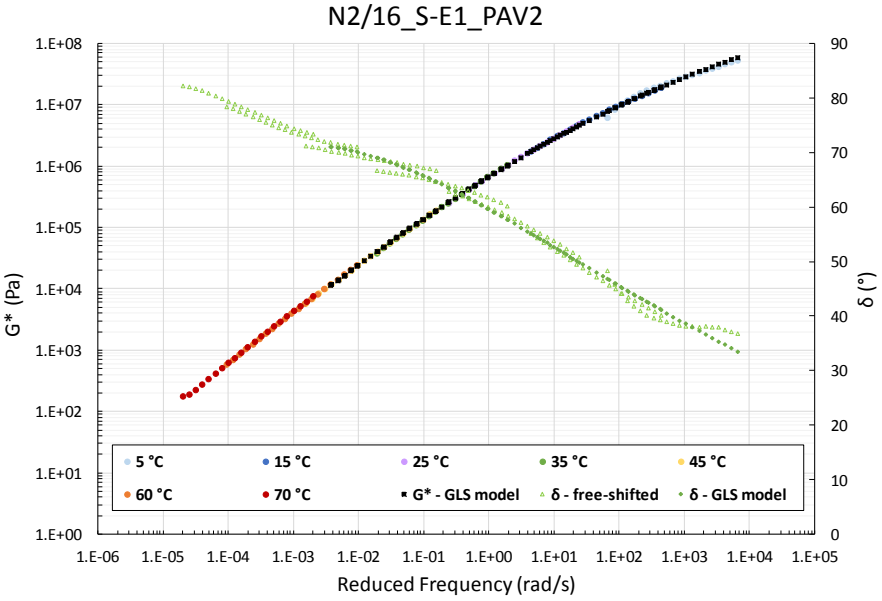

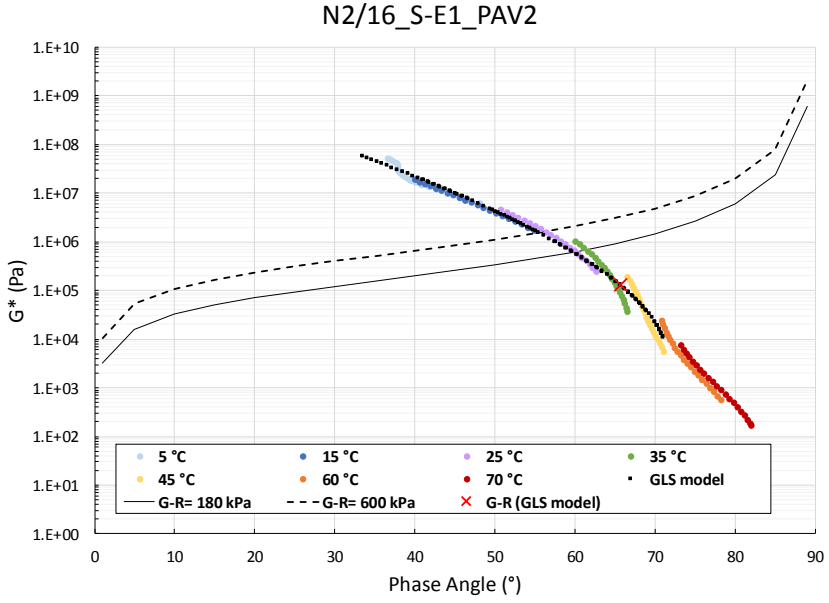

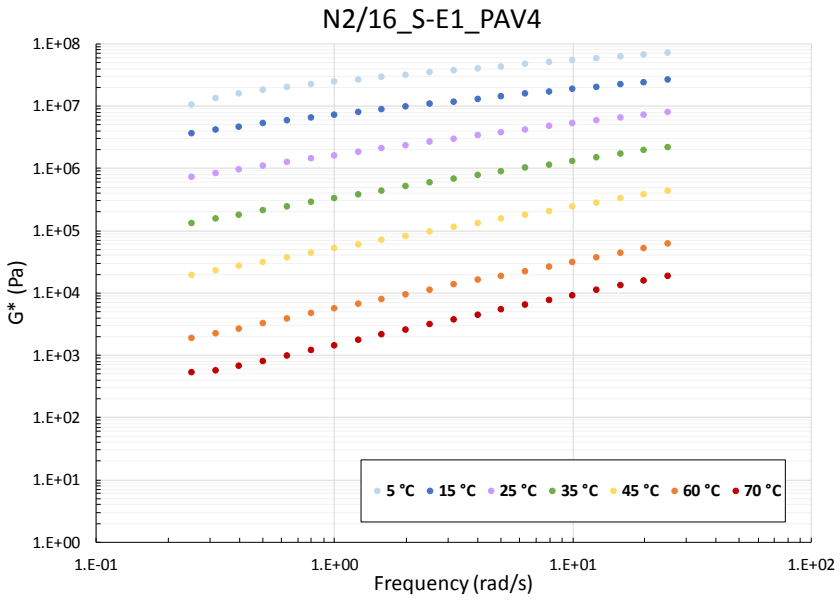

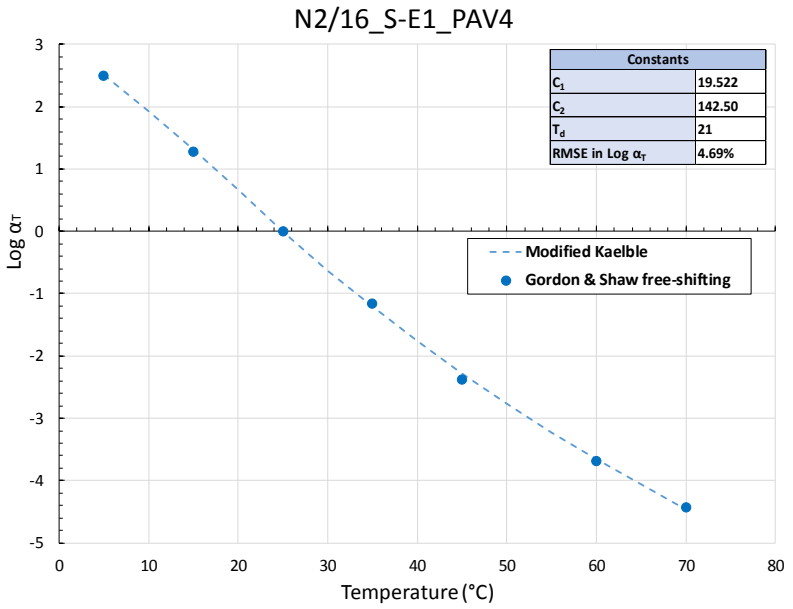

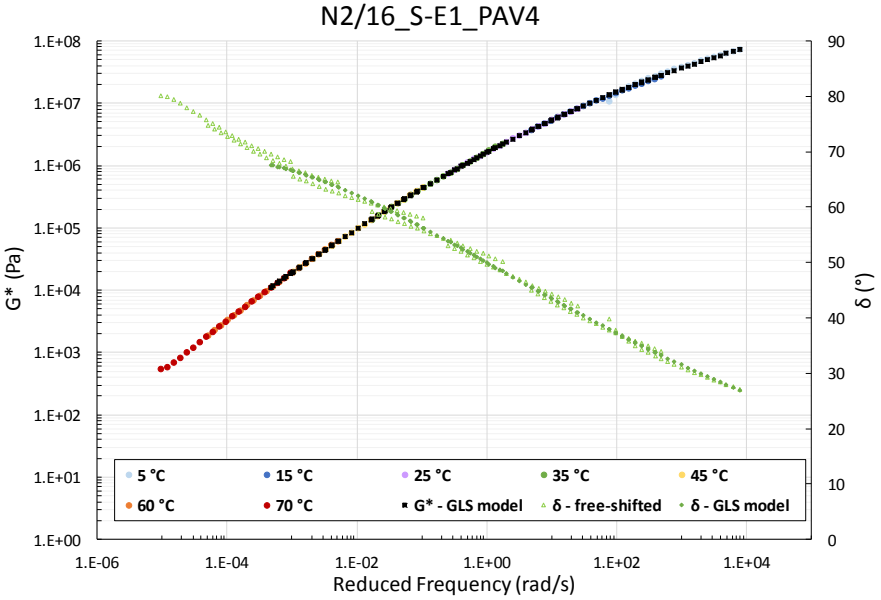

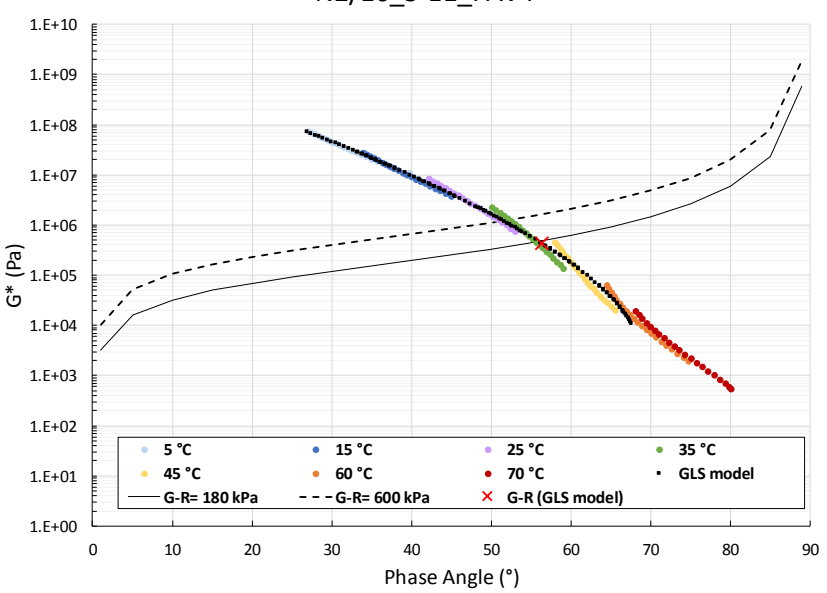

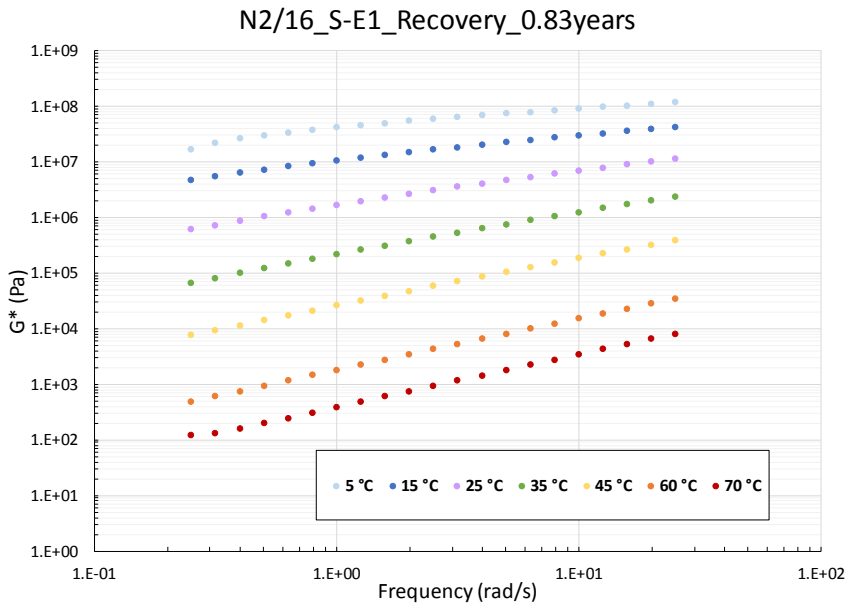

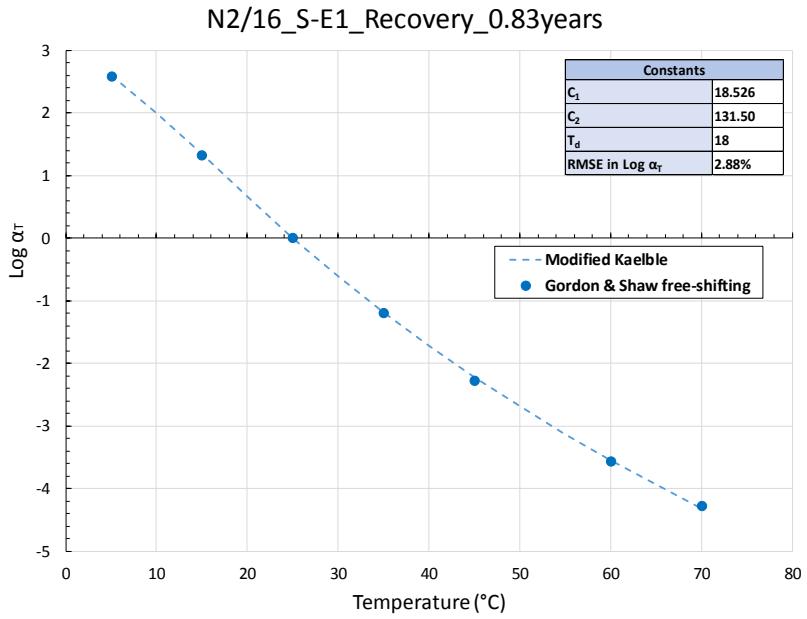

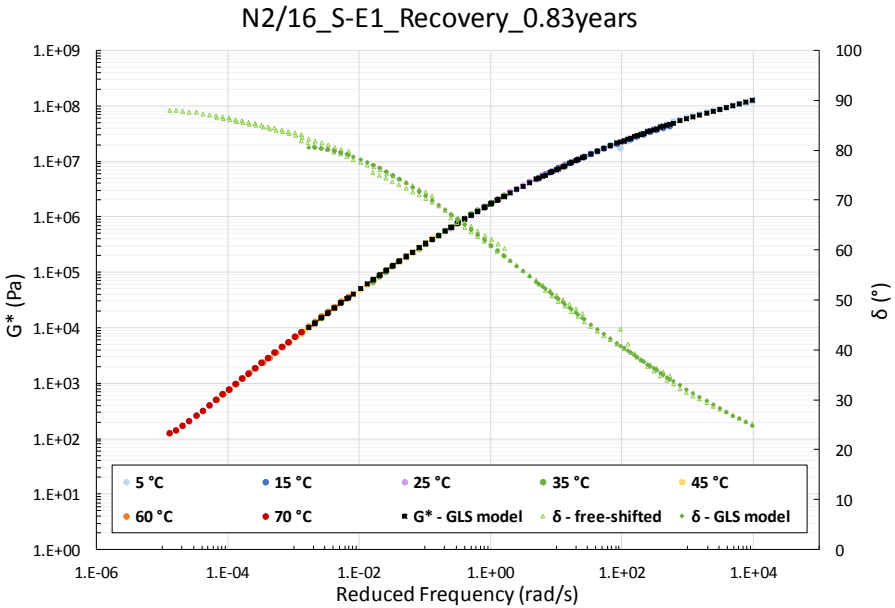

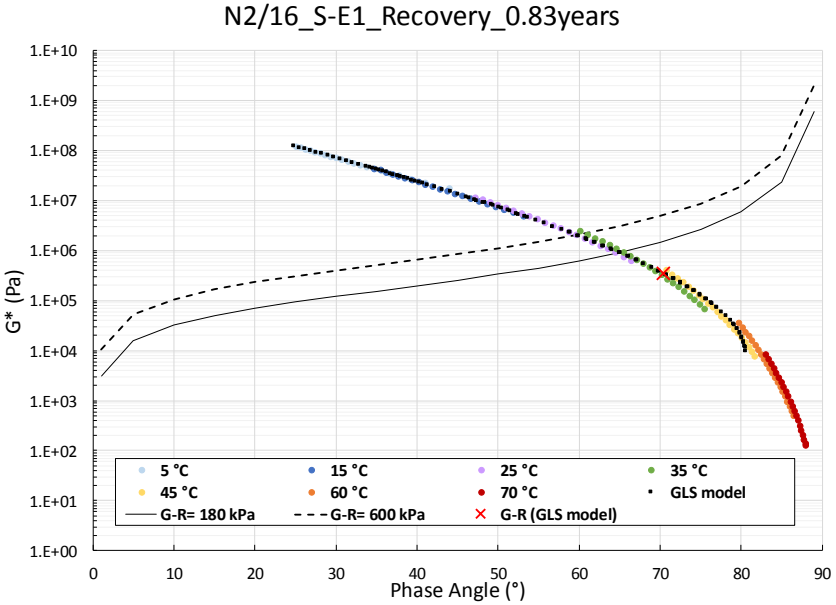

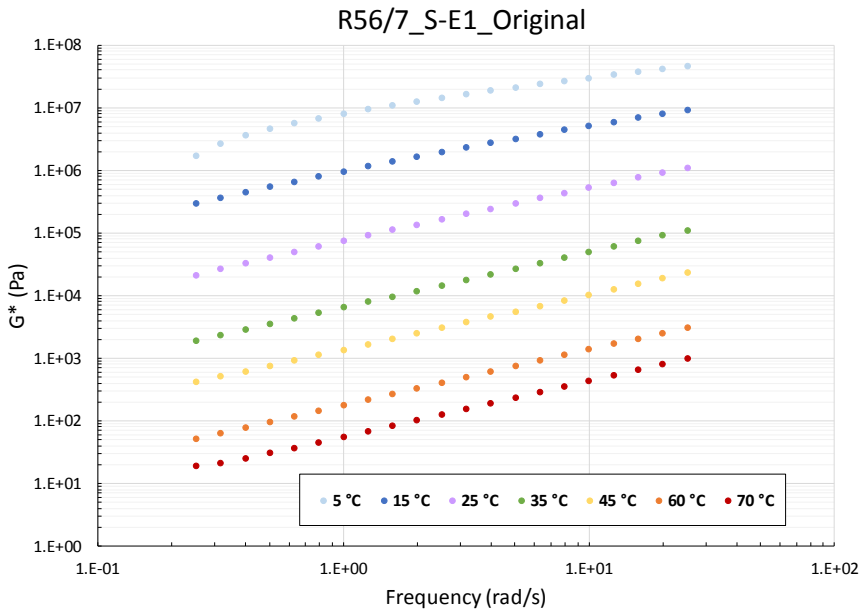

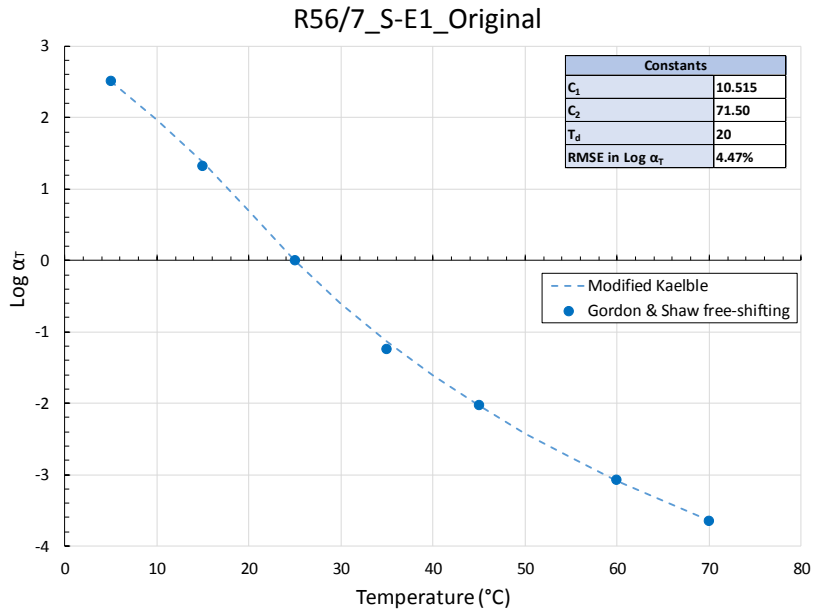

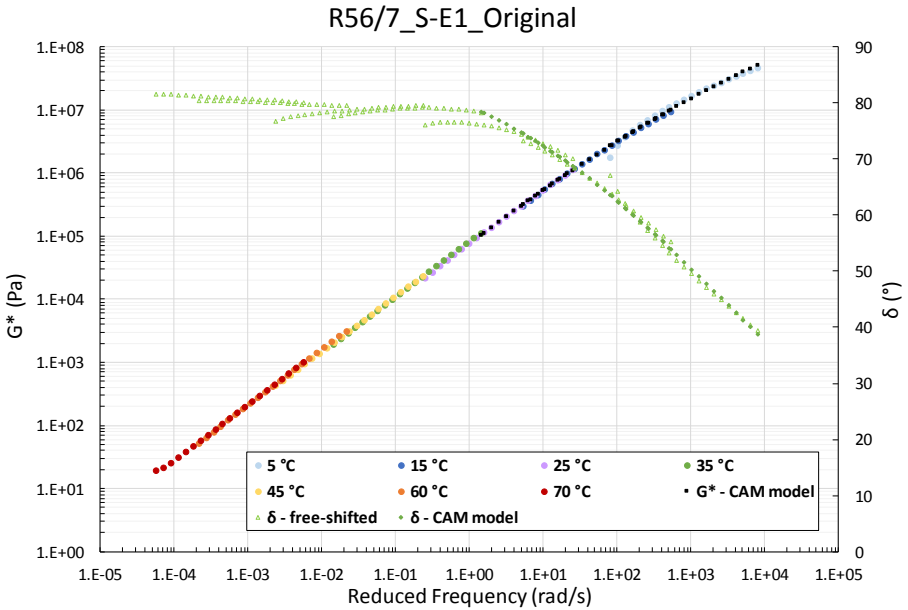

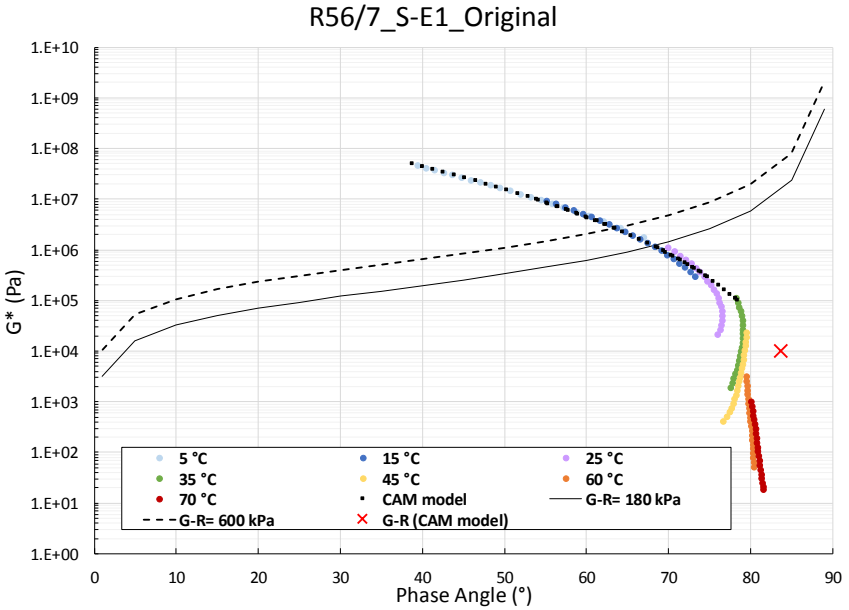

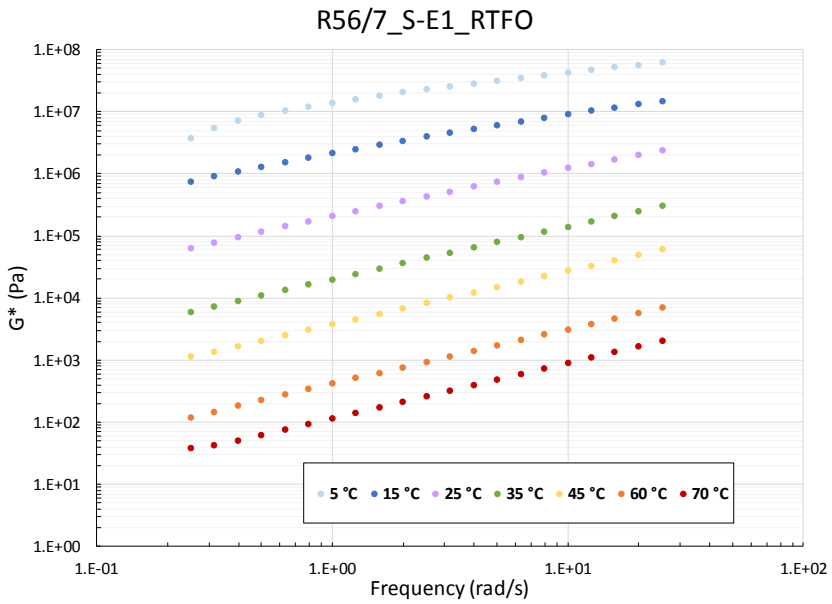

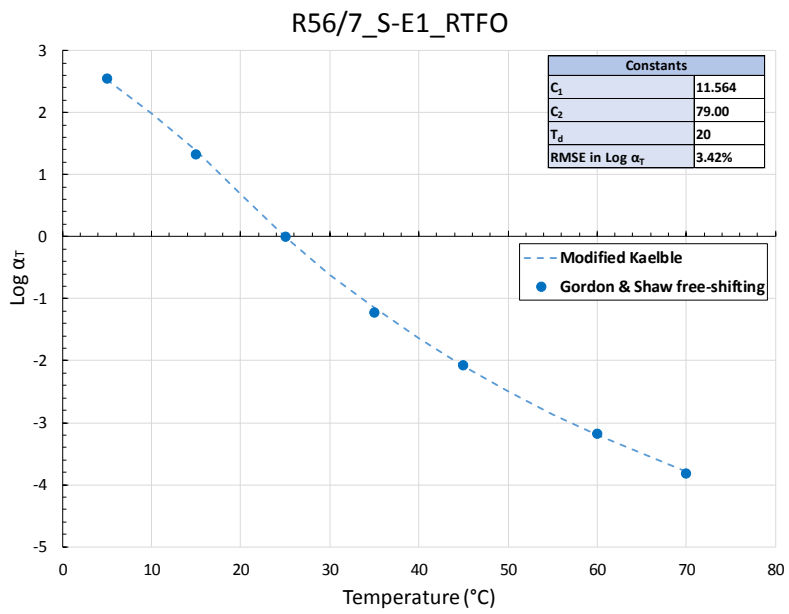

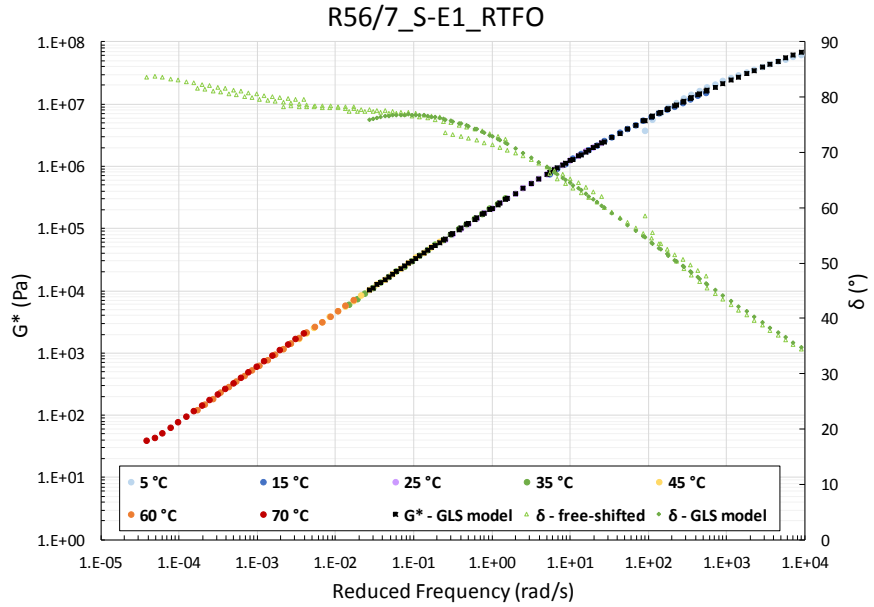

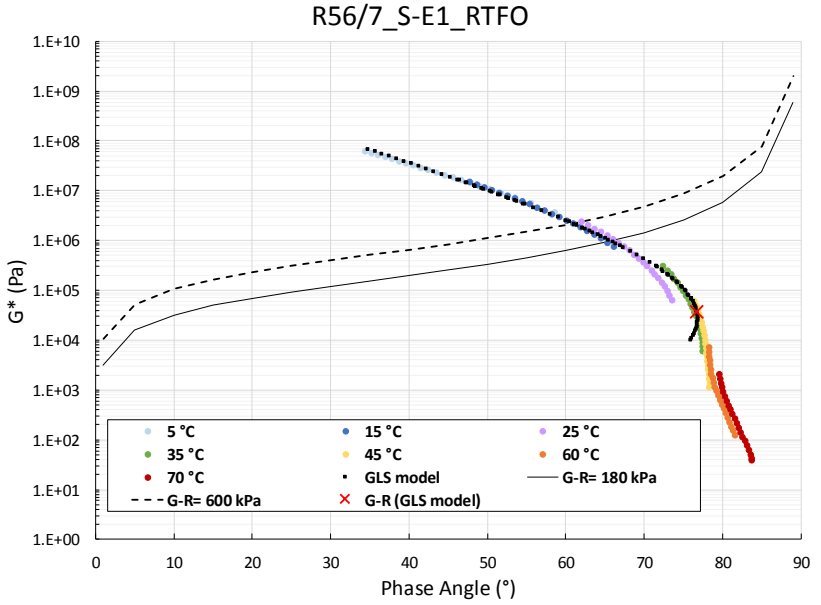

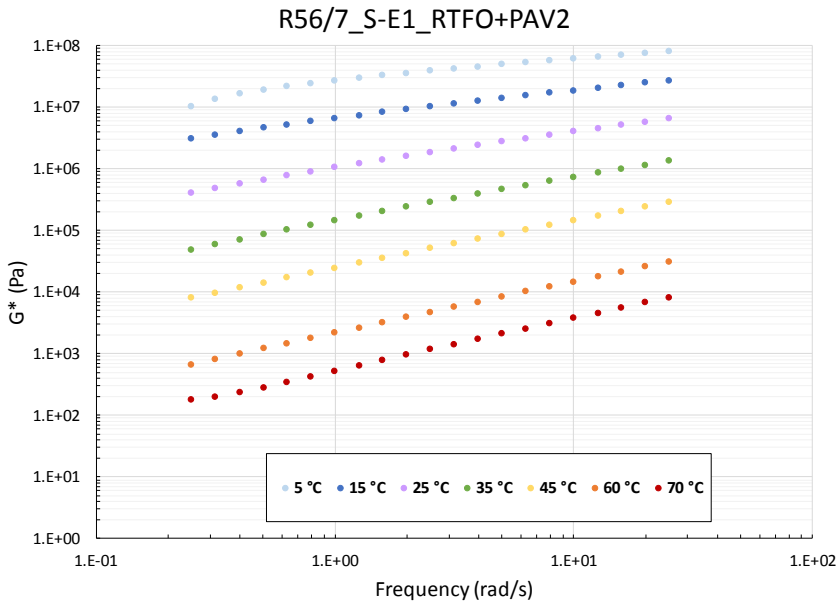

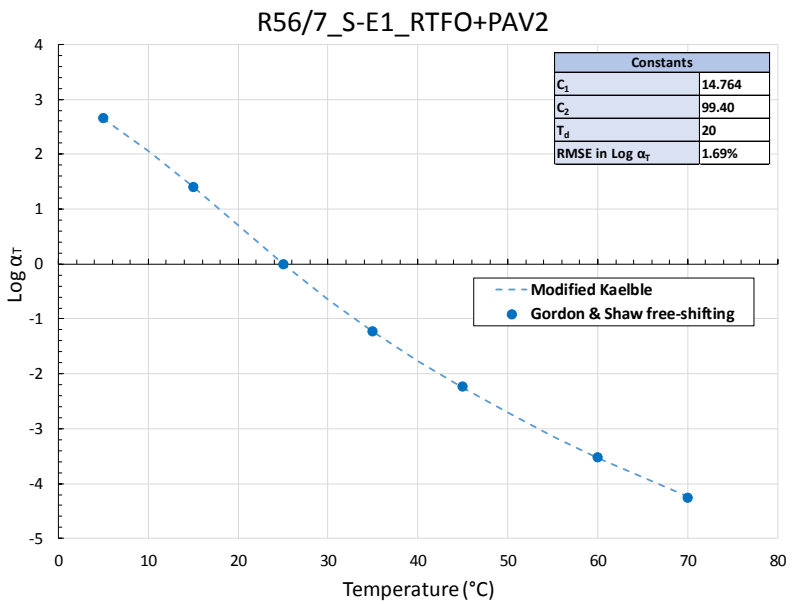

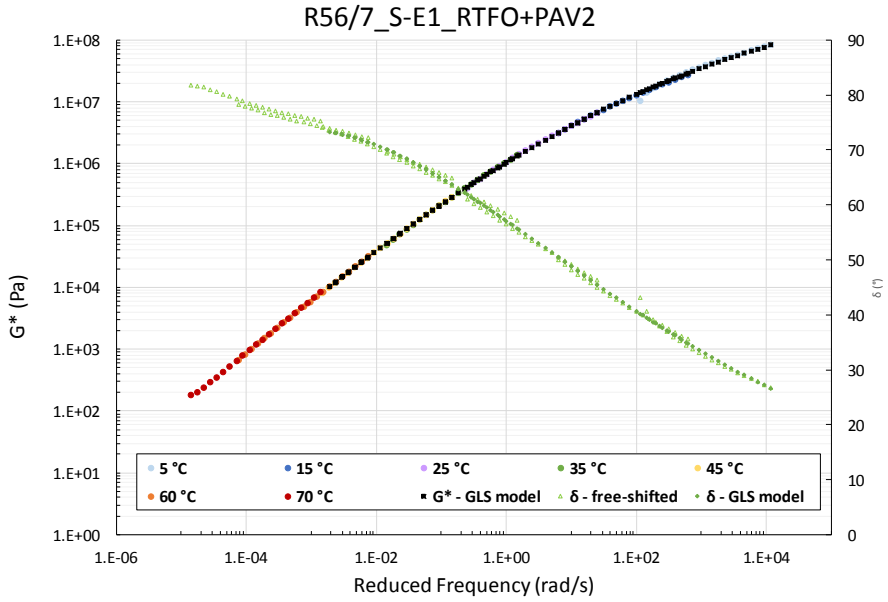

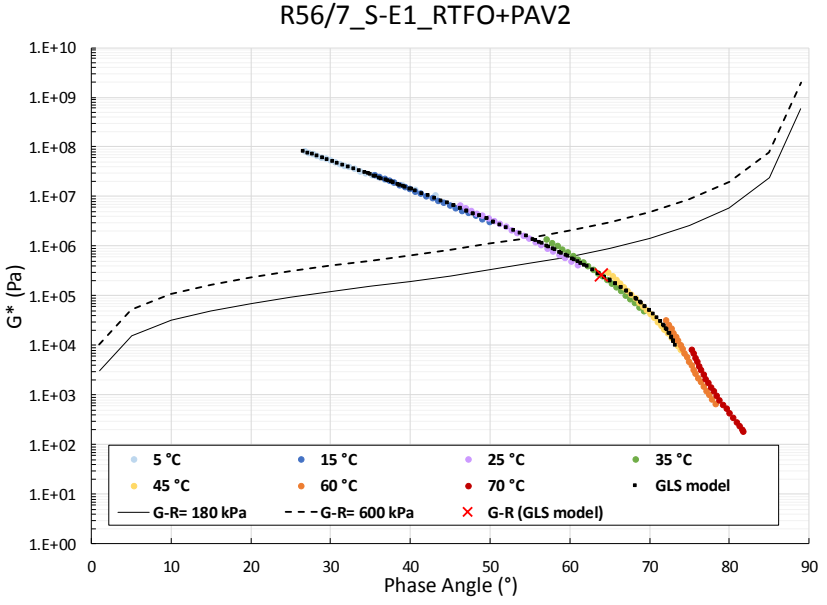

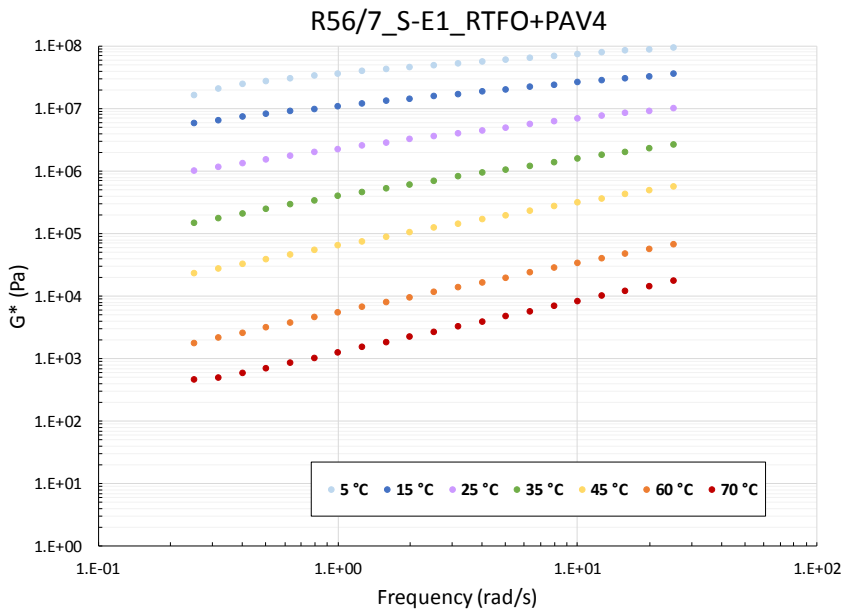

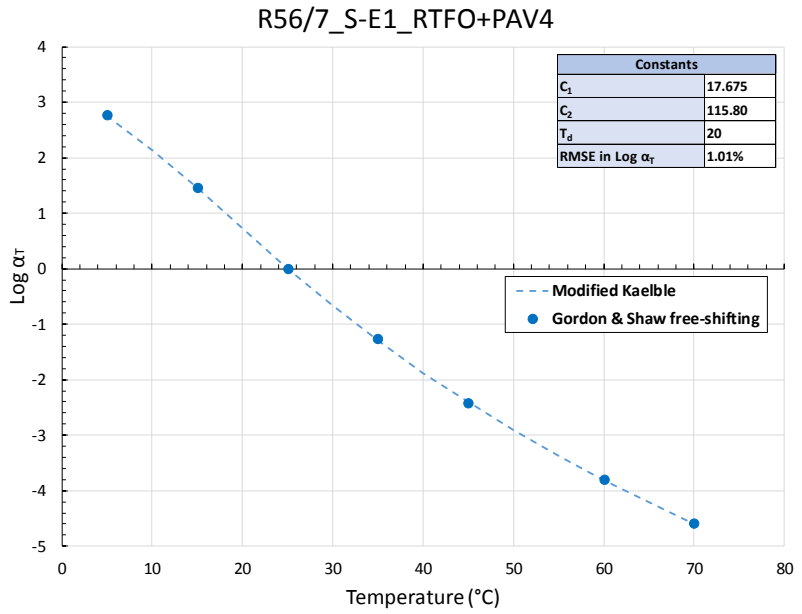

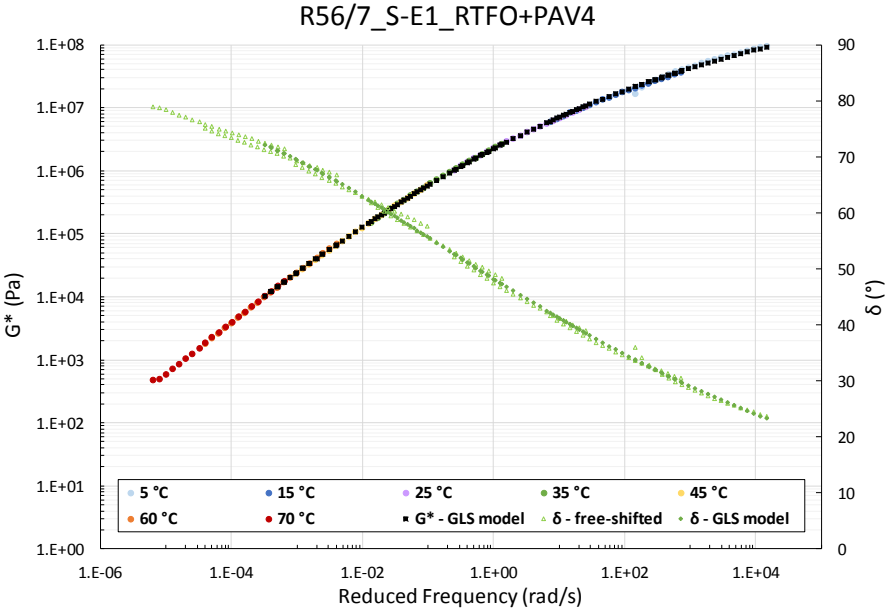

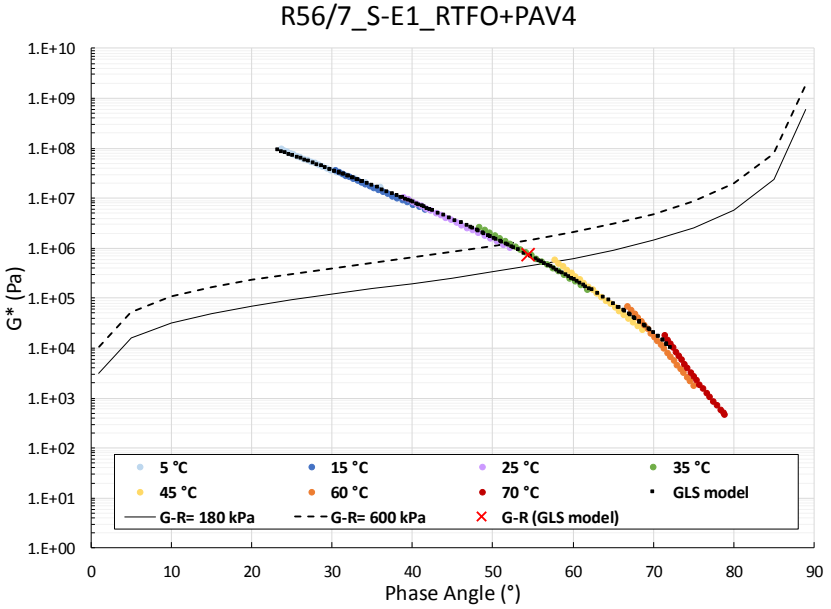

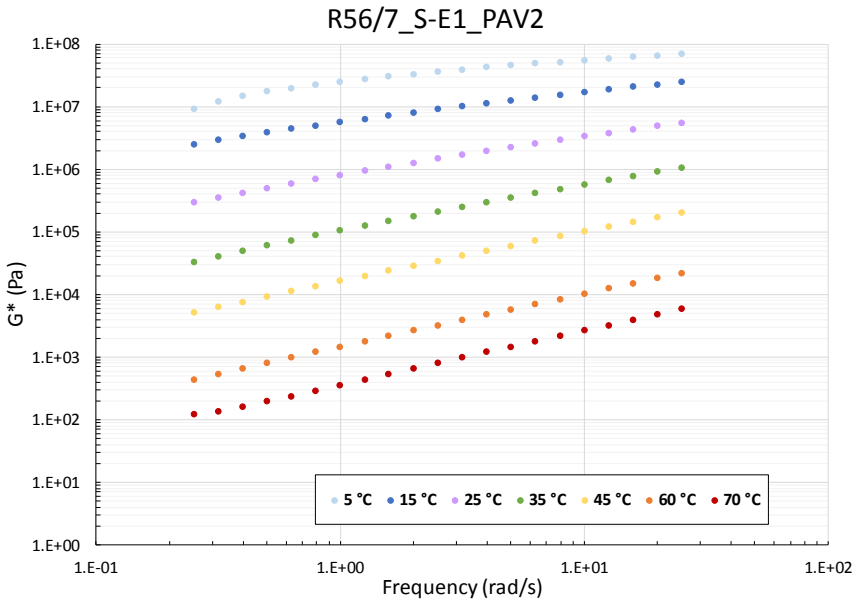

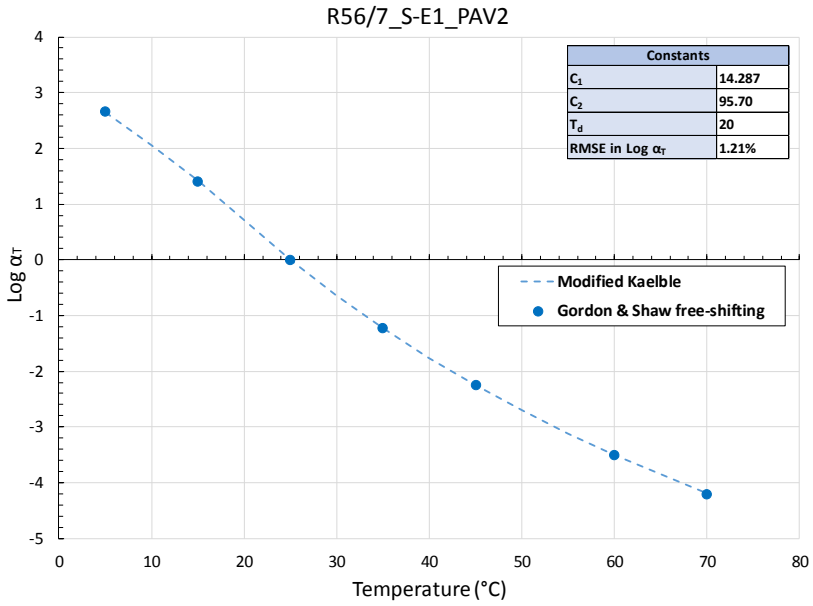

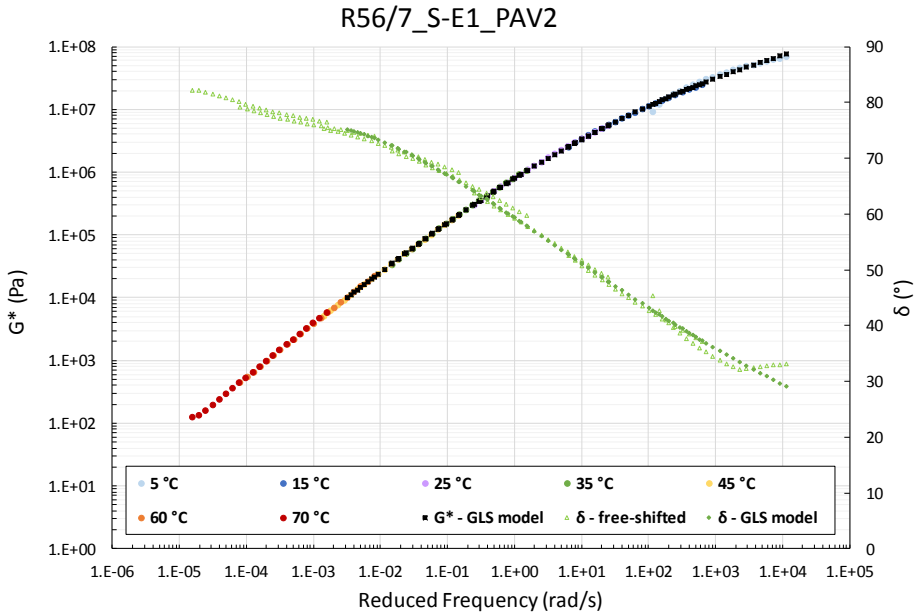

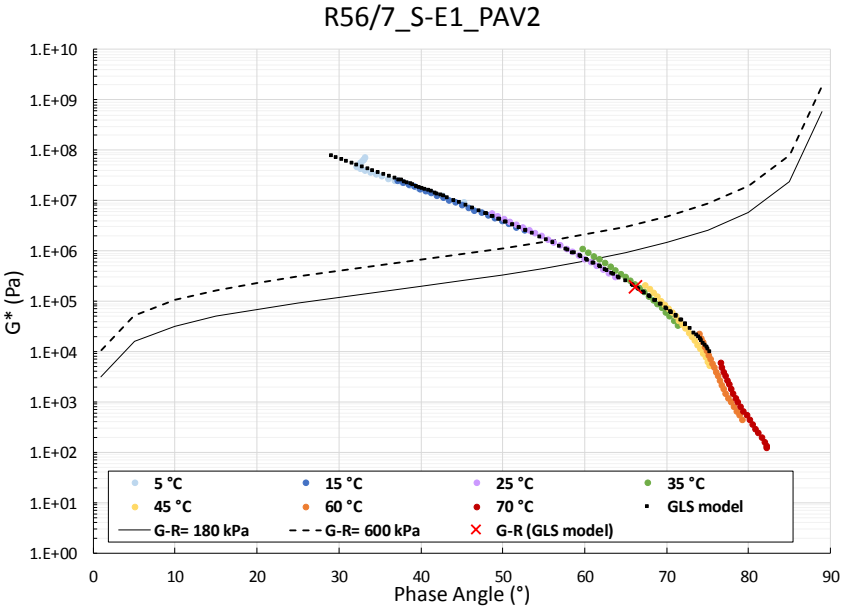

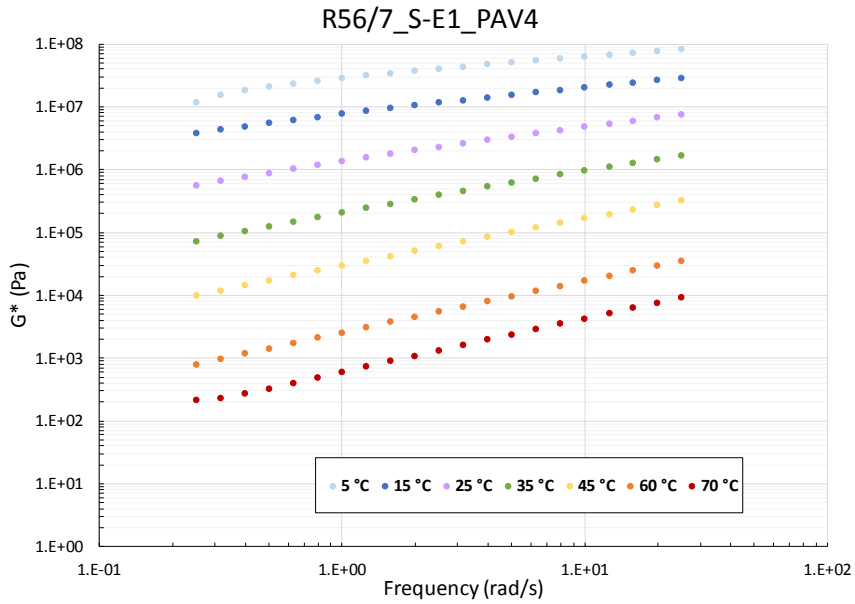

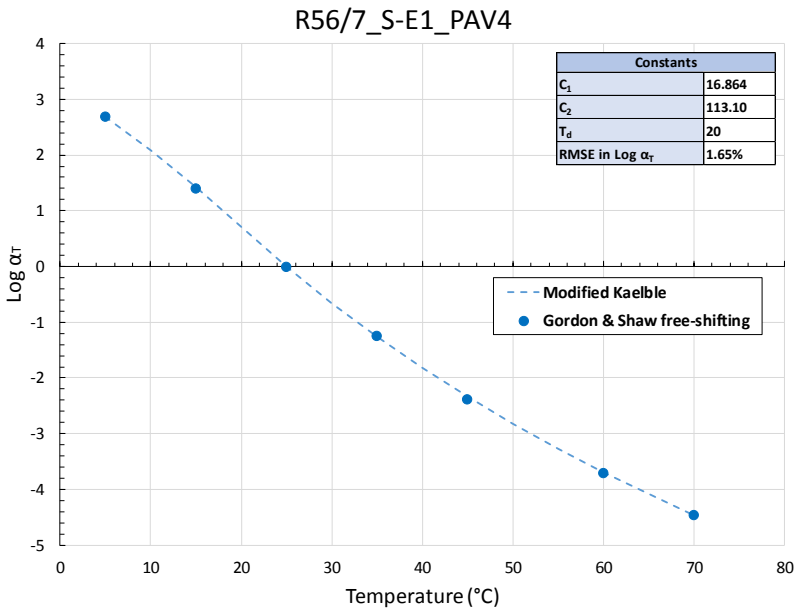

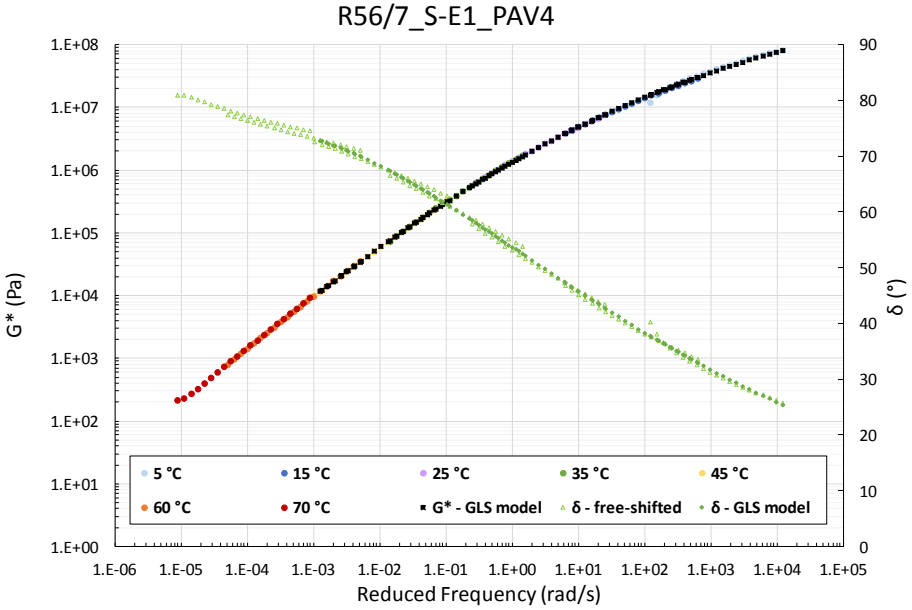

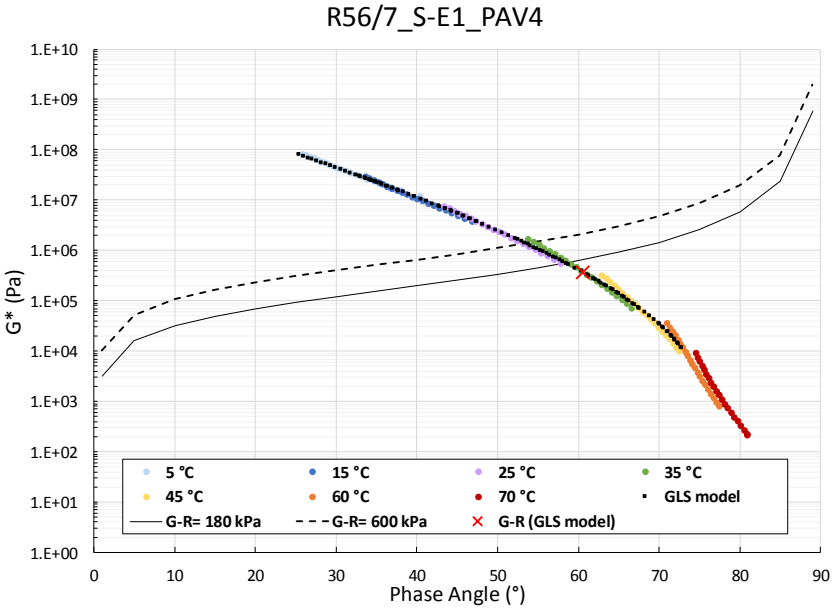

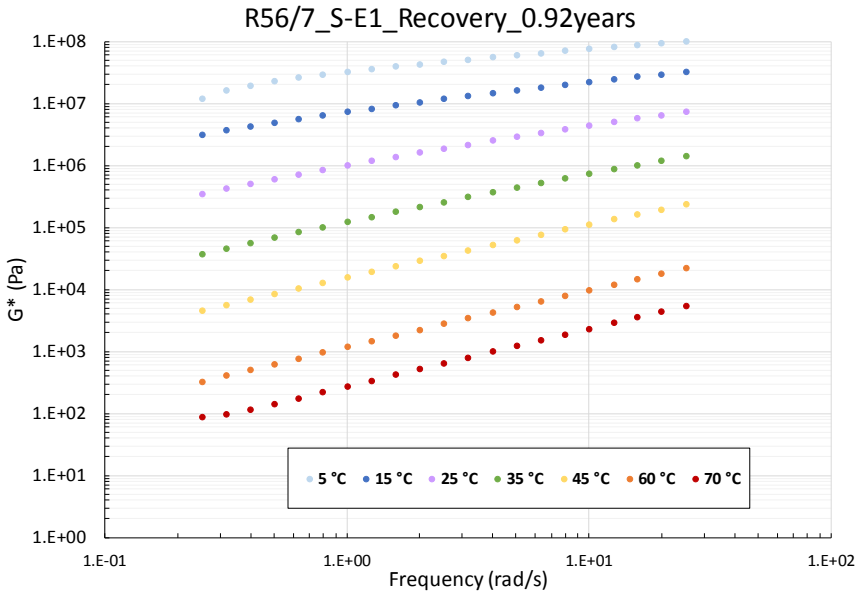

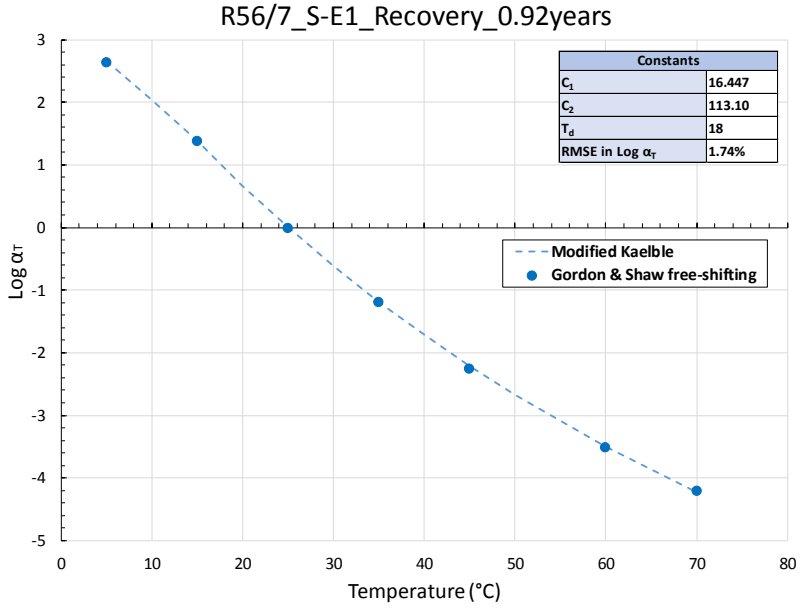

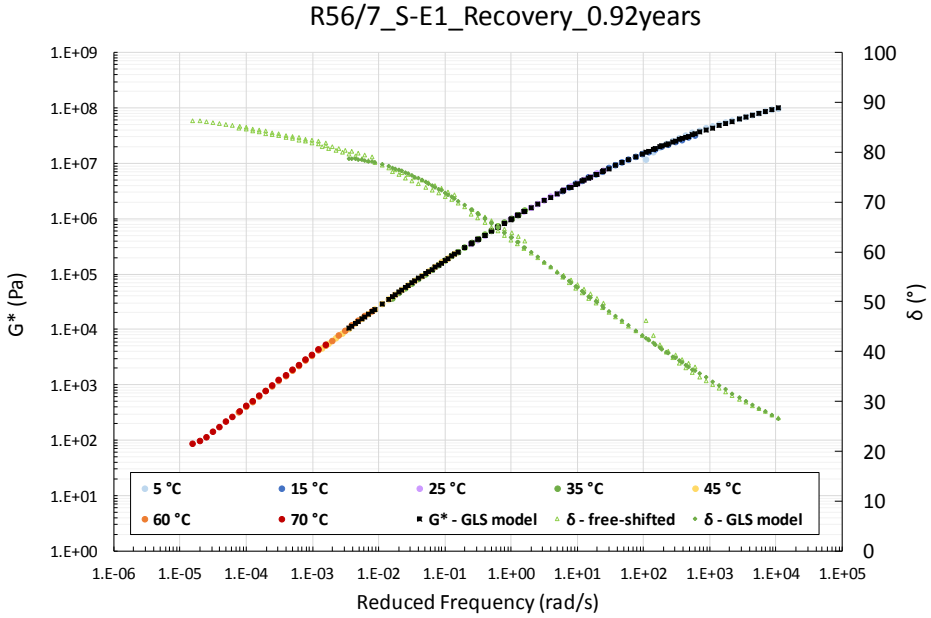

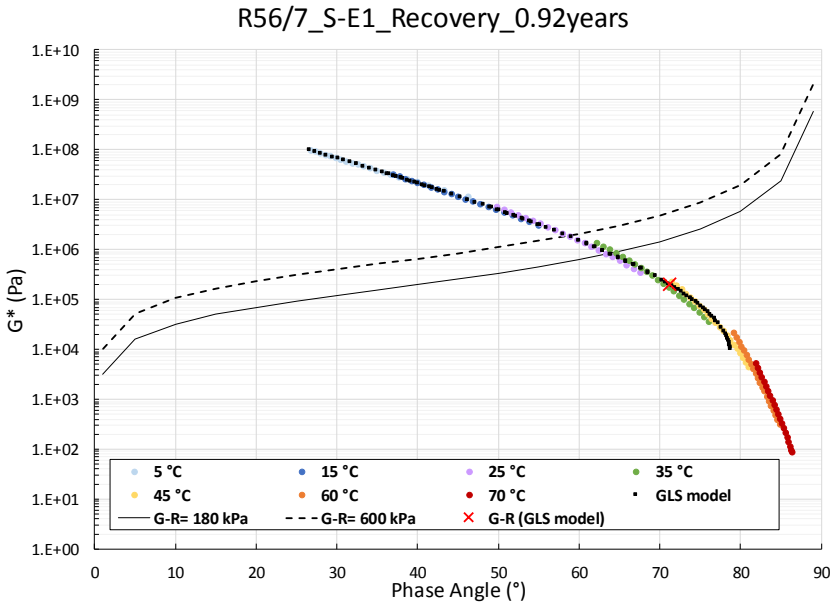

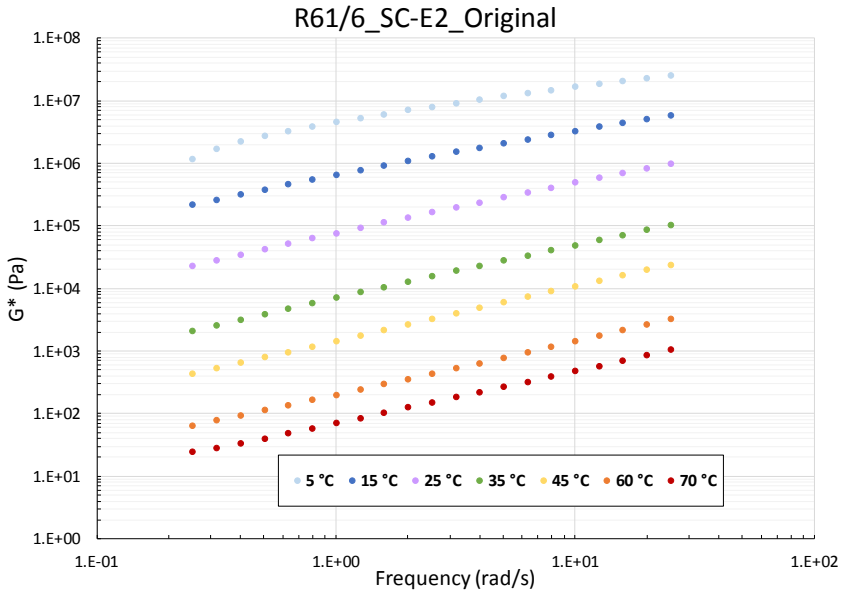

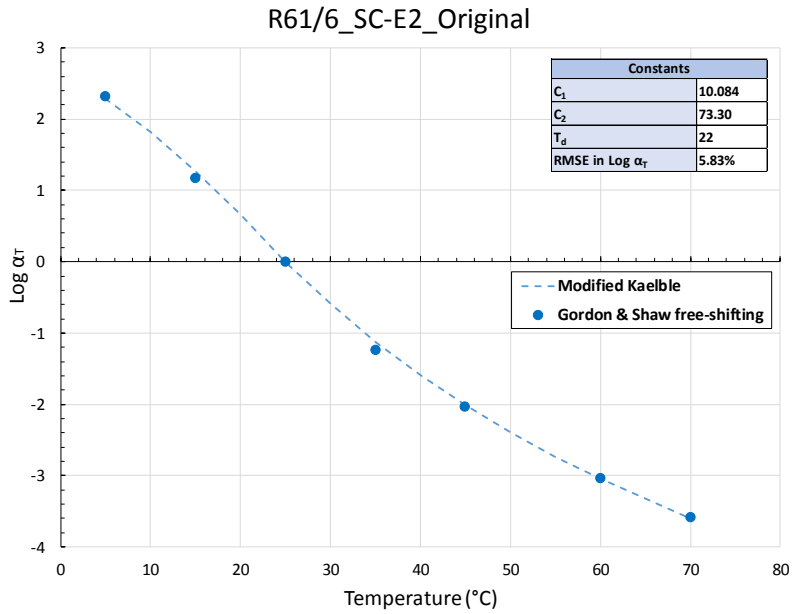

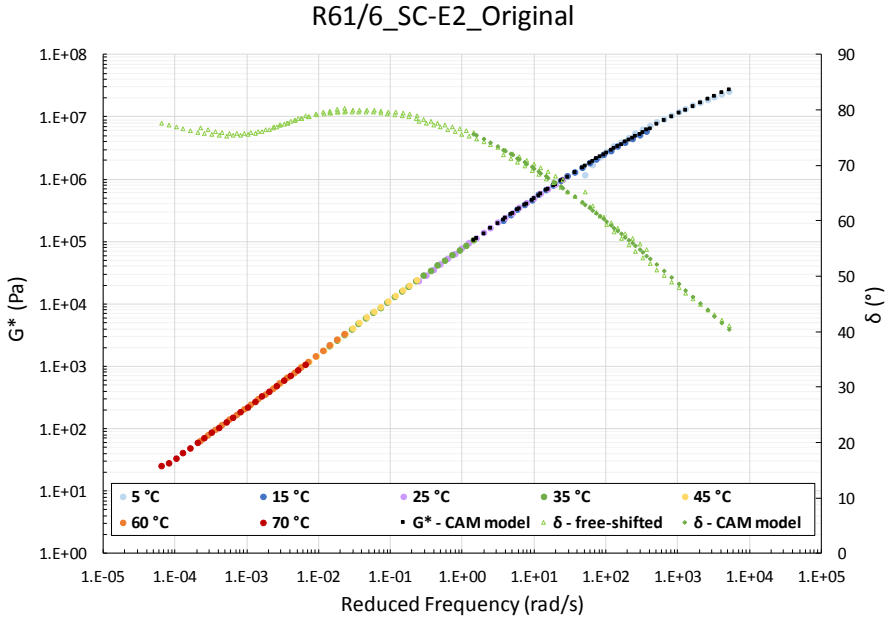

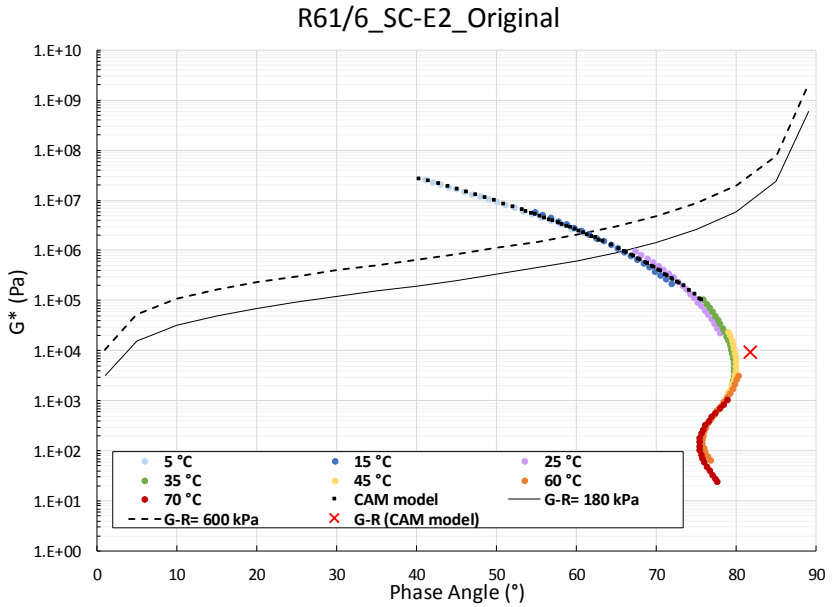

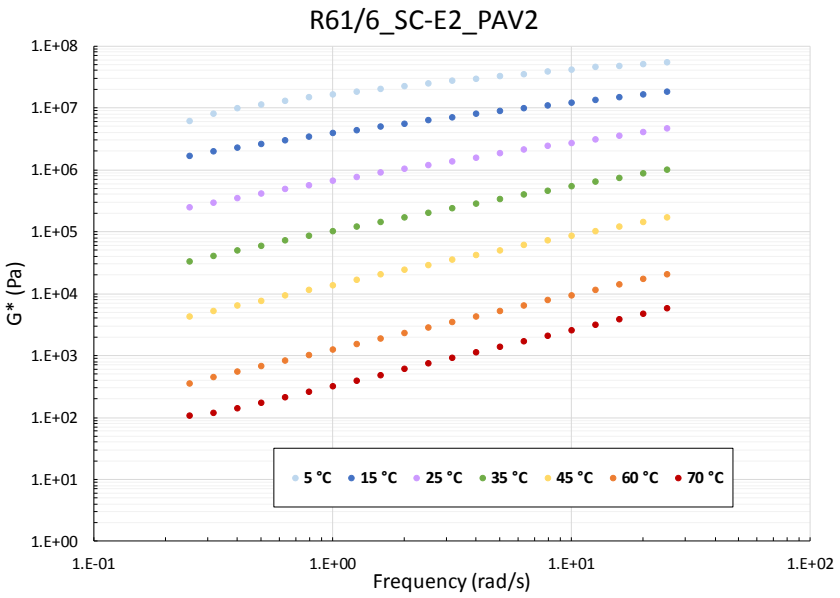

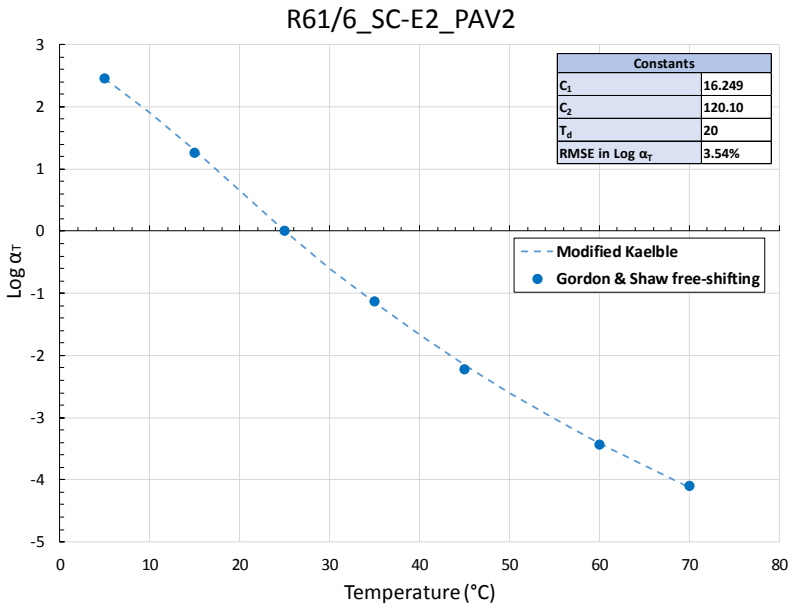

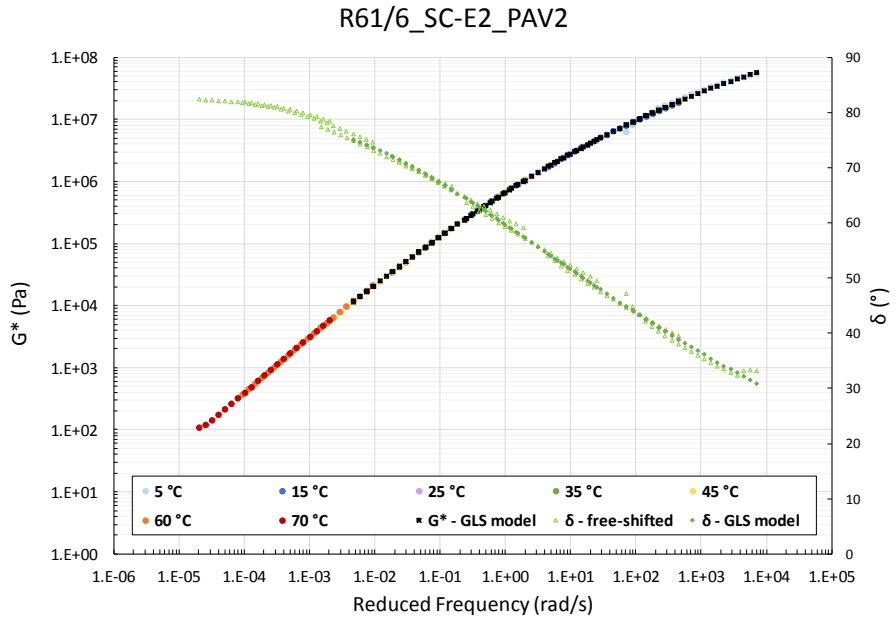

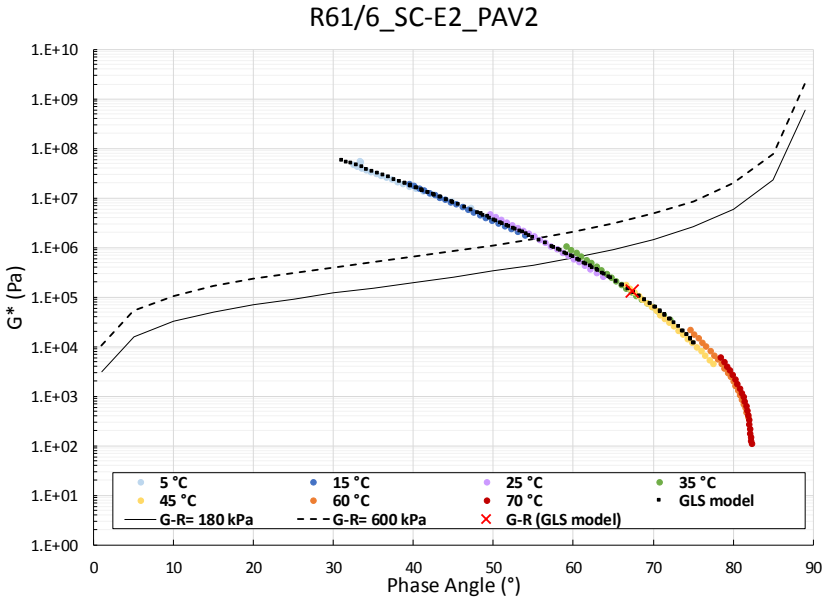

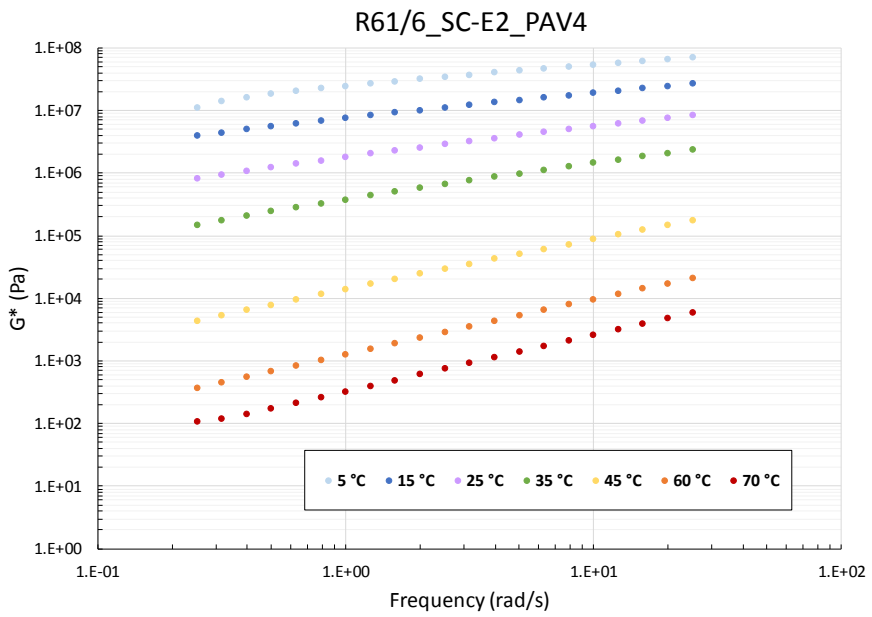

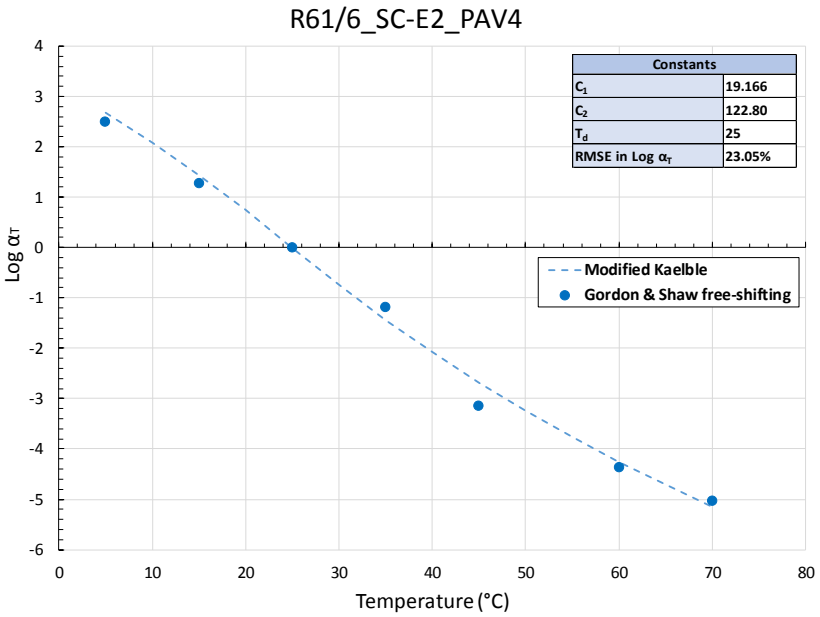

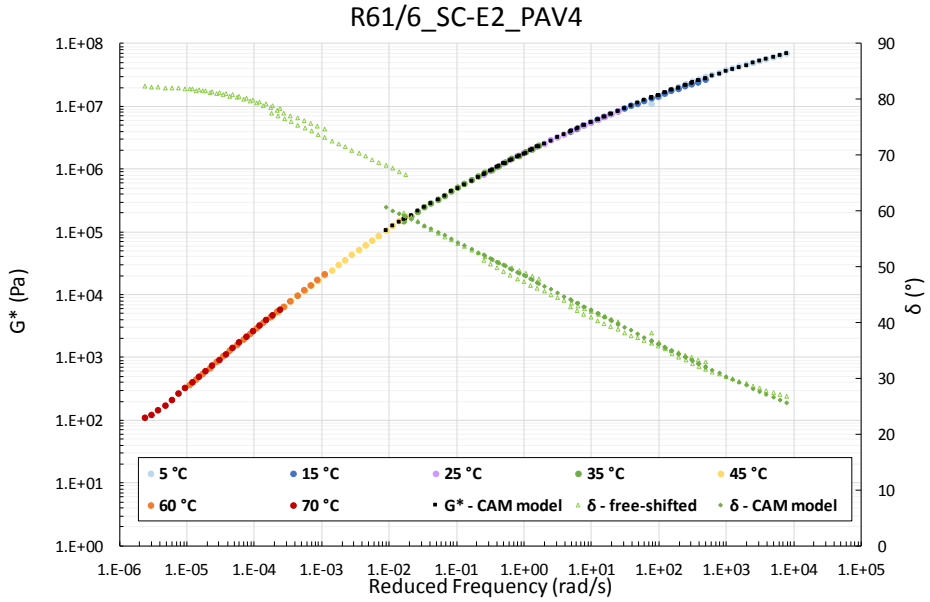

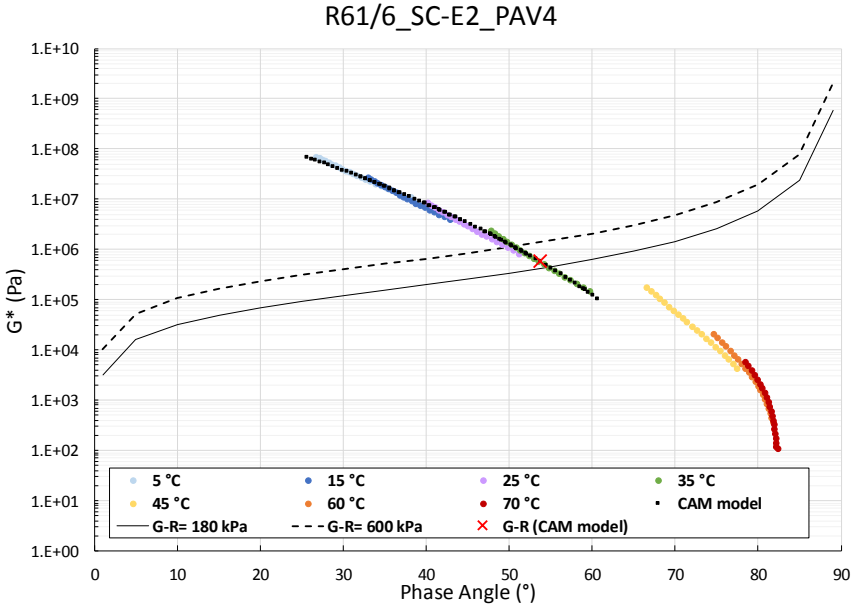

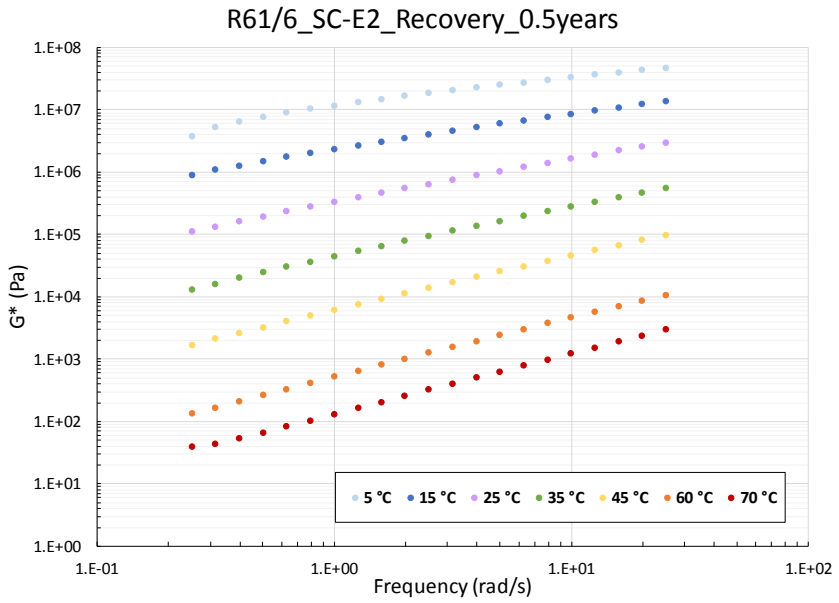

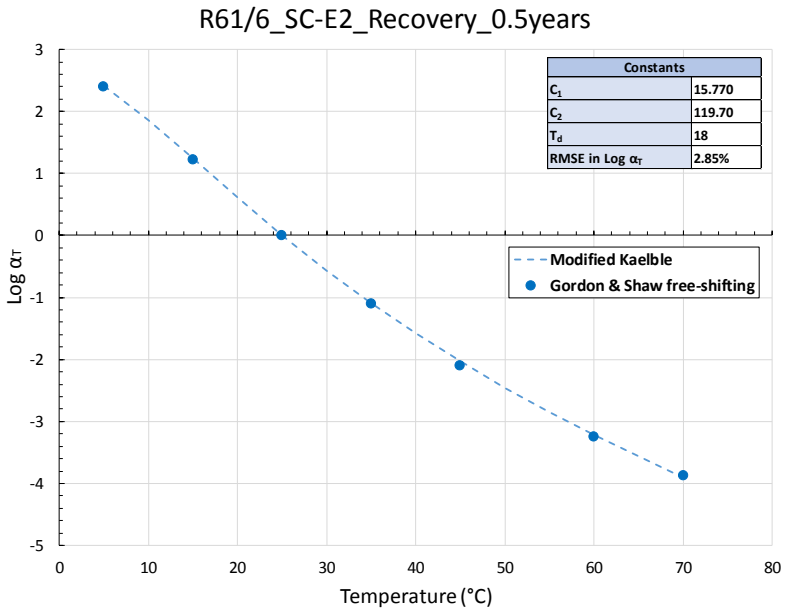

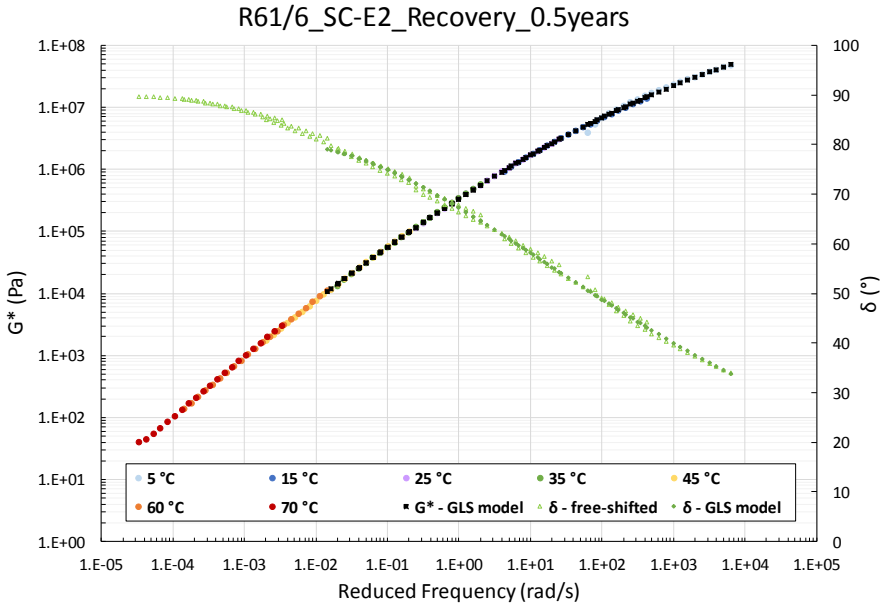

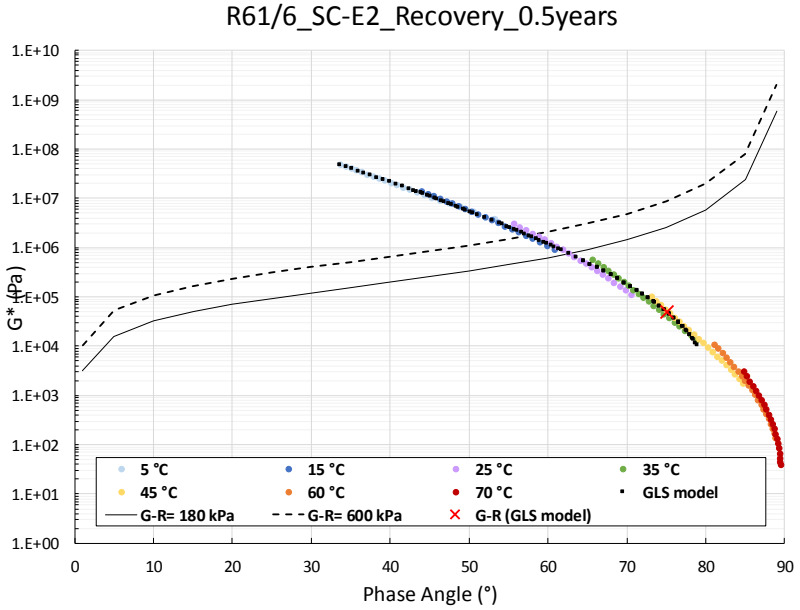

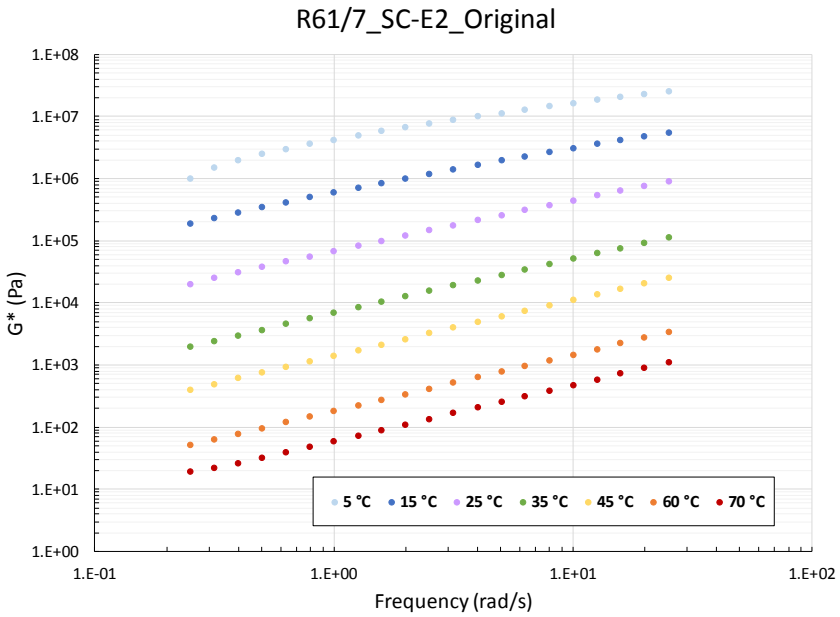

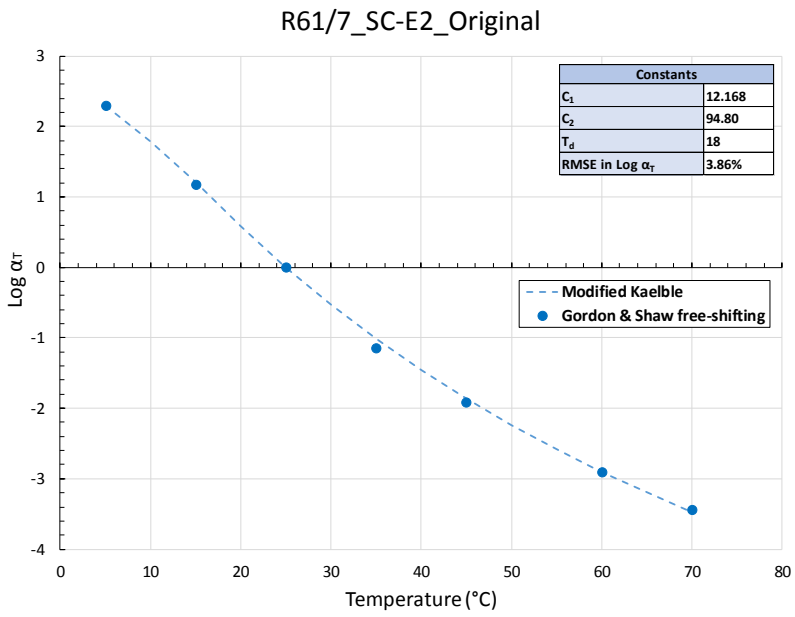

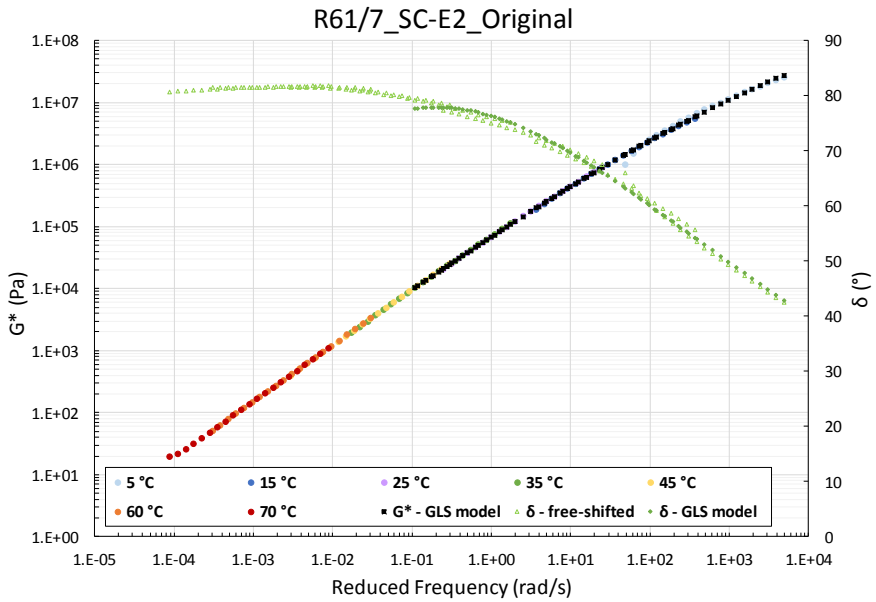

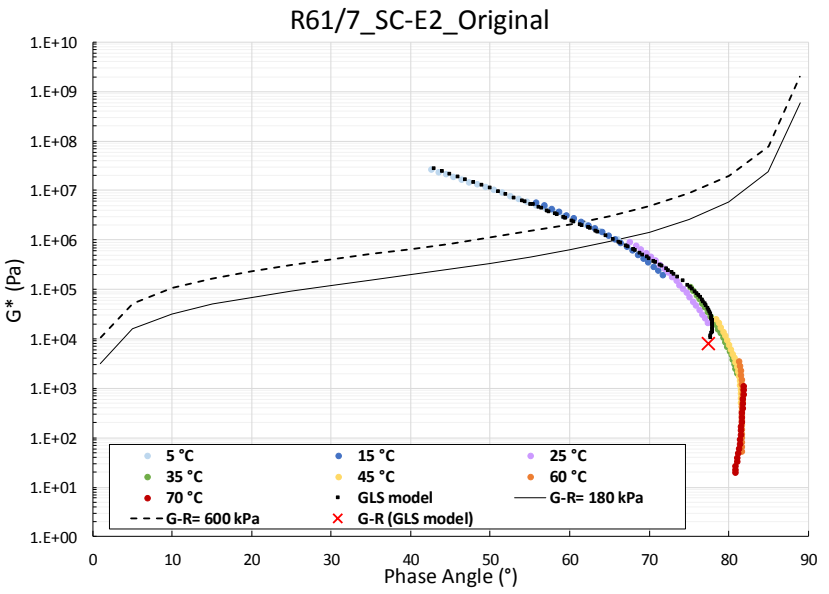

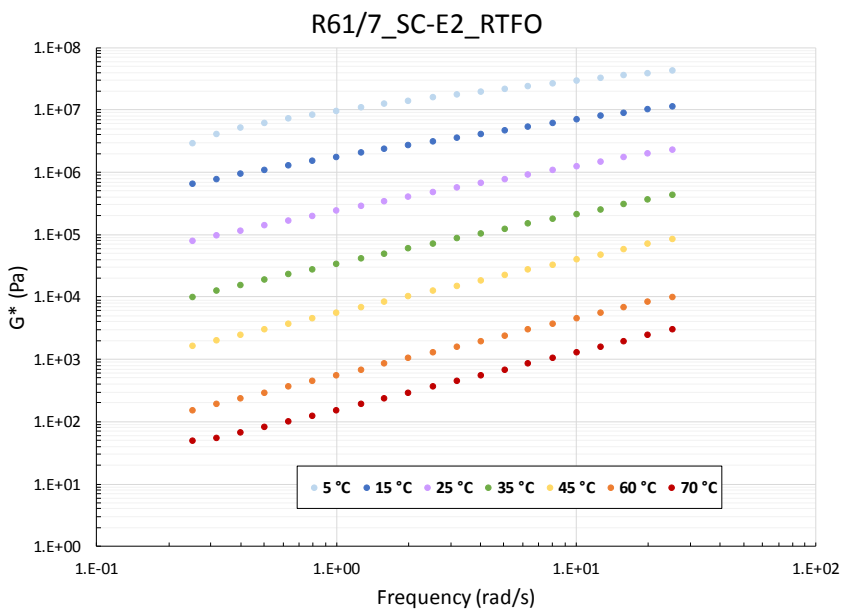

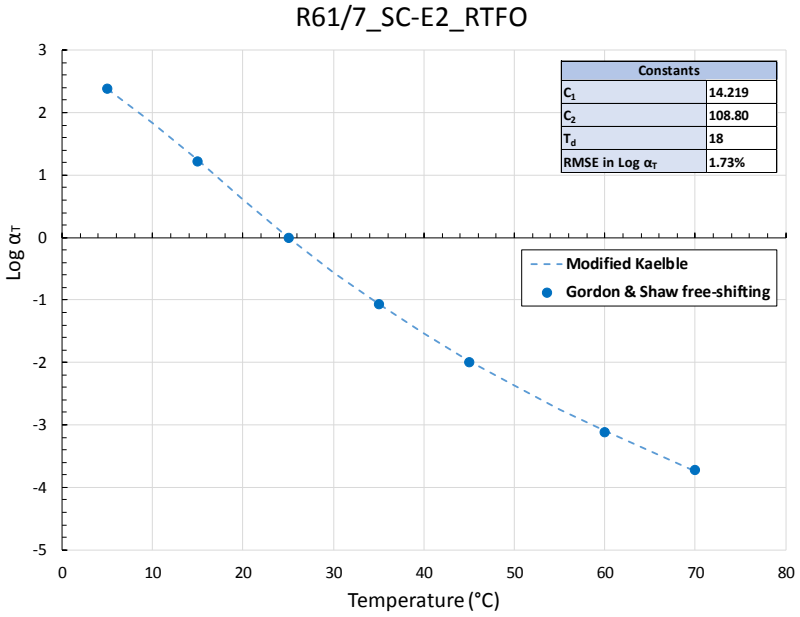

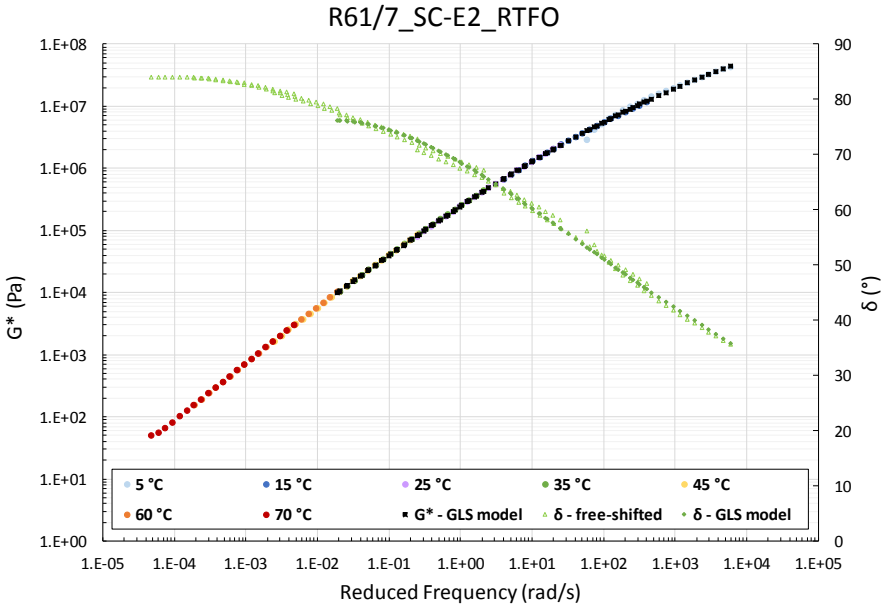

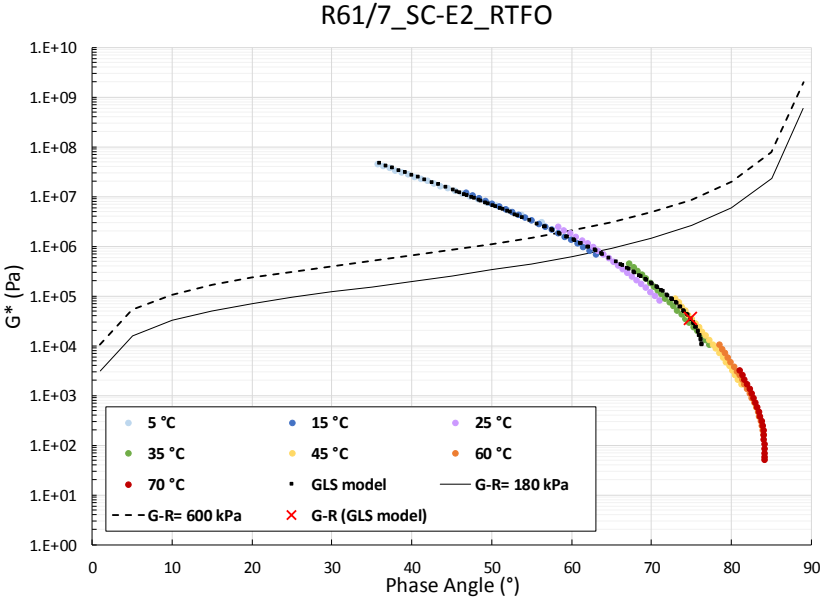

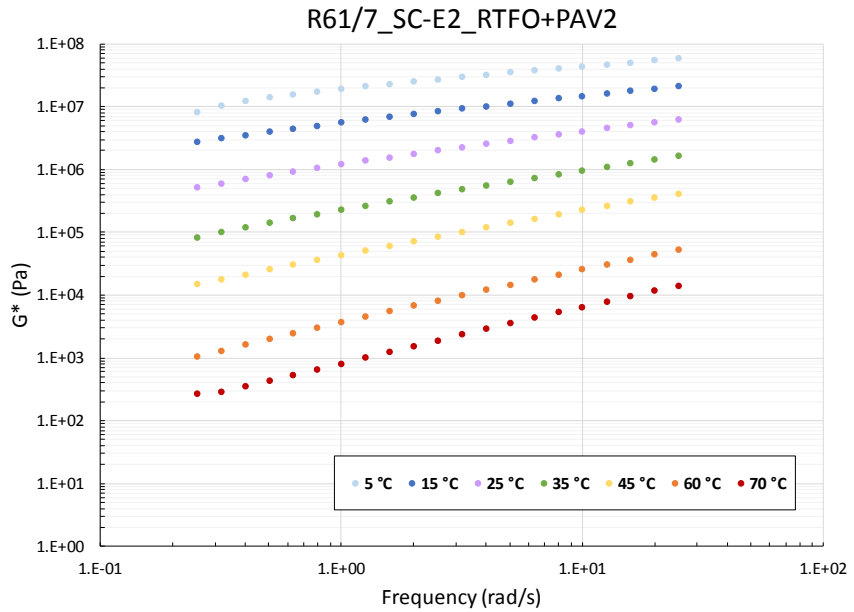

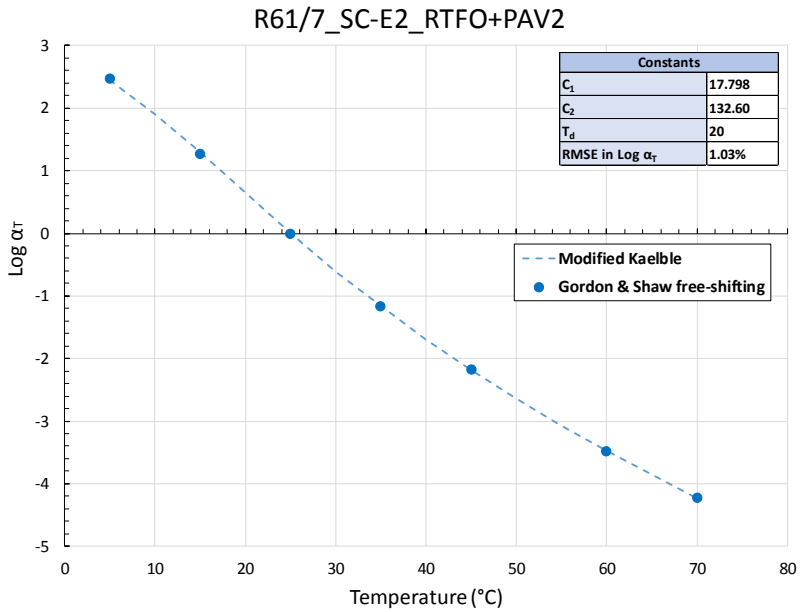

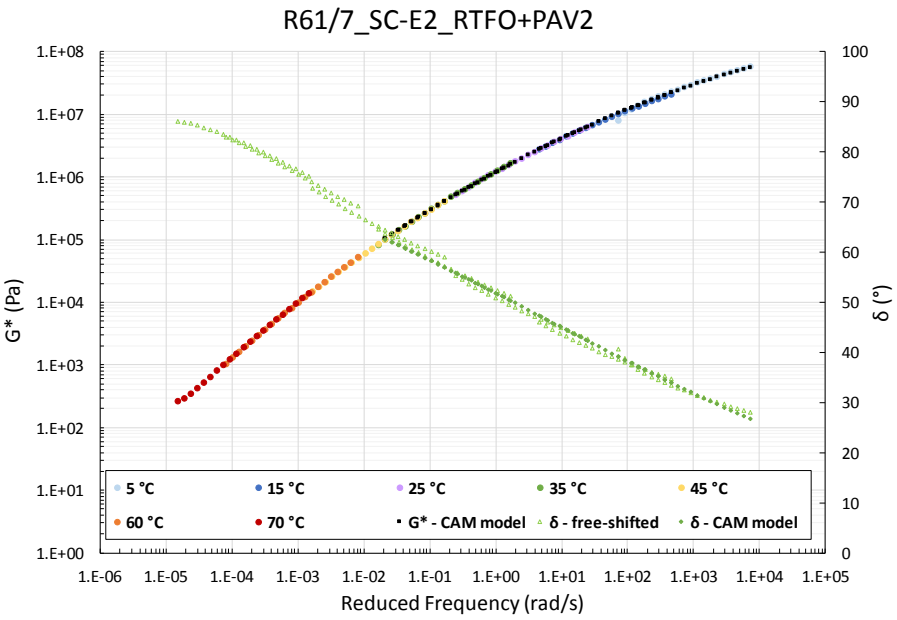

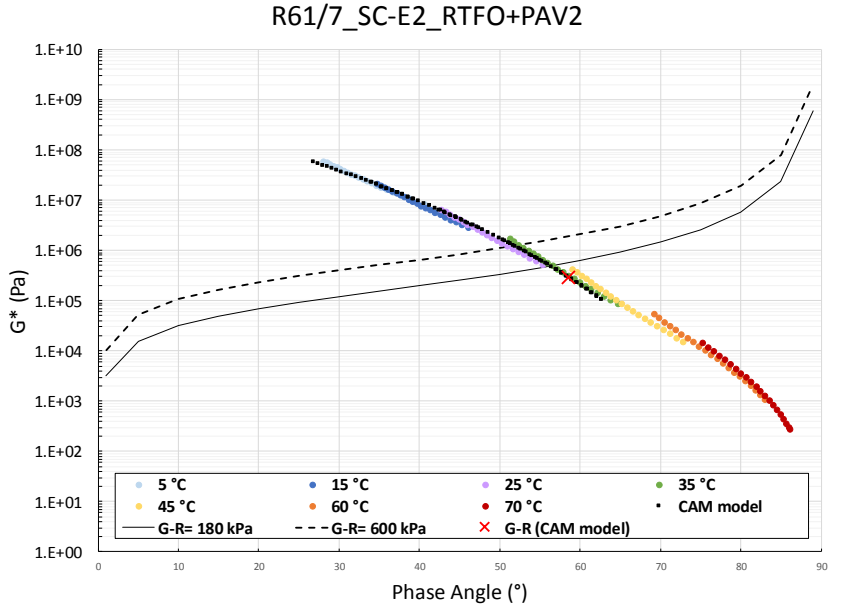

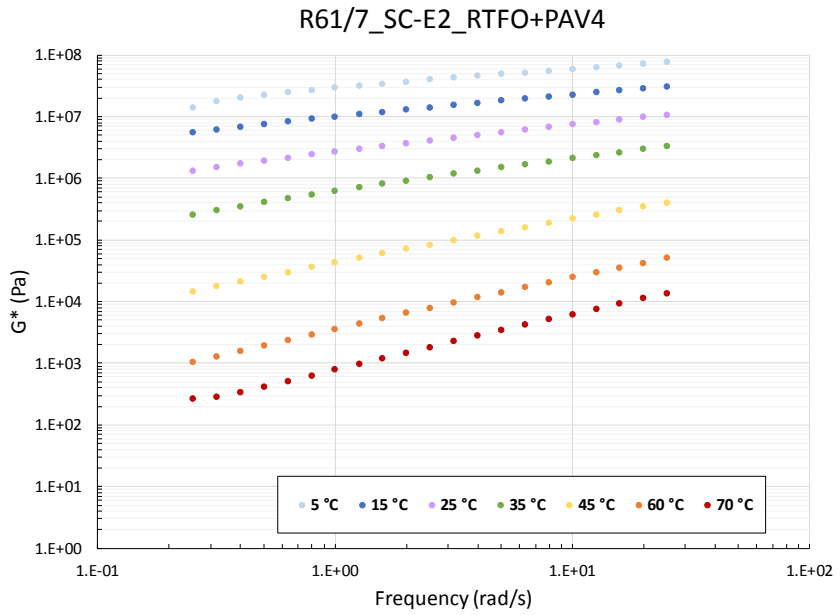

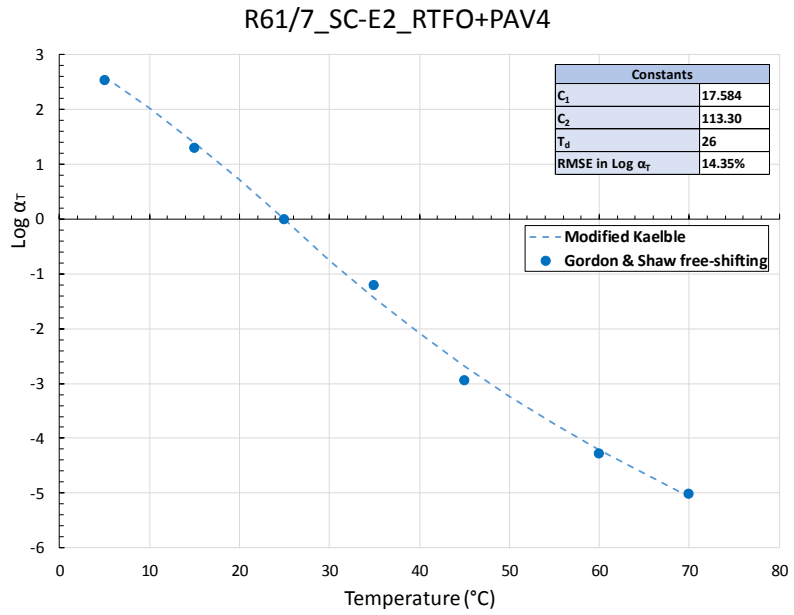

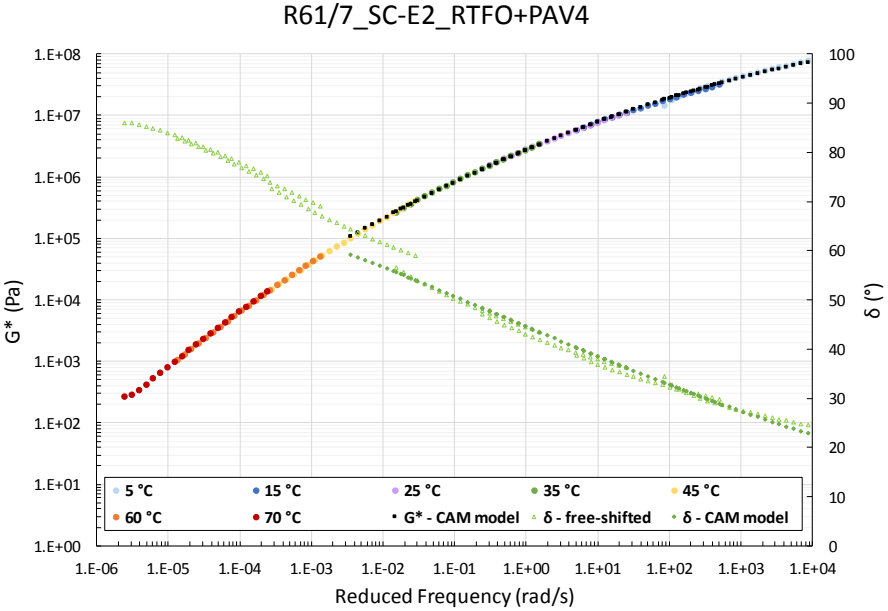

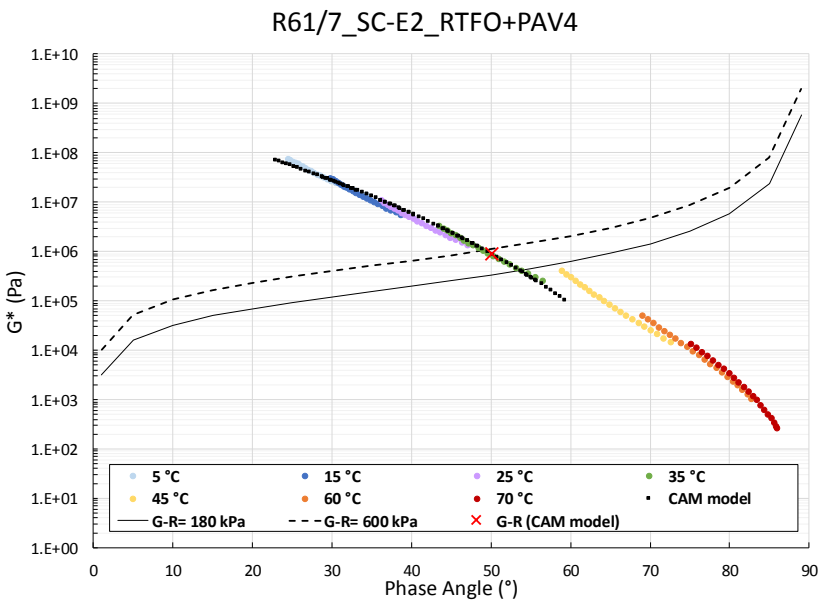

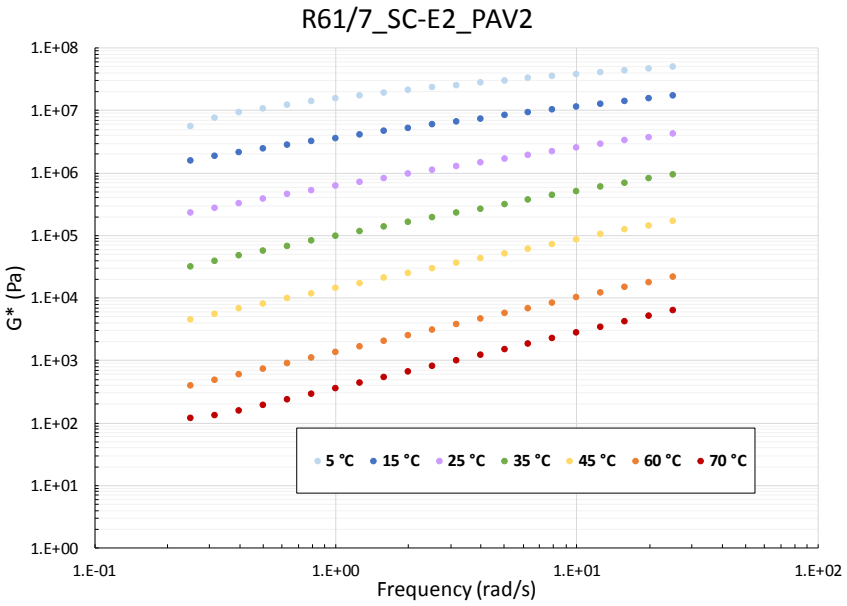

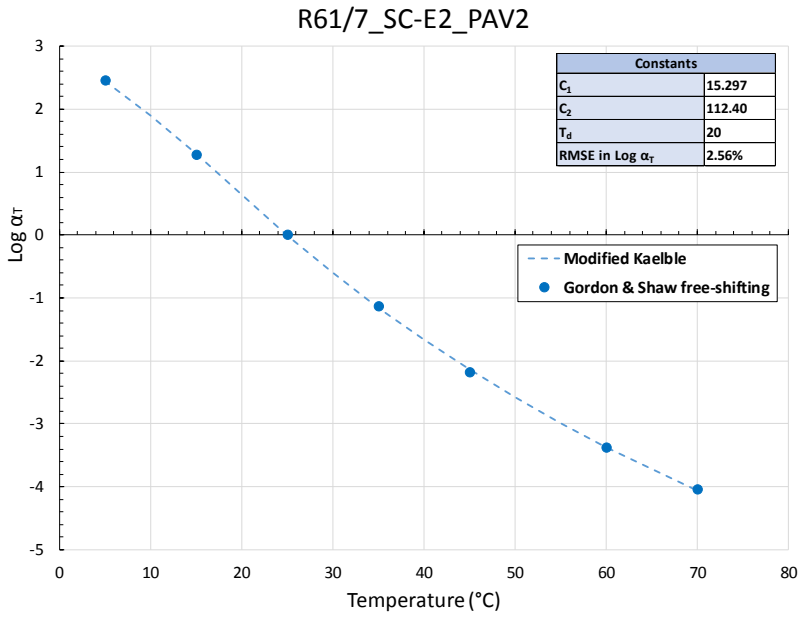

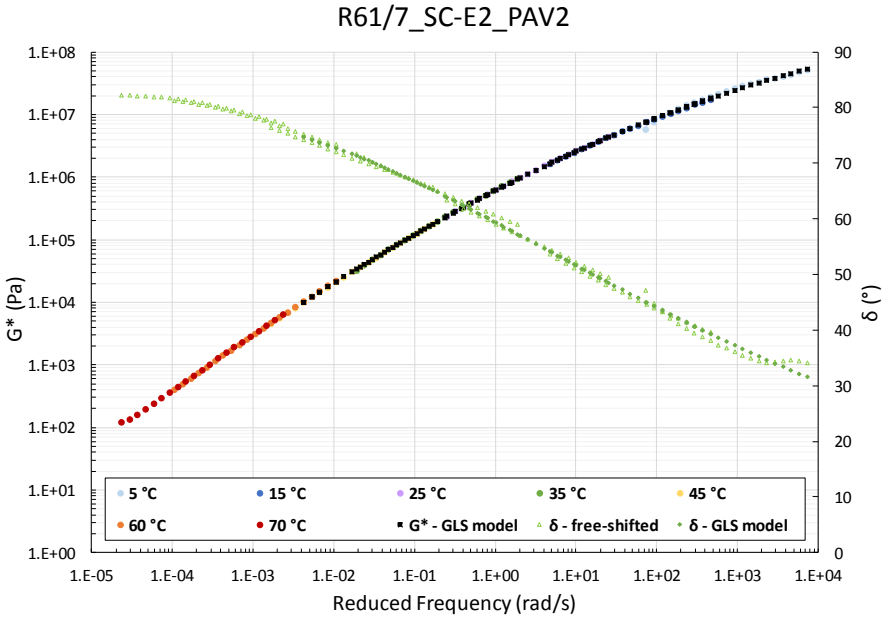

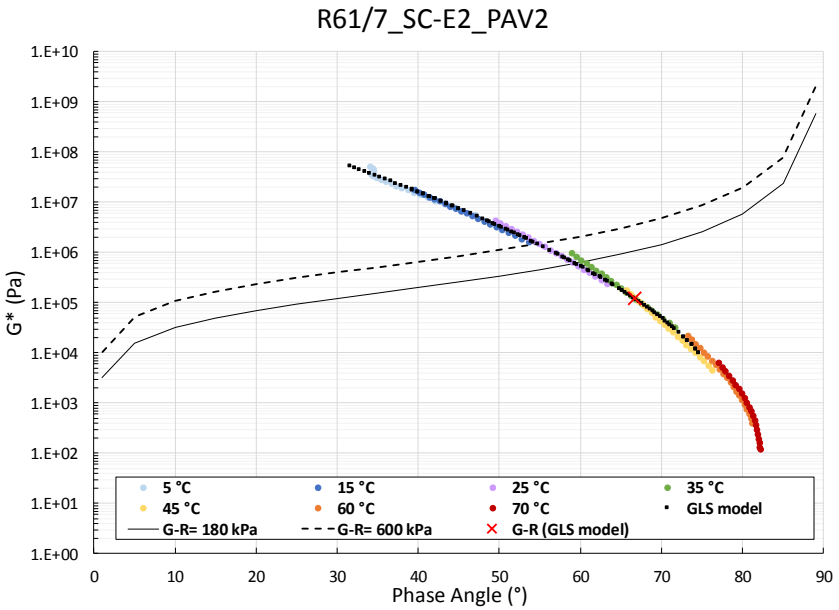

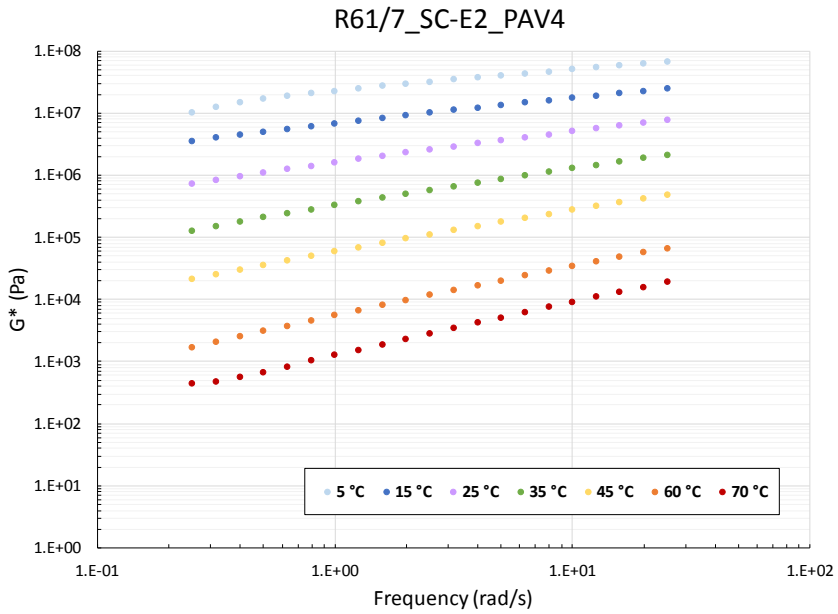

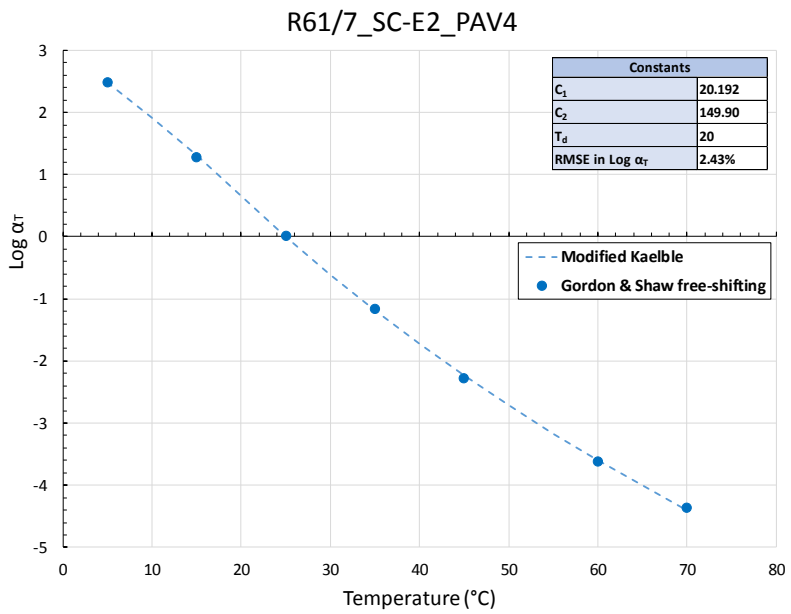

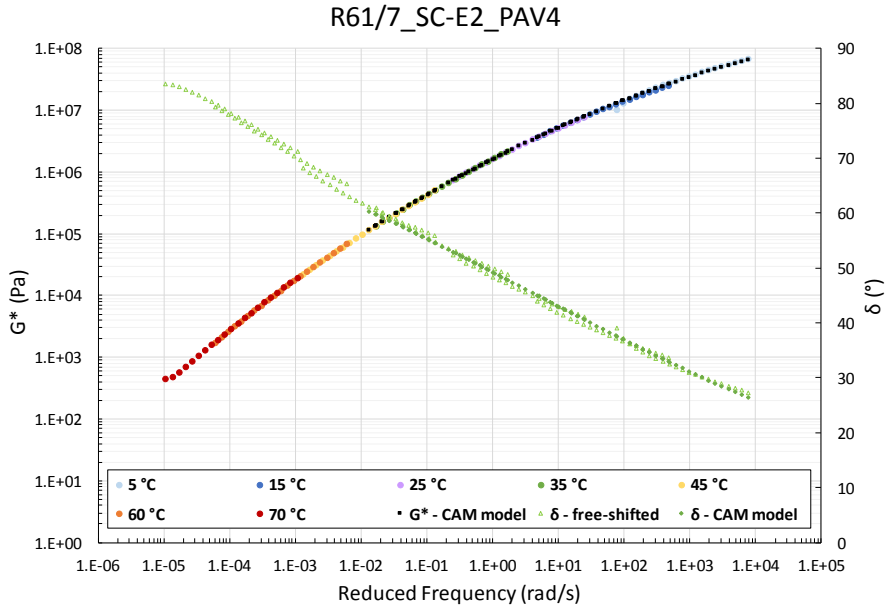

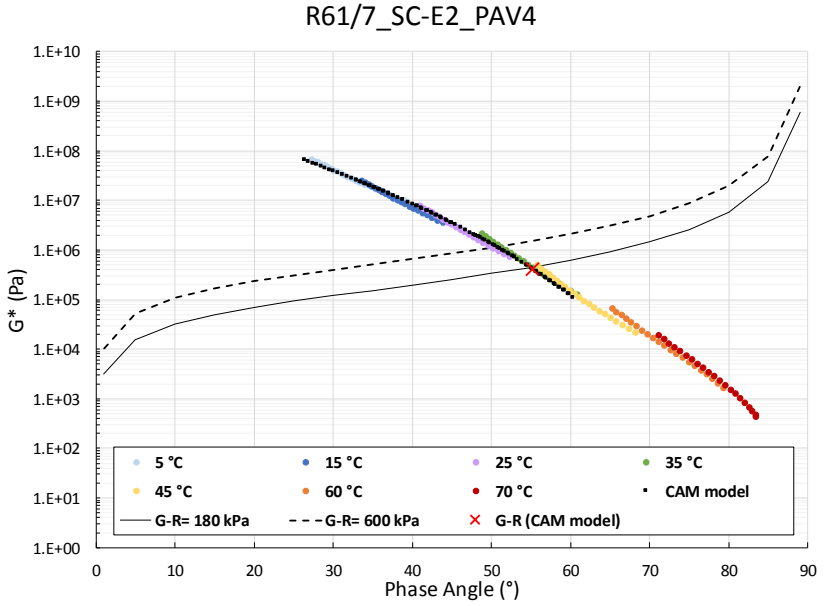

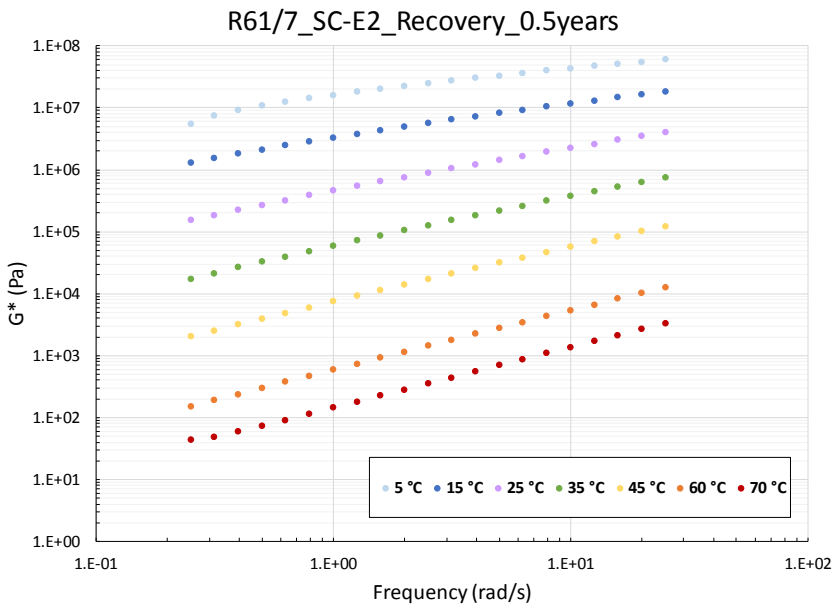

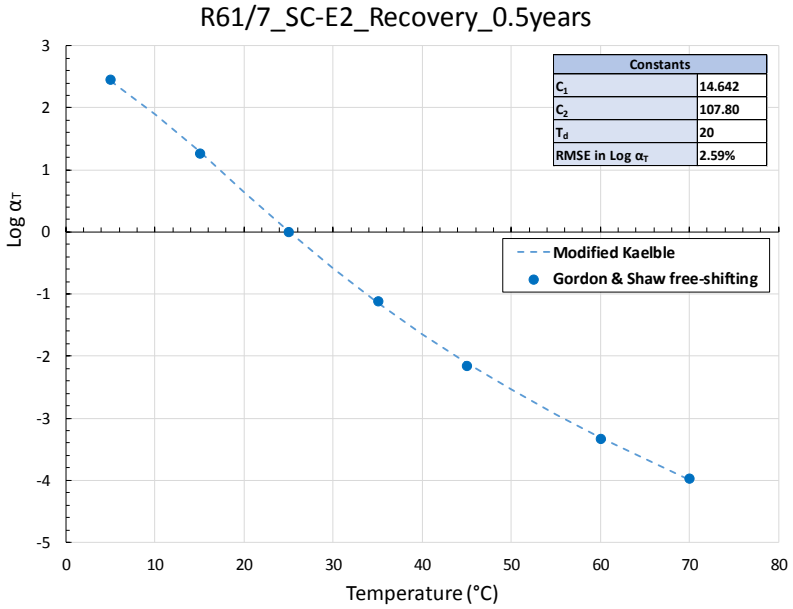

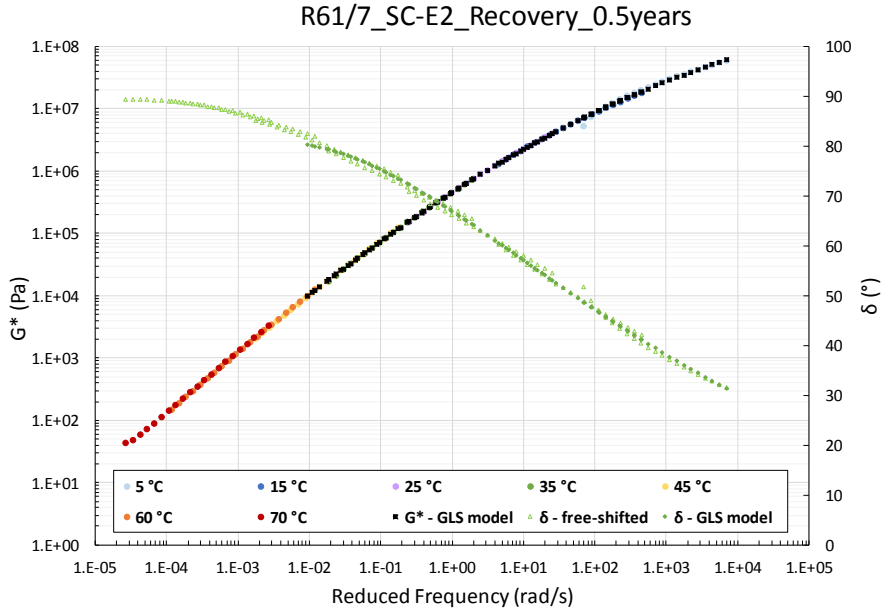

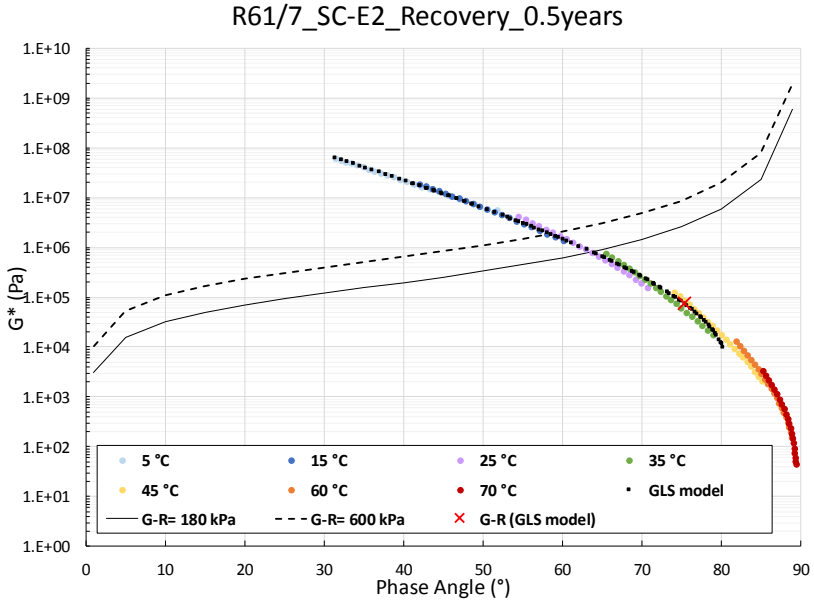

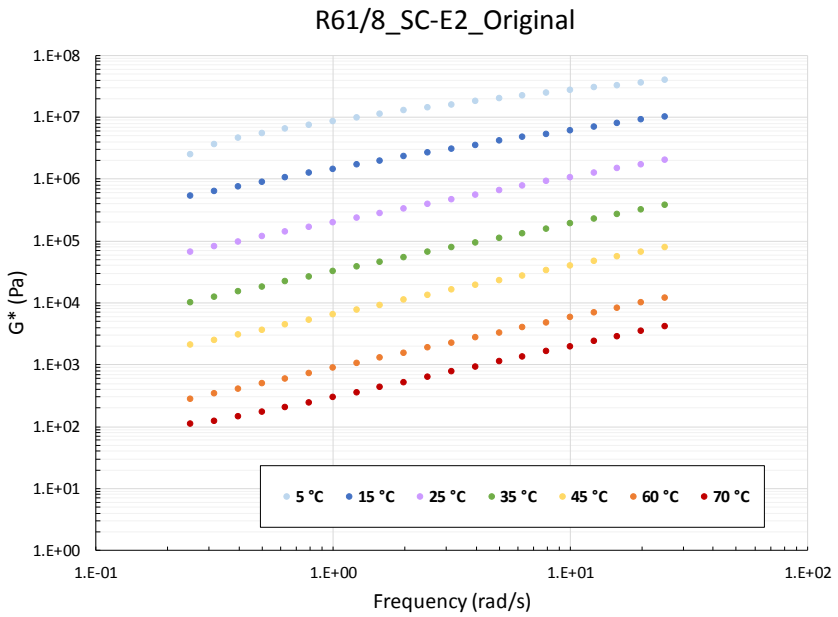

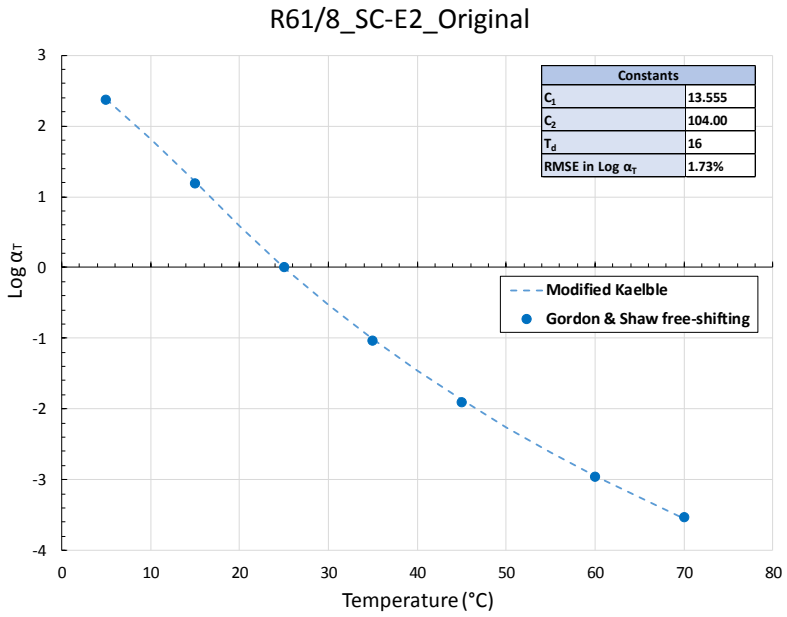

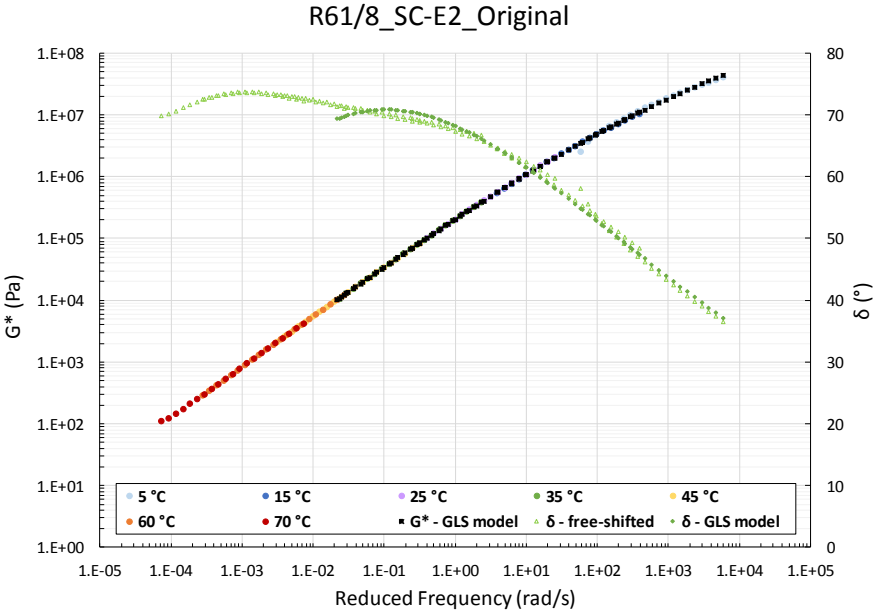

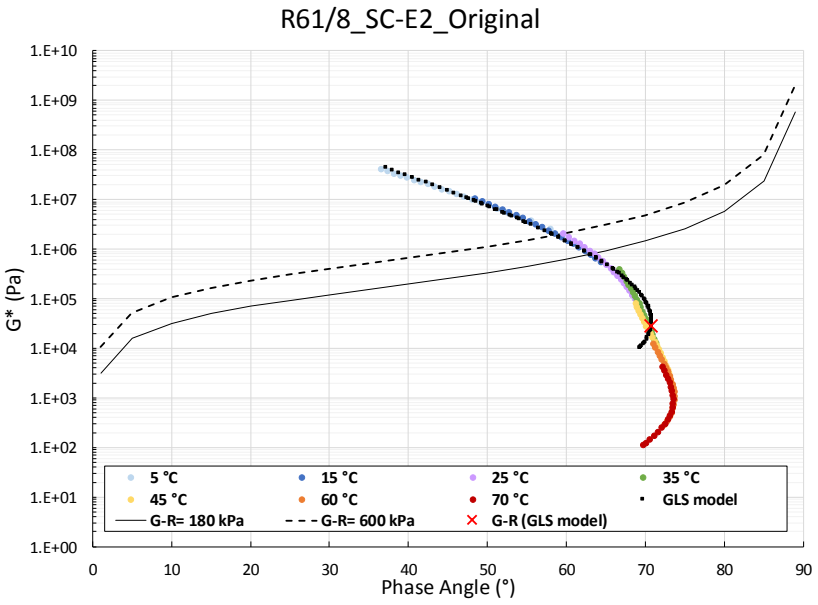

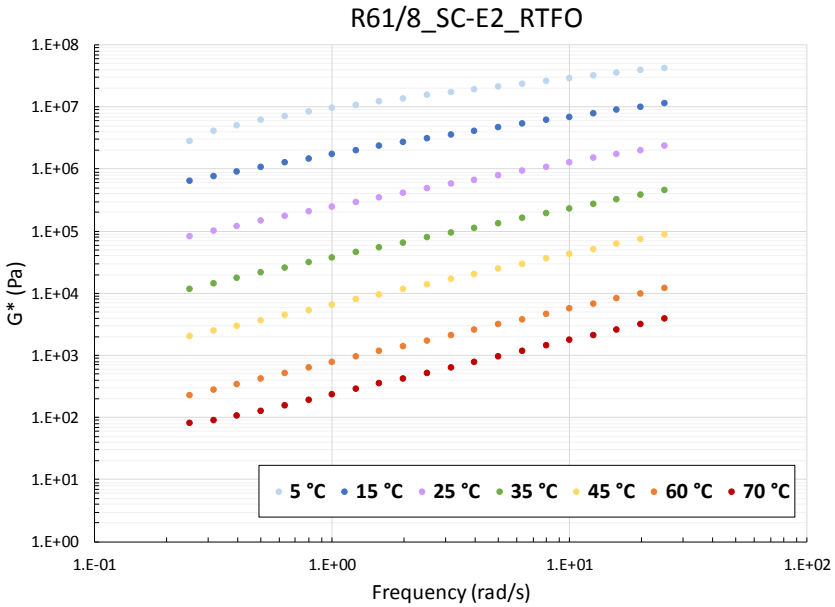

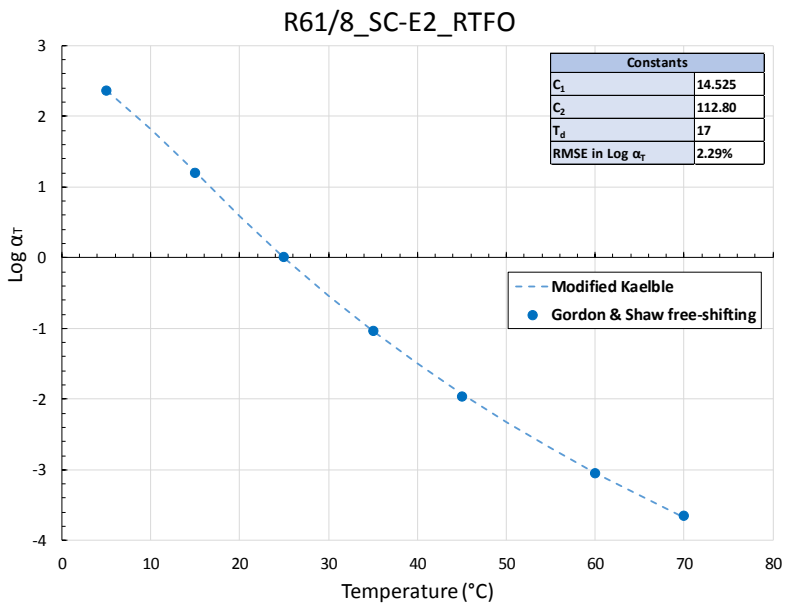

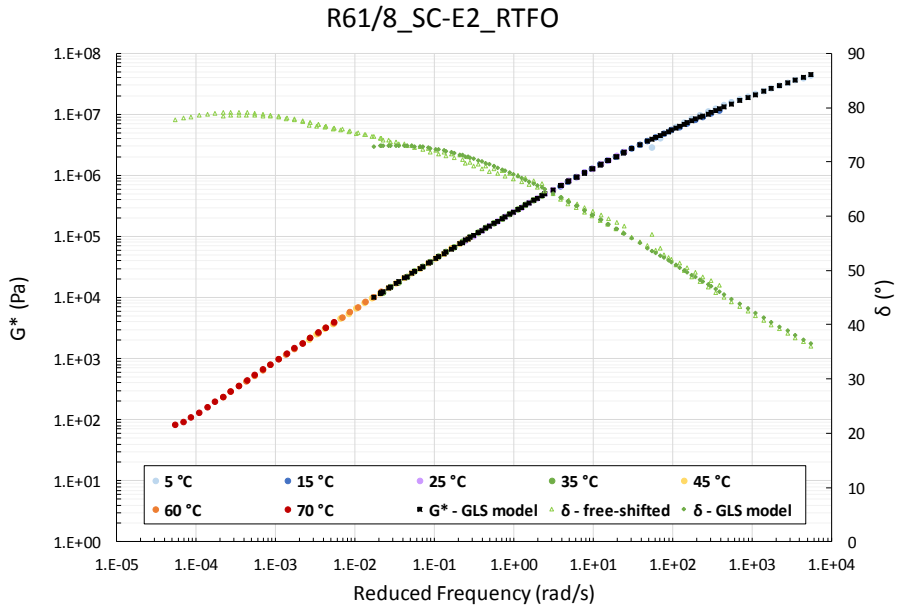

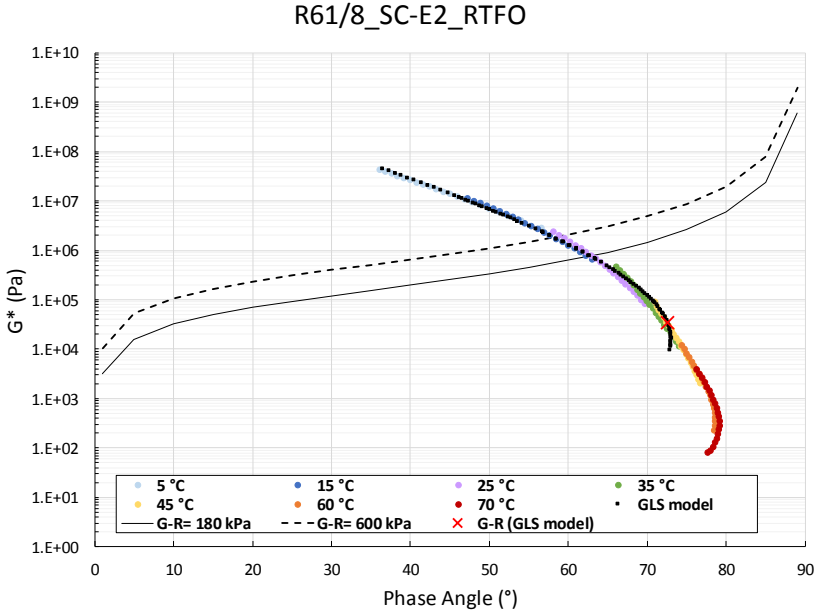

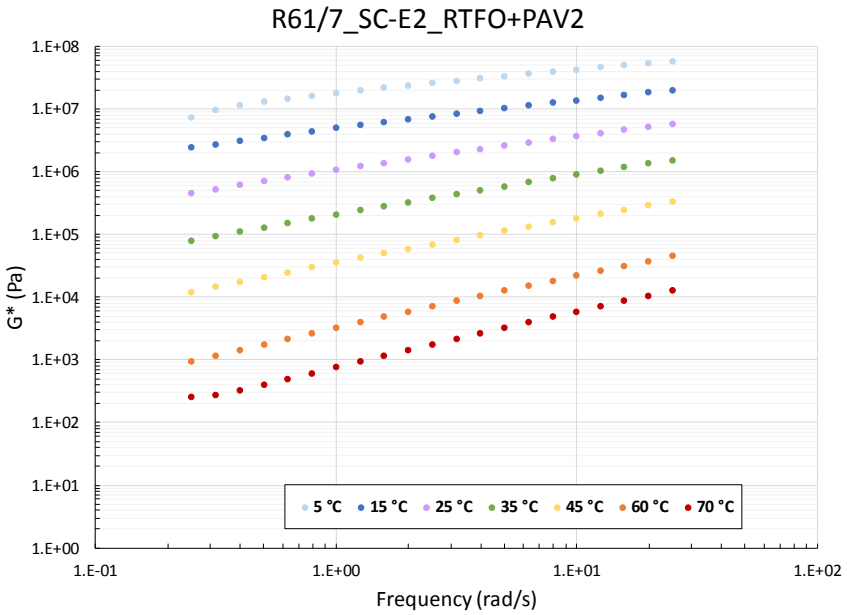

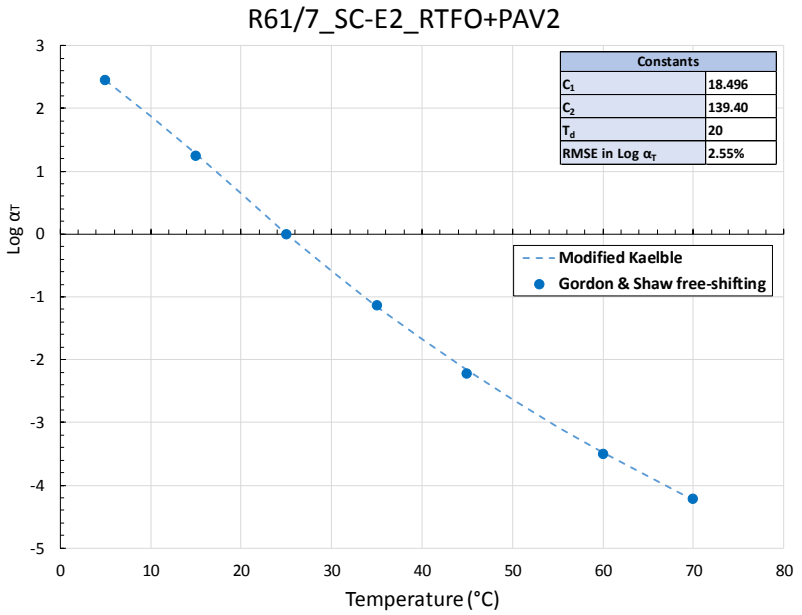

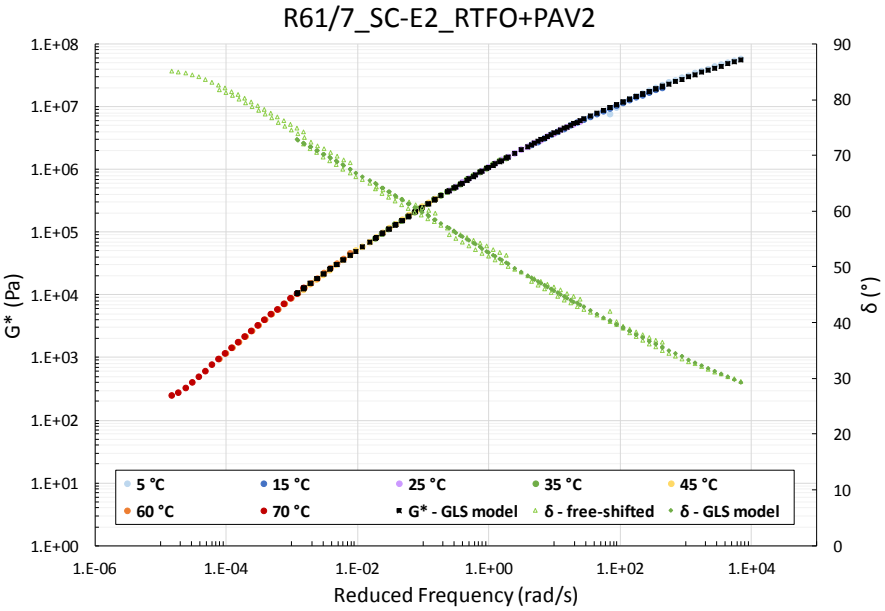

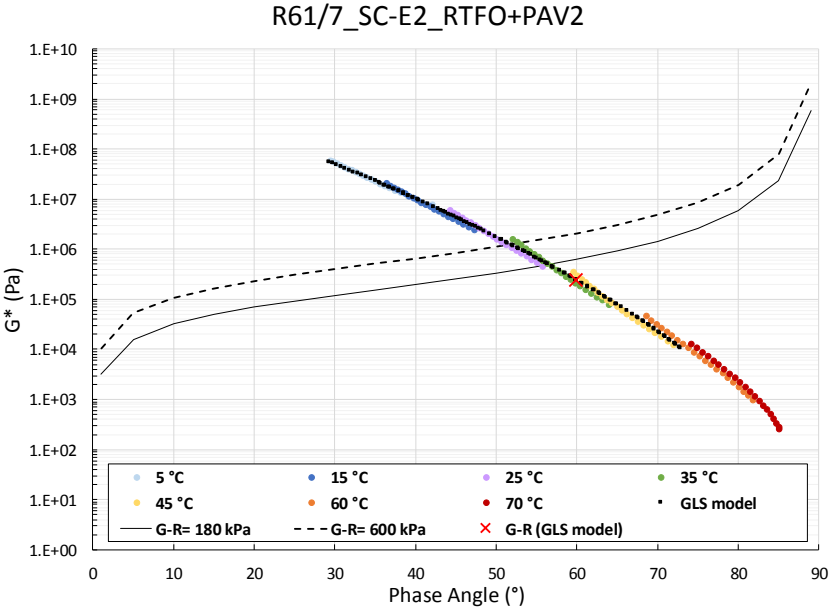

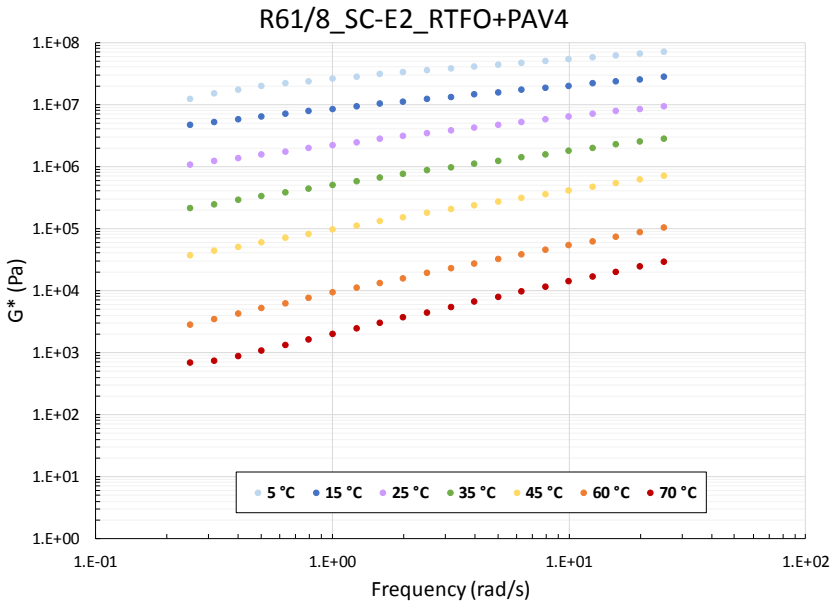

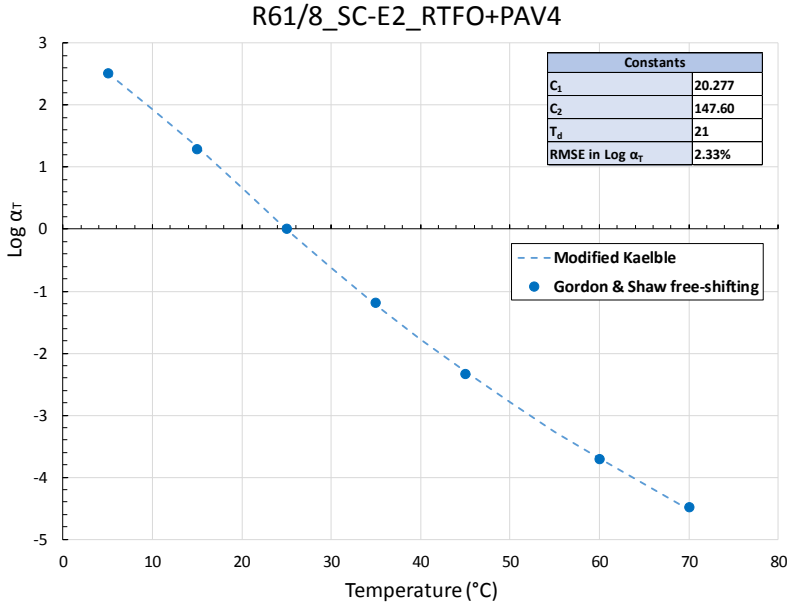

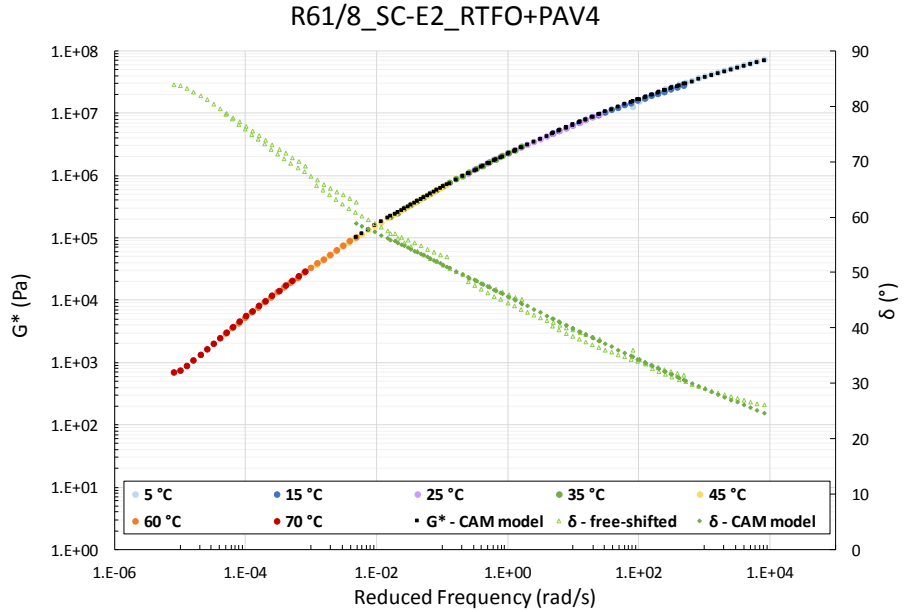

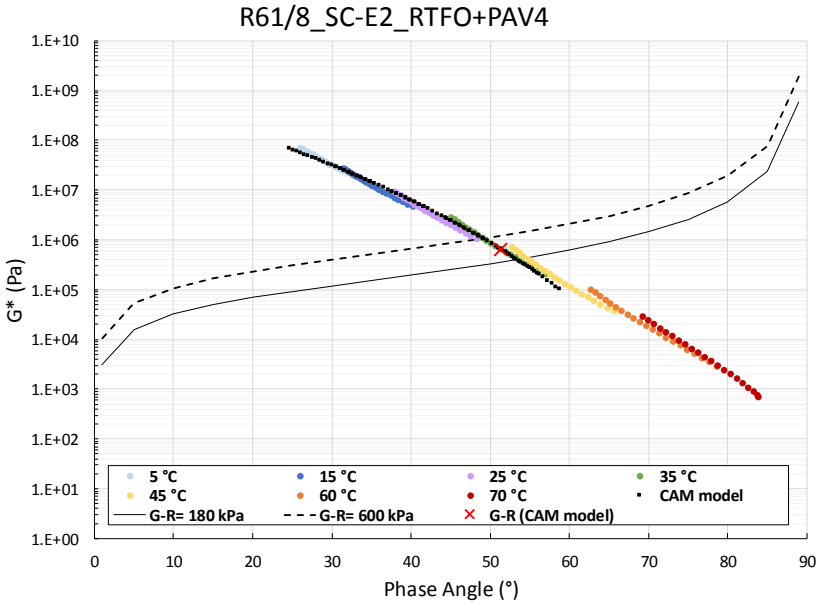

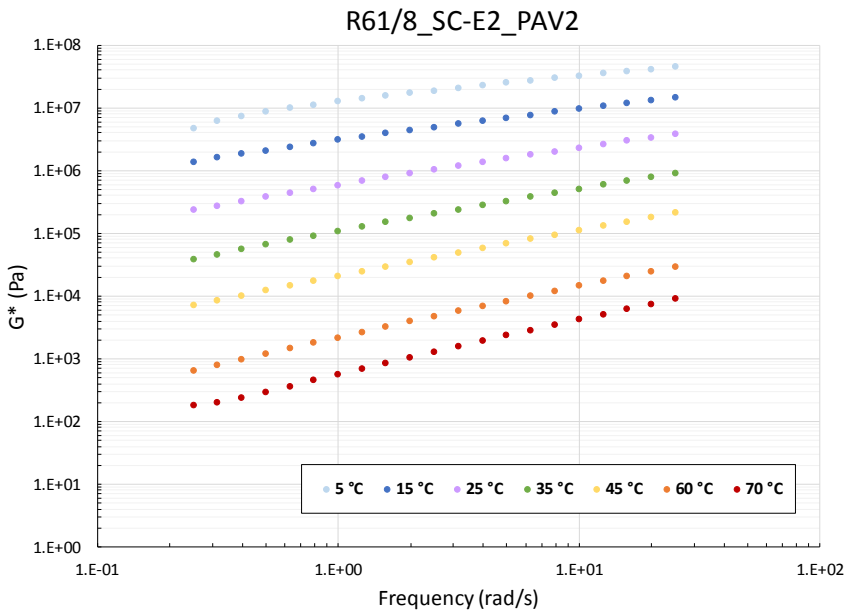

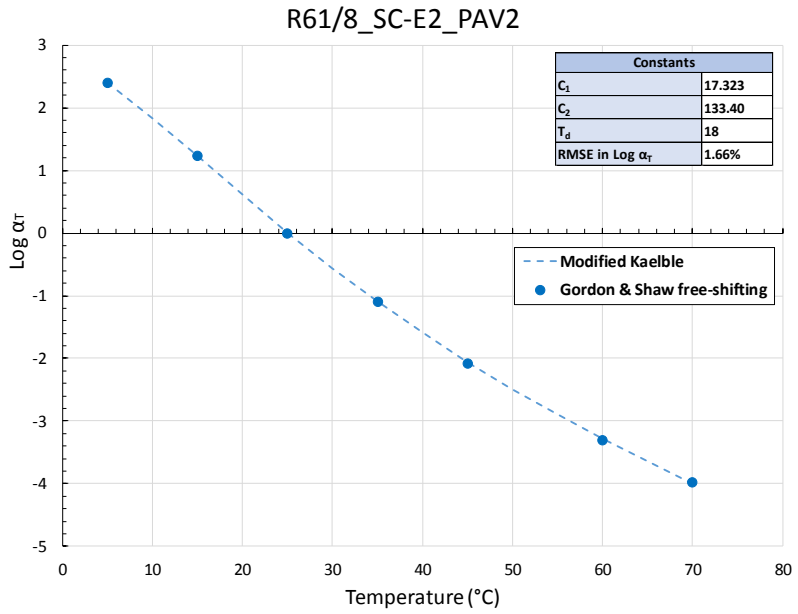

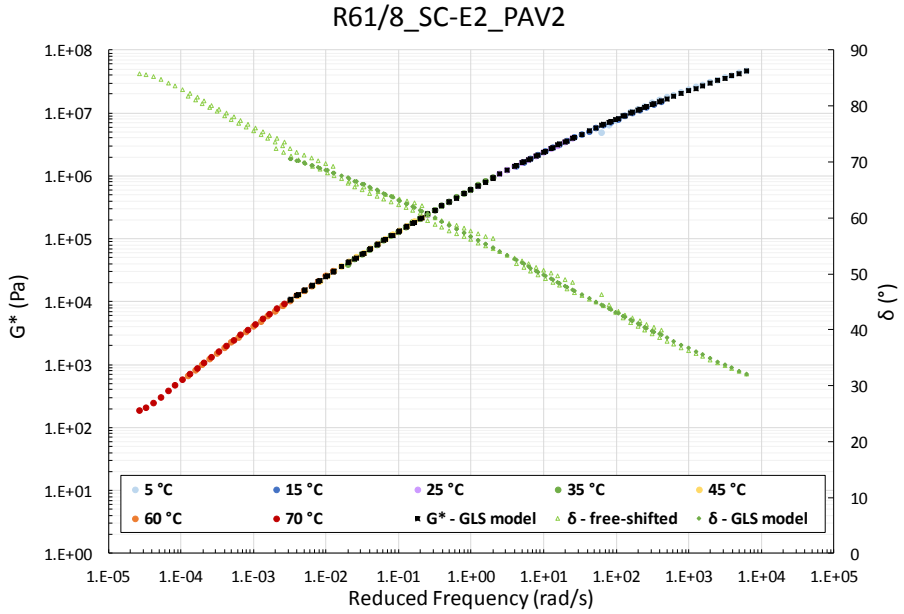

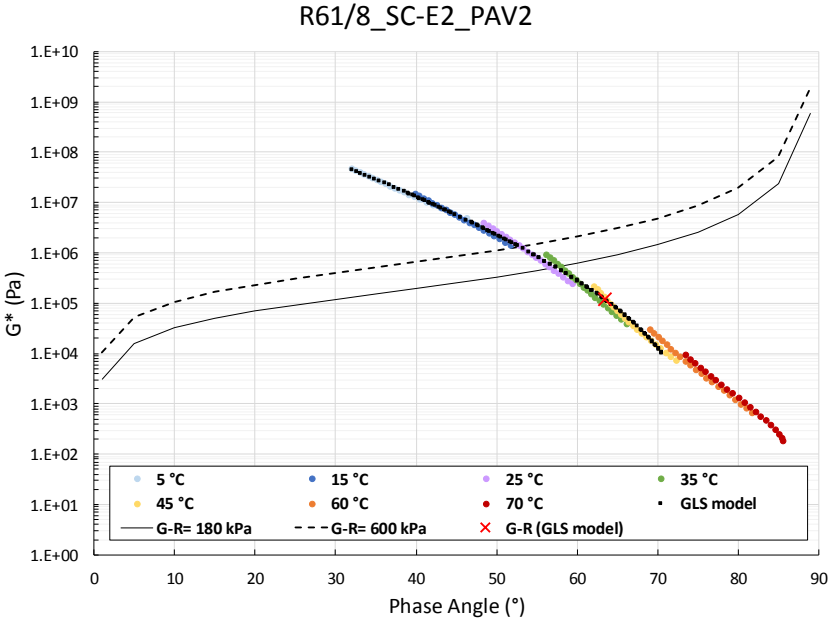

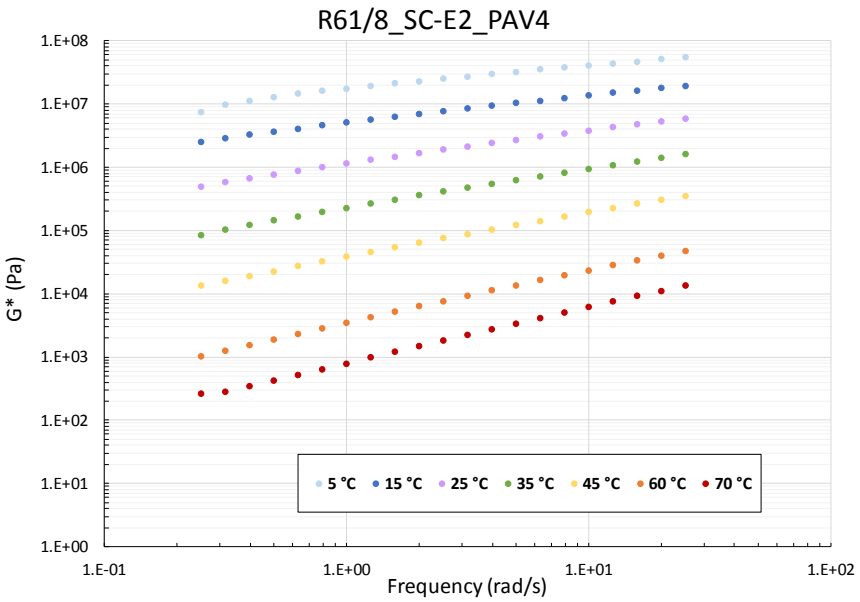

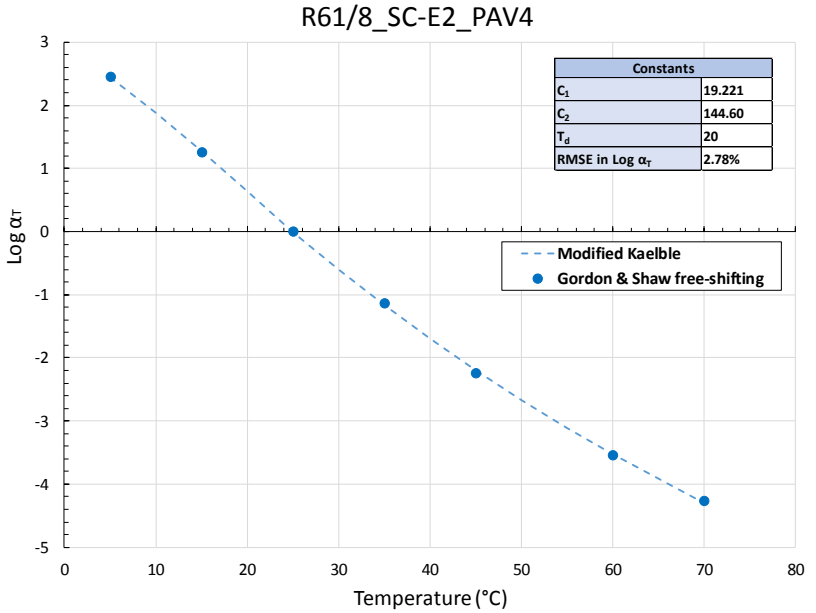

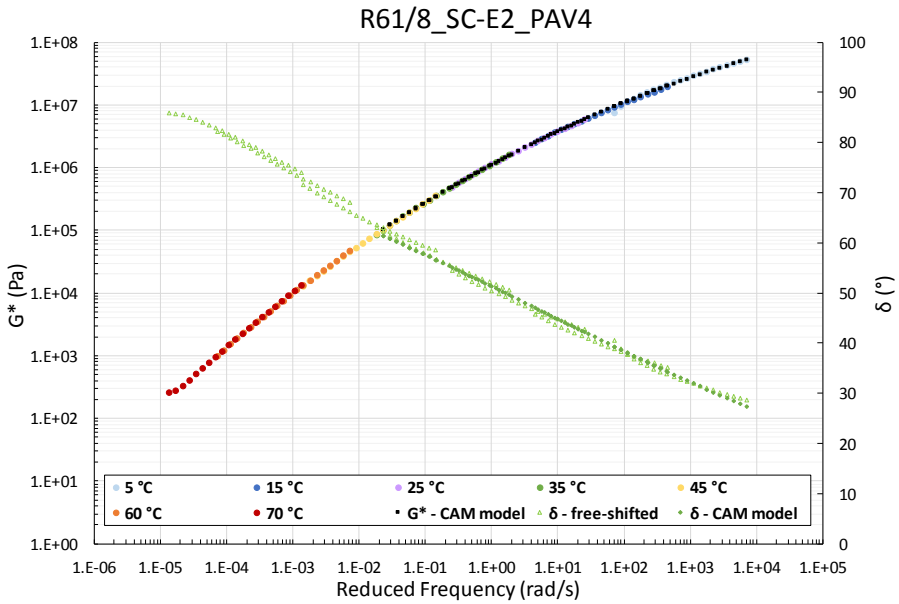

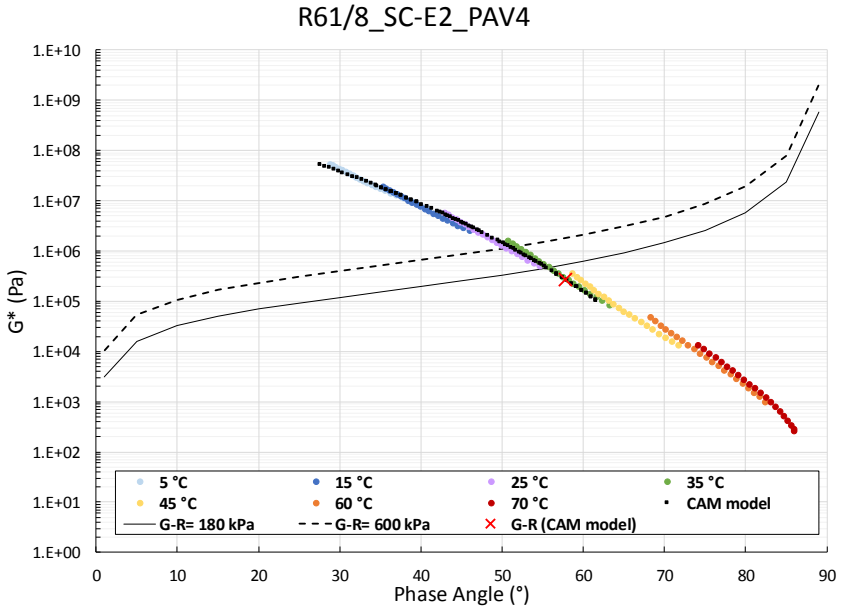

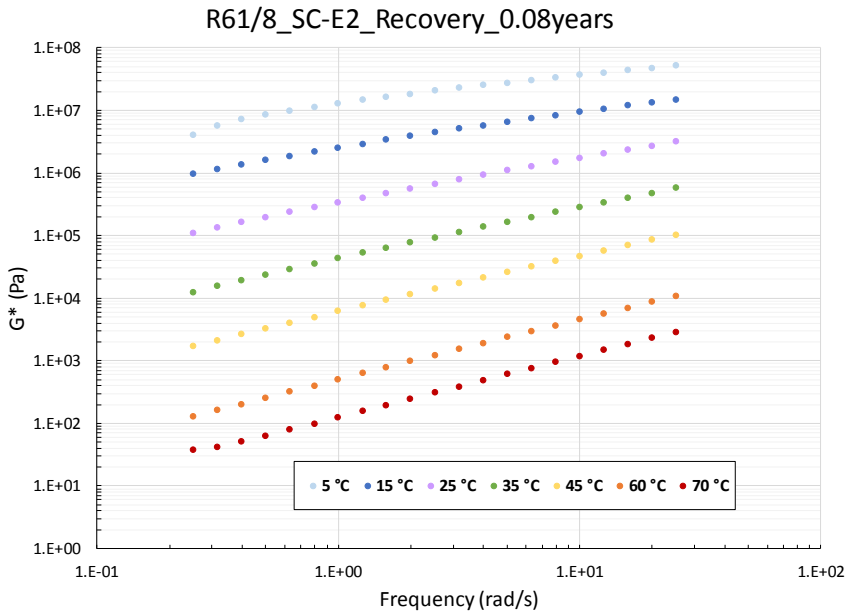

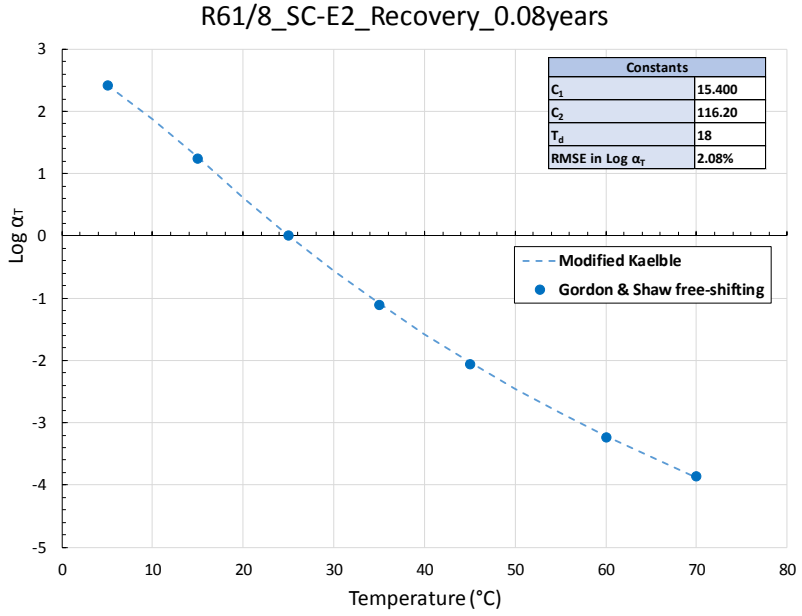

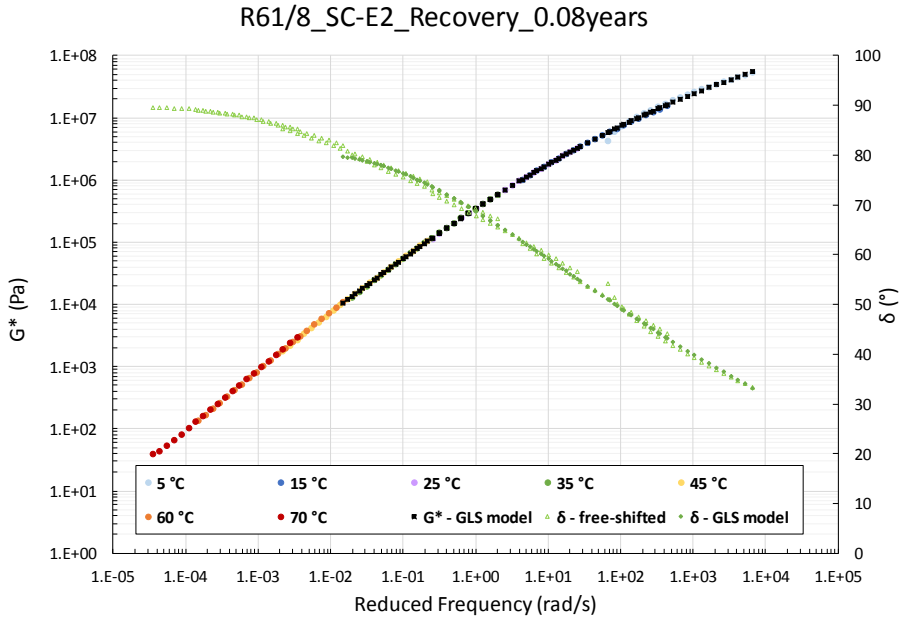

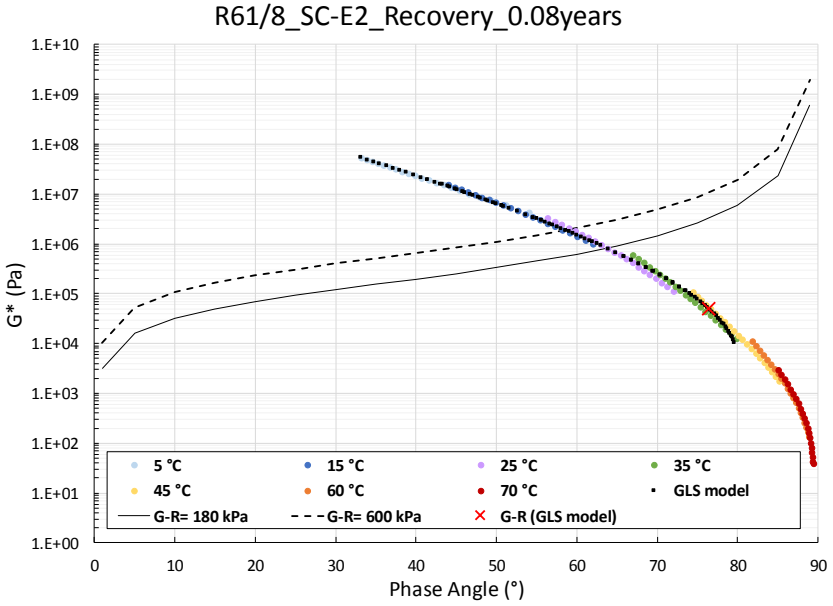

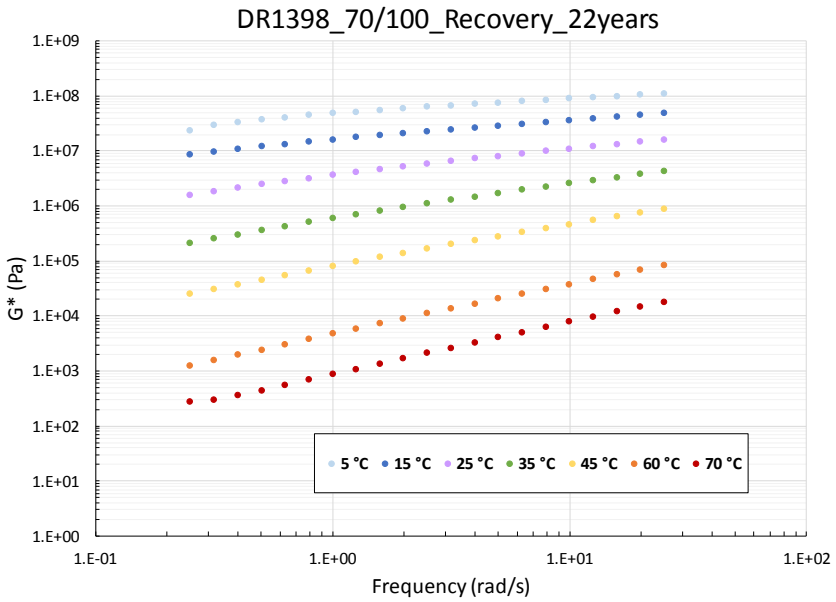

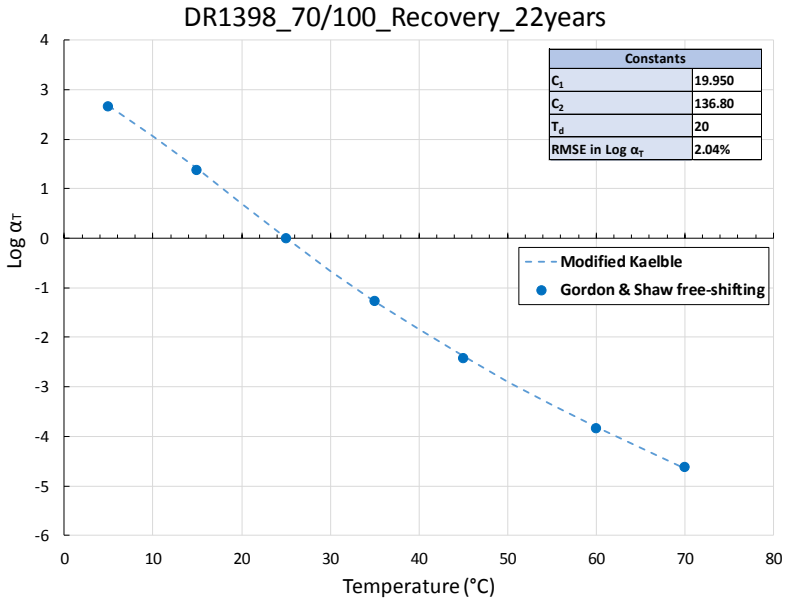

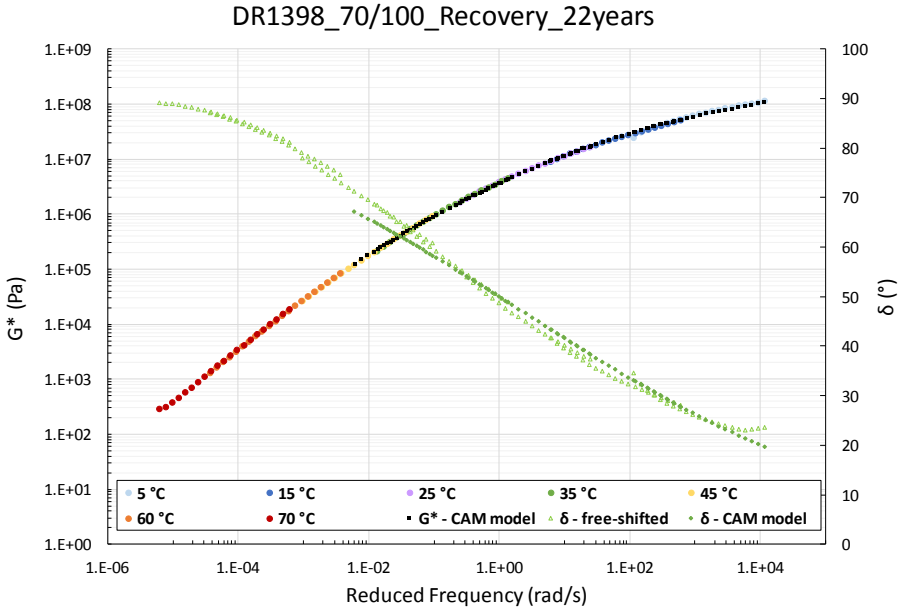

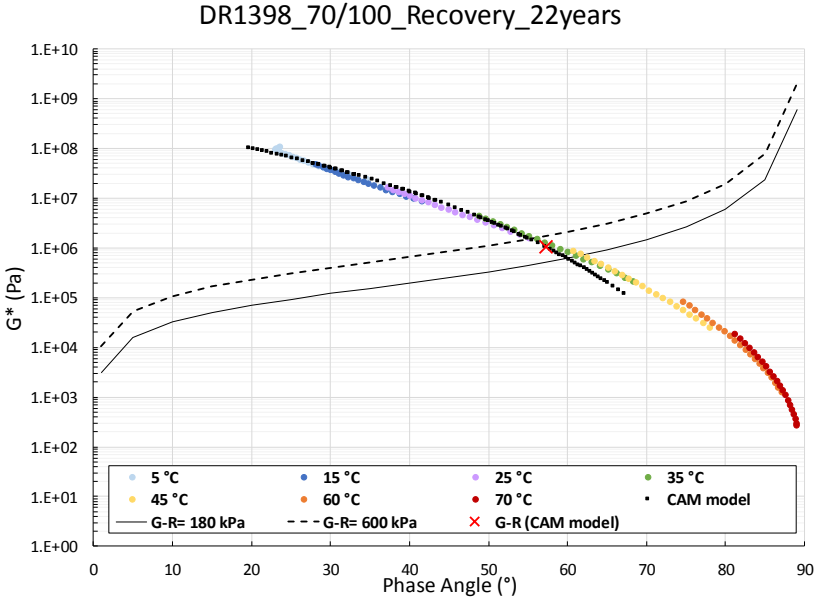

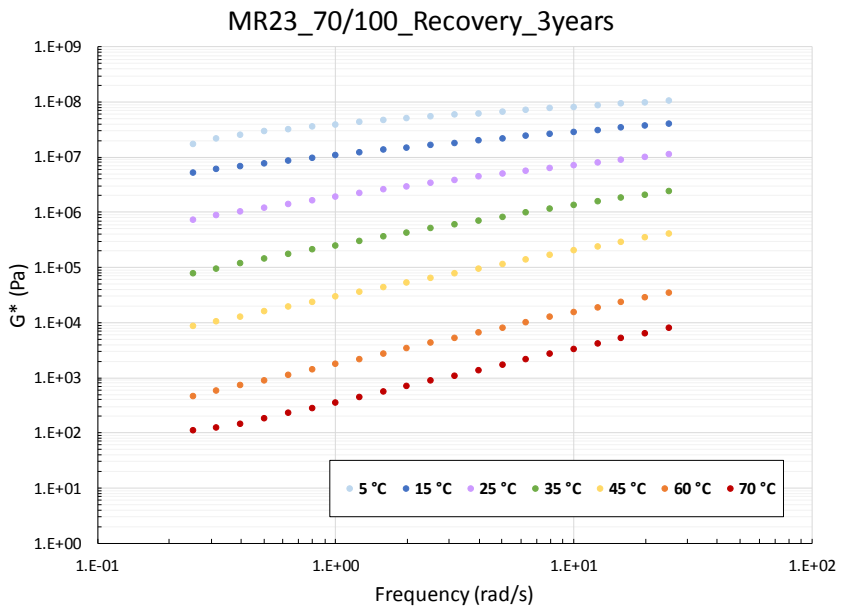

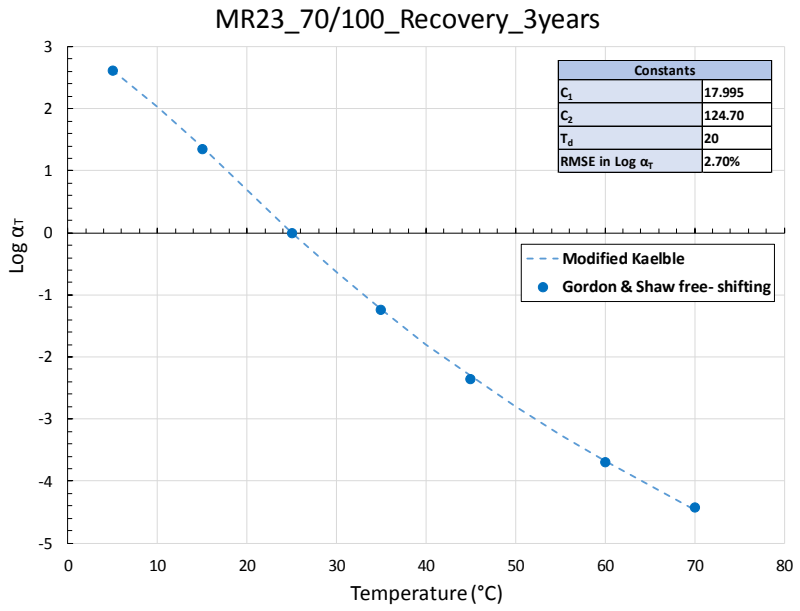

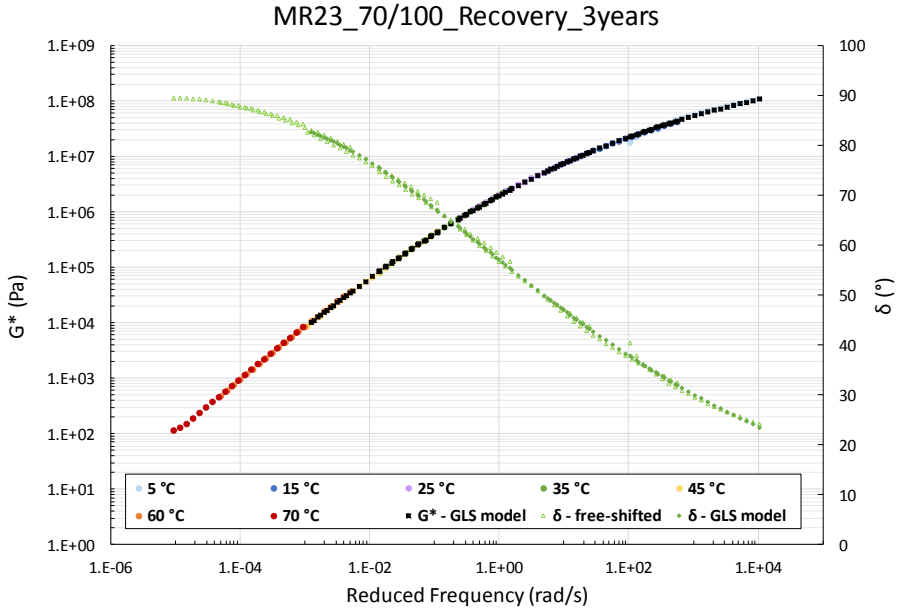

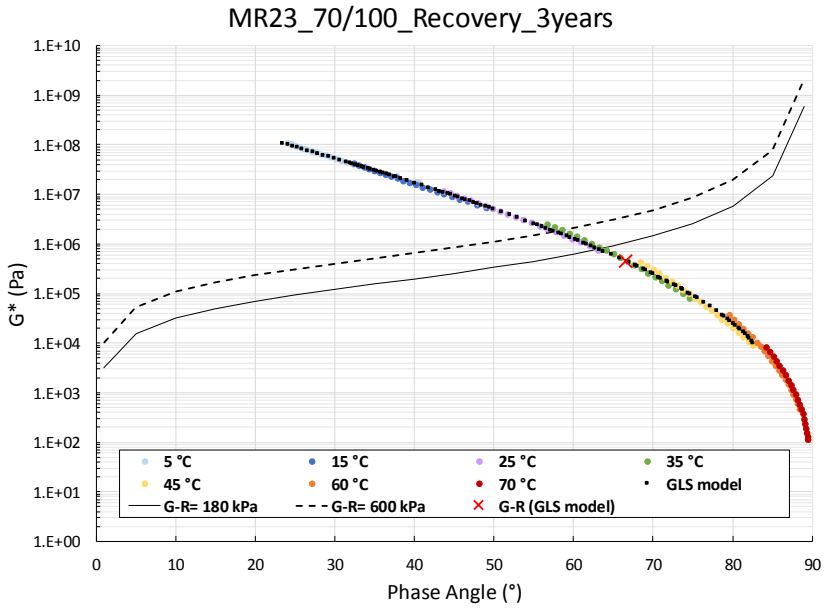

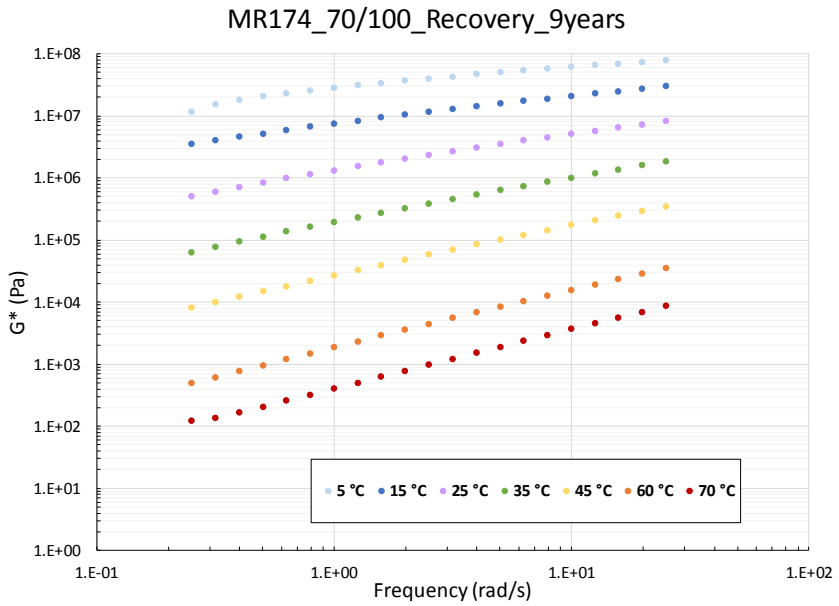

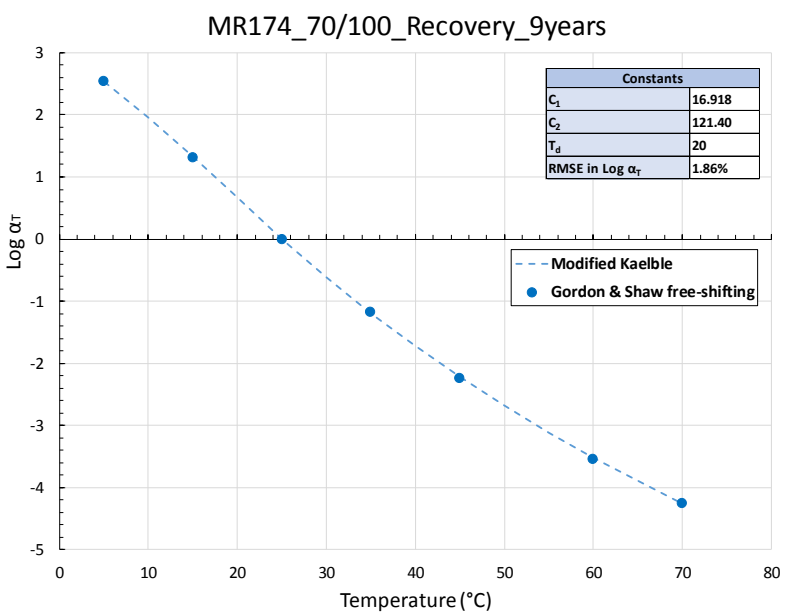

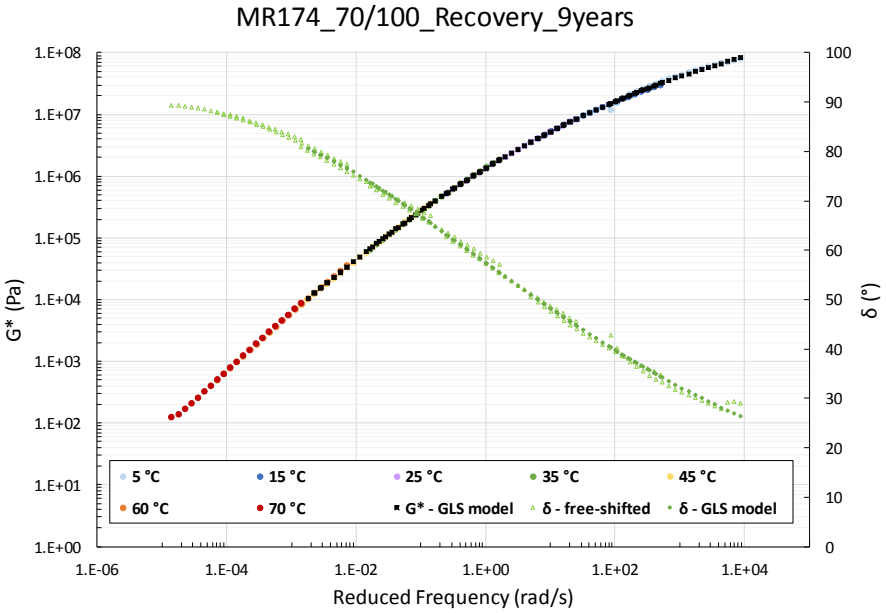

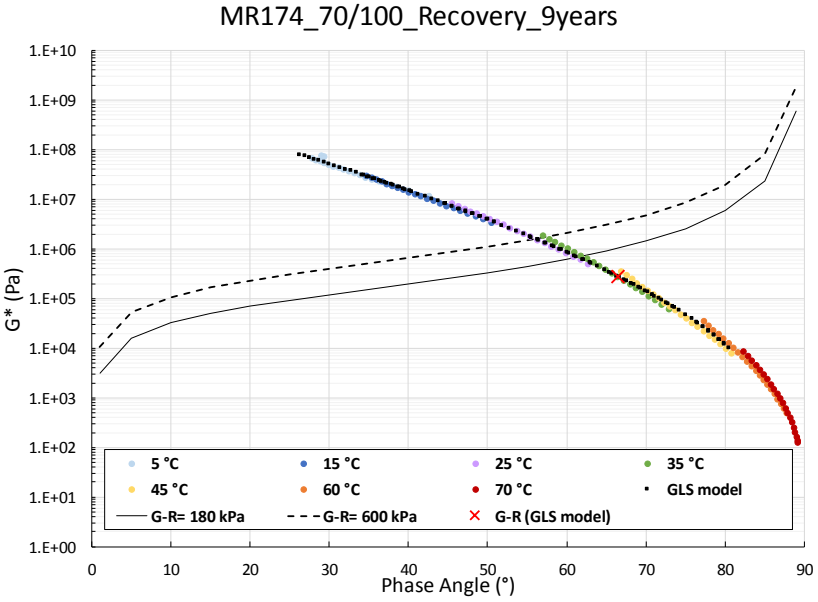

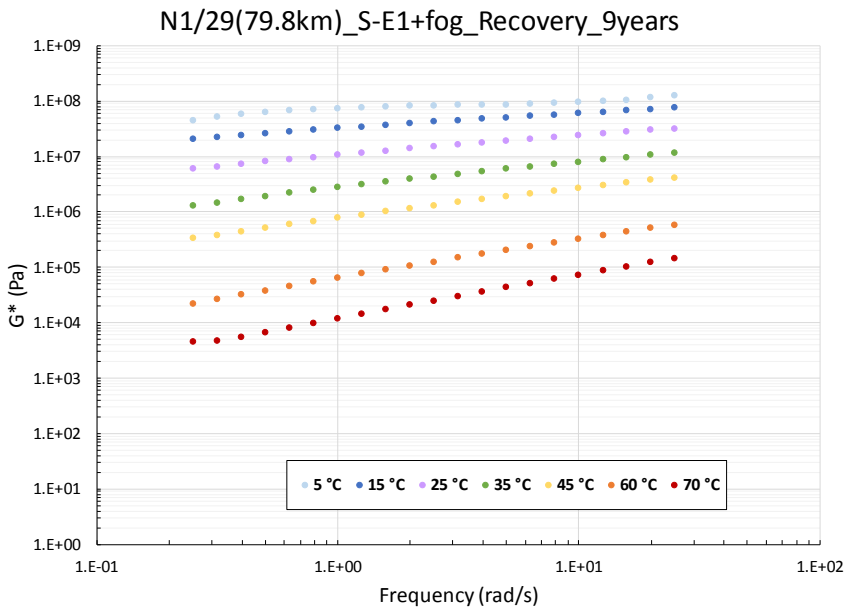

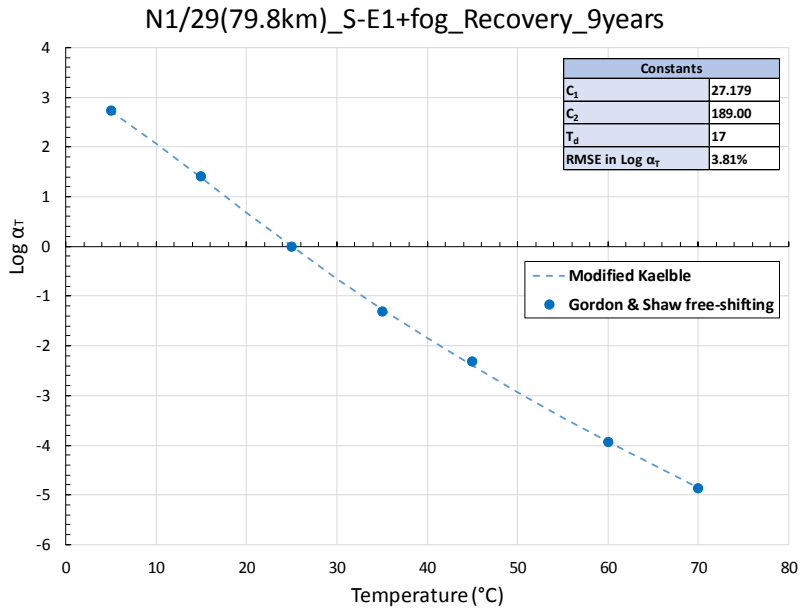

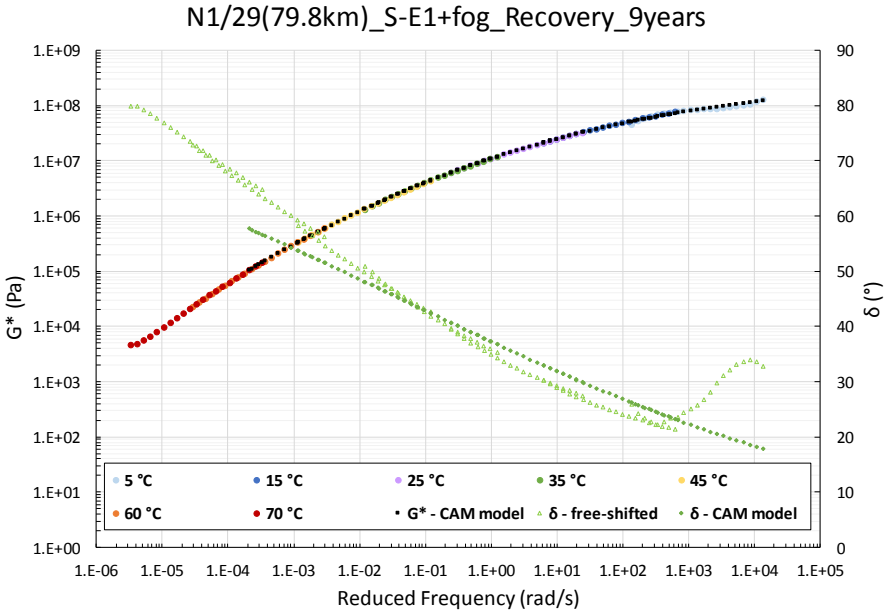

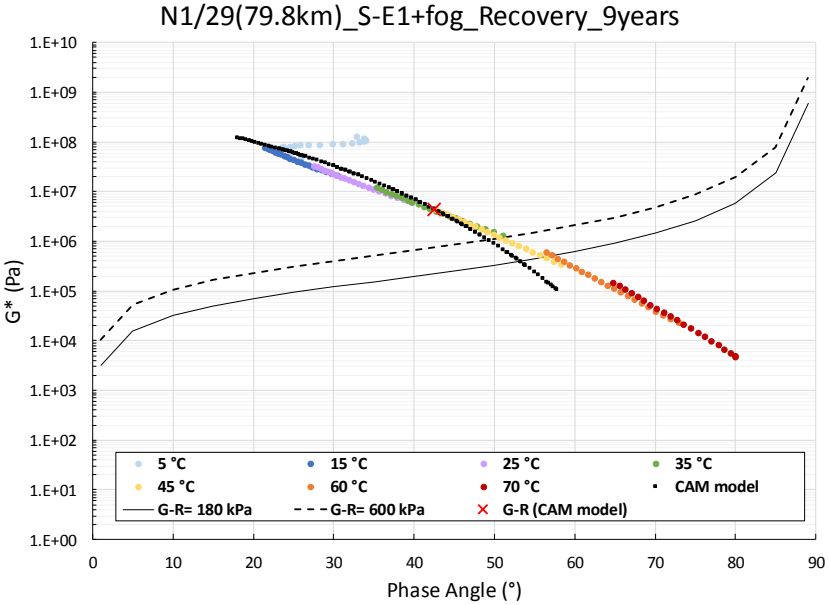

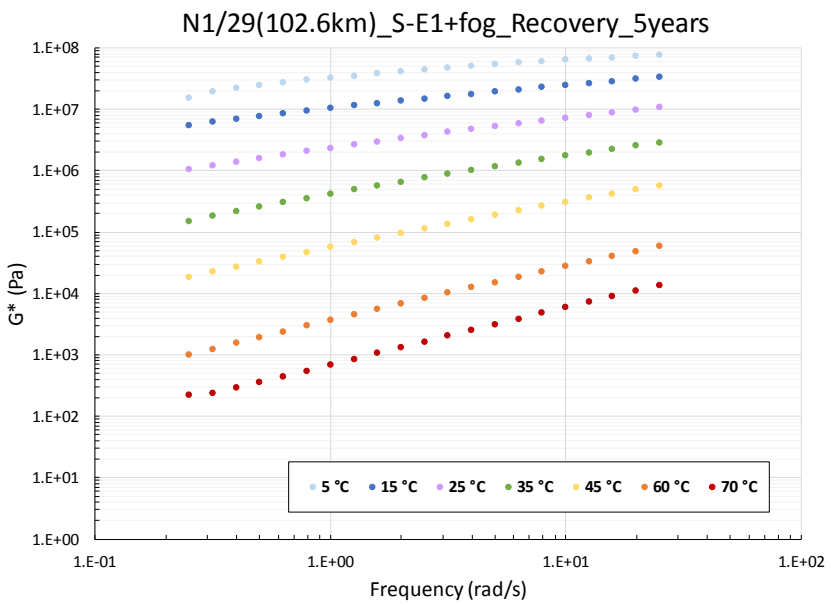

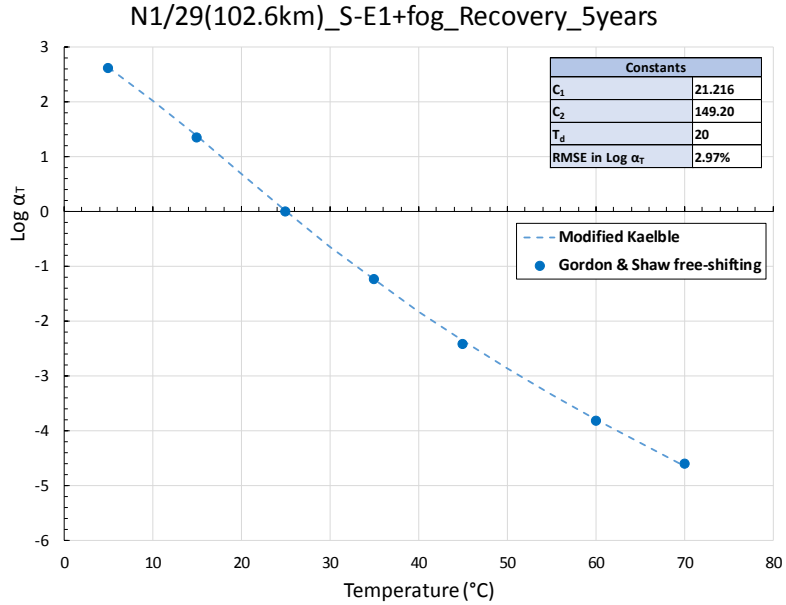

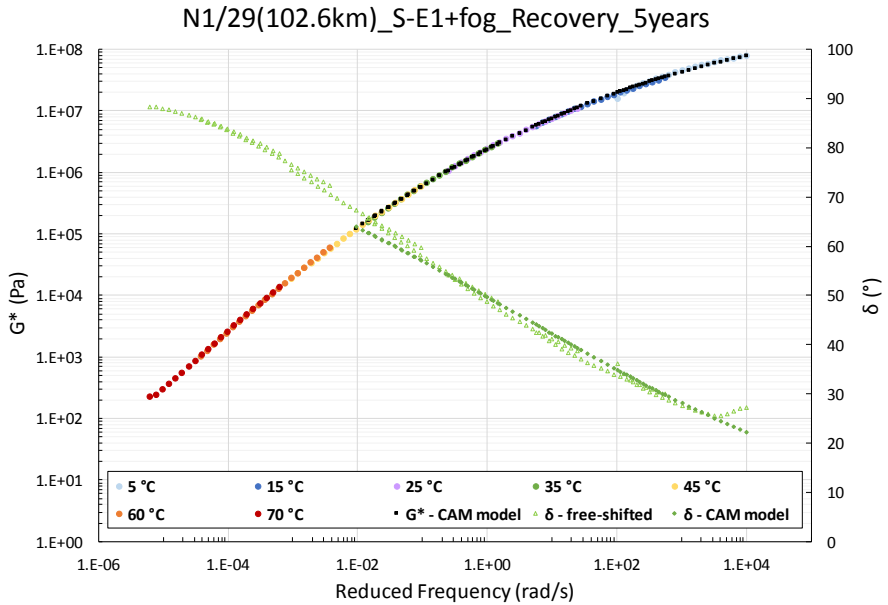

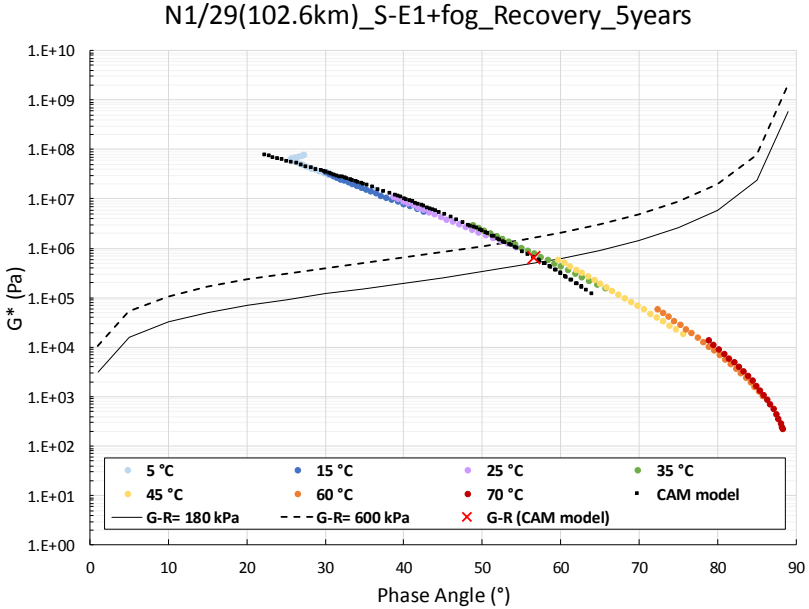

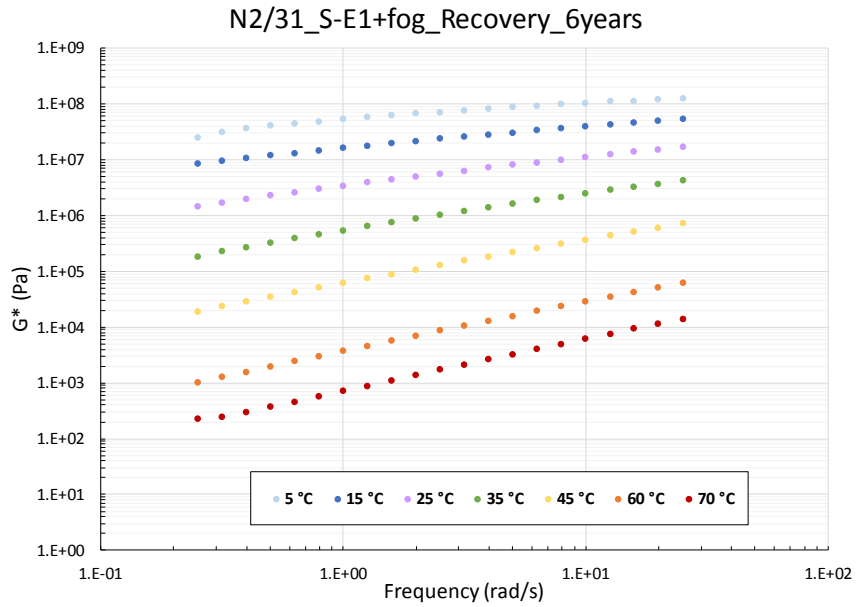

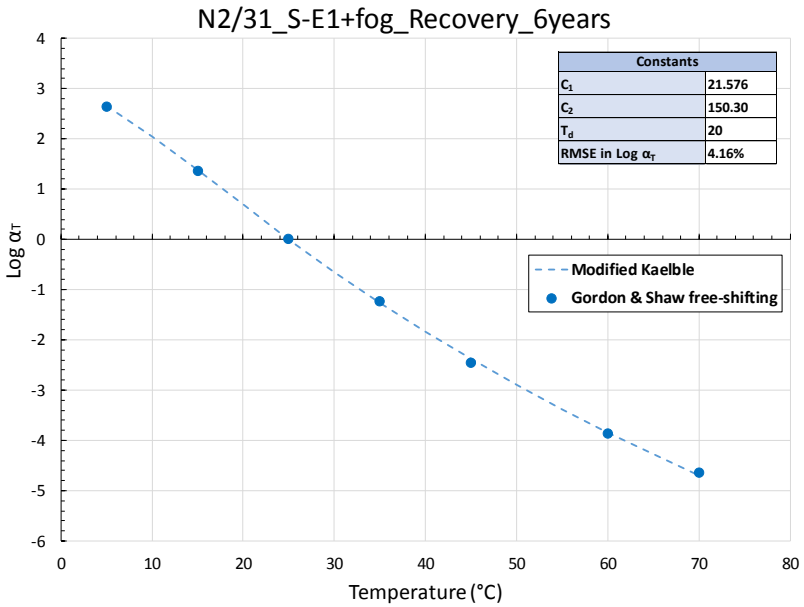

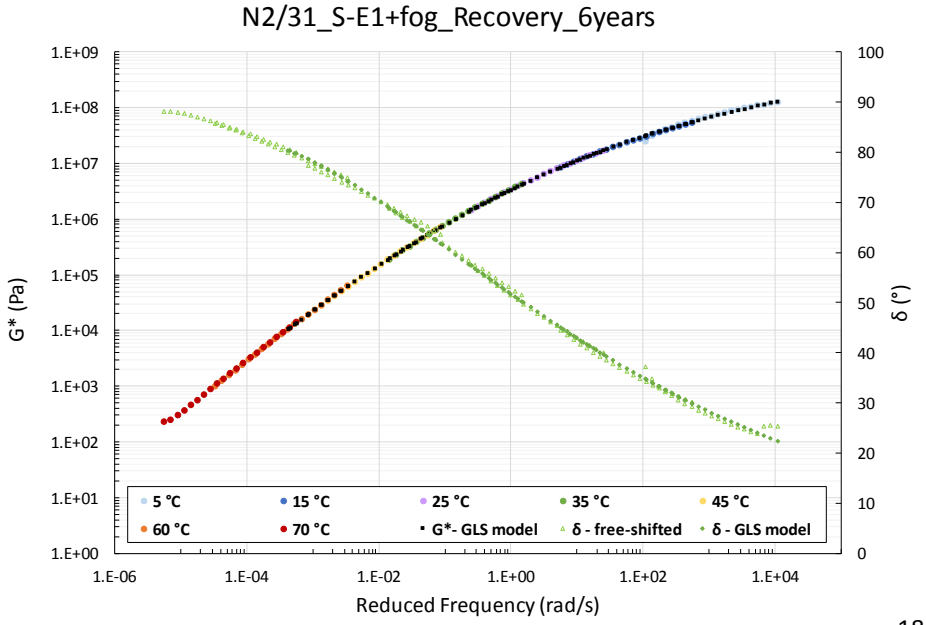

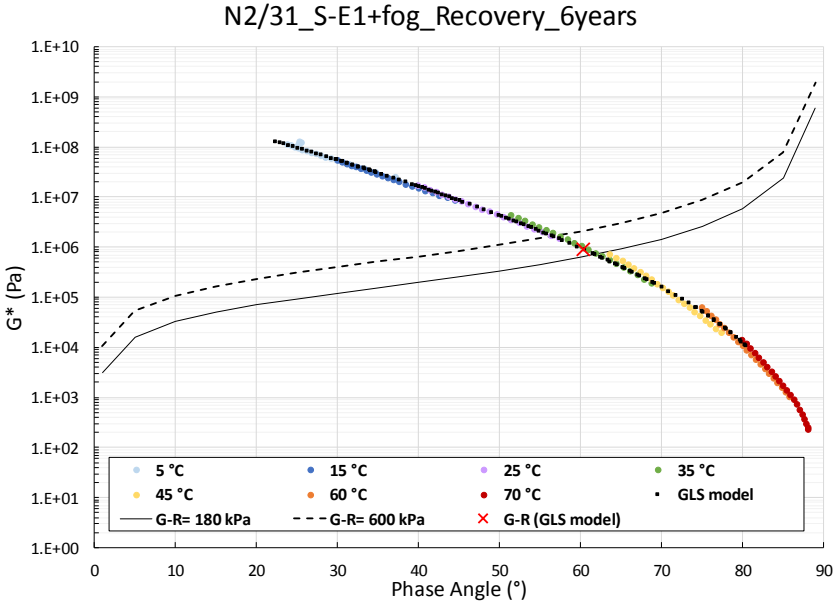

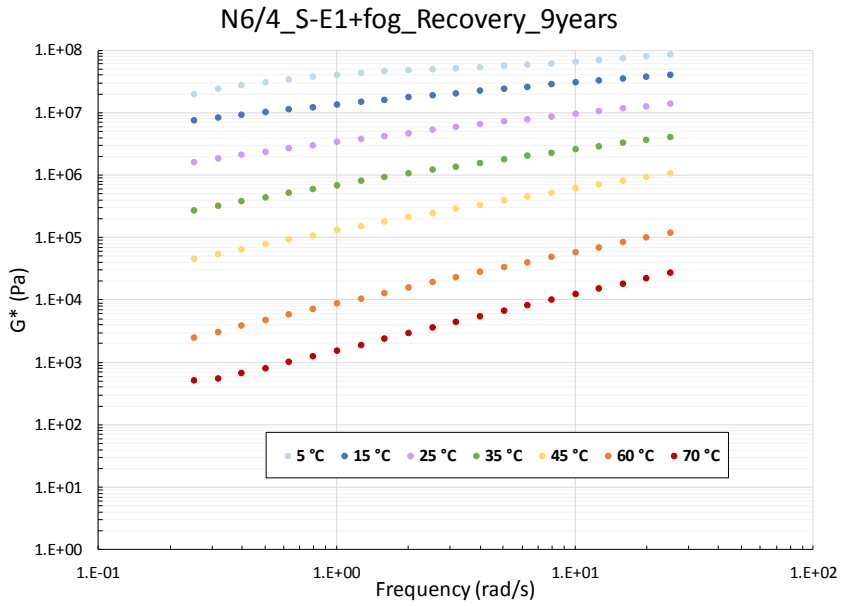

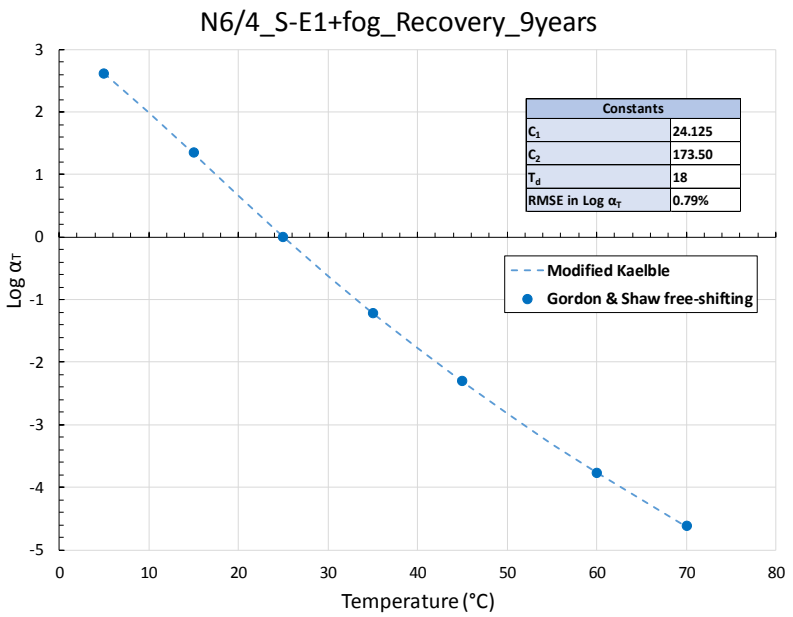

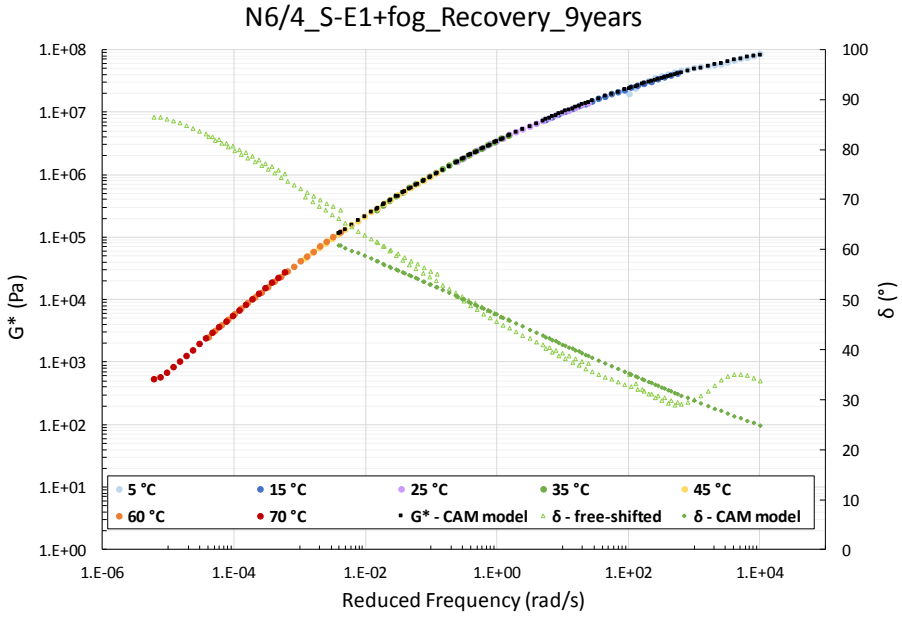

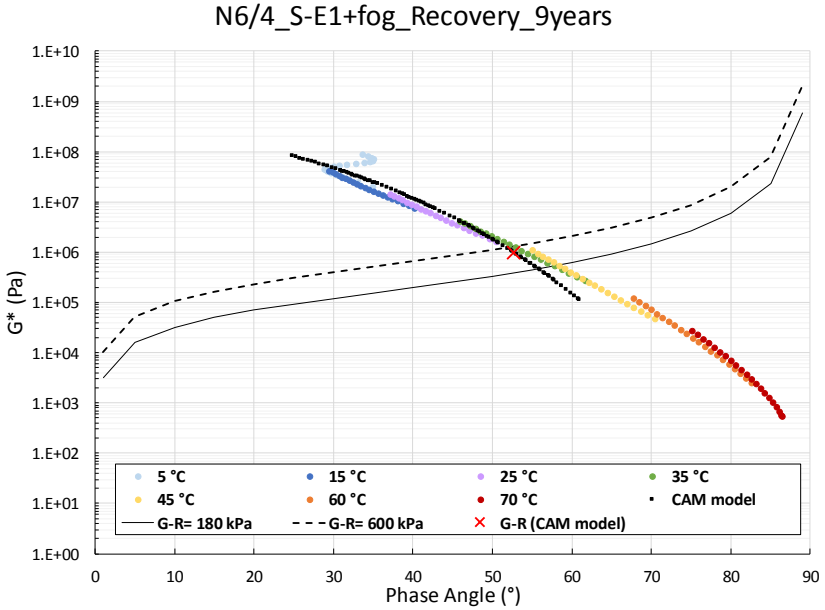

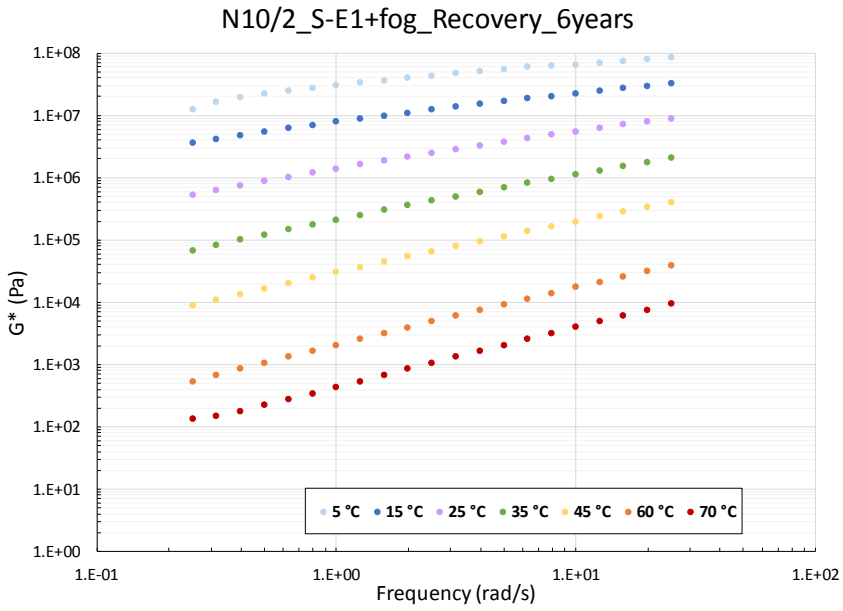

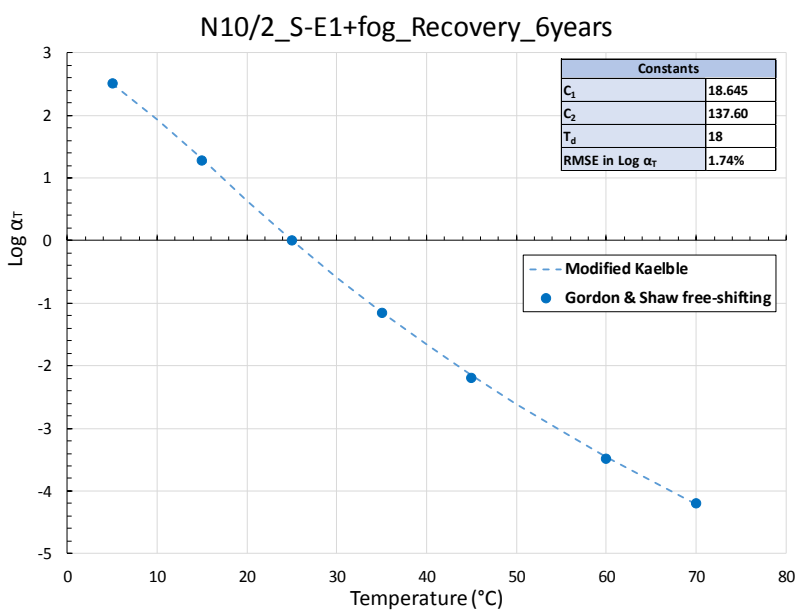

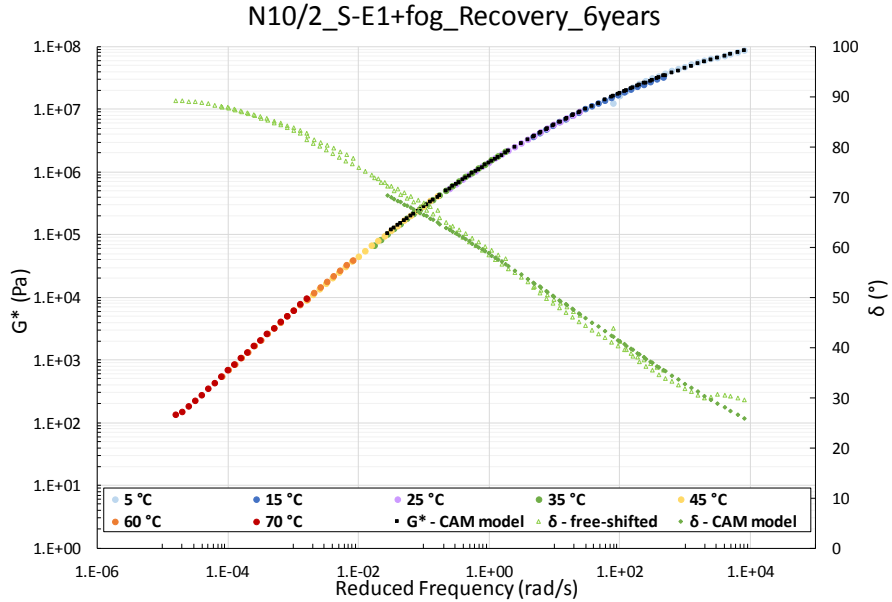

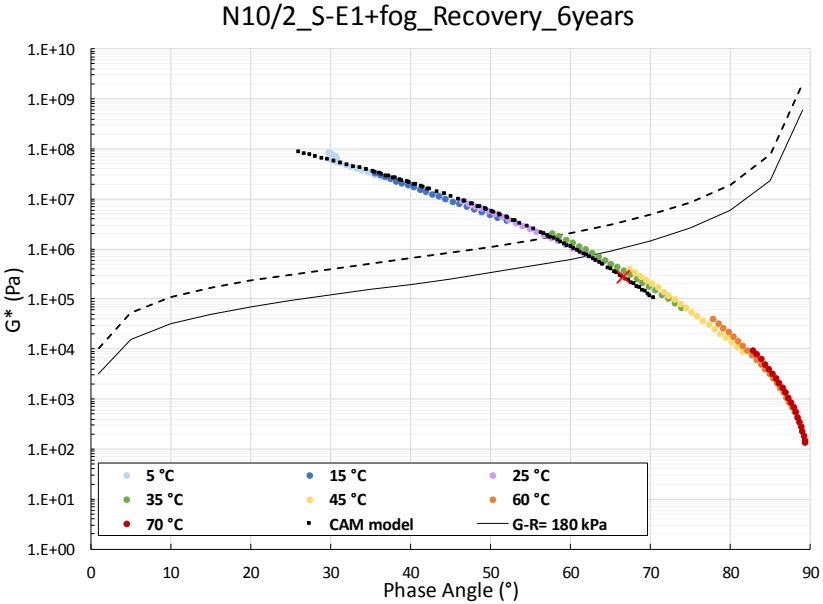

Appendix B: Combined Master Curves & Black Space Diagrams before modelling

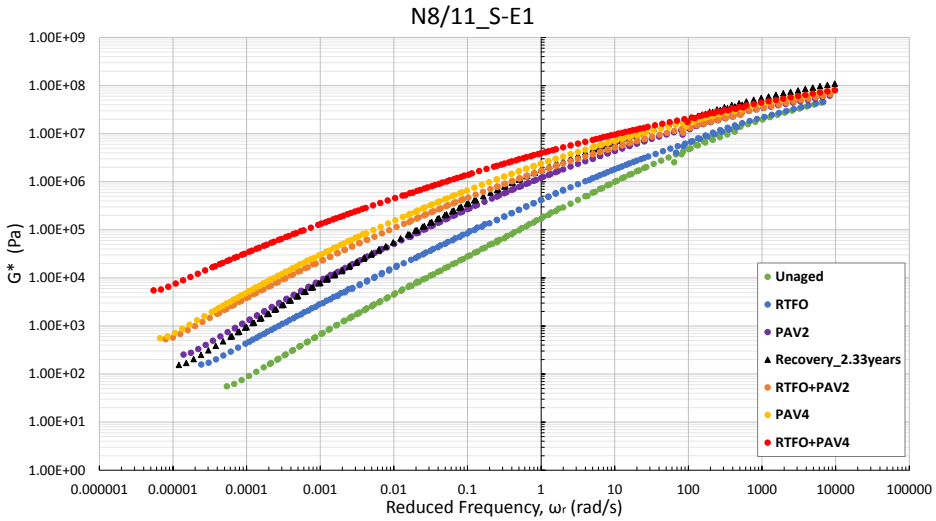

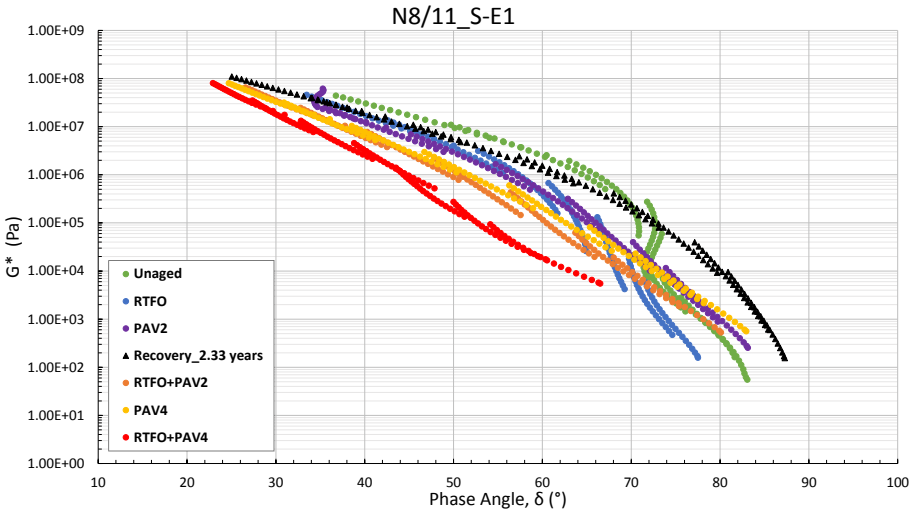

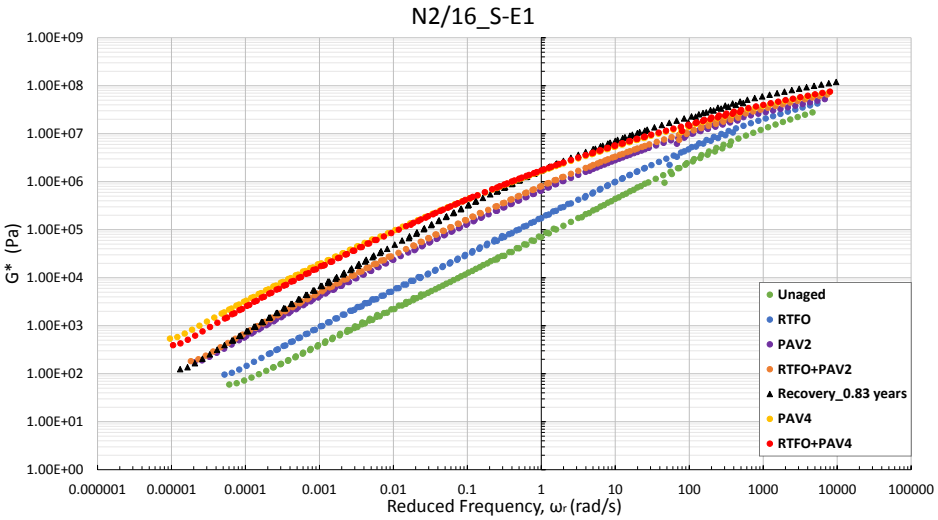

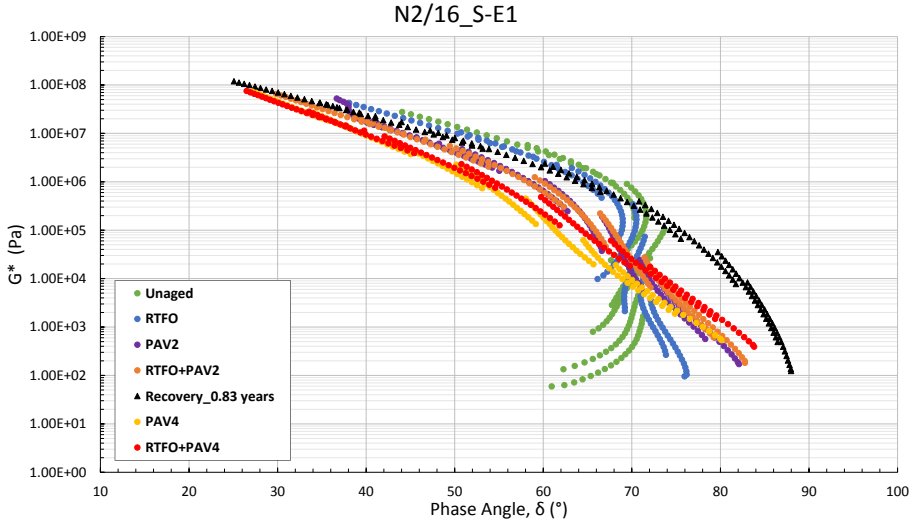

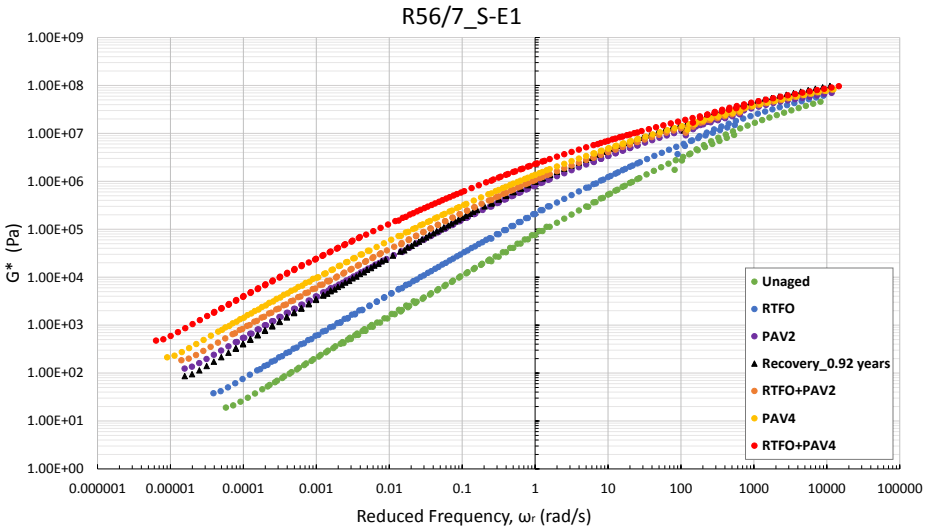

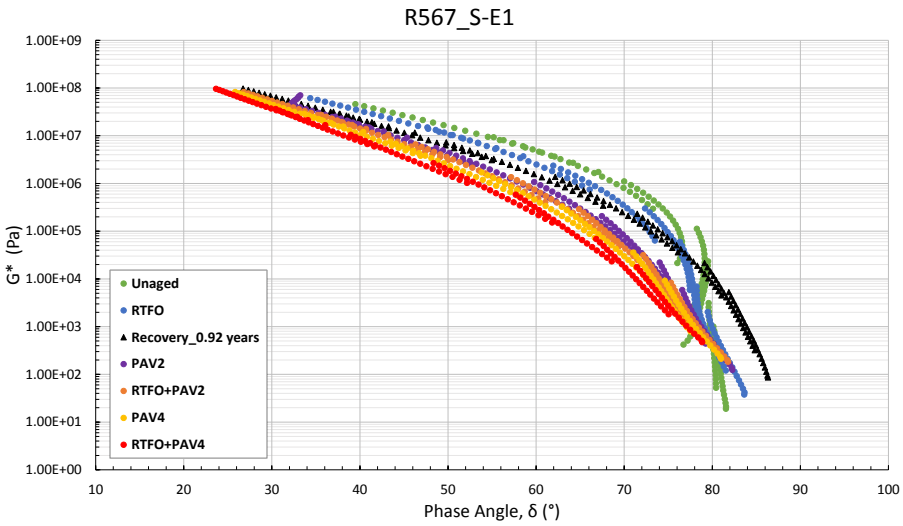

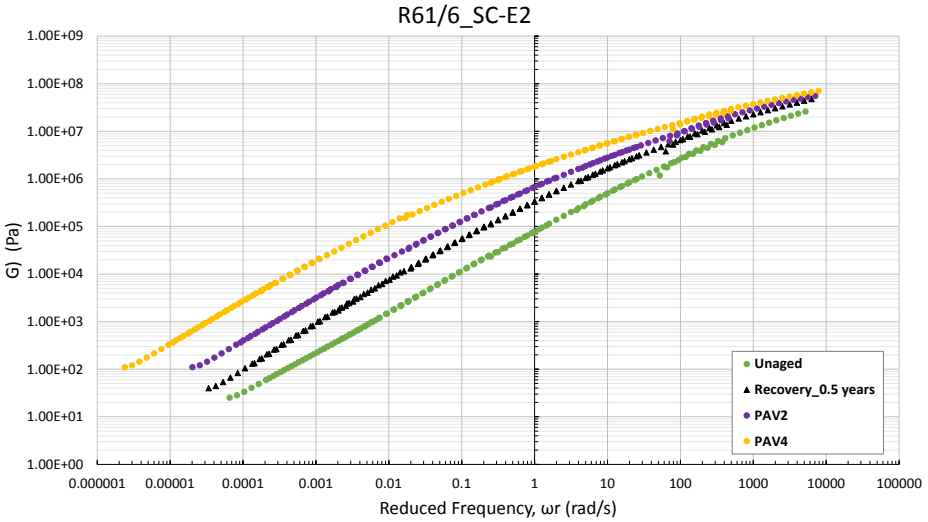

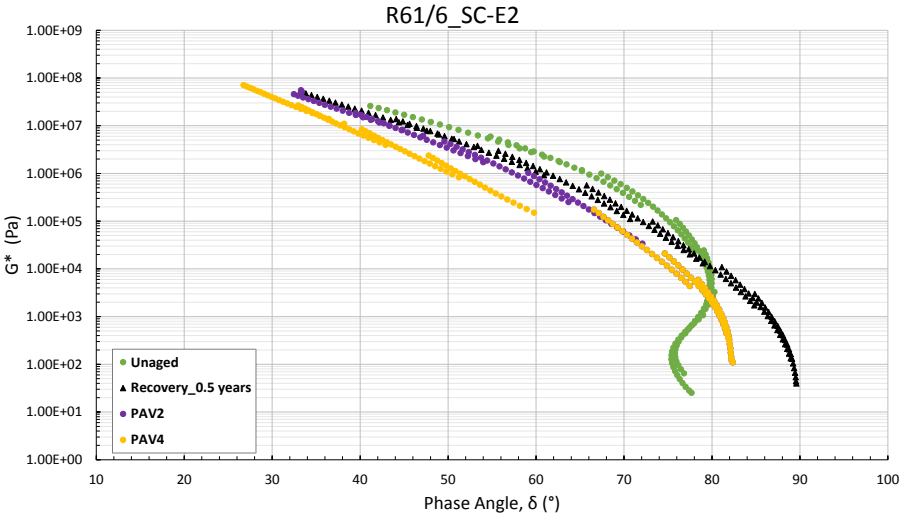

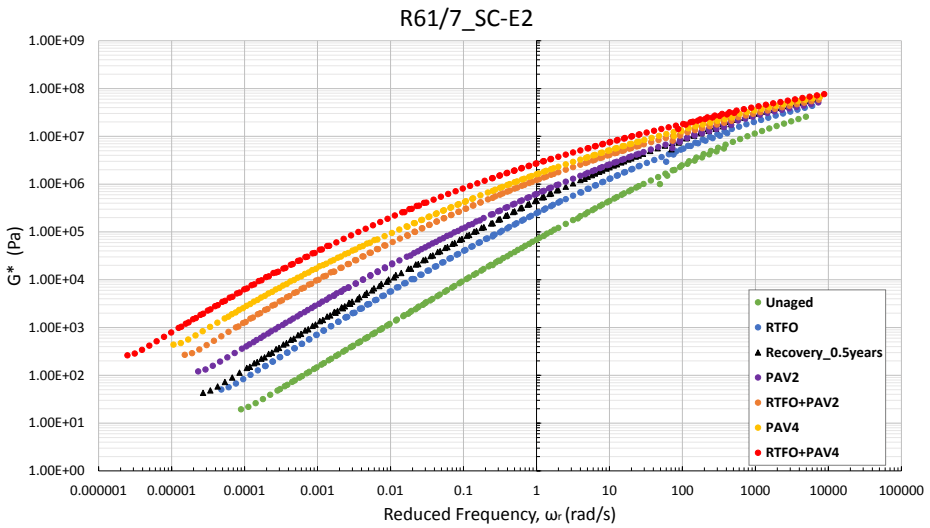

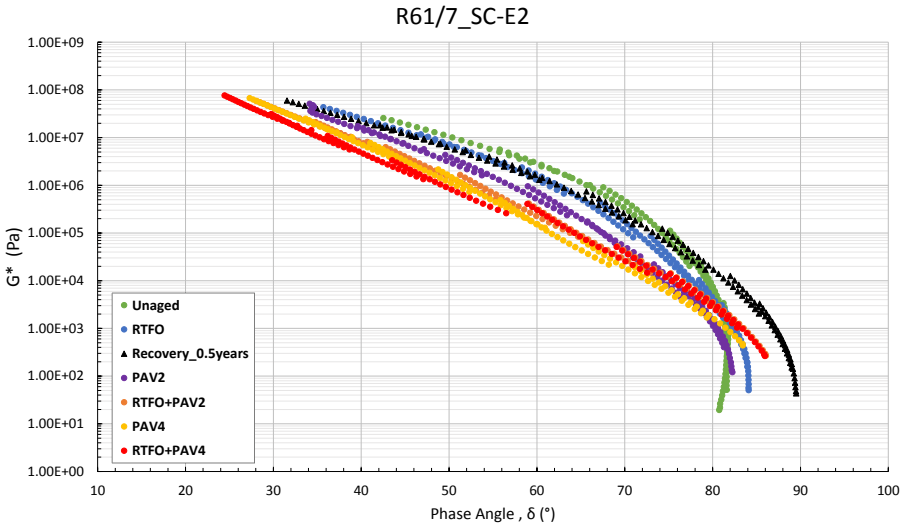

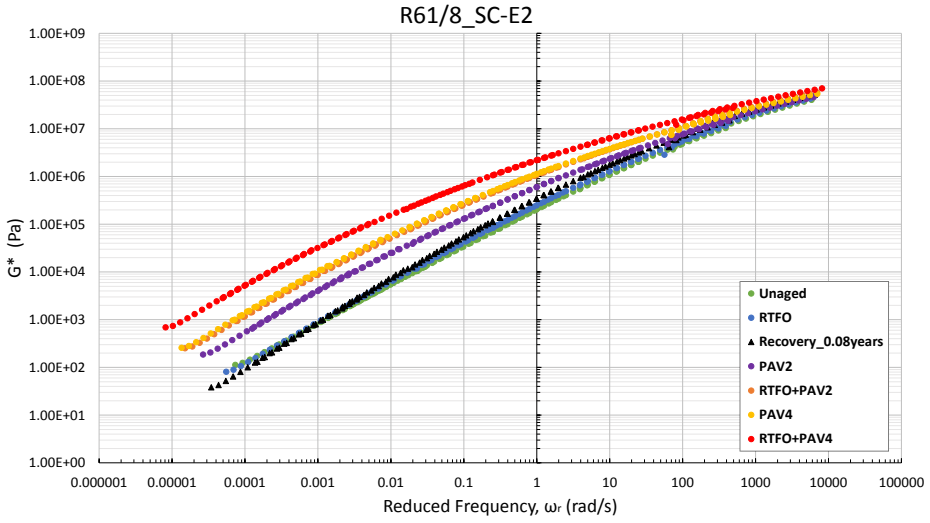

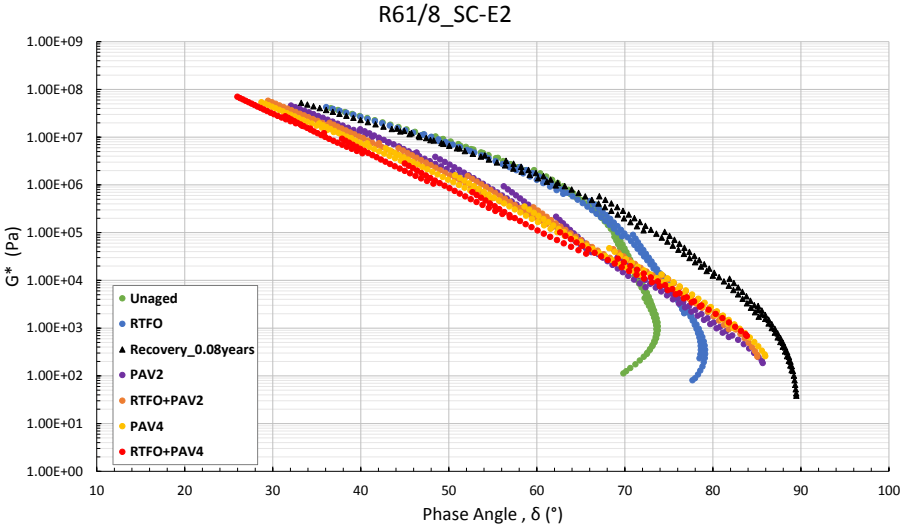

Appendix C: Measured vs modelled correlation

Binder	Parameters	R^2	
		CAM	GLS
Original Binders			
N8/11_S-E1_ORIG	G*	0.9962	0.9946
	δ	0.9889	0.9916
N8/11_S-E1_RTFO	G*	0.9980	0.9981
	δ	0.9879	0.8810
N8/11_S-E1_RTFO+PAV2	G*	0.9988	0.9984
	δ	0.9928	0.9963
N8/11_S-E1_RTFO+PAV4	G*	0.9990	0.9982
	δ	0.9955	
N8/11_S-E1_PAV2	G*	0.9980	0.9967
	δ	0.9690	
N8/11_S-E1_PAV4	G*	0.9984	0.9979
	δ	0.9931	
N2/16_S-E1_ORIG	G*	0.9945	0.9938
	δ	0.9644	
N2/16_S-E1_RTFO	G*	0.9955	0.9928
	δ	0.9753	0.9794
N2/16_S-E1_RTFO+PAV2	G*	0.9989	0.9985
	δ	0.9948	0.9946
N2/16_S-E1_RTFO+PAV4	G*	0.9988	0.9988
	δ	0.9946	
N2/16_S-E1_PAV2	G*	0.9980	0.9959
	δ	0.9790	0.9867
N2/16_S-E1_PAV4	G*	0.9990	0.9990
	δ	0.9944	0.9955
R56/7_S-E1_ORIG	G*	0.9931	0.9924
	δ	0.9926	
R56/7_S-E1_RTFO	G*	0.9954	0.9958
	δ	0.9944	0.9940
R56/7_S-E1_RTFO+PAV2	G*	0.9984	0.9984
	δ	0.9963	0.9981
R56/7_S-E1_RTFO+PAV4	G*	0.9978	0.9979
	δ	0.9939	0.9982
R56/7_S-E1_PAV2	G*	0.9962	0.9950
	δ	0.9824	0.9948
R56/7_S-E1_PAV4	G*	0.9984	0.9984
	δ	0.9953	0.9982
R61/6_SC-E2_ORIG	G*	0.9970	0.9960
	δ	0.9943	
R61/6_SC-E2_PAV2	G*	0.9979	0.9980
	δ	0.9923	0.9971
R61/6_SC-E2_PAV4	G*	0.9988	0.9968
	δ	0.9676	
R61/7_SC-E2_ORIG	G*	0.9965	0.9968
	δ	0.9933	0.9927
R61/7_SC-E2_RTFO	G*	0.9976	0.9983
	δ	0.9953	0.9954
R61/7_SC-E2_RTFO+PAV2	G*	0.9987	0.9983
	δ	0.9922	
R61/7_SC-E2_RTFO+PAV4	G*	0.9978	0.9951
	δ	0.9689	
R61/7_SC-E2_PAV2	G*	0.9974	0.9974
	δ	0.9888	0.9962
R61/7_SC-E2_PAV4	G*	0.9988	0.9985
	δ	0.9950	

Binder	Parameters	R^2	
		CAM	GLS
R61/8_SC-E2_ORIG	G*	0.9969	0.9970
	δ	0.9884	0.9918
R61/8_SC-E2_RTFO	G*	0.9976	0.9979
	δ	0.9941	0.9952
R61/8_SC-E2_RTFO+PAV2	G*	0.9990	0.9986
	δ	0.9938	0.9966
R61/8_SC-E2_RTFO+PAV4	G*	0.9986	0.9971
	δ	0.9895	
R61/8_SC-E2_PAV2	G*	0.9989	0.9990
	δ	0.9944	0.9956
R61/8_SC-E2_PAV4	G*	0.9989	0.9984
	δ	0.9927	
Recovered Binders			
N8/11_S-E1_3y4m	G*	0.9985	0.9988
	δ	0.9953	0.9987
N2/16_S-E1_10m	G*	0.9984	0.9986
	δ	0.9953	0.9983
R56/7_S-E1_11m	G*	0.9987	0.9982
	δ	0.9941	0.9981
R61/6_SC-E2_6m	G*	0.9985	0.9987
	δ	0.9954	0.9969
R61/7_SC-E2_6m	G*	0.9986	0.9985
	δ	0.9953	0.9970
R61/8-SCE2-1m	G*	0.9983	0.9984
	δ	0.9958	0.9969
DR1398_70/100_23y	G*	0.9968	0.9983
	δ	0.9837	
MR23_70/100_4y	G*	0.9980	0.9989
	δ	0.9913	0.9989
MR174_70/100_10y	G*	0.9982	0.9981
	δ	0.9905	0.9977
N1/29(79.8km)_S-E1+fog_9y	G*	0.9950	0.9941
	δ	0.8574	
N1/29(102.6km)_S-E1+fog_5y	G*	0.9977	0.9979
	δ	0.9827	
N2/31_S-E1+fog_6y	G*	0.9976	0.9980
	δ	0.9886	0.9985
N6/4_S-E1+fog_9y	G*	0.9976	0.9977
	δ	0.9072	
N10/2_S-E1+fog_6y	G*	0.9981	0.9976
	δ	0.9891	